Université Mohamed Boudiaf - M'sila

FACULTE DE TECHNOLOGIE

DEPARTEMENT Génie Electrique

Numéro de série……..…

Numéro d'inscription :D.ELM/3C/05/17

Thèse

Présentée pour l'obtention du diplôme de

DOCTORAT LMD

Filière : Electromécanique

Spécialité : Electromécanique

THEME

DIAGNOSTIC DES DEFAUTS ET ANALYS ELECTROMAGNETIQUE EN 2D DES MACHINES ASYNCHRONES

Présentée Par

ABU IBAID Osama ziadibrhim

Soutenue le : 30 / 01 / 2024

Devant le jury composé de :

Nom & Prénom	Grade	Etablissement	Qualité
Khodja Djallal Edinne	**Professeur**	Univ.de **M'sila**	Président
BELHAMDI SAAD	**Professeur**	Univ.de **M'sila**	Encadreur
CHAKROUNE SALIM	**Professeur**	Univ.de **M'sila**	Co-Encadreur
Benyettou Lotfi	**Professeur**	Univ.de **M'sila**	Examinateur
Talhaoui Hicham	**Professeur**	Univ.de **B-B-A**	Examinateur

Année Universitaire : 2023/2024

Université Mohamed Boudiaf - M’sila

FACULTE OF TECHNOLOGIE

DEPARTEMENT ELECTRICAL ENGINEERING

Serial number……

Description number……

Thesis

Presented for graduation of

DOCTORATE LMD

Branch: Electrical engineering

Specialization: Electro mechanics

THEME

DIAGNOSIS OF DEFECTS AND 2D ELECTROMAGNETIC ANALYSIS OF ASYNCHRONOUS MACHINES

Presented By

ABU IBAID Osama ziad ibrhim

Supported on :30 /01 /2024

Name & Family name	Grade	Facility	Quality
Khodja Djallal Edinne	**Professor**	Univ. de **M’sila**	President
BELHAMDI SAAD	**Professor**	Univ. de **M’sila**	Supervisor
CHAKROUNE SALIM	**Professor**	Univ.de **M’sila**	Co-Supervisor
Benyettou Lotfi	**Professor**	Univ.de **M’sila**	Examiner
Talhaoui Hicham	**Professor**	Univ.de **B-B-A**	Examiner
Rahali Hilal	Professor Lecturer	Univ.de M’sila	Examiner

Academic year 2023/2024

شكر

لحمد لله رب العالمين والصلاة والسلام على أشرف الأنبياء والمرسلين سيدنا محمَّد وعلى آله وصحبه ومن تبعهم بإحسان إلى يوم الدين، وبعد

فإني أشكر الله تعالى على فضله حيث أتاح لي إنجاز هذا العمل بفضله،

فله الحمد أولاً وآخرًا

أعرني لساناً أيها الشعر للشكر

وإن تطق شكراً فلا كنت من شعر

وجئني بنور الشمس والبدرِ كي أرى

بمَعْناك نور الشمس يُشرق والبدر

يسرني أن أوجه شكري لكل من نصحني أو أرشدني أو وجهني أو ساهم معي

في إعداد هذا البحث بإيصالي للمراجع والمصادر المطلوبة في أي مرحلة من مراحله، وأشكر على وجه الخصوص أستاذي الفاضل الدكتور (بلحمدي ساعد)

و أستاذي الفاضل الدكتور (شقرون سليم)

كل عبارات الشكر والعرفان لا تكفي من الامتنان بحقكما اساتذتي الموقرين ..

كيف لا.. وقد كاد المعلم أن يكون رسولا ..

أيضا كل الشكر لهذا الصرح العلمي العظيم والذي يزيدني شرفا باني ابن وطالب واليوم خريج باذن الله من جامعة محمد بوضياف بالمسيلة

كل التقدير لطاقم هذه المؤسسة العريقه مع خالص التحيه لكل القائمين علي تسييرها متوجة برئاسة الجامعة وطواقمها الإدارية والتعليميه

الشكر موصول لعميد كليه التكنولوجيا ونائبه المحترم

وبكل اعتزاز كلي فخر وعرفان لكل أساتذة قسم الهندسه الكهربائية

شكرا لهذا البلد العظيم ..كل التحيه للجزائر

إهـــــــداء

بسم الله الرحمن الرحيم

{قل إعملوا فسيري الله عملكم ورسوله والمؤمنون}

صدق الله العظيم

إلي من بلغ الرسالة , وأدي الأمانة , ونصح الامة , نبي الرحمة ونور العالمين ,,

سيدنا محمد الصادق الأمين , عليه افضل صلاة وأشرف تسليم ,,

بدأنا بأكثر من يد , وقاسينا أكثر من هم , وعانينا الكثيرمن الصعوبات , وهان نحن اليوم ,,

والحمد لله نطوي سهر الليالي وخلاصة المشوار وتعب ألف يوم ويوم ,,

وها أنا اهديك أبي , يا مهجة الروح , ونور قلبي , وقرة عيني ,,

لأذكر اسمك مفتخرا به , على الرأس مرفوعا , مزينا لنجاحي ,,

أمي الغالية , يا نهر الحب ونبع الحنان ,,

كيف أهديكي كلماتي , وبحبك تاهت حروفي , وعن نطقها عجز اللسان ,,

كيف لا , وأنتي أغلي ما بدنيتي , وأغلي ما وهب لي الرحمن ,,

أخوتي وأختي , يا من حبكم يجري في عروقي , ويلهج بذكراكم فؤادي ,,

يا نجوما ساطعة في سمائي , ونور كالقمر ينير آمالي , اهديكم نجاحي بأجمل المعاني ,,

ولا أنسي في هذا المقام كل صديق او عزيز او اخ ,,

كان بوجوده الهاما لطريقي ومشواري في غربتي ..

ولفلسطين أهديكي مني أشواق ومودة وحب وعرفان ,,

أهديكي نجاحي , بعنوان قضيتي , يا رمزا لكل الأوطان ,,

وفي الختام ,, أهدي فرحتي اليوم لمن كان سببا بفرحتي , عائلتي الجزائرية ,,

لكم مني كل المودة والاحترام , ولجزائركم أحبتي مني الف سلام

Tables of contents

Figure List

Table List

Symbol List

n_b : The number of rolling elements (balls, rollers or needles). [Ω]

D_b : Diameter of the balls. [m]

D_c : Diameter of the center of the balls. [m]

θ = The contact angle of the ball with the cage. [rd]

f_r *:* The rotational frequency of the inner ring (the outer ring being assumed to be fixed) [Hz]

F_{ext} : The frequency at which a rolling element will pass through an outer ring defect. [Hz]

F_{int} : describes how often a rolling element will travel over an inner ring flaw that is believed to be positioned on the rotating shaft. [Hz]

F_{cage} : The passage frequency (Fcage) of a cage defect. [Hz]

F_b : Used to determine the frequency of passing of a ball (or roller) fault on the inner ring or the outer ring. [Hz]

P : number of pole pairs

g : slip. [%]

N_e : number of rotor slots

n_d : is either 0 or 1 depending on whether the eccentricity is static or dynamic.

f_s : frequency of alimentation. [Hz]

$f_p(k)$: The additive failures.

$w_p(k)$: The noises and disturbances

$f_U(k)$: The additive failures.

$f_Y(k)$: The noises and disturbances

MCSA : The motor current signature analysis .

BRB : the broken bar.

FFT : Fast Fourier Transform.

WT : The wavelet transform .

fb : is the sideband frequency associated to the BRB, [Hz]

s : is the per-unit motor slip,

fs: is the frequency of the power grid in which the motor is connected [Hz]

k : is the number of the broken bar.

CWT: Continuous Wavelet Transforms Description

$\hat{\Psi}(f)$: denotes the Fourier transform of Ψ (x).

C_{Ψ} : The reconstruction formula involves this normalization coefficient.

DWT: Discrete Wavelet Transforms Description.

CA: Approximation wavelet coefficients.

CD: Detail wavelet coefficients.

f_n : the Nyquist frequency. [Hz]

E_j : Each frequency band's energy eigenvalue [Hz]

N_s : Number of stator turns per phase;

I_s : Current of a stator phase;

[Ampere]

$B_{\max}$: The maximal induction in the air gap.

[Tesla]

e : Air gap [m]

μ_0 : Magnetic permeability of vacuum [H.m^{-1}]

$B_s(\theta)$: The Fourier series decomposition of induction the fundamental.

[Tesla]

Φ_s : the magnetic flux in the air gap,

ψ_{sp} : the main flux of the stator winding.

L_{sp} : the main (magnetizing) inductance of the stator phase "n". [H]

Φ_{fs} : The leakage flux.

Symbol List

L_{sc} : The cyclic inductance. [H]

M_s : The mutual inductance between the stator phases.

[H]

N_r : Number of rotor bars,

i_{rk} : current in the loop .

[Ampere]

k=1,..., N_r

B_k : rotor mesh "k" produces a magnetic field in the air gap.

[Tesla]

B_{rk} : the air gap induction produced by a rotor loop

[Tesla]

L_{rb} : The primary inductance of a rotor mesh. [H]

M_{rr} : the mutual inductance between non-adjacent (disjoint) rotor cells [H]

$a = p\frac{2\pi}{N_r}$: The electrical angle between two rotor cells. [rd]

I_{rk} : Represents the current wire flow K ,

[Ampere]

I_{bk} : The current of the bar K .

[Ampere]

R_{bfk} : Resistance of a broken rotor bar [Ω]

R_e : Resistances of a short-circuit ring segment. [Ω]

$[R_r]$: Matrix of rotor resistances.

r : Average machine radius.

[Ω]

r_s : Resistance of each stator phase.

[Ω]

C_e : Electromagnetic torque

[Nm]

θ_r : Angle that defines the position of the rotor relative to the stator. [rd]

u_m : Maximum value of the voltage between two phases. [Volt]

$v_a(t)$: Voltage between two phases. [Volt]

VAO, VBO and VCO : are respectively the voltages between phases A, B and C and the fictitious neutral of the source. [Volt]

ω_r : Mechanical rotor speed.

[rd/s]

FEM: the finite element method.

$\vec{H}$: Magnetic field

[A/m]

$\vec{E}$: Electric field

[V/m]

$\vec{B}$: Magnetic induction

[Tesla]

$\vec{B}_r$: Remanent induction of the magnets

[Tesla]

$\vec{J}$: Total current density

[A/m^2]

μ : Magnetic permeability

[H/m]

σ : Electrical conductivity [$\Omega^{-1}m^{-1}$]

e : The total number of domain elements

[Ω]

$\omega = 2\pi f$: Electric pulse [rad. s^{-1}]

J : imaginary unit ($i^2 = -1$).

E : Element number.

Work done in this thesis

International journal publications:

1. O.Z.I. Abu Ibaid, S. Chakroune, S. Belhamdi, Z. S. Al-Sagar, "**Wavelet packet analysis for broken rotor bar fault detection in squirrel cage induction motor**" Section of Journal, ISSN 2074-272X. Electrical Engineering & Electromechanics. 03(2023). LicenseCC BY-NC 4.0 .no.1.Journal homepage: doi: 10.20998/2074-272X.2023.3.01

International conference publications:

1- O.Z.I. Abu Ibaid, S. Chakroune, S. Belhamdi, M.Abid, "**DIAGNOSIS OF ROTOR FAULTS OF ASYNCHRONOUS MACHINE BY SPECTRAL ANALYSIS OF STATOR CURRENTS**", 5th International Aegean Conference on Innovation Technologies & Engineering, February 25-26, 2022 , Izmir, Turkey.

2- 1- O.Z.I. Abu Ibaid, S. Chakroune, S. Belhamdi, , "Broken rotor bar fault detection in squirrel cage induction engine", Participated in the 4th International Conference on Electromechanical Engineering (ICEE2022) on December 13-14, 2022 at the University of Skikda, Algeria..

General Introduction

The ideal rise in global production competitiveness in a fiercely competitive worldwide environment throughout the previous century has compelled manufacturers to explore for measures to regulate and guarantee the availability and reliability of their production tools, [1].

The monitoring of industrial equipment is a new engineering science that has resulted from these operational safety needs. The latter involves locating and identifying failures. As a result of the diagnostic field's current status as a vital instrument for corrective maintenance, businesses with monitoring systems are increasingly automating the maintenance process, [2].

The asynchronous machine is the most durable and least expensive machine available because to its design. The majority of electric drives in a variety of industrial industries employ this equipment, particularly for applications requiring constant or variable speed. The asynchronous machine is not immune to failure, just like any other machine. It may be impacted by mechanical, electrical, or both simultaneously in the stator, rotor, or both. [2, [3]. The source of the flaws might be a straightforward manufacturing issue or incorrect machine usage. Sometimes the usage environment (a corrosive or chemical environment, for example) may be to blame for the machine's degeneration.

Therefore, any anomaly that causes an abrupt stop might cause financial losses. Therefore, it is advised that defects be discovered early in order to be fixed as soon as possible and reduce any adverse consequences. This encouraged the majority of businesses to create very advanced problem detection and diagnostic systems for their manufacturing lines. These two tasks are intended to maximize production gains while also initially enhancing the safety of people and property, [3, 4 and 5].

Goals

For many academics studying electric machines, rotor failure identification has grown to be a difficult subject in recent years. The combination of many stressors, namely dynamic stresses resulting from shaft torque, centrifugal forces, and cyclic stresses, is what causes the bulk of all rotor failures.

The three stages of diagnosis are the identification of an operating mode, the localization of its source, and the detection of that mode.

If the fault is found promptly, the induction motor could be spared from severe damage.

The goal of the current study is to model a multi-winding asynchronous machine and to identify rotor faults (bar breaks) in an asynchronous machine's variable speed drive.

Thesis Exposition

The dissertation is divided into four chapters in order to carry out this study:

The study's setting is described in the first chapter, which deals with the identification of rotor failures in squirrel-cage asynchronous machines. We first outline the numerous problems (causes and consequences) that may affect each of the components of this sort of machine. In a subsequent section, we provide a list of some of the instruments required for the frequency-domain analysis of time signals, which is a preferred method for finding asynchronous machine flaws.

This chapter comes to a close with a review of the various diagnostic procedures now in use, outlining both their advantages and disadvantages.

The time required for maintenance might be reduced, even with early issue discovery. Bar breaking are the most frequent rotor issue, and the most common rotor faults are found at the rotor level. The connection between it and the rotor ring may be at the notch or the end of the rotor ring, [4, 5].

The models of the asynchronous machine for simulating bar breakage are presented in the second chapter. First, we use an analytical technique to illustrate the multi-winding model's evolution.

Through a change of asynchronous machines in case they are healthy and faults with broken, using the Park benchmark In order to explore the impact of the defect on the diagnosis, the research is even applied to the scenario where the machine is powered by an imbalanced voltage. We next go over modeling an inverter with two voltage levels in MAS, explaining its significance and its obvious effects on managing and operating the equipment.

In the third chapter, we show the simulation results for the machine's reduced model in both a healthy and faulty state (with and without an inverter).

The development of various steady-state condition monitoring strategies has been the subject of much study over the previous 15 years, the majority of which are based on the fast Fourier transform (FFT).

This theory differs from others in that it analyzes signals more quickly, making transactions simpler and saving time. Due to its importance in scientific research and the resurgence of industrial maintenance, it was thus briefly examined, [6].

The utilization of the instrumentation, ease of implementation, and wealth of data supplied for the existence or absence of the problem and its severity are the advantages of signal-processing techniques like the fast Fourier transform (FFT), [7, 8] The benefit of this method is that it is now widely accepted as a standard since it is so straightforward and only requires one current sensor per machine, [9].

By performing a spectrum analysis of the stator current signature of the asynchronous squirrel cage motor under various fault situations in the broken bar of the rotor, we concentrate on the monitoring and diagnosis of induction machine problems. Using the Fast Fourier Transform method FFT, the spectrum analysis is applied to three distinct windows of the signal in steady state and under load, including the Hamming window, Hanning window, and rectangular window.

While the Fourier analysis (FFT) did enable us to identify the various frequencies stimulated in a signal, or its spectrum, we were unable to determine when these frequencies were released.

For the analysis of signals whose frequency fluctuates over time (statistically stationary), this loss of locality in the FFT is not a concern, but it becomes one when studying non-stationary signals. Wavelets are used for this.

The proposed work is innovative in that it uses wavelet analysis technologies in both continuous and discrete systems to identify problems affecting an induction motor's spinning portion that is fed by a three-phase inverter.

In the fourth chapter, a simulation model using the finite element approach in Flux 2D® software will be shown in order to assess how the machine behaves both in the absence and presence of defects (broken bars).

The goal of this study is to diagnose asynchronous machines by simulating and identifying their many windings using the finite element approach.

The study proposes an effective analytical method for induction machines (IM) based on finite elements (FE). In comparison to the traditional analytical models, the research based on finite element models (FEM) provides for more information on the processes defining the functioning of electrical machines. This explains the growing interest in research using finite elements in electrical machinery.

Chapter One :

Asynchronous Machines Fault State

I.1.Introduction

Rotating electrical devices are frequently exposed to extreme stresses throughout their lifespan, which can result in a certain number of failures. It goes without saying that these malfunctions may affect the various electronic propulsion systems.

We conduct a study of the different types of flaws that could exist on each of them. Because a decent diagnosis needs a clear grasp of these ideas, we go over various diagnostic techniques already used in the context of spinning machinery or who may be interested in this context. We then go over a number of signal processing tools that can be applied to finding an electrical or mechanical problem. Knowing the signs is a requirement for making a machine diagnostic.

The first chapter concentrates on the synthesis of the defects that are likely to cause tremors in conjunction with each flaw that may have an impact on the machine in question, which is, let's say if we know the vibratory pictures caused by these defects, [10, 11].

I.2.The causes of asynchronous machine failures

The majority of motor defects are brought on by a confluence of stresses operating on the shaft, bearings, rotor, and windings, [11, 12 and 13].

In these case, Figure (I.1) shows the fault tree of the asynchronous machine where the faults are classified according to their location: rotor and stator.

I.2.1Stator

The limitations imposed on the stator may have several causes:

a) Thermal: Over time, the temperature affects the aging of the insulation system, which can lead to a short circuit in the stator's windings, heating that result from an excess, prolonged use, or repeated beginning of the motor.
b) Electrically, an insulation issue could result in a straight short-circuit between phases, between turns, or between turns and the ground. We can also experience the corona effect in the high voltage generator.
c) Mechanical: The coils' vibrations, which can harm the insulation, can be brought on by the electromagnetic force generated by the current running in the stator windings during beginning. When there is contact between the rotor and the stator due to a gear or bearing problem, several things may occur.
d) Environmental factors like moisture content, chemical interactions, a combustible atmosphere, and outside objects.

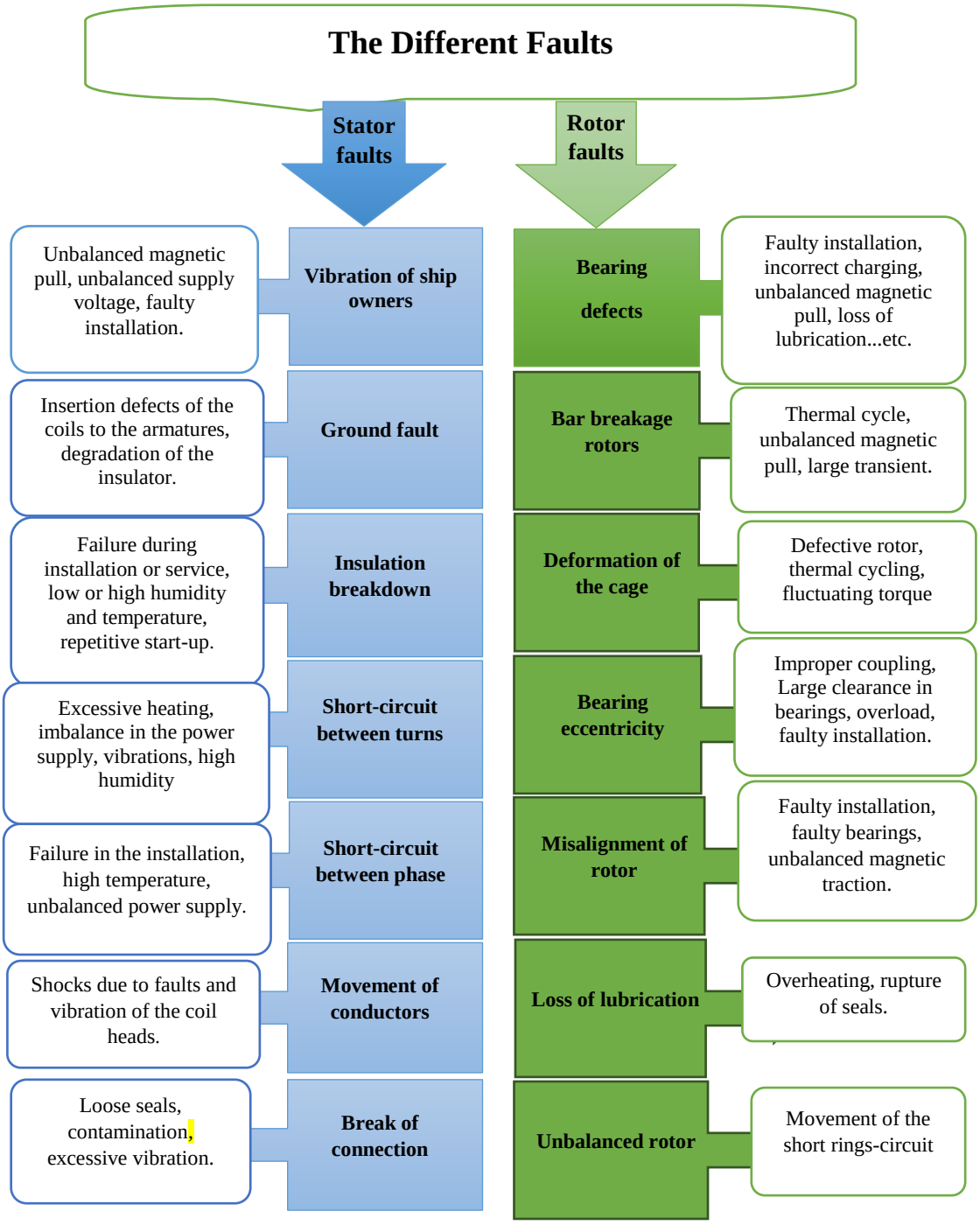

.

Figure I.1: Main faults in the asynchronous machine and their cause's, [14].

I.2.2 Rotor

These pressures for the rotor derive from the following factors and have thermal, electromagnetic, dynamic, mechanical, and external origins:

1. The working force;
2. Dynamic energy that is out of equilibrium;
3. Transient torques and rotational tremors;

4. The notch following flux moving twice at the rotor current frequency produces an electromagnetic force;

6. Thermal pressures brought on by the short-circuit ring's warmth.

7. Thermal pressures brought on by the bars' starting-up temperature differential (skin effect).

I.3. Different types of asynchronous machine faults

1.3.1 Mechanical defects

Mechanical failures are, in general, the most encountered among all the defects in the asynchronous machine. These defects can appear at the level of the ball bearings, the flanges or the motor shaft, [15].

- **Bearing faults**

All sorts of electrical apparatus depend heavily on ball bearings to function properly. A poor material selection throughout the production process might result in bearing flaws.

The electromechanical interaction between the stator and the rotor is made out of ball bearings. Additionally, they stand in for the component that keeps the machine's shaft in place to guarantee appropriate rotor spinning, [16].

A broken, chipped, or cracked winding might lead to rotational issues in the bearings, which can produce disturbances inside the machine.

The majority of induction motor problems and causes of bearing aging are found in the bearings. This kind of failure, as was previously mentioned, occurs most frequently on powerful equipment. It is typically related to bearing wear, and more particularly, to the tread or ball deterioration. Its potential causes include wear brought on by age, high operating temperatures, lubrication loss, and polluted oil (by metallic flakes brought on by the wear and tear on the balls or tread).

• The manufacturing flaw;

• Skew currents (Shaft Current);

The following are the immediate effects of this failure on the bearings: holes in the inner and outer bearing grooves; undulation of their running surface; and marble attack.

•Water-related corrosion, lack of lubrication, and temperature-related issues.

• Surface separation and cracking brought on by overburden.

This kind of flaw affects the system by creating vibrations from the motions of the rotor along the longitudinal axis of the machine, oscillations of the load torque, the emergence of

extra losses, and other issues. A faulty bearing might, in the worst case scenario, cause the engine to stall.

Most often, a bearing's rolling element or one of its raceways degrades by separating, creating a shock with each pass. Vibrations caused by defective bearings have frequencies corresponding to the rotational rates of the rolling components. They are in accordance with the balls, rollers, cage, and the movement of the balls on the rings. The characteristic frequencies provided by the formulae below can be taken into consideration for each kind of bearing and in accordance with its production, [17, 18].

n_b : The number of rolling elements (balls, rollers or needles);

D_b : Diameter of the balls;

D_c : Diameter of the center of the balls;

θ = The contact angle of the ball with the cage;

f_r : The rotational frequency of the inner ring (the outer ring being assumed to be fixed).

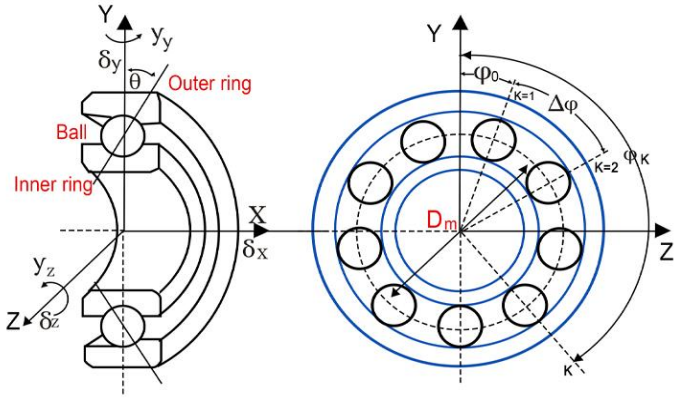

Figure I.2: Geometric characteristics of a bearing

Thus, we have:

• The following equation provides the frequency at which a rolling element will pass through an outer ring defect:

$$F_{ext} = \frac{n_b}{2} f_r \left[1 + \frac{D_b}{D_c} \cos\theta\right] \quad \text{(I-1)}$$

• The following equation describes how often a rolling element will travel over an inner ring flaw that is believed to be positioned on the rotating shaft:

$$F_{int} = \frac{n_b}{2} f_r \left[1 - \frac{D_b}{D_c} \cos\theta\right] \quad \text{(I-2)}$$

•The equation (I-3)gives the passage frequency (Fcage) of a cage defect:

$$F_{cage} = \frac{1}{2} f_r \left[1 - \left(\frac{D_b . \cos\theta}{D_c}\right)\right]$$

So

$$F_{cage} = \frac{F_{bint}}{n_b} \qquad \text{(I-3)}$$

• The following equation can be used to determine the frequency of passing of a ball (or roller) fault on the inner ring or the outer ring:

$$F_b = \frac{D_c}{D_b} f_r \quad 1 \quad \frac{D_b}{D_c} \cos\theta \quad ^2 \qquad \text{(Hz)} \qquad \text{(I-4)}$$

- **Flask defects**

The asynchronous machine's flanges most frequently produce errors throughout the production process. In reality, incorrect flange location leads to misaligned ball bearings, which result in eccentricity at the machine shaft level. A vibration study or harmonic analysis of the currents absorbed by the machinery can find this kind of failure.

- **Shaft faults**

These failures are brought on by fractures in the shaft that result from poor material selection or poor machine assembly. Cracks can result in the shaft's net fracture under the influence of different mechanical, dynamic, thermal, electromagnetic, and environmental loads, which will immediately halt the machine.

- **Misalignment**

The three types of misalignment are parallel, angular, and mixed. The main effect of bearing flaws (Figure I.3), improper machine assembly poor mechanical connection or shaft deformation is the causes of misalignment.

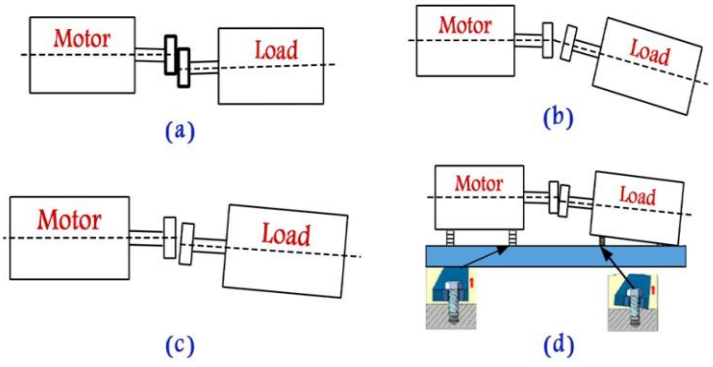

Figure I.3: Incorrect installation of an induction motor

Figure I.3 shows how an induction motor was installed incorrectly. The motor shaft axis is linked to the load in the same plane in (a), and the shaft's center of motion is parallel, but there is a parallel misalignment. The axial motor shaft is linked with the load in the same plane in (b), and the shaft's center of motion is angular. This causes an angular misalignment. The center of motion is parallel and angular in (c), which depicts a combined misalignment caused by the axial motor shaft paired with the load in the same plane. In (d), the installation of the rotor shaft coupled to a load calibrated using a dial gauge is adjusted, [19].

- **Eccentricity**

Natural asymmetries may be found in the rotor's geometry. These basically fall under three categories, which are:

- Static eccentricity: Refers to the situation where the rotor shaft's center of rotation differs from the stator's geometric center.

- The dynamic eccentricity: It relates to a rotor center of rotation that is different from the stator's geometric center, yet the rotor also revolves about the stator's geometric center.

- The two situations mentioned above add together to create the mixed eccentricity.

Figure I.4: Static, dynamic and mixed eccentricity, [20].

By monitoring the side rails of the f_s frequency of alimentation, it is possible to identify enteric eccentricities.

$$F_{exc} = f_s\left[1 \pm k\frac{(1-g)}{p}\right] \qquad \text{(I-5)}$$

k=1, 2.3..., p: number of pole pairs, and *g*: slip

Monitoring the current notch main harmonics and some of their spectrum components is another method for spotting eccentricities. The number of rotor slots N_e must be known in order to use this strategy.

$$F_{enc+exc} = f_s\left[(kN_e \pm n_d)\frac{(1-g)}{p} \pm n_w\right] \quad \text{(Hz)} \quad \text{(I-6)}$$

With: $n_w = 1, 3, 5, 7, \ldots$

N_e stands for "number of rotor slots," p for "number of pole pairs," g for "slip," and n_d is either 0 or 1 depending on whether the eccentricity is static or dynamic.

While a dynamic eccentricity reveals new spectral lines, a static eccentricity alters the amplitude of the principal harmonics of the slots of the stator current.

1.3.2. Failure due to the supply network

Random occurrences occur on networks and in electrical infrastructure, with the following being the most frequent:

- Interphase short circuit;

-Power phase failure and supply voltage imbalance.

The effects of these anomalies on service continuity and equipment performance vary depending on the fault's kind. The latter is brought about by limitations imposed by nature or by aerial networks:

-The climate (rain, lightning, etc…);

- The environment (tree branches, shotgun pellets, etc...);

- As a result of the numerous networks' connections.

Electrical infrastructure can therefore resist a variety of difficult to predict voltage disturbances whose effects are defined by either a transitory voltage drop, or a momentary blackout. This results in the long-term cut in the worst scenarios, [21].

I.3.2.1. Electrical faults

- **Stator faults**

The winding insulation is one of an electric machine's most vulnerable parts, both physically and electrically. Partial stator winding insulation failures are the root cause of stator defects. Such partial stator winding insulation failures may in turn be brought on by one or more of the following factors, including frequent machine overloading, coil vibration, frequent motor starts and stops, transient voltage stress, PWM inverter induced surges, ambient stresses, and aging of the stator winding insulation. This is especially true when there is a significant cable length between a motor and its drive. Heat is produced in

the faulty area of a winding as a result of inter-turn faults, which leads the fault to quickly proceed to more severe forms like phase-to-phase and phase-to-ground faults, [22].

Additionally, there have been instances of short circuits between two phases of a stator as well as between a phase and the machine's metal frame. These flaws are typically mechanical in nature. In fact, extreme vibrations might cause the machine's terminal board bolts to become loose, resulting in a short circuit. A phase opening may be caused by a loose lug at the point where the machine terminals and power supply line converge. The melting of a protection fuse is still the defect that is most frequently seen. A harmonic study of the currents the machine absorbs can find these flaws. The most recurrent faults, located at the stator level, can be defined as follows, [23]:

A. Insulation faults in a winding

Short circuits may result from the deterioration of the insulators in the windings. In fact, the many losses (Joule, iron, mechanics, etc.) cause thermal phenomena that raise the temperature of the engine's numerous parts. However, the temperature, voltage, and mechanical limits of insulating materials exist. As a result, if an insulating material's working environment surpasses one of these limitations, it will begin to degrade sooner or more quickly and eventually stop serving its purpose. The following are some of the potential causes of this sort of fault:

- The insulation degrading during production;
- A winding voltage that exceeds the insulating material's maximum;
- The rumbling of machines;
- High current in the winding as a result of a short circuit, a converter malfunction, or an overload. This causes a spike in temperature, which causes the insulation's substance to prematurely deteriorate;
- The insulation's maturing naturally. Every insulating substance has a finite shelf life;
- The insulation inevitably loses its effectiveness even under "normal" use;
- Working in a hostile atmosphere.

B. Short circuit between turns

A reasonably common issue is a short-circuit between turns of the same phase. One or more insulation problems in the impacted winding are the root of this failure. It alters the power factor, increases the currents in the rotor circuit, increases the stator currents in the affected phase, and somewhat changes the amplitude on the other phases. This causes the temperature to rise at the winding level, which accelerates the insulators' deterioration and

may result in a chain fault (appearance of a second short-circuit). On the other hand, except from an increase in oscillations corresponding to the defect, the machine's average electromagnetic torque delivery stays almost unchanged.

C. Short-circuit between phases

Any point along the winding can experience this kind of failure, but the effects will vary depending on where it happens. Analyzing the effect of this malfunction on the system is challenging because of this attribute.

When short-circuit occurs between phases of the supply, it would cause extremely high currents that would cause the supply conductors to melt and/or trip the safeguards. On the other hand, a short circuit between two phases that is near to neutral creates an imbalance without melting the conductors.

The stator currents are completely out of balance, and the fault that manifests is inversely proportionate to this unbalance. When this defect arises, the currents in the bars and rings are increased. The imbalance of the phase currents may be used to detect this kind of malfunction.

D. Phase-to-frame short circuit

Although the frame typically has a floating potential, it is frequently linked to ground for mechanical connections. With the exception of the capacitive effects, a short circuit between the winding and the frame is unimportant from a material standpoint if the potential is floating. Instead, the frame absorbs the winding's potential at the location of the short circuit.

However, this form of failure can be extremely hazardous to personal safety, necessitating the installation of protection equipment (residual circuit breakers). The voltage of the affected phase remains unchanged in the event of this kind of failure.

The lowering of resistance and inductance, however, causes the current flowing in this phase to grow. The rise in temperature brought on by this increase in current may cause insulation problems in the winding. Additionally, this failure will produce a zero-sequence component that will cause a pulsing torque to emerge. The leakage current might be measured in order to identify this kind of defect.

E. Magnetic circuit faults

The majority of the time, these flaws cause the machine to operate asymmetrically, which can exacerbate the issue through overheating, overvoltage, considerable increases in current, etc….

The various possible short-circuit faults can be clarified by the Figure (I-5), [24, 25].

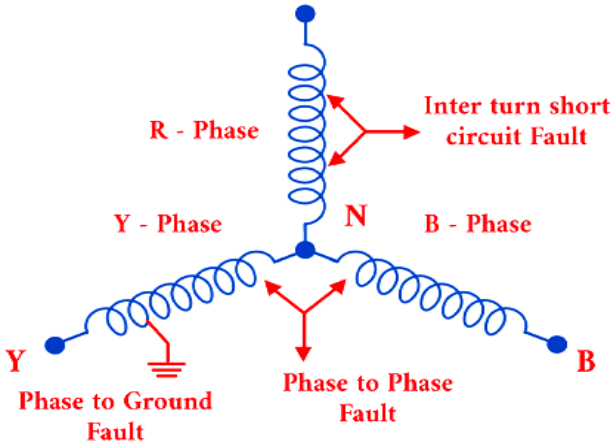

Figure I.5: Representation of the various possible stator faults

- **Rotor faults**

One of the most frequent rotor problems is the breaking or breakage of the bars. Either its notch or the end that links it to the rotor ring might house it. The degradation of the bars lowers the electromagnetic torque's average value and raises its average amplitude, which in turn causes oscillations in rotational speed and, as a result, mechanical vibrations and irregular machine functioning. The machine's degeneration is sped up by the huge amplitude of these oscillations. As a result, the torque declines substantially as the number of broken bars increases, leading to a cumulative failure. With more broken bars, the impact of each one rises quickly. When a result, the torque drops substantially when more bars are broken, leading toa chain reaction of failure, [26].

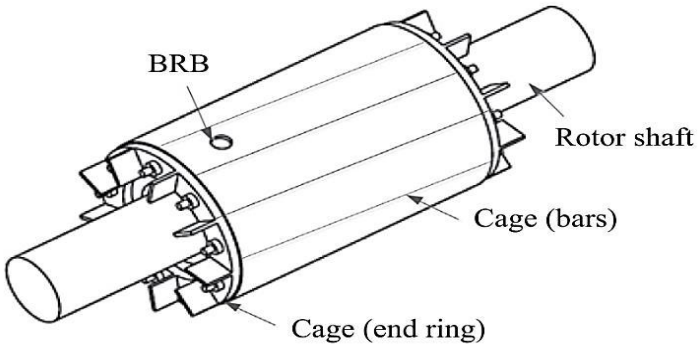

Figure I.6: The solid model of the BRB in an induction motor

I.4. Methods of diagnosis

The diagnosis is the process of determining the most likely reason for the failure(s) based on a collection of data from an inspection, check, or test. Is a series of steps designed to find the most failure cause.

When electrical machinery malfunction, it's common for the entire industrial process to be stopped. If an early warning system against potential problems were available, such unexpected equipment shutdowns would save time and money. A system like this may help enhance process safety, which is important in many industrial settings.

The two primary diagnostic duties are the identification and localization of problems to deliver early alerts of developing errors, allowing remedial action to be conducted without negatively impacting process continuity. Electrical machine fault diagnostics can result in improved plant availability, longer plant life, higher-quality products, and more efficient plant operations, [27].

While localization seeks to pinpoint the specific kind of defect, detection consists on indicating the issue's presence. Therefore, the goal of diagnostic is to find a flaw early on before it causes the industrial installation to fail completely.

The identification of symptoms frequently makes reference to one's understanding of healthy conduct. The shape this knowledge takes determines how and in what form the symptoms are produced. For instance, if new spectral lines in an electrical amount reveal the defective operation, a signal processing analysis will enable the symptoms to be obtained. The method used to treat symptoms varies on both the type of symptom and the manner the information is applied in.

With the resurgence of interest in the diagnosis, a number of strategies are emerging, but they may all be categorized along two axes: [28].

- The application of mathematical techniques that allow for the modeling of the systems, their
- Failure causes and symptoms to aid inductive and deductive procedures, which fall under the category of internal diagnostic techniques;
- The application of techniques that can simulate human reasoning in computer form. The latter fall under the category of external diagnostic techniques and are based on the discipline of artificial intelligence.

Simply said, the taxonomy of diagnostic techniques permits categorization into two significant families:

Diagnostic techniques may be divided into two primary groups, [15, 28 and 29]:

- Internal and outside techniques;
- Deductive and inductive reasoning.

I.4.1 Diagnosis by internal methods

This approach is based either on the estimate of intangible signals or on the operational parameter monitoring. They presumptively have a complete understanding of the procedure represented by a numerical model. Modeling in the comparable three-phase or two-phase reference frame is required in the case of the asynchronous machine, [21, 29].

This model could change based on the goals. It may be more or less aggregated, illustrative of a model of proper functioning, or indicative of one or more faults in operation.
A model is often a formal (mathematical) description of the system under observation. Different versions of the may be described mathematically using differential equations or difference equations, and they can be continuous or discrete time.

Mechanical and electrical model parameters are documented and utilized as a "signature" of the flaws. Quantities characterized by the state of the process, known as residuals, are used to check the agreement between measurements and model calculations.

These internal diagnostic techniques compare real measurements taken from the system to be monitored with the data given by the model. The system's functioning is characterized by deviations: a deviation of zero indicates that everything is operating as it should; a divergence of more than zero indicates that something is wrong.

In addition, these procedures may be divided into two categories: parametric estimation techniques, which try to estimate the model's parameters, and analytical redundancy methods, which employ state estimation techniques.
Depending on the model being used, internal diagnostic techniques vary:

- **Diagnosis by analytical redundancy (parity space)**

The word "parity" was taken from the lexicon of logic systems, where error detection is made possible by the creation of parity bits from an analytical redundancy relationship.
An equation with known variables is known as an analytical redundancy relationship (ARR). It must be insensitive to disruptions and sensitive to defects. By projecting the measured data into a space and using the relationships created, residuals may be produced. It is sometimes described as the orthogonal of the observe ability matrix, which essentially means that the state's impact on the residue is eliminated. This technique's explanation will focus on how to utilize it to find and locate faults. The idea is to develop parity relationships that are independent of unknown parameters but nevertheless sensitive to faults in order to assess the consistency of the measurements and find errors. The state and

measurement equations are rewritten using this method, allowing only known variables (commands and outputs) to appear.

It is important to model the system realistically enough (actuators, control devices, alarms, etc…) to be able to account for all failures at all levels since the quality of a choice depends on the quality of the model. The majority of techniques rely on linear representations of discrete-time equations of state; alternatively, linearization is performed in the vicinity of the operational points. We may think of the system parameters as being independent of time (constant) around the operational point since we presume that they slowly vary over time.

Through the use of the constant matrices *A*, *B*, and *C*, the state, [15, 30]. *A*, *B*, *C* are real and constant matrices of dimensions n .n, n .p and q .n

With: n, p, q whole numbers. Space model connects the state vector x(k) to the input vector u(k) and the output vector y(k), [15].

$$x(k+1) = Ax(k) + Bu(k) \tag{I-7}$$

$$y(k) = Cx(k) \tag{I-8}$$

By taking into account the additive failures $f_p(k)$, and the noises and disturbances $w_p(k)$ in the model becomes:

$$x(k+1) = Ax(k) + Bu(k) + f_p(k) + Qw_p(k) \tag{1-7}$$

The model becomes by factoring in the additive failures $f_U(k)$, as well as the sounds and disturbances $f_Y(k)$:

$$\acute{U}(k) = U(k) + Bu(k) + f_U(k) + w_U(k) \tag{I-9}$$

$$\acute{Y}(k) = Y(k) + B_Y(k) + f_Y(k) + w_Y(k) \tag{I-10}$$

As the new actuator command, $\acute{U}(k)$, is now used, and $\acute{Y}(k)$ is used to measure the output $Y(k)$.

When comparing the parameter matrices to those of the actual system, we obtain:

$$A^* = A + \Delta A(k) \tag{I-11}$$

$$B^* = B + \Delta B(k) \tag{I-12}$$

$$C^* = C + \Delta C(k) \tag{I-13}$$

Through these relationships, the mathematical representation of the system is changed to account for the numerous additive defects.

- **Diagnosis using observers**

The fundamental idea behind this approach is to treat the outputs' estimate mistakes as residuals. Building structured residues, or determining where flaws are, is the goal.

To assure the location of defects, it may occasionally be required to deploy several observers To assure the location of defects, [31].

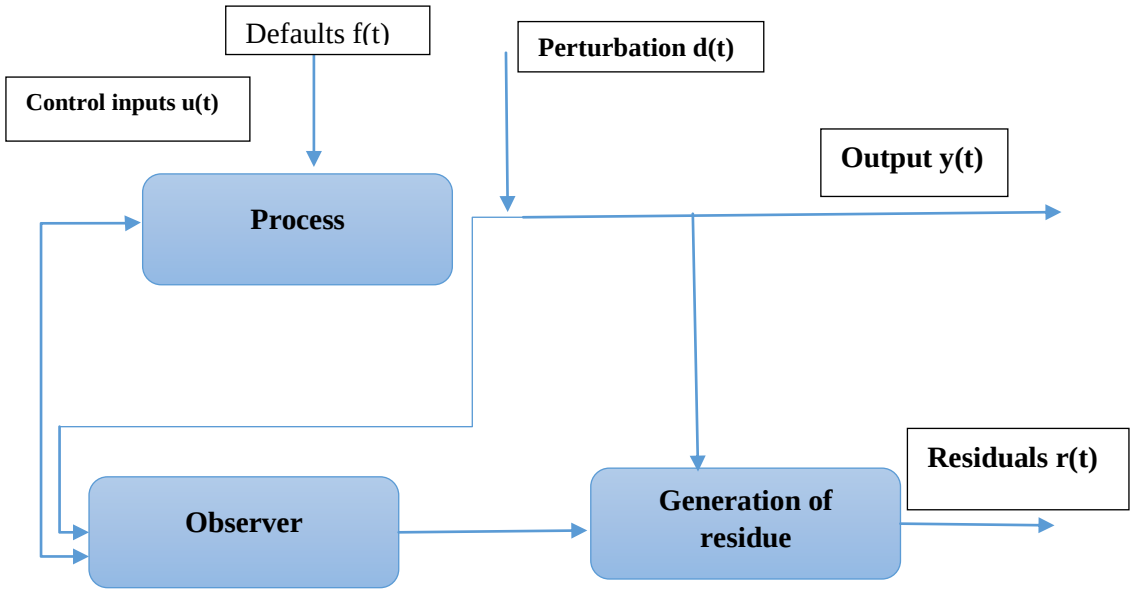

Figure I.7: Diagnostic methods by observers, [33].

- **Parametric estimation**

The parametric estimating technique takes into account the fact that flaws have an impact on the parameters that control the system's dynamic behavior. The fundamental idea behind this approach is to continually estimate process parameters using input/output data and assess how far they deviate from the reference values of the process's steady state. By parameter, we mean one or more aggregates of physical properties, such as the system's mass, viscosity coefficient, etc. The benefit of parametric estimate is that it can reveal the significance of variances.

In order to identify and pinpoint faults, this diagnostic technique first extracts the system parameters from the knowledge rules of a knowledge model.

Determine the numerical values of the structural parameters of a knowledge model that controls the dynamic behavior of the system in order to discover and locate faults using parametric estimate, [31, 32].

To characterize the system in both healthy and impaired functioning, the first step is to create a mathematical model of appropriate complexity. In fact, the model used will depend on the kind of defect we're trying to find.

To identify and find the stator or rotor flaws, it is necessary to distinguish at the level of the estimated physical characteristics. Parametric estimate diagnostics frequently employ Park's model. The apparent rotor resistance rises as a result of bar breakage, [16, 34].

However, the method's primary disadvantage is the requirement for a physically stimulated system that is always present. Thus, in the event of risky, pricey, or immovable procedures, practical issues arise. Additionally, unitarily invertible correlations between mathematical and physical quantities are not always present, which makes residual-based diagnosis more challenging.

I.4.2 Diagnosis by external methods

The premise behind external diagnostic techniques is that no model is available to explain cause and effect connections. The sole source of information is human skill acquired through learning. The recognizer looks for cause and effect links using observers from the system, including inputs and outputs. The categorization algorithm is what makes these diagnostic approaches work.

I.4.3 Diagnosis by inductive methods

In general, there are two types of classification techniques: supervised learning methods and self-learning techniques. The classes linked to the training data must be known beforehand by methods that use supervised learning.

Supervised learning methods involve training a model on a labeled dataset, where each instance is already classified into one of several categories. The model then uses this training data to learn patterns and relationships between the input features and the output labels, allowing it to classify new instances that it has not seen before.

Self-learning techniques, on the other hand, do not require labeled data. Instead, they use unsupervised learning algorithms to cluster similar instances together based on their features. The model then assigns labels to these clusters based on the majority class of the

instances within them. Over time, as more data is collected and labeled, the model can refine its clustering and labeling algorithms to improve accuracy.

Both supervised learning and self-learning techniques have their advantages and disadvantages depending on the specific application and available data. Supervised learning is generally more accurate but requires labeled data, while self-learning can be used with unlabeled data but may be less accurate initially.

The traits of the classes are always determined by analyzing a vector that summarizes the data (individual) and corresponds to the system samples.
The learning phase distinguishes the two types of approaches.
The approaches found in "Machine Learning" in the context of methods based on data mining allow for the creation of simpler categorization rules or expressions, resulting in results that are straightforward to understand.

One of the goals of these techniques is to minimize human involvement in the learning process while still making the lessons that are produced simple to understand.
These diagnostic techniques fit into a bottom-up or forward-looking strategy. It is a matter of identifying the flaw based on how it affects the system. To understand the symptoms and their combinations in order to identify the fault, these systems employ a forward reasoning mechanism.

I.4.4 Diagnosis by deductive methods

The primary characteristic of these approaches is backward thinking. The impacts in the systems must be discovered using deductive techniques. It is feasible to establish or disprove the existence of the fault by comparing the "effects found in relation to the possible effects". A diagnosis may be made using either one kind of reasoning (forward or backward) or both forward and backward reasoning. Reasoning is referred to be mixed or forward-backward reasoning in the latter scenario. Knowing the "defect" cause "a priori" entails being aware of certain effects, [16, 29].

The motor current signature analysis (MCSA) is one of the most widely utilized fault detection techniques. This method relies on pinpointing specific harmonic components via spectrum analysis in the line current generated by abnormal rotating flux components brought on by flaws such broken rotor bars, air-gap eccentricity, and shorted stator winding turns, among others. It should be noted that this approach only needs one current transducer, which can be in any one of the three phases. The motor current signature

analysis approach can identify these issues early on, helping to prevent subsequent damage and total motor failure, [36, 37]. This technique is an effective tool for finding mechanical and electrical defects. It differs from previous methods in that it simply needs a current sensor (effect probe), rather than introducing a sensor at the machine level or using pricey, bulky equipment. A device (such as a current transformer or hall) that displays the stator phase current. The FFT (Fast Fourier Transform) is one of the most popular and well-established methods of signal analysis that has been offered for the diagnosis of problems, [38].

Unfortunately, FFT-based approaches cannot extract the information included in non-stationary signals and are not suited for signal analysis, [39]. Non-stationary parts typically have a wealth of information concerning mechanical issues.

The wavelet transform (WT), a different method for dealing with such non-stationary signals, has the advantage of being able to capture how the parameters of the signals, their frequencies and instantaneous amplitudes change with time. To put it another way, the WT makes it possible to describe the signal in the time-scale domain, which eliminates the Fourier transformation's issue of losing temporal information. It is becoming clear that the booming wavelet approach is an effective instrument for signal processing, [40, 41 and 42].

I.4.4.1 Fast Fourier transform (FFT)

A key component of both mathematics and physics is Fourier analysis. The first reason is that the idea of frequency, on which it is founded, is universal. The second reason concerns Fourier analysis' inherent structure, which lends itself well to basic transformations like linear filtering by translating them in a particularly straightforward manner, [43]. A true image of the imbalances that occur in the machine can be obtained through signal processing analysis of the line values (current, voltage, and power), [44].

A popular method for locating faults in asynchronous devices is the Fast Fourier Transform (FFT). It performs well in applications that need for a lot of power or constant torque. The bearing fault component's FFT analysis will show all of the fault's characteristics, including frequency and magnitude responses, [45].

Over the years, numerous investigations using the fast Fourier transform (FFT), [47, 48]. The spectrum of stator currents can be employed in FFT-based motor current signature analysis (MCSA) to identify BRBs and stator winding defects in motors, [49]. By

contrasting the effectiveness of various diagnostic techniques to identify and quantify BRBs in induction machines, the superiority of diagnostic techniques based on FFT analysis of sideband current components is shown, [50].

A set of precise signal spectrum values can be broken down using the FFT method from one domain to another. Each step of the process consists of a signal spectrum that may be analyzed using a little amount of data to ascertain the variation in the dataset [46, 51].

Any periodic function can be represented as the sum of a series of sins and cosines whose amplitudes are changed by multiplying them by coefficients on the one hand, and whose phases are changed by shifting them so that they add up or balance each other on the other, [52, 53].

$$\mathrm{X(f)} = \int_{-\infty}^{+\infty} x(t).e^{-j2\pi.f.t}dt \qquad \text{(I-14)}$$

$$x(t) = \int_{-\infty}^{+\infty} \mathrm{X(f)}.e^{j2\pi.f.t}dt \qquad \text{(I-15)}$$

But Fourier analysis immediately reveals its limitations because of the nature of the method: Its calculation necessitates understanding the entire temporal history of the signal (equations (I-14), Fourier transformation, and (I-15), inverse Fourier transformation). In addition, while time information is present in a Fourier transform (making the inverse transform possible), it is buried in the phases and is therefore nearly impossible to extract. The choice of a weighted window for the analysis (Blackmann window, Hanning, Hamming, etc…), as well as the window size that will affect the resolution, is necessitated by the study of a signal across a known interval. The greatest resolution that can be used will also depend on the size of the window. In fact, N: Δf=fs/N. states that the frequency accuracy depends on the sampling frequency and the number N of samples. This fluctuation can be used by the FFT method to find induction motor defects. As a result, the method will be quicker than DWT in signal analysis, [54].

The formula below can be used to examine the FFT data, [55].

$$f_b = (1 \pm 2sk)fs. \quad HZ \qquad \text{(I-16)}$$

Where:

f_b :is the sideband frequency associated to the BRB;

s: is the per-unit motor slip;

fs: is the frequency of the power grid in which the motor is connected and k is the number of the broken bar.

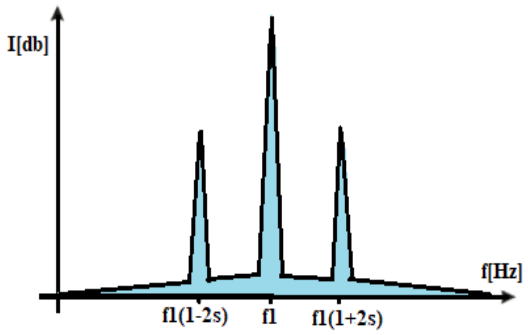

Figure I.8: Idealised current spectrum

One of the most well-known methods for rotor problem diagnostics in induction motors is based on processing stator currents to find recognizable spectrum lines. Due to the rotor asymmetry, an induction motor operating with defective rotor bars generates a negative sequence of stator current. At a frequency *(1± 2s)fs* near the fundamental frequency, this main component grows.

By observing the current spectral components, it is possible to identify the two frequencies *(1-2s)fs* and *(1+2s)fs* that enable broken rotor bars. Using the stator currents Isa phase 'a', observe how the machine behaves in both healthy and malfunctioning states (broken one bar, broken two bars, broken three bars, broken four bars). Analysis of the current's frequency spectrum at about 50 Hz.dsqw

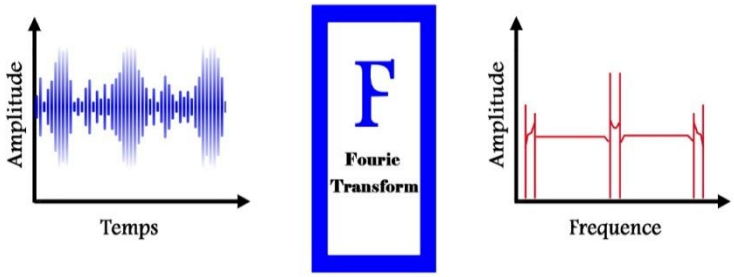

Figure I.9:Fast Fourier transform (FFT) principal

I.4.4.2 Wavelet transform (WT)

The position and amplitude of fault-related features might be affected by external influences, making frequency domain analysis unreliable for fault identification. The fault frequency components of this parameter depend on the motor's slip, its amplitude depends on load, its frequencies are affected by voltage fluctuations, and its fourth classification requires a long sampling interval for a high-resolution frequency. As a result, frequency domain studies are often appropriate for steady-state conditions.

The time-frequency analysis of the signal, which depicts the signal in three dimensions as time, frequency, and amplitude, can avoid the issue associated with the analysis of non-stationary signals. Wavelet transform is the most often used time-frequency representation. A signal is expressed using the wavelet transform as a series of oscillatory functions at various frequencies and times. The original signal is divided into time-scale space via the wavelet transform, where the dimensions of the windows at time and scale (frequency) are flexible, [58]. In order to extract the dominating characteristics from the original signals in the fault diagnostics domain, wavelet transform has been utilized, [59].

Because wavelets have a finite time length and frequency bandwidth, they are localized in both the time and frequency domains. Because of the localization feature of wavelets, the wavelet transform may represent a signal with a small number of coefficients, [62].

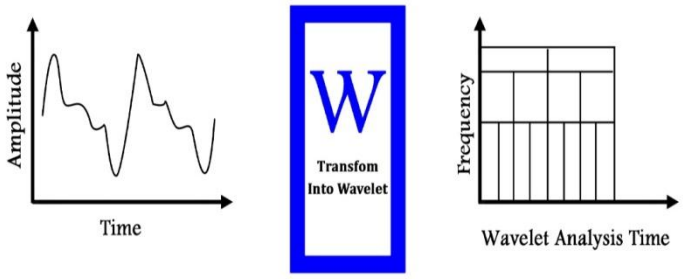

Figure I.10: Wavelet transform (WT)

I.4.4.2.1 Continuous wavelet transforms description (CWT)

In this transformation, the spectral development of the signal frequencies is first ascertained and then contrasted with the spectra of other signals. The CWT is a subtype of the WT that is employed particularly when it is difficult to detect overlap between the neighboring signal and the frequency supply signal. How the scale parameter is discretized distinguishes the CWT from the DWT. Scale is discretized more precisely by the CWT than by the DWT. The no orthogonal collection of wavelets used in CWT results in highly correlated data with significant levels of redundancy, [63, 64].

Two parameters; "a" for the scale parameters and "b" for the translation parameters make up the continuous wavelet transform. It is comparable to the Fourier transform with sliding window, with the exception that the analysis's sliding window is changeable over time.

The mother wavelet $\psi \in L^2(R)$, which is a fixed function, is translated and enlarged by the wavelet transform. The translation and dilation parameters change continually in the case of the continuous transform, [65].

In other words, the following functions were employed by the transform:

$$\psi_{a,b}(x) = \frac{1}{\sqrt{a}}\Psi\left(\frac{x-b}{a}\right) \tag{I-17}$$

The distance is used to dilate (compress or lengthen) the function ψ, and b is used to translate (move it along the time axis) it using $a,b \in R, a \neq 0$, or a scaling factor x.

When we use these wavelets to analyze a signal f(x), we turn it into a function of two variables, the time and the scale of analysis, which we may denote by $W(a,b)$:

$$W(a,b) = \left\langle f, \Psi_{a,b} \right\rangle \tag{I-18}$$

Which can also be noted:

$$W(a,b) = \frac{1}{\sqrt{|a|}}\int f(x)\Psi_{a,b}(x)dx \tag{I-19}$$

The factor $\frac{1}{\sqrt{|a|}}$ normalizes $\Psi_{a,b}$ in order to preserve the energy of the analyzing motif:

$$\left\|\Psi_{a,b}\right\|_2^2 = \int\left|\Psi_{a,b}(x)\right|^2 dx = 1 \tag{I-20}$$

Since the wavelet is continually translated, this transformation is theoretically eternally redundant. However, there are ways to limit this redundancy, and one of these ways involves using the discrete wavelet transform, [66]. A sizable family of wavelets includes the following:

Name of wavelet families	**Short name in Matlab**
Haar wavelet	Haar
Daubechies wavelet	DB
Biorthogonal wavelets	Bior
Meyer wavelet	Meyr
Discrete approximation of the Meyer wavelet	Dmey
Battle and Lemarié wavelets	Btlm
Gaussian wavelets	Gauss
Mexican hat wavelet	Mexh
Morlet wavelet.	Morl
Shannon complex wavelet.	Shan

Table 1.1: Wavelet Families

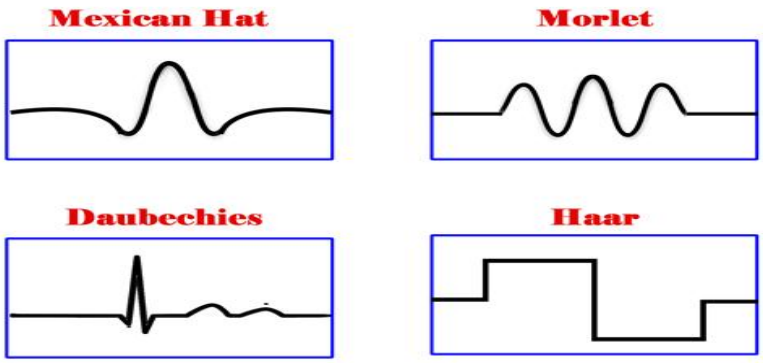

Figure I.11: Some forms of usual wavelets

I.4.4.2.2 Discrete wavelet transforms description (DWT)

In situations where time-frequency domain signal analysis is required, discrete wavelet transform is widely used. This is the most effective method for obtaining transient-based nature signals. The discrete wave transform is used to generate an approximation for low frequency feature points and detail coefficients for high frequency feature points, [67, 68]. The DWT uses a scaling factor and a discretized translation, whereas the continuous wavelet transform results in the discrete version. A dyadic discrete wavelet transform is any basis of wavelets that acts with a scale factor of a = 2. Evidently, the discrete wavelet transform may be successfully applied to any digital system (PC, DSP, CARTE a P...). Although the continuous nature of the scale factor and the dilation need extra processing, the continuous wavelet transform CWTmay also be utilized on digital systems, [69].

For scaling functions , we provide the following foundation: for any $i \in z$:

$$\varphi_{i,j}(t) = 2^{\frac{-i}{2}} \varphi(2^{-i}t - j) \tag{I-21}$$

And similarly the wavelet basis:

$$\psi_{i,j}(t) = 2^{\frac{-i}{2}} \psi(2^{-i}t - j) \tag{I-22}$$

The dyadic scaling factor leads to:

$$\phi(t) = \sum_j 2h(j)\varphi(2t - j) \tag{I-23}$$

$$\psi(t) = \sum_j 2g(j)\varphi(2t - j) \tag{I-24}$$

The breakdown of the ladder function and the wavelet into linear combinations of the ladder function at high resolution is directly represented in equations (1.23) and (1.24).

Another way to think about the wavelet transform is as a method of breaking down the signal into approximations and details.

The original signal f(t) goes through two complimentary high pass and low pass filters and emerges as two signals, correspondingly the approximations signal A and the details signal D. As illustrated in Figure (I.12), [70].

• The signal's large-scale, low-frequency portion is the approximation.

• The details signal is the high-frequency, small-scale portion of the signal.

As we previously mentioned, we must choose two signals that are the same size as the original signal in order to conduct this operation on a real signal. The result of the two signals, each with 1000 samples, results in a total of 2000 samples, assuming for the time being that the initial signal had 1000 samples.

To offer two vectors, correspondingly abbreviated as CA (Approximation wavelet coefficients) and CD (Detail wavelet coefficients). Both are around half the original size of the vector. The decimation by two (down sampling) method is what led to this, [71].

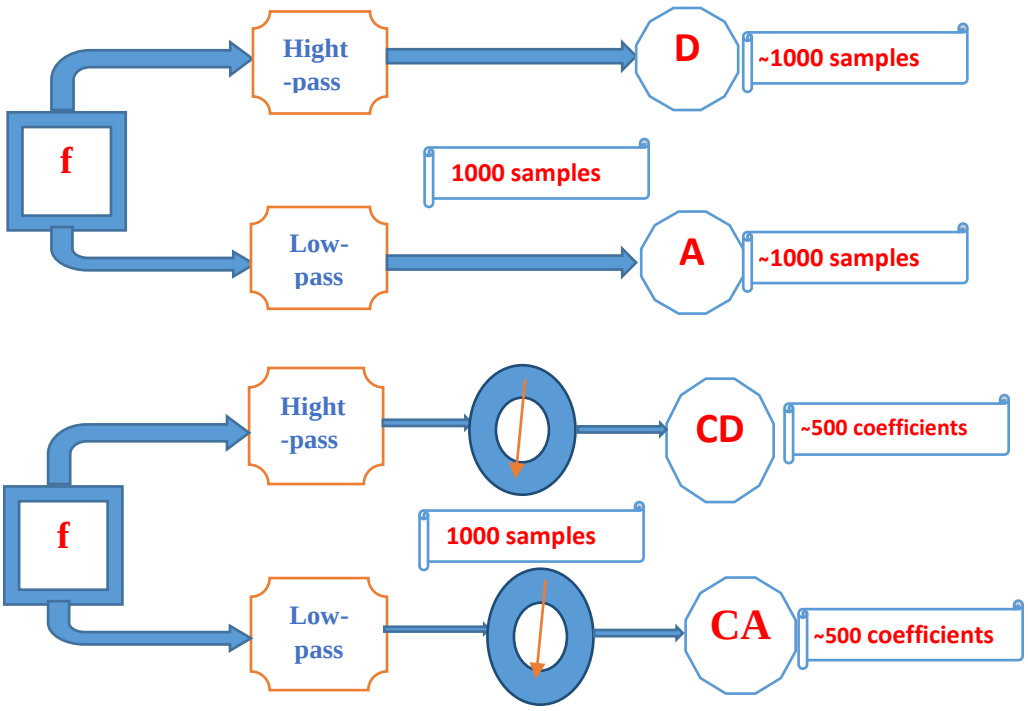

Figure I.12: Simple decomposition of signal f into approximations and details

Iterative decomposition, which alternately decomposes consecutive approximations, can divide a signal into many high resolution components. This is the wavelet decomposition tree. Since parsing is an iterative process, it is possible that it will never end. Actually, just one sample or pixel at a time may be used to decompose the specific information. The correct number of levels will really be chosen based on the characteristics of the signal to

be decomposed or another suitable criterion, [71, 72]. Using Mallat's approach, the signal may be separated into several levels, as seen in Figure 1.13.

The discrete temporal signal f(n) may be broken down into its approximate and precise forms using multi-resolution analysis. The initial decomposition coefficients, A_j and D_j, describe the original signal f(n) in approximate and detailed ways, respectively. It is possible to separate a signal into its individual frequency bands using wavelet decomposition. After dividing by the number of times, we will get frequency bands with the same bandwidth.

$$\left[\frac{(i-1)f_n}{2}, \frac{if_n}{2}\right], i = 1,2,.....,2^l \qquad \text{(I-25)}$$

The various stages of breakdown can be represented with their respective frequency bands using relation (I.25) is illustrated in Figure I.13, [73].

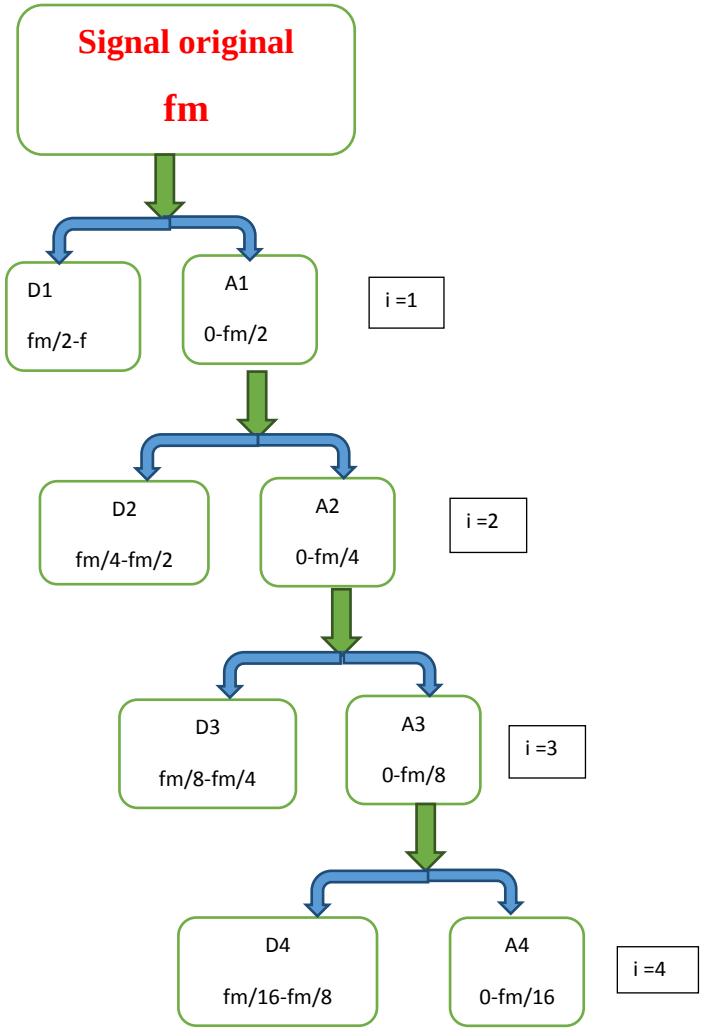

Figure I.13: Tree of decomposition of a signal into four levels

The total of the approximation and detail signals may be used to estimate the original signal at any level, per the decomposition tree (Figure I.13).

The original signal is recreated for a breakdown into four levels as follows:

$$\begin{cases} i=1,\ f(n)=A_1(n)+D_1(n) \\ i=2,\ f(n)=A_2(n)+D_2(n)+D_1(n) \\ i=3,\ f(n)=A_3(n)+D_3(n)+D_2(n) \\ i=4,\ f(n)=A_4(n)+D_4(n)+D_3(n) \\ i=k,\ f(n)=A_k(n)+D_k(n)+D_{k-1}(n) \\ i=1,\ f(n)= \end{cases} \quad \text{(I.26)}$$

Such that in frequency band i, f_n is the Nyquist frequency.

A extension of the discrete wavelet decomposition that provides a wider variety of options for signal analysis is the wavelet packet approach. A signal is divided into approximation and detail in wavelet analysis.

Following that, the approximation is divided into second-level approximation and detail, and the procedure is repeated. There are (n+1) potential methods to deconstruct or encode the signal for an n-level decomposition.

Wavelet packet analysis allows for the decomposition of both specifics and approximations. More than 22-1 distinct signal decompositions are produced as a result.

$$\begin{cases} i=1,\ f(n)=A_1(n)+D_1(n) \\ i=2,\ f(n)=AA_1(n)+DA_2(n)+AD_2(n)+DD_2(n) \\ i=3,\ f(n)=AAA_3(n)+DAA_3(n)+ADA_3(n)+DDA_3(n)+AAD_3(n) \\ +DAD_3(n)+ADD_3(n)+DDD_3(n) \end{cases} \quad \text{(I-27)}$$

The original signal in the wavelet packet decomposition is calculated by adding the approximation and detail signals at each level, much like in the wavelet decomposition. Whose basic principle is given by the Figure I.14.

The original signal, whether it is stationary or not, is divided into several frequency bands by the wavelet packet.

The separated frequency bands include no duplicate data. It may be suggested as a defect diagnostic technique and is an effective analytical strategy based on multi-resolution, [75].

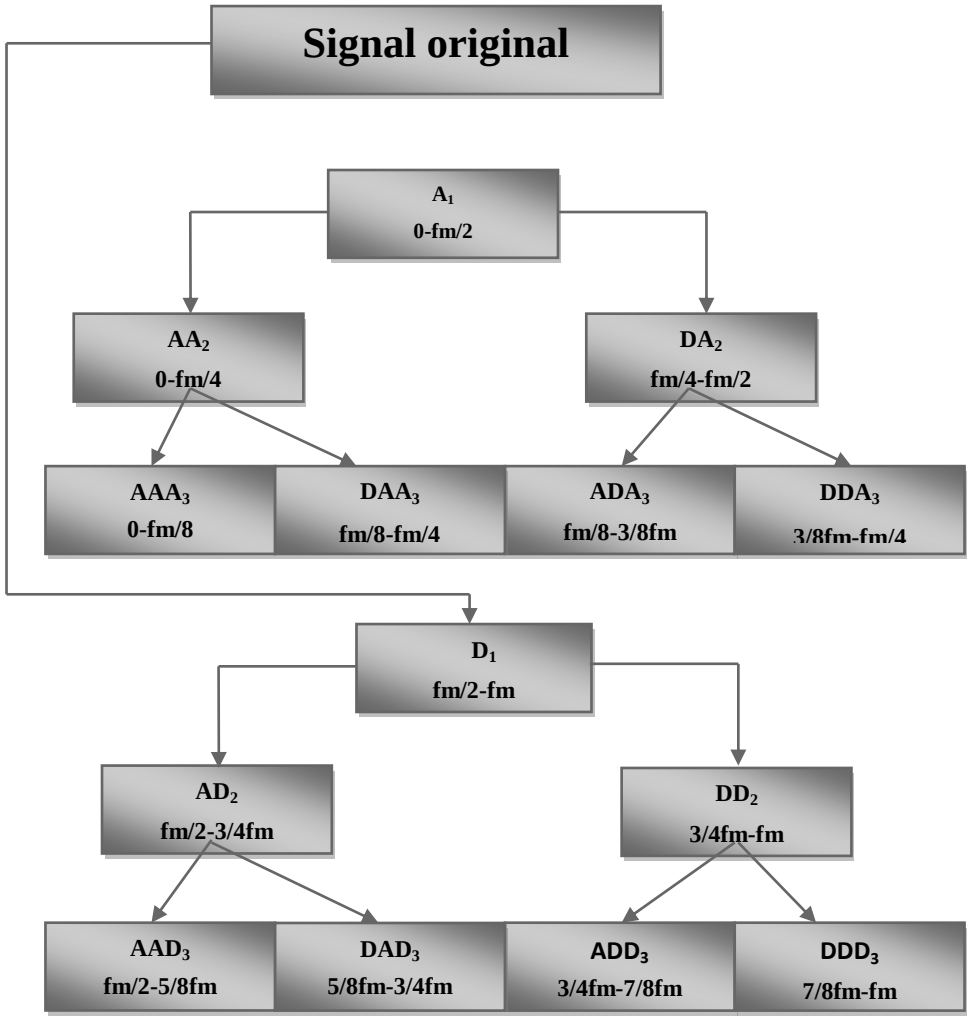

Figure I.14: 3rd order wavelet packet decomposition

After differentiation, the extraction of the fundamental of the stator current, or any other pre-processing, the diagnosis of the defect is based on observation and comparison between the layers of decomposition that carry the knowledge of the issue for different machines to be diagnosed.

When the fault of the rotor bars, a section of the short-circuit ring, or a short-circuit at the level of the stator windings of the asynchronous machine manifests, the wavelet or wavelet packet decomposition results in the inclusion of the fault information of the stator current signal in each frequency band.

By calculating the energy associated with at each level or node of the decomposition process, a very effective diagnostic tool may be built, [76, 77]. Each frequency band's energy eigenvalue is described.

$$E_j = \sum_{k=1}^{k=n} D_{j,k}^2(n) \quad \text{(I-28)}$$

such that degree of decomposition j is met.

The plot of these values may be used to detect defects in the squirrel-cage asynchronous machine and to determine the degree of default. The eigenvalues of energies of the levels of the decompositions contain the information of the signals in an asynchronous motor. The degree of the fault is indicated by the divergence of a particular eigenvalue.

I.5 Conclusion

We reviewed the structure of the asynchronous machine at the beginning of this chapter before classifying the problems that are most likely to damage the various components of electrical machines (eccentricity, short circuit, breaking of the bars, etc.). The reasons of mechanical and electrical failures of these equipment were then listed in a non-exhaustive manner.

The three critical processes of detection, localisation, and identification make up all diagnostic techniques discussed in the literature. The diagnostic method used for system monitoring relies on the way the system is presented (with or without a model) and the kind of defects (sensor, actuator, or system failure) that are present.

We concentrated on techniques based on identifying particular machine parameters, such as diagnostic techniques (FFT and WT), and we observed that the detection of a fault, whether mechanical or electrical, is based on the spectral content of signals and frequently from the current absorbed by the asynchronous machine.

In general, when a problem manifests, the machine's topology is altered, implying the emergence of certain fingerprints on specific physical quantities or specific parameters that are reflective of its structure. The implementation of the detection and localization algorithms that are the focus of this thesis work revolve around the extraction, exploitation, and analysis of these changes.

Knowing the components that make up the asynchronous cage machine allows one to locate a simulation-specific model that provides a rough idea of the machine's condition during various operating regimes (healthy or defective), and which will be the focus of the second chapter.

Therefore, picking an identification model is an important first step since it will have a big impact on how well the associated identification algorithm performs in terms of stability and precision.

Chapter Two :

Asynchronous Machine Multi-Winding Model

II.1.Introduction

Research in the diagnosis of the asynchronous machine on primarily mechanical faults (vibrations generated by a defect in the bearings) or electrical faults (short-circuit at the level of the stator of the machine and broken bar) requires modeling in the presence of faults. They enable the comprehension of flawed operation and the validation of algorithms for fault identification. Additionally, they enable us to create databases on how these defects manifest themselves electrically and magnetically. So, the main reason for creating a model in the context of diagnostics is the capacity to simulate mistakes. It is evident that this modeling stage is a necessary step in understanding how the machine behaves in all operational scenarios. The generalized machine and its accompanying equations of state are used as the foundation for this modeling of the asynchronous machine.

To describe the diagnosis, a model built using the circuits' electrical and mechanical equations typically work well. Short simulation times are a result of the algebraic formulation's simplicity.

The modeling's accuracy is also respectable the traditional approaches to investigating this kind of machine rely on straightforward models in the frame (d, q).However they ignore a few occurrences [78].

The physical models are based on the electromagnetic principles to explain how the machine works. Depending on the modeling technique employed, these models can have varying degrees of complexity and/or precision. Therefore, Behavioral models as for them, they alter the physics-derived models by adding new parameters that permit the detection and, in certain circumstances, the localization of the detected fault. Direct use of these behavioral models in diagnostic processes is possible [79].

Numerous studies [81, 80] on the modeling and simulation of asynchronous machines have been conducted in recent years in an effort to find the model that most closely approximates the behavior of the real machine as well as one that can simulate both the state of proper operation (the healthy case) and the state of malfunction (the case with a defect).

These models are regularly transformed and have their reference axes changed, which results in theoretical interpretations that cannot be utilized to study localized effects like the breakage of the machine's rotor bars by separating them from the impacts of other incidences. These models, however, lack precision and can only accurately depict a

machine's sound functioning [12]. Due to this, more complex models (such as the multi-winding model in closed loop) had to be used to create a description that was appropriate for the faults. For an asynchronous cage machine, the modeling techniques discussed in this chapter's objective are to enable the description of a bar break.

II.2.Multi-winding model of the asynchronous machine in closed loop

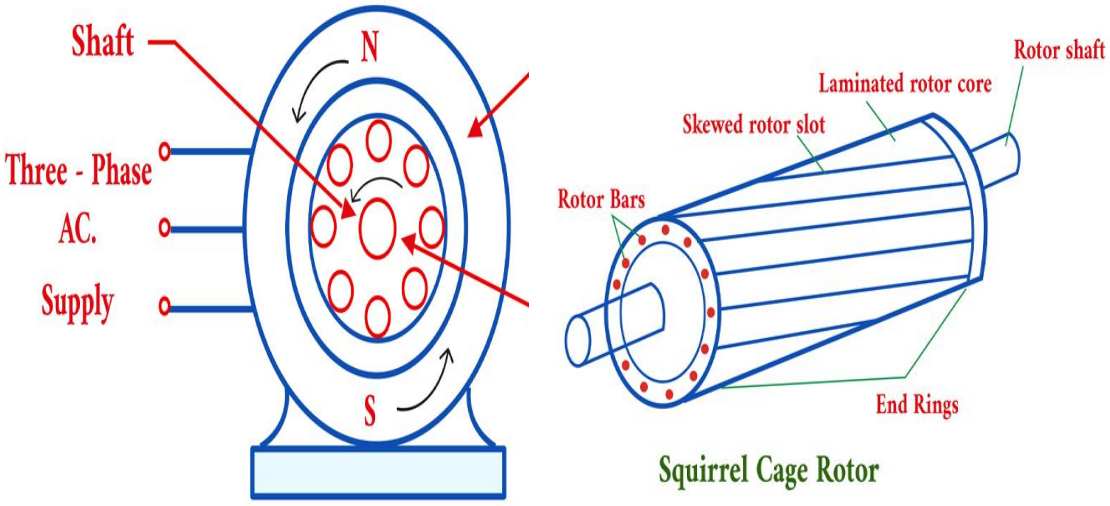

Figure II.1: Three-phase squirrel cage motor.

As is well known, maintaining and diagnosing the rotor is challenging due to its inaccessibility. The process of creating new models caused a significant revolution in the industrial world because of the enormous diversity and diverse goals of the simulation model in diagnosing the electrical machine.

The goal is to move forward with the creation of an asynchronous machine model that emphasizes the impact of the researched faults on the machine's observable quantities, namely the currents, in order to investigate the underlying phenomena. There are several options. The finite element allows for the simulation of the machine's operation under malfunctioning situations [79, 82] and is based on the distribution of fields and currents at any location of the machine. This approach is computationally costly and necessitates an understanding of the asynchronous motor-related geometrical factors and material properties. The second strategy used in this case understands the machine from the perspective of circuit theory.

Considered is a three-phase squirrel cage motor. Its rotor is made up of Nb insulated bars that are evenly spaced throughout its surface and are short-circuited by two rings. The cage

is modeled as a mesh circuit in a model that is used to analyze its performance, as seen in Figure II.1. In order to account for one of the two rings, the number of differential equations derived for the model is equal to the number of bars plus one [78, 83].

These simplifying hypotheses are typically used in the research of this device to translate the laws of electromagnetism.

- A continuous air gap;
- Neglecting the impact of the notches;
- Sinusoidal distribution of the magnetomotive forces in the air gap;
- A magnetic circuit with constant permeability that is unsaturated;
- Minimal losses in ferromagnetic field;
- The skin impact and heating's effects on the features are not taken into consideration;

The following are significant repercussions of the assumptions: [84, 85].

- The flows' additively;
- The self-inductances' constant;
- The mutual inductances between the devices are subject to the law of sinusoidal variation.
- The windings of the stator and rotor in accordance with the electrical angle of their magnetic axes.

II.2.1 Calculation of inductances

II.2.1.1 Stator part

The circulation of the magnetic field H produced by a i^{th} stator phase at any place may be estimated by using Ampere's theorem to a closed contour.

Ampere's theorem states that we have [86, 87]:

$$\oint Hdl = \frac{N_s I_s}{p} \qquad \text{(II -1)}$$

N_s Number of stator turns per phase;

I_s Current of a stator phase;

p Number of pole pairs;

The maximal induction in the air gap, starting with the formula (II -1), is equal to:

$$B_{\max} = \mu_0 \frac{N_s I_s}{2.p.e} \qquad \text{(II -2)}$$

With:

e Air gap [m]

$\mu_0 = 4\pi 10^{-7}$ Magnetic permeability of vacuum [H. m^{-1}]

The Fourier series decomposition of induction provides the fundamental:

$$B_s(\theta) = \mu_0 \frac{2\mu_0 N_s I_s}{pe\pi} \cos(p.\theta) \qquad \text{(II -3)}$$

In order to obtain the magnetic flux in the air gap, by poles, expression (II -3) is integrated. Along the machine, roughly at a polar interval [88].

We compose:

$$\Phi_s = \iint_s B_s ds = \int_0^t dz \int_{-\frac{\pi}{2p}}^{\frac{\pi}{2p}} B_s R.L.d\theta$$

We obtain:

$$\Phi_s = \iint_s B_s ds = \frac{4}{\pi} \mu_0 \frac{N_s^2}{e.p^2} R.L.I_s \qquad \text{(II -4)}$$

Dou the main flux of the stator winding:

$$\psi_{sp} = \Phi_s.N_s = N_s.I_s \frac{2\mu_0.N_s.R.L}{p.e\pi} \int_{-\frac{\pi}{2p}}^{\frac{\pi}{2p}} \cos(p.\theta).d\theta$$

So:

$$\psi_{sp} = L_{sp}.I_s \qquad \text{(II -5)}$$

Therefore, provides the main (magnetizing) inductance of the stator phase "n" according to (II -5):

$$L_{sp} = 4\mu_0 \frac{N_s^2}{e.p^2\pi} R.L \qquad \text{(II -6)}$$

The leakage flux is given by:

$$\Phi_{fs} = L_{fs}.I_s \tag{II -7}$$

The cyclic inductance L_{sc}:

$$L_{sc} = \frac{3}{2}L_{sp} + L_{sf} = \mu_0 \frac{6\mu_0 N_s^2.R.L}{e.p^2.\pi} + L_{sf} \tag{II -8}$$

Due to the symmetry of the stator windings, which are $\frac{2\pi}{3}$ degrees offset. The three phases' correct mutual inductances are as follows:

$$\begin{cases} L_{ab} = L_{sp}\cos\ (\frac{2\pi}{3}) = -\frac{L_{sp}}{2} \\ L_{ac} = L_{sp}\cos\ (\frac{4\pi}{3}) = -\frac{L_{sp}}{2} \\ L_{bc} = L_{sp}\cos\ (\frac{2\pi}{3}) = -\frac{L_{sp}}{2} \end{cases}$$

The mutual inductance between the stator phases is computed as:

$$\left.\begin{matrix} L_{ab} = L_{ba} \\ L_{ac} = L_{ca} \\ L_{bc} = L_{cb} \end{matrix}\right\} = M_s = -\frac{L_{sp}}{2}$$

II.2.1.2 Rotor part

It is essential to have a model of the machine that can take into consideration its transient behavior during load and voltage fluctuations in order to replicate the functioning of the system.

For this, we created a model of the rotor using meshes that were magnetically and electrically linked, with each mesh consisting of two bars and the two rings that connect them (figure II.2).

It should go without saying that the key to a successful simulation of an induction motor is the computation of all the inductances. We can determine the rotor circuits' inductances thanks to their architecture [33].

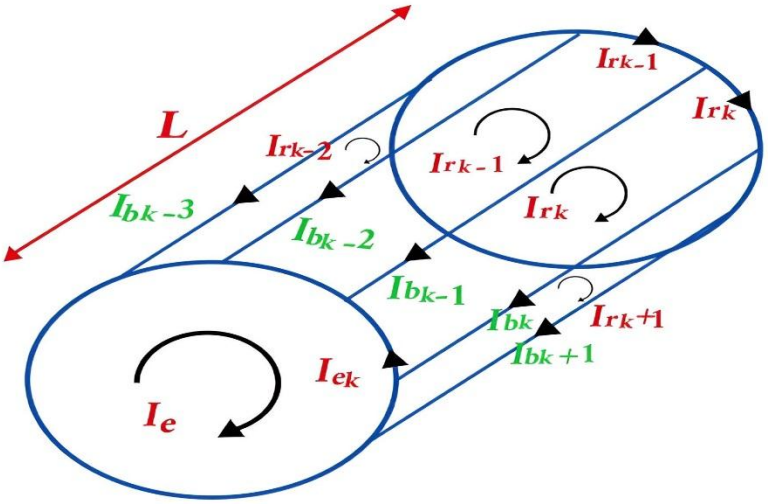

Figuire II.2: Cage rotor mesh

The magnetic induction distribution can be used to determine a rotor mesh's primary inductance. The sum of the primary inductance, the leakage inductance of the two bars, and the leakage inductance of the two segments of rings of the short circuit closing the mesh k determines the total inductance of the k^{th} rotor mesh, The magnetizing inductance of a rotor loop and the mutual inductance between two rotor loops are the result, giving us two different forms of inductance.

Assuming constant air gap permeances, the expression for the air gap induction produced by a rotor loop is as follows:

$$B_{1rk} = \frac{\mu_0}{e}\frac{N_r - L}{N_r} i_{rk} \qquad \text{(II -9)}$$

$$B_{2rk} = \frac{-L}{N_r}\frac{\mu_0}{e} i_{rk} \qquad \text{(II -10)}$$

A rotor mesh k producing magnetic induction in the air gap is seen in Figure II.3 as a function θ of its presumed radial form.

N_r Number of rotor bars, i_{rk} current in the loop [A], k=1,..., N_r and B_k rotor mesh "k" produces a magnetic field in the air gap.

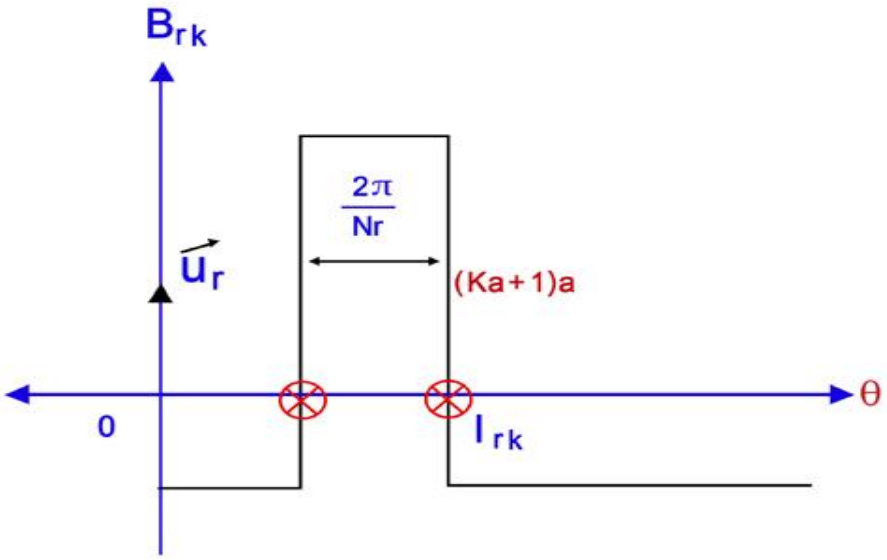

Figure II.3: Magnetic induction produced by a rotor mesh

If each single-turn coil in the rotor mesh, through which a current i_{rk} travels, serves as the location of the primary flux, then:

$$\Phi_{rbk} = \frac{(N_r - L)}{N_r^2}\mu_0 \frac{2.\pi.R.L}{e} i_{rk} \qquad \text{(II -11)}$$

The primary inductance of a rotor mesh is thus:

$$L_{rb} = \frac{(N_r - L)}{N_r^2}\frac{\mu_0}{e} 2.\pi.R.L \qquad \text{(II -12)}$$

So the expression is given by:

$$L_{rr} = L_{rp} + 2.L_b + 2.L_e \qquad \text{(II -13)}$$

The Winding Function reduced size makes it simple to compute these inductances. The following equations can be used to calculate the inductance between any two windings " i_{rk} " and "j" in any electric machine.

$$\Phi_{rjrk} = \int_0^t dz \int \left[-\frac{1}{N_r}\frac{\mu_0}{e} R.L.i_{rk} \right] d\theta \qquad \text{(II -14)}$$

As a result, the following relation may be used to represent the mutual inductance between non-adjacent (disjoint) rotor cells:

$$M_{rr} = -\frac{1}{N_r^{\,2}}\frac{\mu_0}{e}2.\pi.R.L \qquad \text{(II -15)}$$

The following equation describes how the kth cell and its surrounding cells' mutual inductance.

$$\begin{cases} L_{(k+1)k} = -\dfrac{1}{N_r^{\,2}}\dfrac{\mu_0}{e}2.\pi.R.L - L_{(k+1)b} \\ L_{(k-1)k} = -\dfrac{1}{N_r^{\,2}}\dfrac{\mu_0}{e}2.\pi.R.L - L_{(k-1)b} \end{cases} \qquad \text{(II -16)}$$

II.2.1.3 Stator and rotor mutual inductance

Since our rotor is caged, only the inclination coefficient is taken into consideration when calculating these inductances. The mechanical angle is then introduced between the stator phase and the rotor loop for the flux calculation [89, 90], with n= (1,2 and 3) giving us:

$$B_{smr} = \frac{2\mu_0 N_s I_s}{pe\pi}\cos(p.\theta - n\frac{2\pi}{3}) \qquad \text{(II -17)}$$

The flux may be used to compute the mutual inductance stator-rotor expression, which is provided by:

$$\Phi_{smrk} = \frac{2\mu_0}{\pi.e.p}N_s R.L.I_{sm}\frac{1}{p}\left[\sin\left(p\theta - n\frac{2\pi}{3}\right)\right]_{\frac{\theta}{\pi}+k\frac{2\pi}{N_r}+\frac{\pi}{N_r}\,s}^{\frac{\theta}{\pi}+k\frac{2\pi}{N_r}+\frac{\pi}{N_r}} \qquad \text{(II -18)}$$

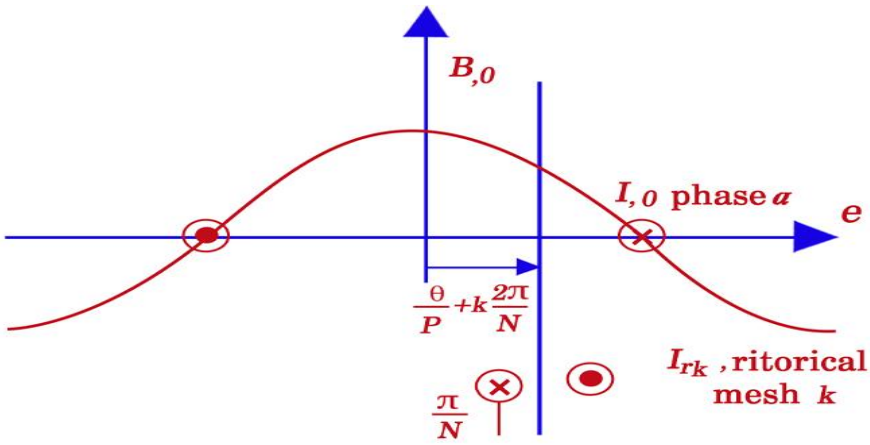

Figure II.4: Position of the rotor mesh, relative to the coil stator of the phase

The mutual inductance between the kth cell and phases "b" and "c" of the rotor is provided by e^{me}, while the mutual inductance between phase "n" of the stator and the kth rotor mesh is represented as:

$$M_{rkm} = -M_{sr}\cos\left[p\theta - n\frac{2\pi}{3} + ka\right] \qquad \text{(II -19)}$$

With :

$$M_{sr} = -\frac{4\ \mu_0 N_s R.L}{e.\pi.p^2}\sin\frac{a}{2}$$

$a = p\frac{2\pi}{N_r}$ The electrical angle between two rotor cells.

II.2.2 The Park transform

We employ the magnetically equivalent two-phase representation produced by the Park transformation in order to streamline the machine model and create a system with constant coefficients.

With the help of this transformation, a three-phase system called Xabc with windings along the Sa, Sb, and Sc axes can be changed into a system with windings along the orthogonal Sd, Sq, and So axes, which is equivalent in terms of the strength of the magnetic fields and the instantaneous electric and magnetic energies.

In the three-phase quantity system, the instantaneous total of the three phases equals zero. As a result, the homopolar component can be cancelled. It is possible to reduce the marker (o, d, q) to a two-phase marker (d, q) [108].

In this work the Park transform was used and applied to the equations and The Park transformation consists of transforming a three-phase system (abc) into an equivalent two-phase system (dq), as shown in Figure II.5 .

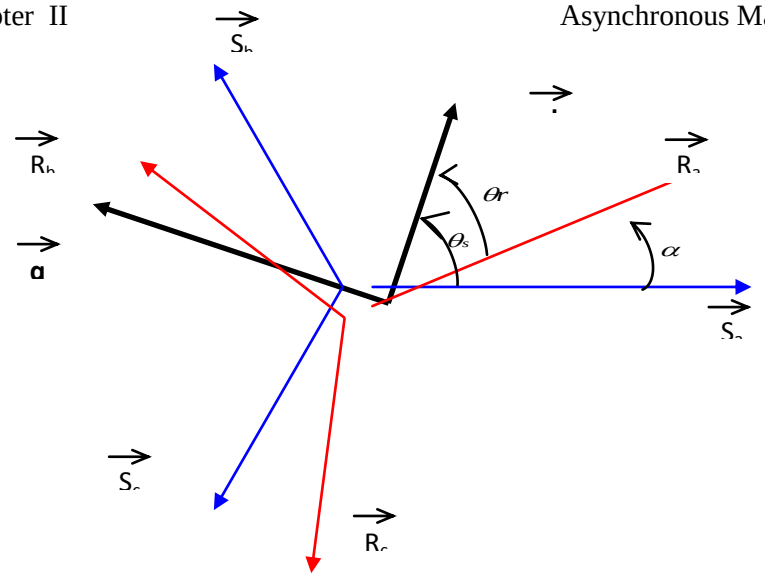

Figure II.5: Angular identification of axis systems in electrical space

We have :

$$[V_{abc}] = [R]\,[I_{abc}] + \frac{d}{dt}\,[\Phi_{abc}] \tag{II.20}$$

$$R=\begin{bmatrix} r & 0 & 0 \\ 0 & r & 0 \\ 0 & 0 & r \end{bmatrix}$$

(II.21)

The linear transformation $[p]$ is applied to the previous equation [108].

$$[p]^{-1}[V_{dqo}] = [R]\,[p]^{-1}[I_{dqo}] + \frac{d}{dt}\,[[p]^{-1}[\Phi_{dqo}]] \tag{II.22}$$

With :

$$[p] = \sqrt{\frac{3}{2}}\begin{bmatrix} \cos(\theta) & \cos(\theta-\frac{2\pi}{3}) & \cos(\theta+\frac{2\pi}{3}) \\ -\sin(\theta) & -\sin(\theta-\frac{2\pi}{3}) & -\sin(\theta+\frac{2\pi}{3}) \\ \frac{1}{\sqrt{2}} & \frac{1}{\sqrt{2}} & \frac{1}{\sqrt{2}} \end{bmatrix} \tag{II.23}$$

This matrix is orthogonal, that is to say $[p(\theta)]^t = [p(\theta)]^{-1}$ The Park transformation can be applied to voltages, currents and flows.

By multiplying (II.22) by $[p]$:

$$\left[V_{dqo}\right] = \left[R\right]\left[I_{dqo}\right] + \frac{d}{dt}\left[\Phi_{dqo}\right] + \left[p\right]\left(\frac{d}{dt}\left[p\right]^{-1}\right)\left[\Phi_{dqo}\right]$$

(II.24)

We demonstrate that:

$$\left[p\right]\left(\frac{d}{dt}\left[p\right]^{-1}\right) = \begin{bmatrix} 0 & -1 & 0 \\ 1 & 0 & 0 \\ 0 & 0 & 0 \end{bmatrix} \frac{d\theta}{dt} \qquad \text{(II.25)}$$

We finally obtain the system of Park's equations. which thus constitutes a dynamic electrical model for the equivalent two-phase winding:

$$\begin{cases} V_d = rI_d + \left(\frac{d\Phi_d}{dt}\right) - \left(\frac{d\theta}{dt}\right)\Phi_q \\ V_q = rI_q + \left(\frac{d\Phi_q}{dt}\right) + \left(\frac{d\theta}{dt}\right)\Phi_d \\ V_o = rI_o + \left(\frac{d\Phi_o}{dt}\right) \end{cases}$$

(II.26)

For the reduction of the matrix of the inductors the transformations proposed establish the relations between the fluxes of axis d , q , o et axis flows a , b , c :

$$\left[\Phi_{sdqo}\right] = \left[p(\theta s)\right]\left[\Phi_{sabc}\right] \text{ et } \left[\Phi_{rdqo}\right] = \left[p(\theta_r)\right]\left[\Phi_{rabc}\right] \qquad \text{(II.27)}$$

The usual stator power supply mode and the structure of the rotor windings giving zero to the sums of the stator currents and of the rotor currents, the index components (0) are zero.

Under these operating conditions in non-degraded mode, the flow of axes d et q are simply defined by the three constant parameters Ls , Lr , M , and linked to the currents by the relation (II.28) :

$$\begin{bmatrix} \Phi_{ds} \\ \Phi_{qs} \\ \Phi_{dr} \\ \Phi_{qr} \end{bmatrix} = \begin{bmatrix} L_s & 0 & M & 0 \\ 0 & L_s & 0 & M \\ M & 0 & L_r & 0 \\ 0 & M & 0 & L_r \end{bmatrix} \begin{bmatrix} I_{ds} \\ I_{qs} \\ I_{dr} \\ I_{qr} \end{bmatrix}$$

(II.28)

Substitution of dummy windings Sd , Sq , Rd , Rq to three-phase windings allows, by interpretation of their representation in figure (II.6), quick equation writing (II.28).

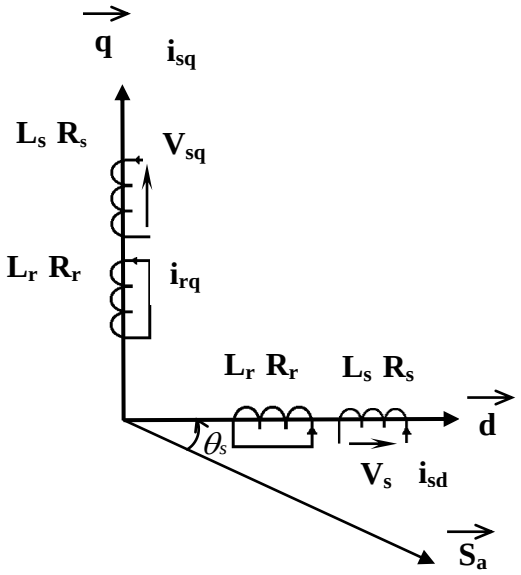

Figure II.6 : Representation of fictitious axis windings **d** and **q**

Park's equations of the tensions, stator and rotor are written:

$$V_{ds} = R_s I_{ds} + \frac{d\Phi_{ds}}{dt} - \frac{d\theta_s}{dt}\Phi_{qs}$$

$$V_{qs} = R_s I_{qs} + \frac{d\Phi_{qs}}{dt} + \frac{d\theta_s}{dt}\Phi_{ds} \qquad \text{(II.29)}$$

$$V_{dr} = R_r I_{dr} + \frac{d\Phi_{dr}}{dt} - \frac{d\theta_r}{dt}\Phi_{qr} = 0$$

$$V_{qr} = R_r I_{qr} + \frac{d\Phi_{qr}}{dt} + \frac{d\theta_r}{dt}\Phi_{dr} = 0$$

II.2.3 The Equations for of the asynchronous machine in closed loop a Multi-winding reduced size model

II.2.3.1. stator :

For the entirety of the static phases, deduction is made [91,92].

$$[V_{sabc}] = [R_s][I_{sabc}] + \frac{d}{dt}[\Phi_{sabc}] \qquad \text{(II -30)}$$

The electrical equations in the rotating representation are written as follows:

$$V_{ds} = R_s\ I_{ds} - \omega\,\Phi_{qs} + \frac{d\Phi_{ds}}{dt} \qquad \text{(II -31)}$$

$$V_{qs} = R_s\ I_{qs} + \omega\,\Phi_{ds} + \frac{d\Phi_{qs}}{dt} \qquad \text{(II -32)}$$

With :

$$\Phi_{sdq} = \begin{bmatrix} L_{sc} & 0 \\ 0 & L_{sc} \end{bmatrix}\begin{bmatrix} I_{ds} \\ I_{qs} \end{bmatrix} - M_{sr}\begin{bmatrix} \cdots & \cos j\alpha & \cdots \\ \cdots & \sin j\alpha & \cdots \end{bmatrix}\begin{bmatrix} I_{r0} \\ \vdots \\ I_{rj} \\ \vdots \\ I_{r(Nr-1)} \end{bmatrix} \qquad \text{(II -33)}$$

So :

$$\Phi_{ds} = L_{sc}I_{ds} - M_{sr}\left[\cos 0\alpha\ I_{r0} + \cos 1\alpha\ I_{r1} + ... + \cos\ j\alpha\ I_{rj} + ... + \cos(Nr-1)\alpha\ I_{r(Nr-1)}\right] \qquad \text{(II -34)}$$

In the same way for Φ_{qs}

$$\Phi_{qs} = L_{sc}I_{qs} - M_{sr}\left[\sin 0\alpha\ I_{r0} + \sin 1\alpha\ I_{r1} + ... + \sin\ j\alpha\ I_{rj} + ... + \sin(Nr-1)\alpha\ I_{r(Nr-1)}\right] \qquad \text{(II-35)}$$

Following the derivation of equations (II -34)and (II -35), one came to:

$$\frac{d\Phi_{ds}}{dt} = L_{sc}\frac{dI_{ds}}{dt} - M_{sr}\begin{bmatrix} \cdots & \cos j\alpha & \cdots \end{bmatrix}\frac{d}{dt}\begin{bmatrix} I_{r0} \\ \vdots \\ I_{rj} \\ \vdots \\ I_{r(Nr-1)} \end{bmatrix} \qquad \text{(II -36)}$$

And:

$$\frac{d\Phi_{qs}}{dt} = L_{sc}\frac{dI_{qs}}{dt} - M_{sr}\left[\ \cdots \quad \sin j\alpha \quad \cdots\ \right]\frac{d}{dt}\begin{bmatrix} I_{r0} \\ \vdots \\ I_{rj} \\ \vdots \\ I_{r(Nr-1)} \end{bmatrix} \qquad \text{(II -37)}$$

So ,the equations are written in the following format:

$$[L]\frac{d}{dt}[I] = [V] - [R][I] \qquad \text{(II -38)}$$

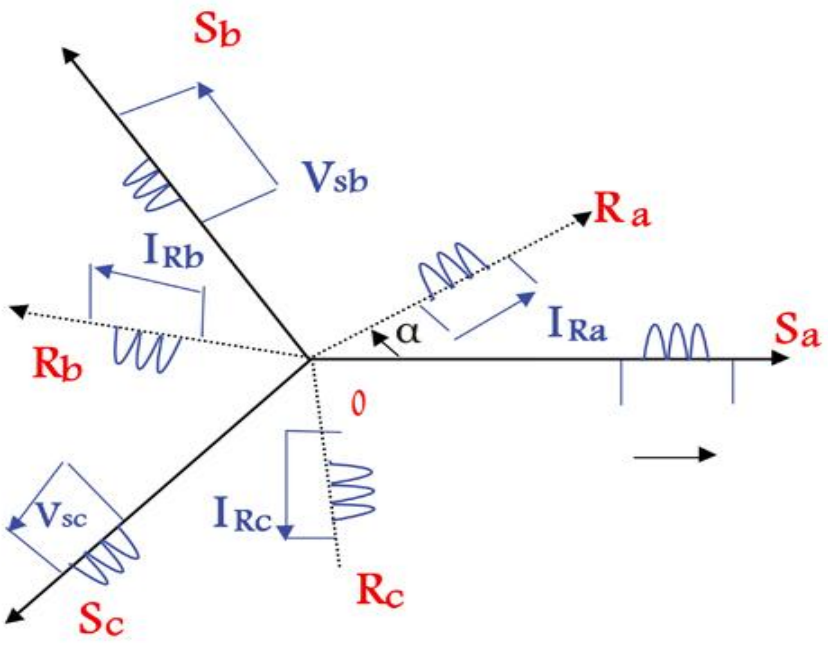

Figure II.7: Representation of the windings of the three-phase asynchronous machine

II.2.3.2. rotor:

The Figure II.8 depicts a caged rotor [93, 94 and 108].

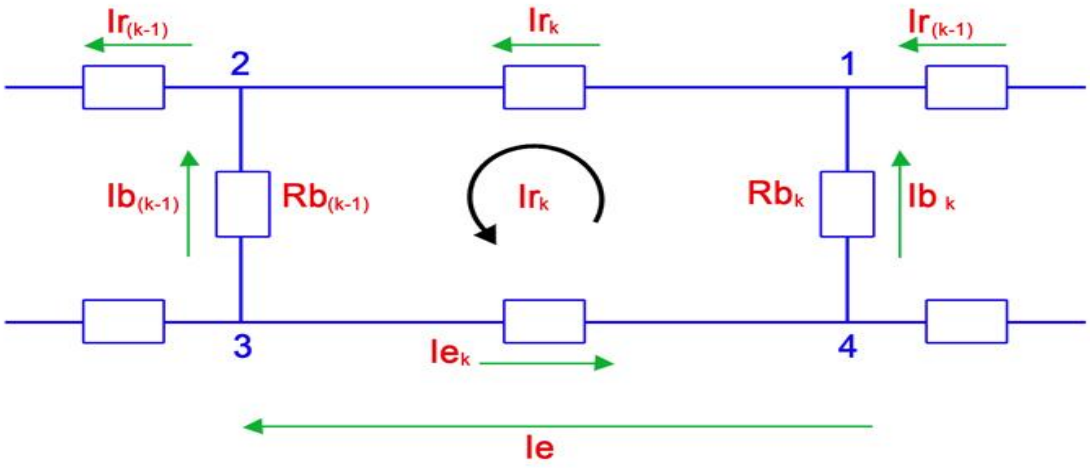

Figure II.8: Representation of a rotating maille

Irk Represents the current wire flow K , Ibk the current of the bar K .

For the k n° 1

$$I_{bk} = I_{rk} - I_{r(k+1)} \qquad \text{(II -39)}$$

For the k n° 2

$$I_{b(k-1)} = I_{r(k-1)} - I_{rk} \qquad \text{(II -40)}$$

The electric equation relating to the mesh K is:

$$0 = \frac{R_e}{N_r} I_{rk} - R_{b(k-1)}\left[I_{r(k-1)} - I_{rk}\right] + \frac{R_e}{N_r}\left[I_{rk} - I_e\right] + R_{bk}\left[I_{rk} - I_{r(k+1)}\right] + \frac{d\Phi_{rk}}{dt} \qquad \text{(II -41)}$$

Formulas (II -39) and (II-40) are replaced in equation (II-41); so the electric equation relating to the mesh K becomes:

$$0 = \frac{R_e}{N_r} I_{rk} - R_{b(k-1)} I_{b(k-1)} + \frac{R_e}{N_r}\left[I_{rk} - I_e\right] + R_{bk} I_{bk} + \frac{d\Phi_{rk}}{dt} \qquad \text{(II -42)}$$

The following determines the flow into the rotating maille:

$$\Phi_{rk} = L_{rp} I_{rk} + M_{rr} \sum_{\substack{j=0 \\ j \neq k}}^{Nr-1} I_{rj} - \frac{3}{2} M_{sr}\left(I_{ds} \cos K\alpha + I_{qs} \sin K\alpha\right) + \frac{L_e}{N_r}\left(I_{rk} + I_{ek}\right) + L_b\left(-I_{b(k-1)} + I_{bk}\right)$$

(II -43)

The term L_{rp} represents the main flux that represents the mutual flux Mrr with the other rotor meshes, then come the coupling terms with the stator. Note the factor $\frac{3}{2}$ with respect to the stator equation [93,94].The terms in L_b and L_e represent the rotor leakage.

The equation (II -43)is attempted to be written solely in terms of mail flow, using the formulas (II -39), (II -40), and:

$$I_{rk} - I_e = I_{ek} \qquad (\text{II -44})$$

Where: I_e represents the current of the short circuit rings.

So:

$$\Phi_{rk} = L_{rp} I_{rk} + M_{rr} \sum_{\substack{j=0 \\ j \neq k}}^{Nr-1} I_{rj} - \frac{3}{2} M_{sr} (I_{ds} \cos K\alpha + I_{qs} \sin K\alpha) + \frac{L_e}{N_r} I_{rk} + \frac{L_e}{N_r} I_{ek} + L_b \left[-I_{r(k-1)} + I_{rk} + I_{rk} - I_{r(k+1)} \right] \qquad (\text{II -45})$$

$$\Phi_{rk} = L_{rp} I_{rk} + M_{rr} \sum_{\substack{j=0 \\ j \neq k}}^{Nr-1} I_{rj} - \frac{3}{2} M_{sr} (I_{ds} \cos K\alpha + I_{qs} \sin K\alpha) + \frac{L_e}{N_r} I_{rk} + \frac{L_e}{N_r} (I_{rk} - I_e) + L_b \left[-I_{r(k-1)} + 2I_{rk} - I_{r(k+1)} \right] \qquad (\text{II -46})$$

$$\Phi_{rk} = L_{rp} I_{rk} + M_{rr} \sum_{\substack{j=0 \\ j \neq k}}^{Nr-1} I_{rj} - \frac{3}{2} M_{sr} (I_{ds} \cos K\alpha + I_{qs} \sin K\alpha) + \frac{2L_e}{N_r} I_{rk} - \frac{L_e}{N_r} I_e - L_b \left[I_{r(k-1)} + I_{r(k+1)} \right] + 2L_b I_{rk} \qquad (\text{II -47})$$

Finally, let's move on to:

$$\Phi_{rk} = \left(L_{rp} + \frac{2L_e}{N_r} + 2L_b \right) I_{rk} + M_{rr} \sum_{\substack{j=0 \\ j \neq k}}^{Nr-1} I_{rj} - L_b \left(I_{r(k-1)} + I_{r(k+1)} \right) - \frac{3}{2} M_{sr} \left(I_{ds} \cos K\alpha + I_{qs} \sin K\alpha \right) - \frac{L_e}{N_r} I_e \qquad (\text{II -48})$$

- On calculation $\frac{d\Phi_{rk}}{dt}$

$$\frac{d\Phi_{rk}}{dt}=(L_{rp}+\frac{2L_e}{N_r}+2L_b)\frac{dI_{rk}}{dt}+M_{rr}\sum_{\substack{j=0\\ j\neq k}}^{Nr-1}\frac{dI_{rj}}{dt}-L_b(\frac{dI_{r(k-1)}}{dt}+\frac{dI_{r(k+1)}}{dt})-\frac{3}{2}M_{sr}(\frac{dI_{ds}}{dt}\cos k\alpha+\frac{dI_{qs}}{dt}\sin k\alpha)$$

$$-\frac{L_e}{N_r}\frac{dI_e}{dt}$$

(II -49)

In place of $\frac{d\Phi_{rk}}{dt}$ while using equation (II -42)

$$0=\frac{R_e}{N_r}I_{rk}-R_{b(k-1)}\left[I_{r(k-1)}-I_{rk}\right]-\frac{R_e}{N_r}I_e+\frac{R_e}{N_r}I_{rk}+R_{bk}\left[I_{rk}-I_{r(k+1)}\right]+\left(L_{rp}+\frac{2L_e}{N_r}+2L_b\right)\frac{dI_{rk}}{dt}$$

$$+M_{rr}\sum_{\substack{j=0\\ j\neq k}}^{Nr-1}\frac{dI_{rj}}{dt}-L_b(\frac{dI_{r(k-1)}}{dt}+\frac{dI_{r(k+1)}}{dt})-\frac{3}{2}M_{sr}(\frac{dI_{ds}}{dt}\cos k\alpha+\frac{dI_{qs}}{dt}\sin k\alpha)-\frac{L_e}{N_r}\frac{dI_e}{dt}$$

(II -50)

Equation (II -50)is written in the following format:

$$[L]\frac{d[I]}{dt}=[V]-[R][I]$$

Equation (II -50) results in:

$$(L_{rp}+\frac{2L_e}{N_r}+2L_b)\frac{dIrk}{dt}+M_{rr}\sum_{\substack{j=0\\ j\neq k}}^{Nr-1}\frac{dI_{rj}}{dt}-L_b(\frac{dI_{r(k-1)}}{dt}+\frac{dI_{r(k+1)}}{dt})-\frac{3}{2}M_{sr}(\frac{dI_{ds}}{dt}\cos k\alpha+\frac{dI_{qs}}{dt}\sin k\alpha)$$

$$-\frac{L_e}{N_r}\frac{dI_e}{dt}=-\left[\left(\frac{2R_e}{N_r}+R_{bk}+R_{b(k-1)}\right)I_{rk}-R_{b(k-1)}I_{r(k-1)}-R_{bk}I_{r(k+1)}-\frac{R_e}{N_r}I_e\right]$$

(II -51)

For the court circuit [95, 96]:

$$L_e\frac{dI_e}{dt}-\frac{L_e}{N_r}\sum_{k=0}^{Nr-1}\frac{dI_{rk}}{dt}=-\left(R_eI_e-\frac{R_e}{N_r}\sum_{k=0}^{Nr-1}I_{rk}\right)$$ (II -52)

The entire system $[L]\frac{d[I]}{dt}=[V]-[R][I]$ become:

$$\begin{bmatrix} L_{sc} & 0 & \cdots & \cdots & \cdots & -M_{sr}\cos j\alpha & \cdots & \cdots & 0 \\ 0 & L_{sc} & \cdots & \cdots & \cdots & -M_{sr}\sin j\alpha & \cdots & \cdots & 0 \\ \vdots & \vdots & L_{rp}+\frac{2L_e}{N_r}+2L_b & M_{rr}-L_b & M_{rr} & \cdots & M_{rr} & M_{rr}-L_b & -\frac{L_e}{N_r} \\ \vdots & \vdots & M_{rr}-L_b & L_{rp}+\frac{2L_e}{N_r}+2L_b & M_{rr}-L_b & M_{rr} & \cdots & M_{rr} & \vdots \\ -\frac{3}{2}M_{sr}\cos k\alpha & -\frac{3}{2}M_{sr}\sin k\alpha & & & & & & & \vdots \\ \vdots & \vdots & & & & & & & \vdots \\ \vdots & \vdots & M_{rr}-L_b & M_{rr} & \cdots & M_{rr} & M_{rr}-L_b & L_{rb}+\frac{2L_e}{N_r}+2L_b & -\frac{L_e}{N_r} \\ 0 & 0 & -\frac{L_e}{N_r} & \cdots & \cdots & \cdots & \cdots & -\frac{L_e}{N_r} & L_e \end{bmatrix} \begin{bmatrix} I_{ds} \\ I_{qs} \\ I_{r0} \\ \vdots \\ I_{rj} \\ \vdots \\ I_{r(Nr-1)} \\ I_e \end{bmatrix} =$$

$$\begin{bmatrix} V_{ds} \\ V_{qs} \\ 0 \\ 0 \\ 0 \\ 0 \\ 0 \\ 0 \end{bmatrix} - \begin{bmatrix} R_s & -WL_{sc} & \cdots & \cdots & M_{sr}W\sin j\alpha & \cdots & \cdots & 0 \\ -WL_{sc} & R_s & \cdots & \cdots & -M_{sr}W\cos j\alpha & \cdots & \cdots & 0 \\ 0 & 0 & 2\frac{R_e}{Nr}+R_{b0}+R_{b(Nr-1)} & -R_{b0} & 0 & 0 & -R_{b(Nr-1)} & -\frac{R_e}{N_r} \\ 0 & 0 & & & & & & \vdots \\ 0 & 0 & 0 & -R_{b(k-1)} & 2\frac{R_e}{N_r}+R_{bk}+R_{b(k-1)} & -R_{bk} & 0 & \vdots \\ 0 & 0 & & & & & & \vdots \\ 0 & 0 & -R_{b(Nr-1)} & 0 & 0 & -R_{b(Nr-2)} & 2\frac{R_e}{N_r}+R_{b(Nr-2)}+R_{b(Nr-1)} & -\frac{R_e}{N_r} \\ 0 & 0 & -\frac{R_e}{N_r} & \cdots & \cdots & \cdots & -\frac{R_e}{N_r} & R_e \end{bmatrix} \begin{bmatrix} I_{ds} \\ I_{qs} \\ I_{r0} \\ \vdots \\ I_{rj} \\ \vdots \\ I_{r(Nr-1)} \\ I_e \end{bmatrix}$$

(II -53)

the corresponding model's dq new resistance matrix is [12]:

$$\left[R_{eq}\right] = \begin{bmatrix} R_s & -WL_{sc} & 0 & -\frac{N_r}{2}WM_{sr} & 0 \\ WL_{sc} & R_s & -\frac{N_r}{2}WM_{sr} & 0 & 0 \\ 0 & 0 & R_r & 0 & 0 \\ 0 & 0 & 0 & R_r & 0 \\ 0 & 0 & 0 & 0 & R_e \end{bmatrix} \qquad (\text{II -54})$$

With : (II -55)

$$R_{rdq} = 2\frac{R_e}{N_r} + 2R_b\left(1-\cos a\right)$$

the analogous model's new inductance matrix is :

$$\left[L_{sq}\right]=\begin{bmatrix} L_{sc} & 0 & -\frac{N_r}{2}M_{sr} & 0 & 0 \\ 0 & L_{sc} & 0 & \frac{N_r}{2}M_{sr} & 0 \\ -\frac{3}{2}M_{sr} & 0 & L_{rc} & 0 & 0 \\ 0 & \frac{3}{2}M_{sr} & 0 & L_{rc} & 0 \\ 0 & 0 & 0 & 0 & L_e \end{bmatrix} \quad \text{(II -56)}$$

With :

$$L_{rdq} = L_{rb} - M_{rr} + \frac{2.L_e}{N_r} + 2L_e(1-\cos a) \quad \text{(II -57)}$$

The electromagnetic torque is produced using co-energy derivation [97,98]:

$$C_e = \frac{3}{2}P\left[I_{sdq}\right]^t \frac{\delta}{\delta\theta}\begin{bmatrix} \cdots & -M_{sr}\cos(\theta+k\alpha) & \cdots \\ \cdots & -M_{sr}\cos(\theta+k\alpha) & \cdots \end{bmatrix}\begin{bmatrix} \vdots \\ I_{rk} \\ \vdots \end{bmatrix} \quad \text{(II -58)}$$

$$C_e = \frac{3}{2}PM_{sr}\left\{I_{ds}\sum_{k=0}^{Nr-1} I_{rk}\sin k\alpha - I_{qs}\sum_{k=0}^{Nr-1} I_{rk}\cos k\alpha\right\} \quad \text{(II -59)}$$

The mechanical equations are then added to obtain the speed. $\Omega = \frac{\omega}{P}$

$$\frac{d\Omega}{dt} = \frac{1}{J}P(C_e - C_r - \frac{f}{P}\omega) \quad \text{(II -60)}$$

$$\frac{d\theta}{dt} = \omega$$

II.2.4 Modeling of ruptures of bars of the asynchronous machine

The technique used for simulating rotor failures entails substituting a finite value for the broken bars' initial resistance value. The resistance method is the name of this technique.

Either by removing the bars under consideration or by increasing the resistance of the damaged bar, the rupture of a rotor bar can be modeled.

Bar breakage is one of the most common rotor faults. Our simulations will allow us to identify the signatures of this fault and predict the damage generated in the motor.

Modeling by omission entails taking into account the whole break of the bar, where no current flows and the bar's current is deleted, and replacing the two currents of the two neighboring meshes and with a single current [99, 100]. By including the two rows and two columns that correspond to the two currents, this adds resistors and inductances to the matrix.

The order of the system to be resolved decreases dramatically by raising the resistance of the broken bar because the current and accompanying stress are eliminated. involves rising the bar's resistance while keeping in mind that the current is not entirely zero to introduce the bar's barrier. The process entails adding a new matrix whose non-zero components correspond to the failed elements to the matrix of rotor resistances .

According to the research of [101,99], an increase in the resistance of the bar by 11 times produces outcomes that are consistent with those attained by experimentation.

As far as we are concerned, increases of 11 times the bar's original resistance have been taken into account.

In fact, in our model, an increase of greater than 11 times causes numerical instability.

A rotor problem necessitates a change to the matrix [R]. We obtain a second order matrix for the rotor using the transformation matrix.

The rotor fault matrix is written:

$$\left[R_{rf}\right]=\left[R_{r}\right]+\begin{bmatrix} 0 & ... & 0 & 0 & 0 & ... \\ & ... & & & & ... \\ ... & ... & ... & ... & & ... \\ & ... & & & & ... \\ 0 & ...0 & 0 & 0 & 0 & ... \\ 0 & ....0 & R'_{bk} & -R'_{bk} & 0 & ... \\ 0 & ...0 & -R'_{bk} & R'_{bk} & 0 & ... \\ 0 & ...0 & 0 & 0 & 0 & ... \\ ... & ... & ... & ... & 0 & ... \end{bmatrix} \quad \text{(II -61)}$$

The resistance matrix is: ou elle sont les resistances R_{dd}, R_{dq}

$$\left[R_{rfdq}\right]=\begin{bmatrix} R_{dd} & R_{dq} \\ R_{qd} & R_{qq} \end{bmatrix}$$

$$R_{rdd} = 2R_b\left(1-\cos a\right)+2\frac{R_e}{N_r}+\frac{2}{N_r}\left(1-\cos a\right)\sum_k R_{bfk}.(1-\cos(2k-1)a) \quad \text{(II -62)}$$

$$R_{rdq} = \frac{2}{N_r}\left(1-\cos a\right)\sum_k R_{bfk}.\sin(2k-1)a \quad \text{(II -63)}$$

$$R_{rqd} = \frac{2}{N_r}\left(1-\cos a\right)\sum_k R_{bfk}.\sin(2k-1)a \quad \text{(II -64)}$$

$$R_{rqq} = 2R_b\left(1-\cos a\right)+2\frac{R_e}{N_r}+\frac{2}{N_r}\left(1-\cos a\right)\sum_k R_{bfk}.(1+\cos(2k-1)a) \quad \text{(II -65)}$$

The broken bar is defined by the index k.

So, taking into account the bar break fault, the electrical equations are rewritten in the following form:

$$\begin{cases} V_{ds} = R_s\ I_{ds} - W\ \Phi_{qs} + \dfrac{d\Phi_{ds}}{dt} \\ V_{qs} = R_s\ I_{qs} + W\ \Phi_{ds} + \dfrac{d\Phi_{qs}}{dt} \\ 0 = R_{rdd}\ I_{dr} + R_{rdq}\ I_{qr} - W\ \Phi_{qr} + \dfrac{d\Phi_{dr}}{dt} \\ 0 = R_{rqd}\ I_{dr} + R_{rqq}\ I_{qr} + W\ \Phi_{dr} + \dfrac{d\Phi_{qr}}{dt} \end{cases} \quad \text{(II -66)}$$

The reduced-size model for the asynchronous machine with a bar break fault is given by:

$$\begin{bmatrix} L_{sc} & 0 & -\frac{N_r}{2}M_{sr} & 0 & 0 \\ 0 & L_{sc} & 0 & \frac{N_r}{2}M_{sr} & 0 \\ -\frac{3}{2}M_{sr} & 0 & L_{dqr} & 0 & 0 \\ 0 & \frac{3}{2}M_{sr} & 0 & L_{dqr} & 0 \\ 0 & 0 & 0 & 0 & L_e \end{bmatrix} \frac{d}{dt}\begin{bmatrix} I_{ds} \\ I_{qs} \\ I_{dr} \\ I_{qr} \\ I_e \end{bmatrix} =$$

$$\begin{bmatrix} V_{ds} \\ V_{qs} \\ 0 \\ 0 \\ 0 \end{bmatrix} - \begin{bmatrix} R_s & -WL_{sc} & 0 & -\frac{N_r}{2}WM_{sr} & 0 \\ WL_{sc} & R_s & -\frac{N_r}{2}WM_{sr} & 0 & 0 \\ 0 & 0 & R_{dd} & R_{dq} & 0 \\ 0 & 0 & R_{qd} & R_{qq} & 0 \\ 0 & 0 & 0 & 0 & R_e \end{bmatrix} \begin{bmatrix} I_{ds} \\ I_{qs} \\ I_{dr} \\ I_{qr} \\ I_e \end{bmatrix} \quad \text{(II -67)}$$

After applying the generalized transformation on the couple's statement for the mechanical part, the following result is obtained:

$$C_e = \frac{3}{2}.P.N_r.M_{sr}\left\{I_{ds}.I_{qr} - I_{qs.}I_{dr}\right\} \quad \text{(II -68)}$$

The sub-matrix that relates to the rotor resistance is a reliable sign of a problem. In fact, unlike with sound machines, R_{rdd} and R_{rqq} are no longer equivalent in default cases. Additionally, the words R_{rdq} and R_{rqd} assume a non-rdq null value, indicating the existence of a rotor malfunction.

II.3 Voltage inverter of an electrical machine

A rotating machine, its power source, its control system, and its load are all often included in an electric drive system, according to [102].

The machine's power source comprises of a DC voltage source that can be acquired via a rectifier, and an inverter that converts this DC voltage into variable AC voltage and variable frequency so that the asynchronous motor's speed may be adjusted. Depending on the receiver provided, there are two main types of inverters: voltage inverters supplied by a DC voltage source and current inverters supplied by a DC source [97, 98].

A static converter known as an inverter makes sure that electrical energy is converted from its continuous form (DC) to its alternating form (AC).

The machine is typically linked to the inverter via shielded three-phase cable, whether it is star or delta mounted. Since the equipment rarely has a neutral point, the inverter is connected to the machine using three wires. In other words, the inverter only imposes two voltages and three potentials. However, we maintain a structure with three electromotive forces for the undulator in order to better integrate it with the control algorithms [103].

The inverter introduces high-frequency components by cutting supply voltages. However, the measurement filters exclude these elements, and we also fail to take into account the machine's high frequency impacts. In order to mimic each arm of the inverter, we simply connect a resistor in series with an excitation, whose value corresponds to the specifications of the control algorithms.

The inverter is considered to have a slot per alternation, full wave (180°), or offset (120°), if the semiconductors are constructed with a single closure and opening per period. But in order to have them operate several times each period, we also utilize semiconductors that operate at a higher frequency. The output voltages and currents of many slots with sufficient widths are then obtained, and PWM inverters are created [104].

The static switch is a crucial component of energy conversion because it controls how much energy is transferred between the various components of the circuit and how average current and voltage values are managed. As such, it was thought interesting to describe the static semiconductor switches currently used in power electronics before beginning the modeling of the inverter.

II.3.1. Modeling of the inverter with two voltage levels

Figure(II.9) illustrates the basic operation of a three-phase inverter with two voltage levels arranged in a bridge to supply a load. Typically, a three-phase rectifier with diodes and an LC filter are used to produce the DC voltage.

The inverter has six switching cells and six freewheeling diodes, and it has two voltage levels. The output of the inverter corresponds to the middle of each arm's two switching cells, which each include a switch and a diode. To avoid damaging the inverter's DC power supply, the control signals of each arm's switches must be complimentary. It is required to provide a waiting period when the switch is closed, which is typically referred to as dead time, to prevent a premature short-circuit. Power transistors (MOSFETs, IGBTs, and bipolar transistors) and fast thyristors (mostly GTOs) are the semiconductors most frequently employed to create switches [105, 106].

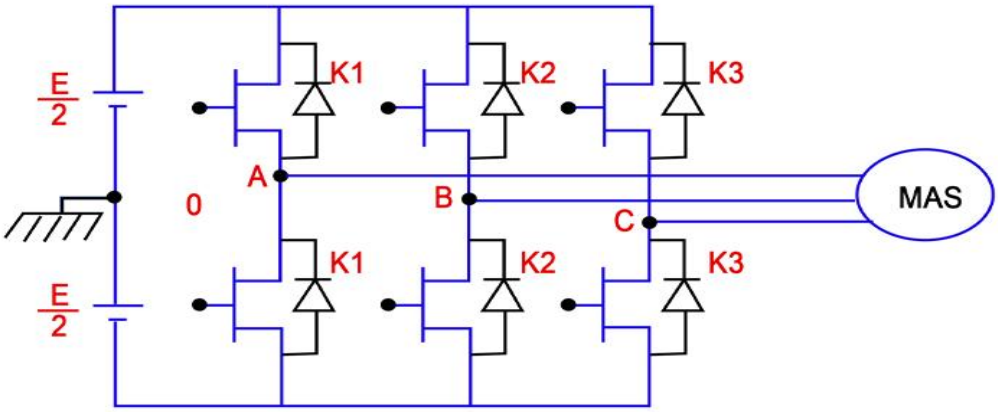

Figure II.9: The voltage inverter associated with the MAS[107]

Three two-level single-phase half-bridges combine to create the six-switch three-phase inverter. The output voltages at the inverter's terminals are expressed in terms of the imaginary point 0 at the inverter's source as follows:

$$v_j - v_0 = \begin{cases} +\dfrac{E}{2} & \text{if } K_i \text{ is closed} \quad j = A,B,C \\ -\dfrac{E}{2} & \text{if } K_i \text{ is closed} \quad i = 1,2,3 \end{cases} \qquad \text{(II -69)}$$

Hence, we can write:

$$\begin{cases} v_{AB} = (v_A - v_0) - (v_B - v_0) \\ v_{BC} = (v_B - v_0) - (v_C - v_0) \\ v_{CA} = (v_C - v_0) - (v_A - v_0) \end{cases} \qquad \text{(II -70)}$$

The voltages at the inverter's terminals can be expressed as follows:

$$\begin{cases} v_{AB} = (v_{A0} - v_{B0}) \\ v_{BC} = (v_{B0} - v_{C0}) \\ v_{CA} = (v_{C0} - v_{A0}) \end{cases} \qquad \text{(II -71)}$$

Knowing that :

$$v_{AN} + v_{BN} + v_{CN} = 0 \qquad \text{(II -72)}$$

We can write :

$$\begin{cases} v_{AN} = (v_{A0} - v_{0N}) \\ v_{BN} = (v_{B0} - v_{0N}) \\ v_{CN} = (v_{C0} - v_{0N}) \end{cases} \quad \text{(II -73)}$$

The following is an expression for the phase-to-neutral voltages at the terminals of the star-connected load:

$$\begin{cases} v_{AN} = \frac{1}{3}(2v_{A0} - v_{B0} - v_{C0}) \\ v_{BN} = \frac{1}{3}(v_{A0} - 2v_{B0} - v_{C0}) \\ v_{CN} = \frac{1}{3}(v_{A0} - v_{B0} - 3v_{C0}) \end{cases} \quad \text{(II -74)}$$

Equation (II -60)may be rewritten as follows in matrix form:

$$\begin{bmatrix} v_{AN} \\ v_{BN} \\ v_{CN} \end{bmatrix} = \frac{1}{3}\begin{bmatrix} 2 & -1 & -1 \\ -1 & 2 & -1 \\ -1 & -1 & 2 \end{bmatrix}\begin{bmatrix} v_{A0} \\ v_{B0} \\ v_{C0} \end{bmatrix} \quad \text{(II -75)}$$

According to the signals, it is possible to determine tensions between phases and the hypothetical neutral by:

$$\begin{cases} v_{A0} = E.S_A \\ v_{B0} = E.S_B \\ v_{C0} = E.S_C \end{cases} \quad \text{(II -76)}$$

The logic functions Sj (j = A, B, and C) reflect the state of the electrical switches (K1, K2, and K3), whose switching is presumed to be instantaneous.

- Sj=1: High switch (K) closed and low switch (K') open.
- Sj=0: High switch (K) open and low switch (K') closed.

$$\begin{cases} v_{AN} = \frac{E}{3}(2S_A - S_B - S_C) \\ v_{BN} = \frac{E}{3}(2S_B - S_A - S_C)\,(\\ v_{CN} = \frac{E}{3}(2S_C - S_B - S_A) \end{cases} \quad \text{(II -77)}$$

The voltages at the terminals of the machine are given by:

$$\begin{cases} v_{AN} = \frac{1}{3}(2v_{A0} - v_{B0} - v_{C0}) \\ v_{BN} = \frac{1}{3}(v_{A0} - 2v_{B0} - v_{C0}) \\ v_{CN} = \frac{1}{3}(v_{A0} - v_{B0} - 3v_{C0}) \end{cases} \quad \text{(II -78)}$$

Equation (II -70) can be rewritten in matrix form:

$$\begin{bmatrix} v_{AN} \\ v_{BN} \\ v_{CN} \end{bmatrix} = \frac{E}{3}\begin{bmatrix} 2 & -1 & -1 \\ -1 & 2 & -1 \\ -1 & -1 & 2 \end{bmatrix}\begin{bmatrix} S_A \\ S_B \\ S_C \end{bmatrix} \quad \text{(II -79)}$$

II.4.Conclusion:

This chapter has a clear presentation of the steps involved in building a mathematical model of a squirrel-cage asynchronous machine that is suitable for simulating bar breakage at the rotor. We presented the simplifying assumptions on which the multi-winding model is based before adapting the model for the simulation of rotor bar breaks, and we then computed the different stator and rotor inductances and mutual's.

Increasing the resistance of the bar that is being influenced by the defect makes it simple to acquire the effects of a bar failure.

In this chapter, the asynchronous machine has been discussed in terms of circuits, and it has been taken into account that the rotor is made up of a number of components, each of which is characterized by an equivalent electrical circuit of Nr magnitudes.

We shall be able to comprehend the physical events connected to this kind of flaw using Park model. In chapter three that is dedicated to the diagnosis of rotor cage problems, we give the simulation results from this model.

Chapter Three :

Size-reduced multi-winding model simulation and results

III.1. Introduction

Once the overall model of the asynchronous cage machine Size-reduced multi-winding model is developed we approach the simulation of it. A program, written in Matlab, makes it possible to highlight the behavior of the asynchronous motor in the case where the machine is healthy and in the case where the machine is faulty.

It makes it possible to solve differential equations that may include certain types of non - linearity's. It includes modules that can perform functions such as summation, integration, multiplication, delay, etc.

Also offers several methods of digital resolution of differential equations by properly choosing the integration step adapting to the dynamics of the system to be resolved.

During the simulation of the model, to observe its good behavior, a torque of 3.5 Nm was subjected to the machine at time t = 0.6 seconds, this torque represents the nominal torque of the machine studied.

We will study in what follows the most frequent faults that appear in the asynchronous motors at the level of the rotor (breakage of bars).

The induction motor was tested under loading conditions first with a healthy rotor, then with 2 broken rotor bars. Every stator current displayed in the study is given in the frequency domain.

The severity of the fault on the stator current spectrum is demonstrated by considering the motor with a fault with one broken bar first, then with two broken bars, then finally with three broken bars.

The stator current spectral analysis in the different cases is applied to three different windows, such as Rectangular window, Hanning window and Hamming window of the signal in steady state and at load using the Fast Fourier Transform algorithm FFT ,In comparison to the healthy conditions, the recommended index significantly raises under the broken bars conditions. It can identify the problematic conditions with clarity. The possibility of detecting potential faults has been demonstrated (broken bars), using discrete wavelet transform and continuous wavelet transform. The diagnostic method is adaptable to temporary situations brought on by alterations in load .

This work aimed to use Wavelet Packet Transform on current window frame samples from an induction motor to diagnose and categorize broken rotor bars using DWT and CWT.

The work in this chapter was split into two halves, and the outcomes were simulated in both scenarios with and without the machine's inverter.

III.2. results of the the multi-winding model reduced size (without inverter.)

We can study the evolution of temporal elements such as stator currents, torque and speed when the rotor cage shows no failure; No-load starting at nominal voltage with a balanced three-phase sinusoidal power supply. The simulation is carried out over a period of 5 sec with at the instant t = 0.6 sec the machine is subjected to a resistive torque Cr = 3.5 N.m he simulation of the model allowed us to obtain the different characteristics of stator current, speed and electromagnetic torque; they are shown in Figures respectively (III.1. a ,b ,c and d)

Then one, two, and three rotor bar is broken for fault analysis and broken rotor bar detection the simulation results they are shown in Figures respectively (III.2 a, b, c, and d) to (III.4 a, b, c, and d).

III.2.1. Case of a healthy machine :

In this section, a squirrel cage induction motor serves as a scaled-down simulation of the multi-winding model.

Five seconds of simulation time was used to test the model's accuracy. At time t = 0.6 seconds, a torque of 3.5 Nm was applied to the machine.

The evolution of temporal factors such as stator currents, torque, and speed, as well as the current in the machine's rotor bars, may be analyzed when the rotor cage shows no symptoms of failure. The number ten bar was used as an example in the research findings. We've displayed the progression of the findings on Figures (III.1. a ,b ,c and d).

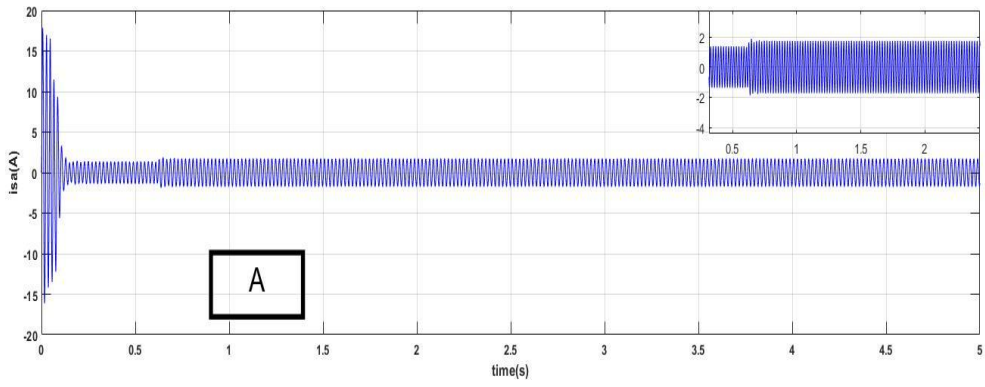

Figure III.1: (a) Evolution of phase a stator current (isa) at no load, on load (healthy).

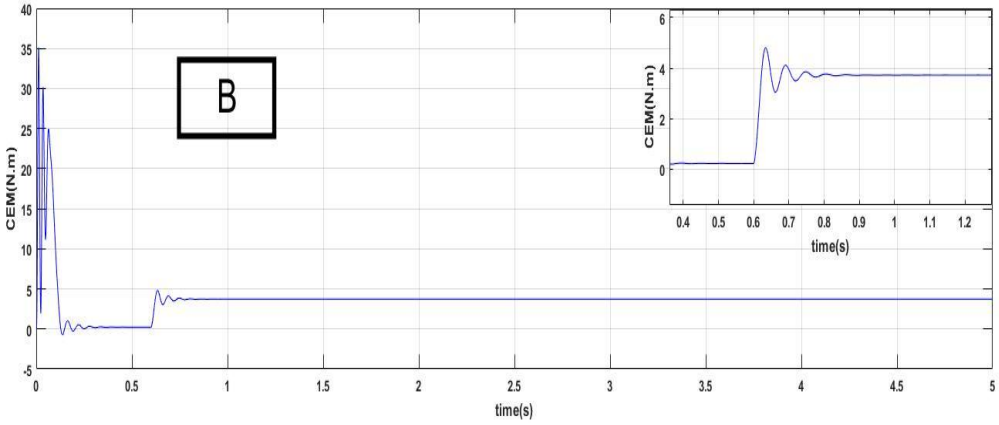

Figure III.1: (b) Evolution of the electromagnetic torque on starting, under load (healthy).

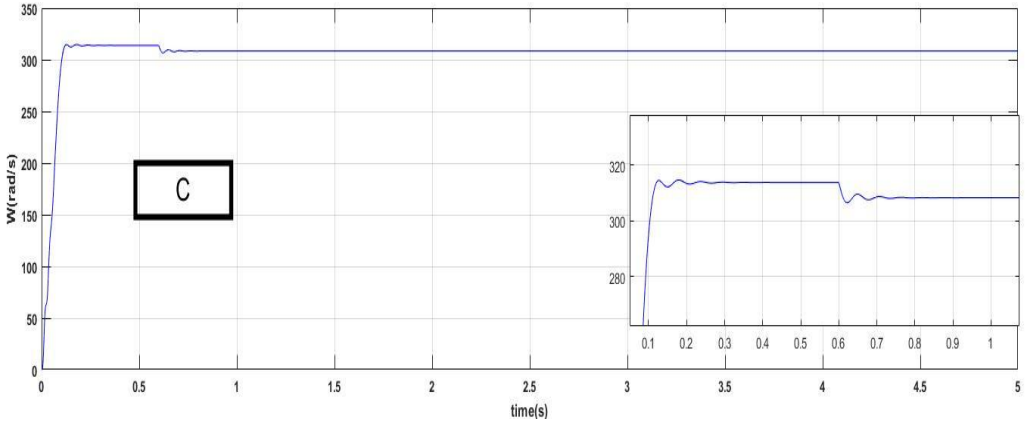

Figure III.1: (c) Rotational speed at start, under load (healthy).

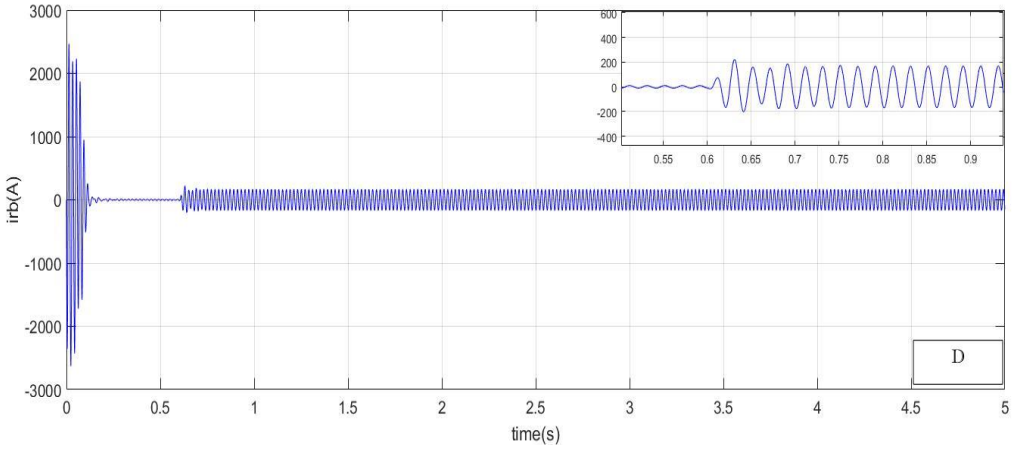

Figure III.1: (d) Evolution of phase a rotor current (irb) bar number ten ,at no load, on load (healthy)

for a healthy motor, the flux lines are distributed symmetrically around each pole as a result of the currents in the bars.

By simulating the asynchronous motor model with a rotor, we were able to estimate the different speed, electromagnetic torque, and stator current characteristics. It should be noted that the speed achieves its nominal value when the machine is loaded and thereafter slightly decreases. Following then, the torque will typically match the load torque amount.

Current amplitudes peak when the rotor is first in a shutdown state, which is why they are so high. After then, a stable regime develops, resulting in the currents decreasing with sinusoidal oscillations around zero.

Figure (III.1.a) depicts the development of the influence of the increasing currents, which are caused by the growing magnetic response of the rotor and the rising amplitude of the rotor currents.

Figure (III.1.b) depicts the electromagnetic torque as it develops, with the transient phase continuing, developing, and having the potential to achieve a maximum value. The torque then rapidly drops to almost nothing, mirroring the torque caused by fluid friction. The electromagnetic torque naturally reacts in the opposite way to counter the resistive torque when we apply a 3.5 Nm torque at (0.6 s).

Figure (III.1.c) depicts the evolution of the rotor's rotational speed. The speed increases as soon as the engine fires up, stabilizing the situation. Then, at time (0.6 s), a resistive torque of 3.5 Nm is applied, which tends to slow the motor shaft and lower the speed.

III.2.2. Result of simulation with machine faults :

III.2.2.1. Case of one broken bar:

The induction motor was first put to the test under duress with one rotor bar destroyed. Each stator current in the study is illustrated in the frequency domain.

Figures (III.2 a, b, c, and d) depict how the machine absorbs a phase as a result of bar breaking.

A resistive torque of 3.5 N.m is applied to the machine at the point t = 0.6 sec during the simulation, which lasts for five seconds.

We recreate the first bar's failure at time t=(2)s by raising the resistance by 11 times.

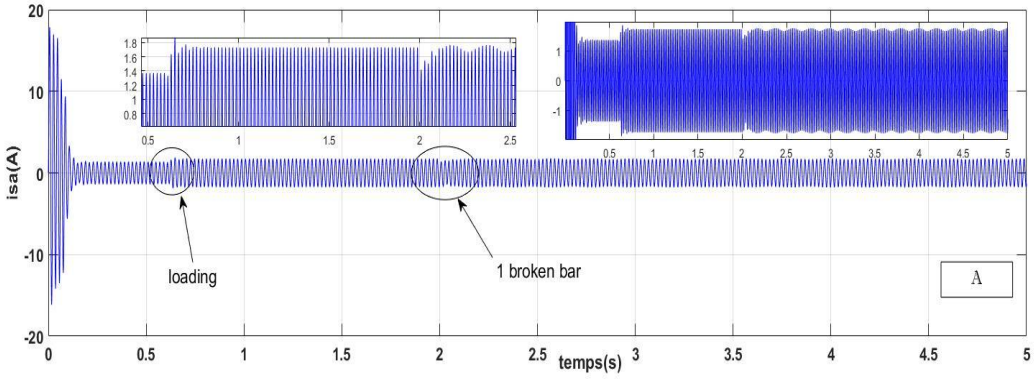

Figure III.2: (a) Evolution of phase a stator current (isa) for one broken bar

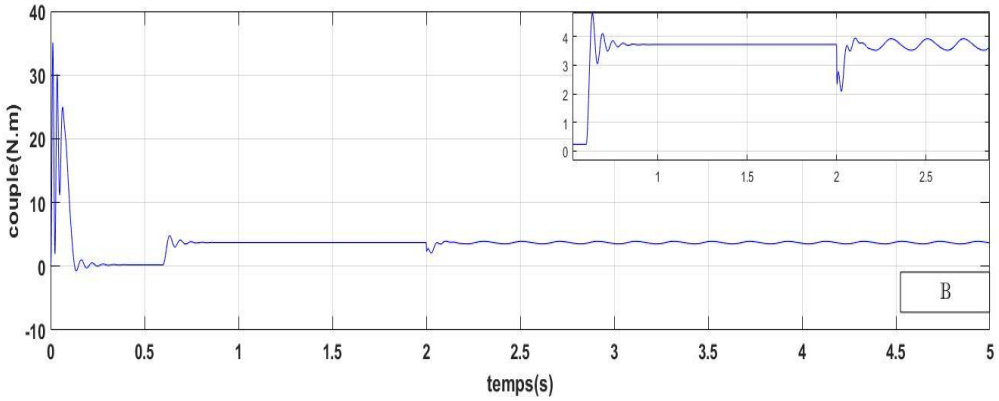

Figure III.2: (b) Evolution of the electromagnetic torque with one broken bar

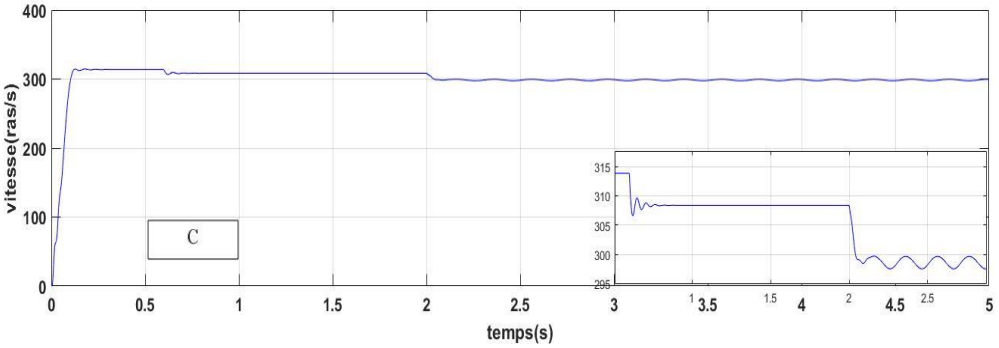

Figure III.2: (c) Rotation speed with one broken bar.

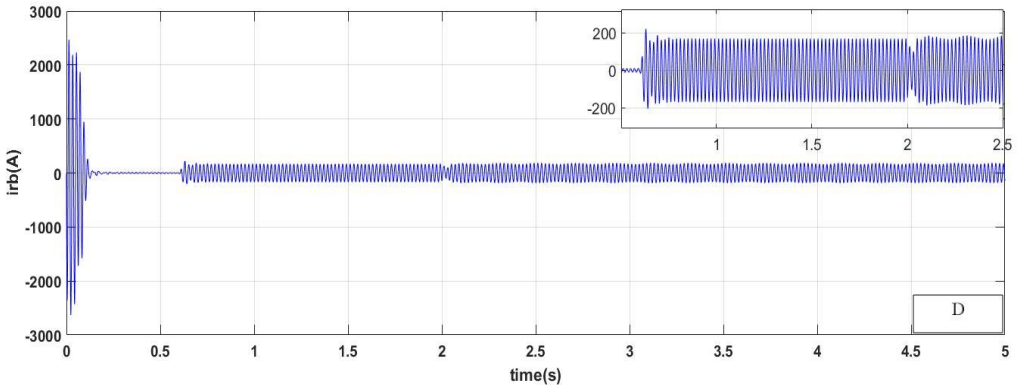

Figure III.2: (d) Evolution of phase a rotor current (irb) bar number ten , with one broken bars.

III.2.2.2. Case of two broken bars:

Second, two broken rotor bars were used in an induction motor stress test. In the research, we have used the frequency domain to illustrate the global quantities (the currents, the electromagnetic torque, and the speed).

Figures (III.3 a, b, c, and d) show how the breaking of two neighboring bars (bars number one and number two) affects a phase that the machine absorbs.

The simulation, which lasts for five seconds, applies a resistive torque of 3.5 N.m to the machine at the point t = 0.6 sec. By increasing the resistance by 11 times, we repeat the failure of the first bar at time t= (2) s and the failure of the second bar at time t= (3) s.

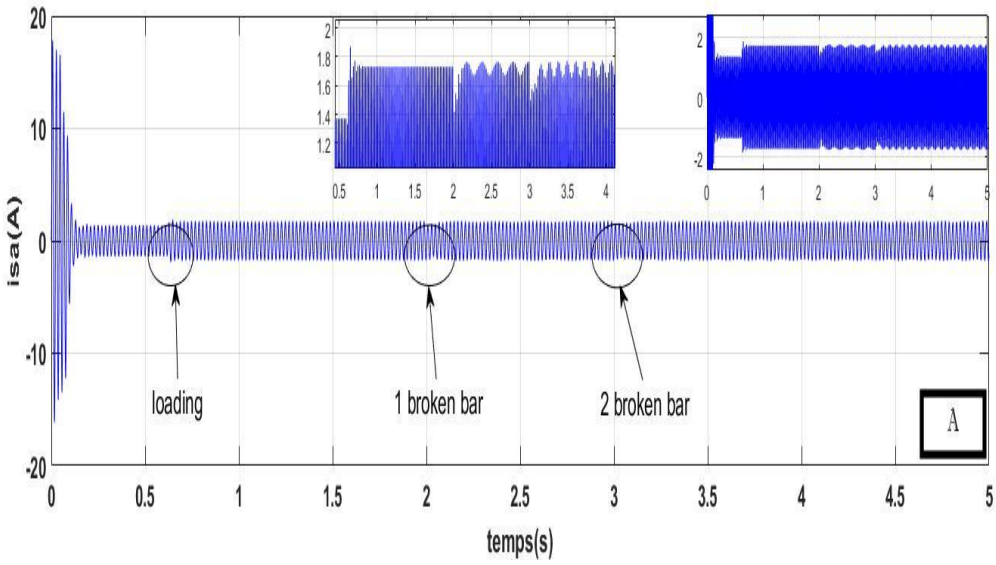

Figure III.3: (a) Evolution of phase a stator current (isa) for two broken bars

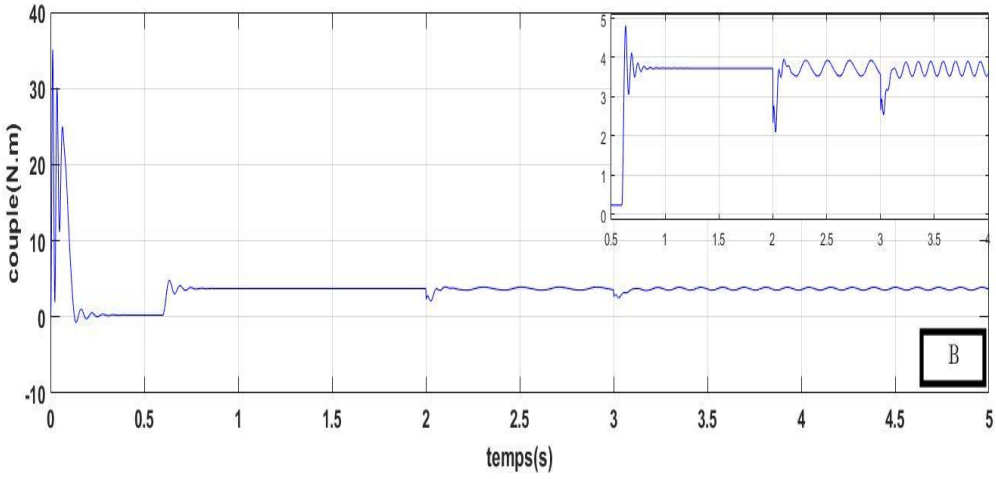

Figure III.3: (b) Evolution of the electromagnetic torque with two broken bars

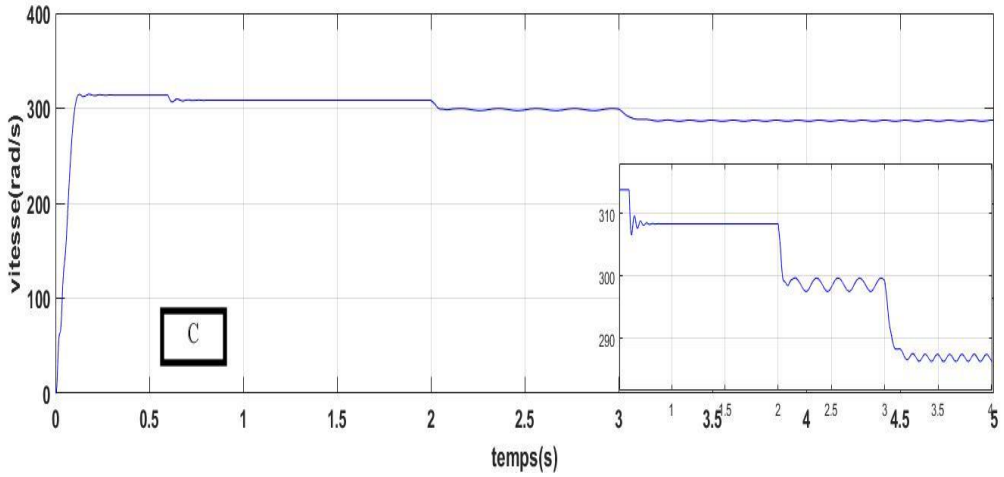

Figure III.3: (c) Rotation speed with two broken bars.

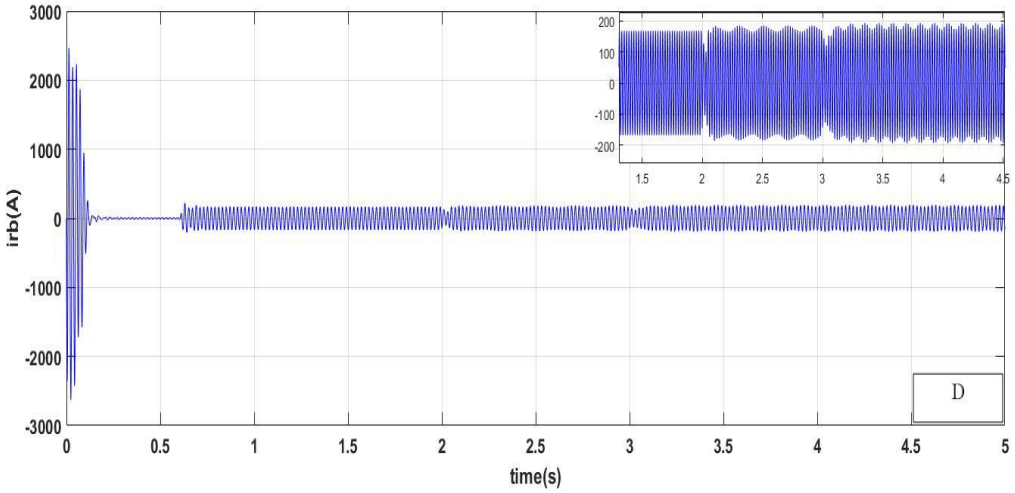

Figure III.3: (d) Evolution of phase a rotor current (irb) bar number ten , with two broken bars.

III.2.2.3. Case of three broken bars:

Third, Figures (III.4 a, b, c, and d) illustrate the consequences of three bar breaking on a phase that the machine absorbs.

The simulation, which lasts for five seconds, applies a resistive torque of 3.5 N.m to the machine at the point t = 0.6 sec. The failures of the first bar at time t= (2) s, the second bar at time t= (3) s, and ultimately the third bar at time t= (4) s may all be successfully reproduced.

The induction motor underwent a stress test using three consecutive broken rotor bars. In the research, we have used the frequency domain to illustrate the evolution of the global quantities (the currents, the electromagnetic torque, and the speed).

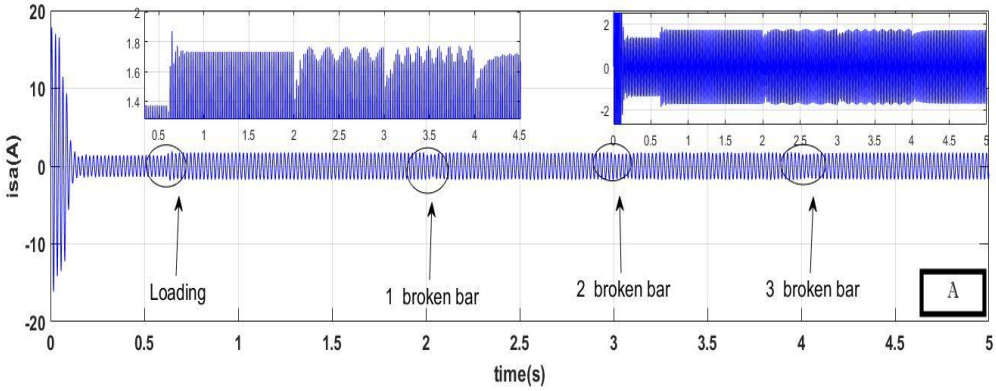

Figure III.4: (a) Evolution of phase a stator current (isa) for three broken bars

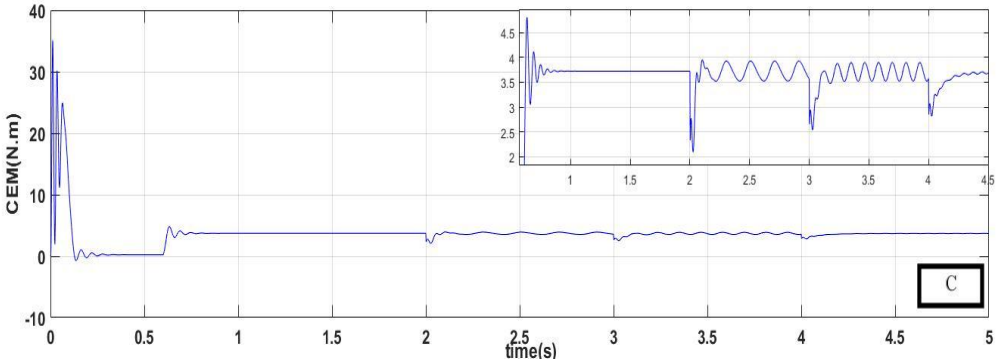

Figure III.4: (b) Evolution of the electromagnetic torque with three broken bars

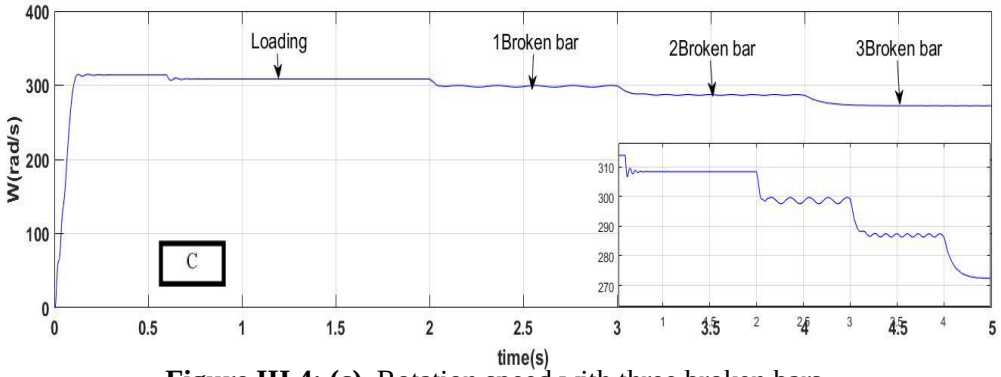

Figure III.4: (c) Rotation speed with three broken bars

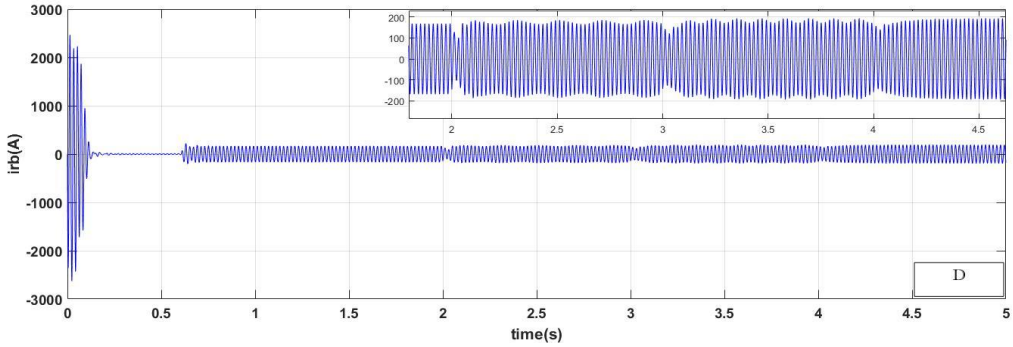

Figure III.4: (d) Evolution of phase a rotor current (irb) bar number ten , with three broken bars.

As evidenced by the earlier findings, we broke the bars to test the machine under three different conditions:

1. The first experiment is shown in Figures III-2(a),(b),(c), and(d)). We broke the first rod in the squirrel cage rotor. The repercussions of the break were evident up to time t = (5)s.
2. In the second situation, we shattered two adjacent bars (bars one and two) in the squirrel cage rotor, as shown in (Figures III-3 a,b,c, and d). At time t = (2)s, the first bar was broken, and up until t = (3)s, its effects were visible. At time t=(3)s, the second rod broke, and its effects persisted until t=(5)s.
3. In the third scenario, as shown in (Figures III-4 a, b, c, and d), we broke three adjacent bars (bars numbers one, two, and three) in the squirrel cage rotor because the first bar was broken at time t = (2).) s and we studied its influence until t = (3) s. After the second rod was broken at time t = (3) s and its effects were not apparent until time t = (4) s, the third rod was broken at time t = (4) s. We tracked its effects up to t=(5)s.

In order to comprehend these effects in the three scenarios, we will describe these adjustments to our analyzed model:

- The currents' amplitude oscillates as a result of the bars' breakage. The amplitude of the oscillation is exactly proportional to the number of broken bars. These dependencies are illustrated in the charts below.
  The broken bars represent the current in the bar adjacent to the broken bars in each of the three cases in figures (III-2 a), (III-3 a), and (III-4 a).
  The images above depict the distribution of the currents in the machine's bars; as the machine's bars crack, the current between the rotor's bars becomes imbalanced and its amplitude rises. Its amplitude increases as more bars are broken. Remember that the amplitude of the oscillations is also influenced by this number.
  The cumulative impact on the breaking of the bars is due to the nearby bars carrying more current, which causes them to heat up and age more quickly.

- Figures (III-2 b), (III-3 b), and (III-4 b) show that the mechanical characteristic in a transient situation, together with the number of broken bars, quickly gives information on the status of the engine. The high amplitude oscillations accelerate the component deterioration of the machine and the traction chain.

As more bars are broken, we observe that the torque is adversely affected. In reality, oscillations increase and the average value decreases as the bars break apart.
These oscillations in the squirrel cage rotor are increased with the number of broken bars, as shown by examination of these faults in the third circumstances, which showed us in each case that the rise in damage develops exponentially with the number of broken bars.

- We can observe from the results in Figures (III-2 c), (III-3 c), and (III-4 c) that the speed is deteriorating and lowering as the number of broken bars slowing the motor shaft increases.
  In our analysis of the evolution of machine speed, the first, second, and third cases confirmed the inverse relationship between machine speed and the number of broken bars.
  These cause rotational speed oscillations, which result in mechanical vibrations and unpredictable machine functioning.

The simulation of the model of the asynchronous motor with a rotor with broken adjacent bars (bar N°01, bar N°02 and bar N°03) allowed us to obtain the different characteristics of speed, electromagnetic torque, currents of rotor bars, and stator current.

Compared to the healthy state of the machine, we note that:

We mimic the bar breaking by raising its resistance by 11 times. In addition to the direct field (g.ws) that is produced when a bar breaks, the rotor also produces an inverse rotor field (-g.ws). An electromagnetic torque is produced as a result of the interaction of these fields with the stator winding and is made up of a constant component and an inverse sinusoidal pulsation component (2g.ws) (see figure III.2,3,4.b). The oscillations on the speed figure III.2,3,4.c will be brought on by the latter. To examine the modulation of the stator current's envelope, utilize Figure III.2,3,4.a.

To demonstrate the impact of the number of broken bars, we simulate the failure of neighboring bar No. 2,3,4 at t=(2,3,4)s. resulting in an overcurrent The torque and speed are produced by an increase in the amplitude of the undulations as a result of the current that passed through the broken bar being spread among the nearby bars. We also see an increase in the stator current's modulation amplitude.

We may quickly draw the conclusion that it is challenging to directly analyze the current's amplitude and that it is thus wise to treat the signal in order to get more accurate data.

III.2.3 Fast Fourier Transform (FFT)

In remark that the direct analysis of the amplitude of the current in the temporal field is difficult and therefore it is advisable to process the signal in order to bring out the more representative data. It is therefore by using the rapid Fourier (FFT) transform that we can highlight more representative criteria such as the appearance of frequency rays.

The stator current spectral analysis in the different cases is applied to three different windows, such as Rectangular window, Hanning window and Hamming window of the signal in steady state and at load using the Fast Fourier Transform algorithm FFT , they are shown respectively in the in Figures (III.5 to III.8).

There are many windows with different features and properties As a result, depending on the specific issue that has to be resolved, the signal's suitable timeframe must be selected Essentially, this trait relates to three things:

the primary lobe's breadth and height, the first sidelobe's height, the subsidiary lobes' attenuation.

In order to demonstrate application the stator current spectral analysis for the diagnostic and detection of faults in the squirrel cage motor, the simulation of the healthy motor supplied with a sinusoidal power supply, operating under a load of 3.5Nm, enables us to visualize the spectrum of the stator current in Figures (III-5 a, b, and c),. Note that the spectrum contains only the fundamental harmonic at the frequency 50 Hz.

The FFT algorithm is widely used for the detection of rotor broken bar fault. The stator current shows the side bands around the fundamental frequency. The fundamental frequency of the motor is 50Hz. If any fault is occurred then amplitude of the side lobes are increased that is clear indication of fault. It is due to the reverse rotating magnetic field in the inductor and mutual inductance.

In the case of a faulty motor with one or two or three broken rotor bars working under the same load above, it is possible to identify from the stator current spectra shown in Figures (III.6 to III.8).

, the harmonics related to the case of one , two and three broken rotor bars respectively. These harmonics appear on either side of the fundamental harmonic at frequencies (1±2k g) fs.

III.2.3.1 Case of a healthy machine:

Figures (III-5 a, b, and c), show The result of stator current spectral analysis for a healthy motor.

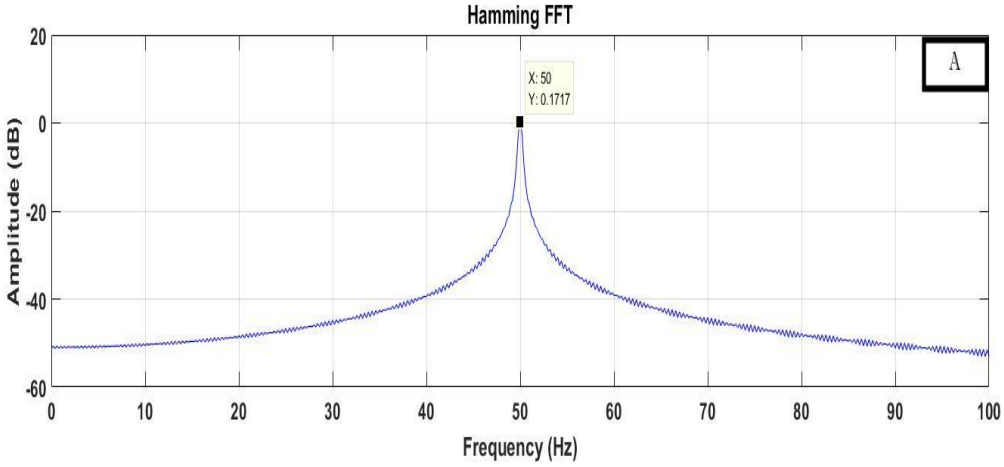

Figure III.5: (a) Spectrum of phase current by hamming spectral analysis .At start-up, under load

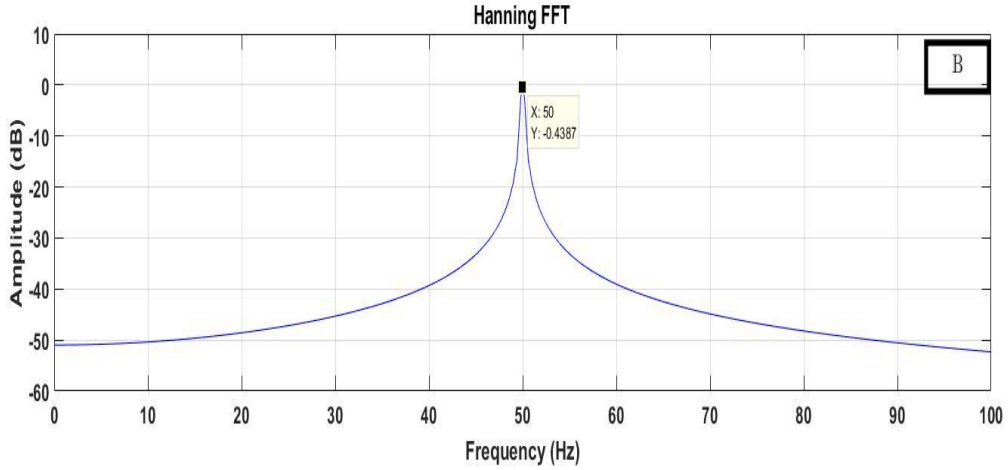

Figure III.5: (b) Spectrum of phase current by hanning spectral analysis .At start-up, under load

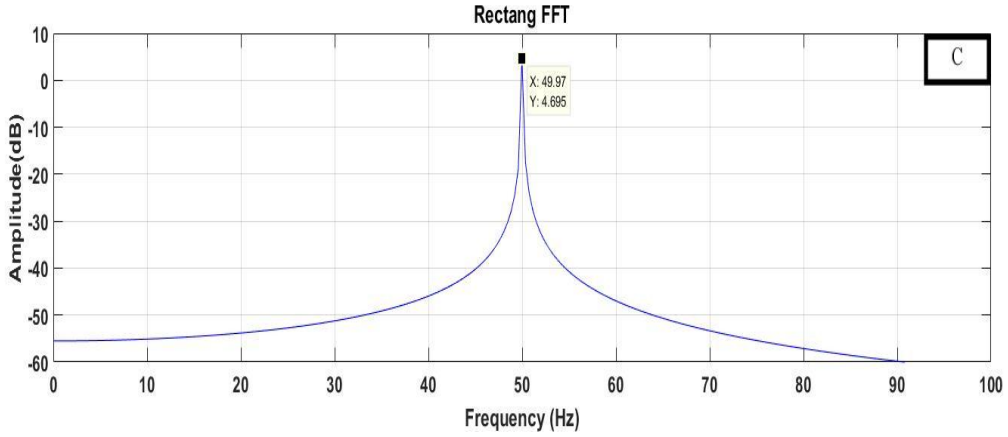

Figure III.5: (c) Spectrum of phase current by Rectangular spectral analysis .At start-up, under load

III.2.3.2 Case of one broken bar:

The induction motor was first put to the test under duress with one rotor bar destroyed.

Figures (III-6 a, b, and c), show the result of stator current spectral analysis for a motor faults (one broken bar).

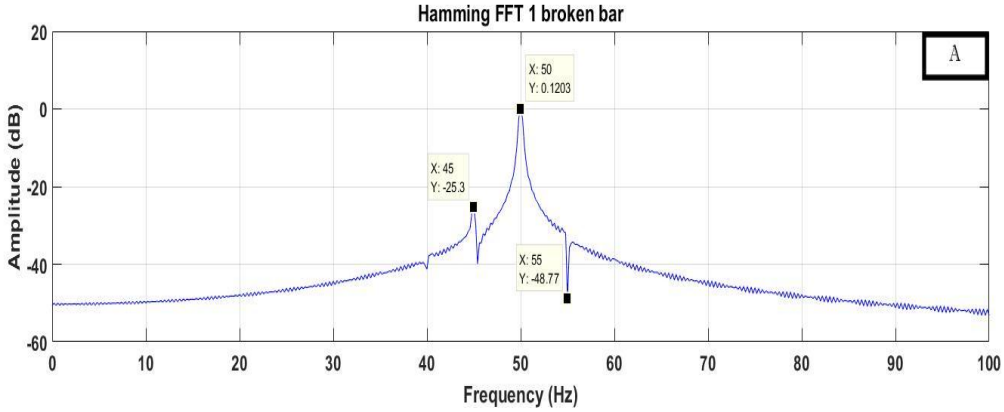

Figure III.6: (a) Spectrum of phase current by hamming spectral analysis . during bar failure(one broken bar)

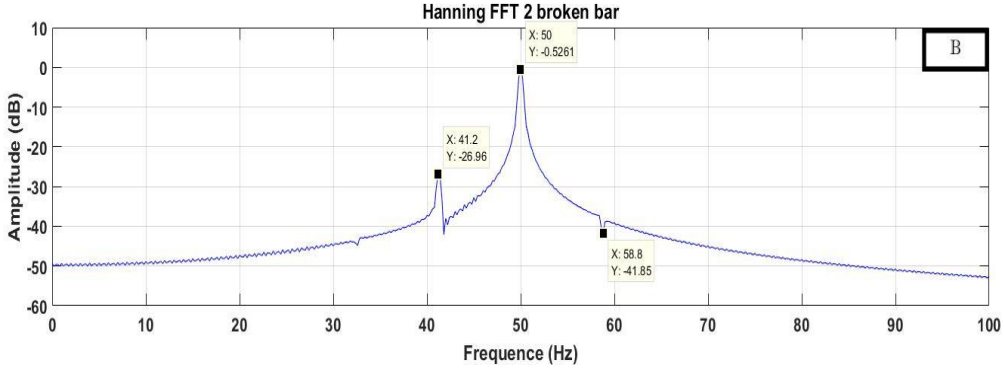

Figure III.6: (b) Spectrum of phase current by hanning spectral analysis . during bar failure(one broken bar)

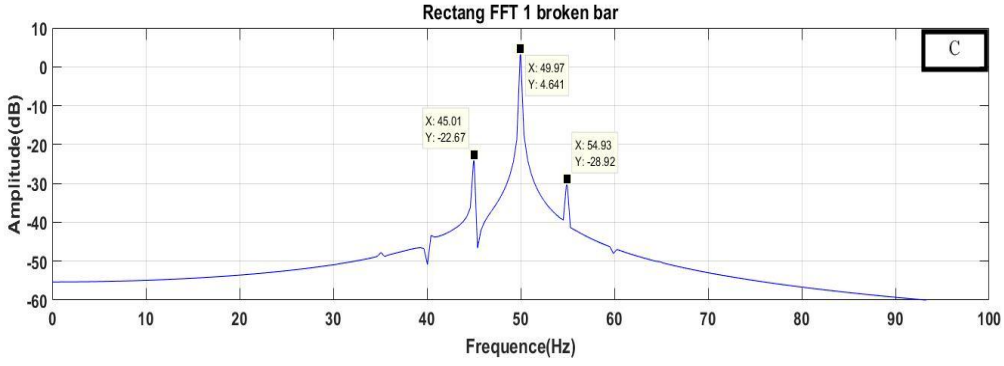

Figure III.6: (c) Spectrum of phase current by Rectangular spectral analysis . during bar failure(one broken bar)

III.2.3.3 Case of two broken bars:

The neighboring rotor bars (bars number one and Number two) were damaged during the second time the induction motor was put under stress.

The results of a stator current spectrum analysis for a motor defect (two broken bars) are shown in Figures (III-7a, b, and c).

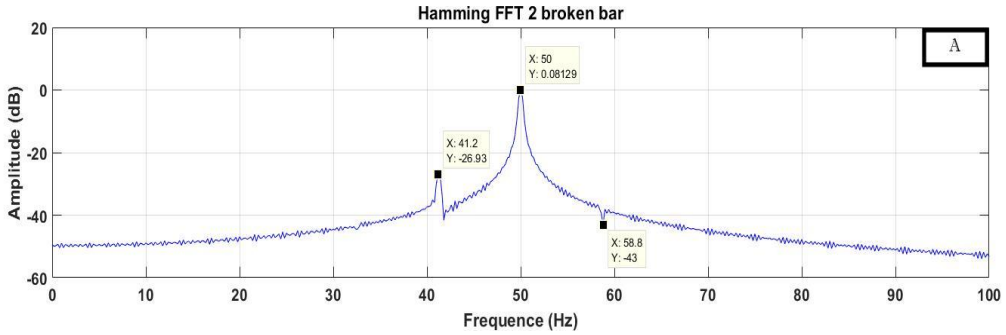

Figure III.7: (a) Spectrum of phase current by hamming spectral analysis . during bar failure(two broken bars)

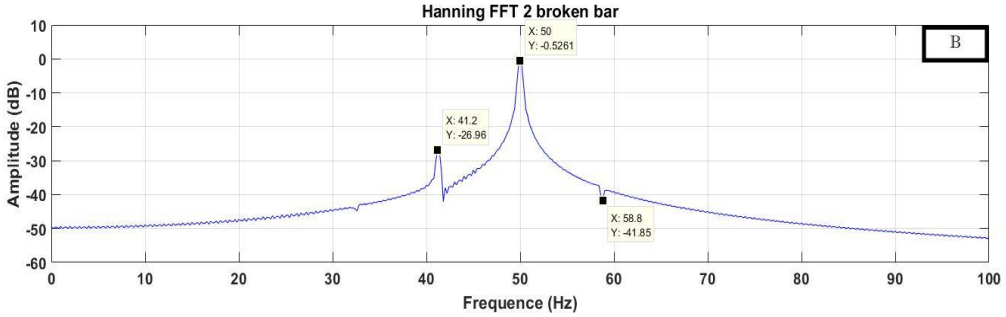

Figure III.7: (b) Spectrum of phase current by hanning spectral analysis . during bar failure(two broken bars)

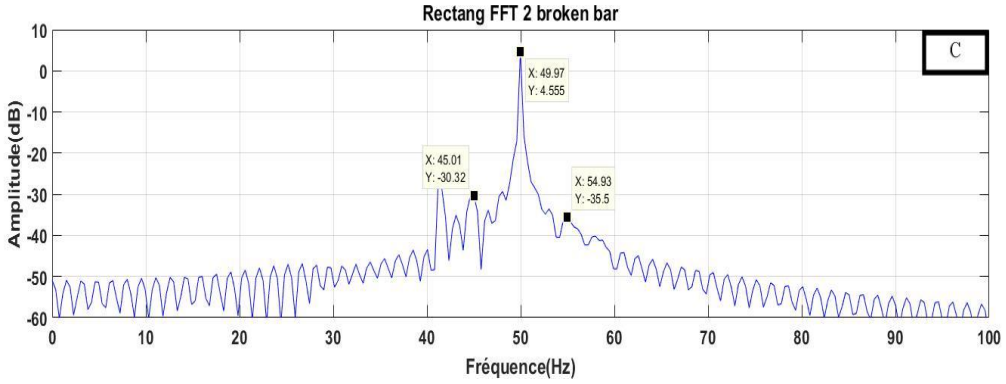

Figure III.7: (c) Spectrum of phase current by Rectangular spectral analysis . during bar failure(two broken bars)

III.2.3.4 Case of three broken bars:

The results of a stator current spectrum analysis for a motor defect (three broken bars) are shown in Figures (III-8 a, b, and c).

The neighboring rotor bars (bar number one, bar number two and bar number three) were damaged during the third time the induction motor was put under stress.

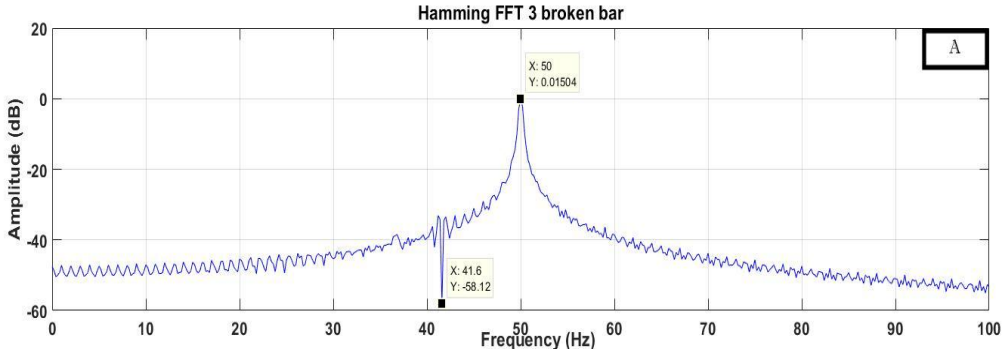

Figure III.8: (a) Spectrum of phase current by hamming spectral analysis . during bar failure(three broken bars)

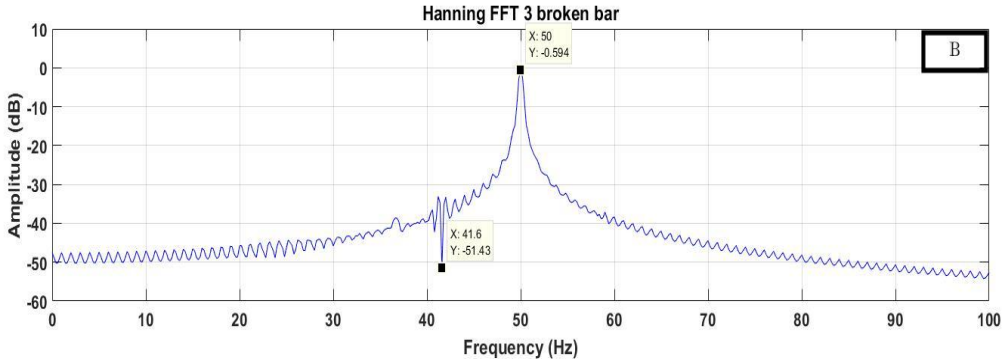

Figure III.8: (a) Spectrum of phase current by hanning spectral analysis . during bar failure(three broken bars)

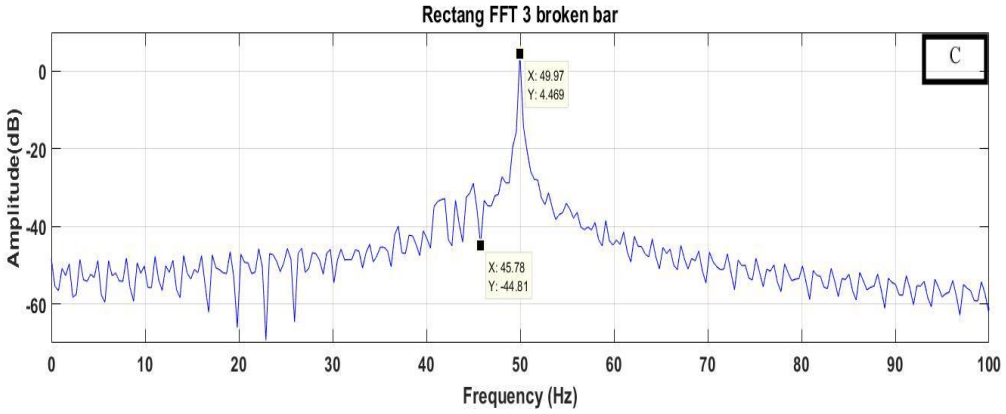

Figure III.8: (a) Spectrum of phase current by Rectangular spectral analysis . during bar failure(three broken bars)

Studied cases	**Estimation results Frequency(Hz)/Amplitude(db)**		
	Spectrum of phase current	***(1-2s)f (Hz)/(db)***	***(1+2s)f (Hz)/(db)***
healthy machine	Rectangular window	0	0
	Hanning window	0	0
	Hamming window	0	0
1 broken bar	Rectangular window	(45.1/-22.67)	(54.93/-28.92)
	Hanning window	(45/-25.65)	(55/-43.58)
	Hamming window	(45/-25.3)	(55/-48.77)
2 broken bar	Rectangular window	(45.1/-30.32)	(54.93/-35.5)
	Hanning window	(41.2/-26.96)	(58.8/-41.85)
	Hamming window	(41.2/-26.93)	(58.8/-43)
3 broken bar	Rectangular window	(45/-44.9)	0
	Hanning window	(41.6/-51.43)	0
	Hamming window	(41.6/-58.12)	0

TABLE III.1: SPECTRUM OF PHASE CURRENT

The power spectrum it is clearly observed when the rotor broken bar is increased then the amplitude of the side lobes around the fundamental frequency is increased. It is also observed that fault frequencies are unique for all the loading condition. All the power spectrums are generated from the motor stator current sometimes it is also called Motor Stator Current Signature analysis (MCSA).

The result of this analysis for a healthy motor is shown in Figures (III-5 a, b, and c),. . Only the line due to the fundamental (50Hz) appears on the spectrum of the stator current. This is quite normal given that the asynchronous motor its model does not present any defect and that the fundamental of the magneto motive force is considered sinusoidal along the air gap.

The stator current spectrum for a break in two consecutive bars is shown in Figures (III-7 a, b, and c). Note the development of substantial amplitudes and lateral frequency lines of the order of (1+-2k g) fs.

As can be seen, the window's function plays a significant part in identifying the frequency components that represent the presence of a defect. Applying this method to the stator current in both a faulted and healthy state yields positive results.

According to the outcomes of the many simulation instances that were run, it can be said that the appearance of the lines is a sign of the presence of the fault, and their amplitude is a measure of how severe the flaw is.

The FFT approach is a very effective and widely used method in the processing of the stationary signal or in permanent diet then that in the time field this signal may lose certain information. On the other hand, the signal of the stator current in transitional regime is rich in frequency information but because of its low duration, it limits the number of acquisition points, which makes the analysis difficult and less precise by the FFT analysis.

In conclusion, standard FFT-based methods cannot be used to detect motor faults or damages in variable load or variable speed applications.

Various solutions have been introduced to reduce problems with proper fault determination under non-standard load conditions.

III.2.4. Wavelet Transform Rotor Fault Diagnosis

A very rich source of information about the faults that frequently occur in asynchronous machines can be found in the signature of the stator current. The wavelet transform is used successfully in the early fault detection of the motor because it has variable window size at different frequencies.

The majority of the diagnostic work for this purpose is based on the examination of the stator current, either in its permanent component or in its transitional part.

In order to identify potential machine problems, we based our study on the use of the CWT and DWT to process and evaluate the current of the machine's stator phase during steady state.

III.2.4.1. The continuous wavelet transform's simulation results

In this part, we suggest utilizing the continuous wavelet transform (CWT) to examine the stator current of the asynchronous motor's signature. In the circumstances of a healthy motor, a broken bar, then two broken bars, then three broken bars at t=2 s, and with the application of a load torque of 3.5 Nm starting at t=0.6 s, the figures below demonstrate the evolution of the coefficients of the current (CWT) of a stator phase for scales between 0 and 64, respectively.

In the process of simulation and examination of the results, we relied on four types of the Wavelet family:

a- Daubechies wavelet (DB).

b- Discrete approximation of the Meyer wavelet (Dmey).

c- Morlet wavelet (Morl).

d- Reverse biorthogonal wavelets (rbio).

III.2.4.1.1. Case of a healthy machine

Figures (III-9 a, b, c, and d), show result continuous wavelet transform (CWT) for a healthy motor.

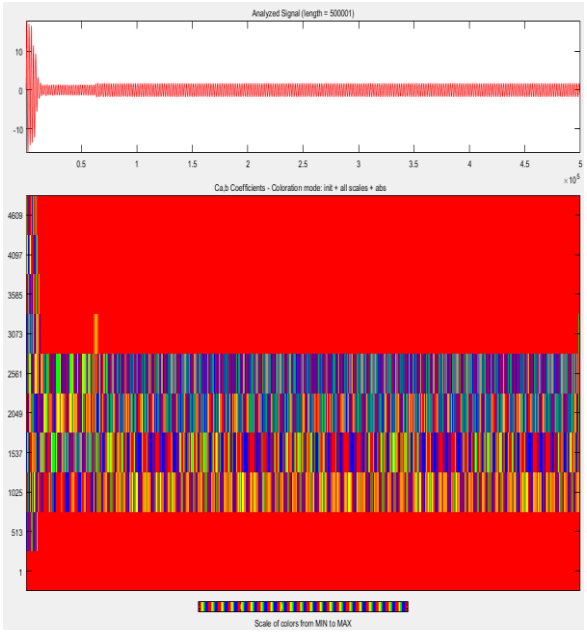

Figure III.9: (a) CWT case of (DB)

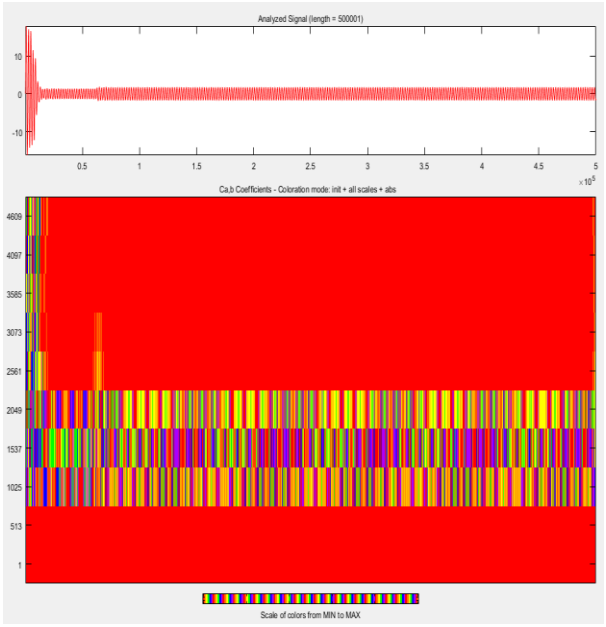

Figure III.9: (b) CWT case of (Dmey)

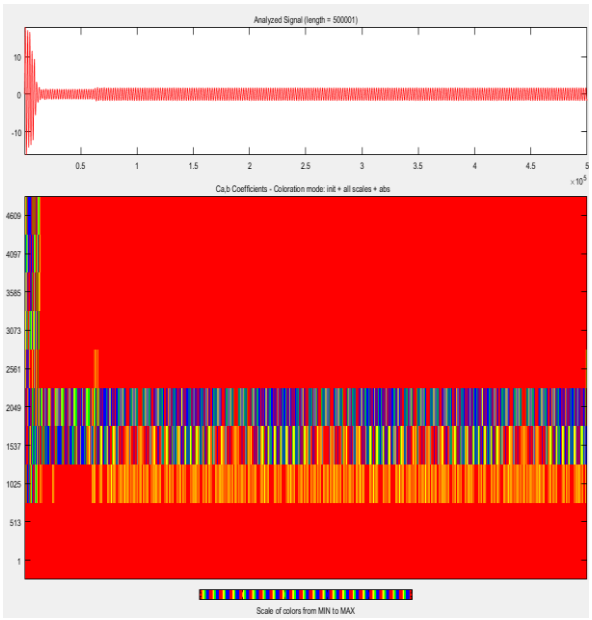

Figure III.9: (c) CWT case of (morl)

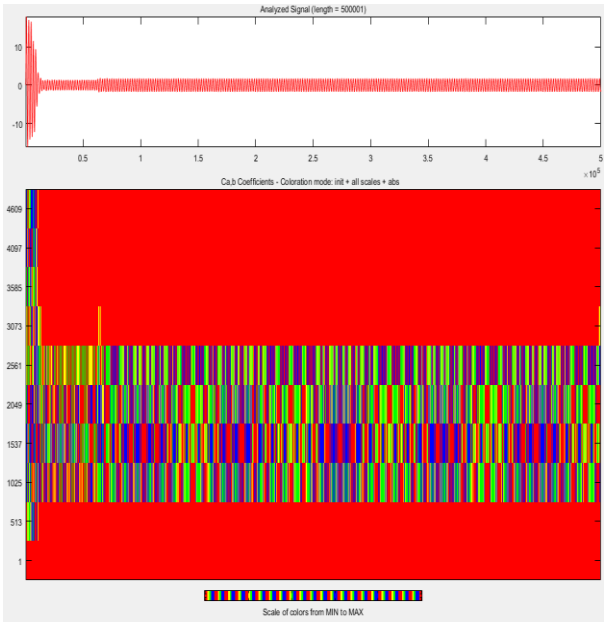

Figure III.9: (d) CWT case of (rbio)

III.2.4.1.2. Case of one broken bar:

The induction motor was first put to the test under duress with one rotor bar destroyed.

Figures (III-10 a, b, c ,and d), show result continuous wavelet transform (CWT) for a motor faults (one broken bar).

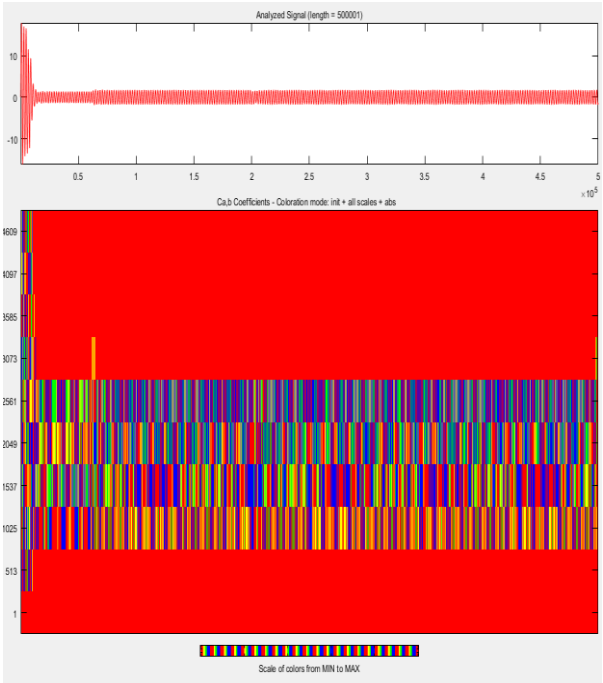

Figure III.10: (a) CWT case of (DB)

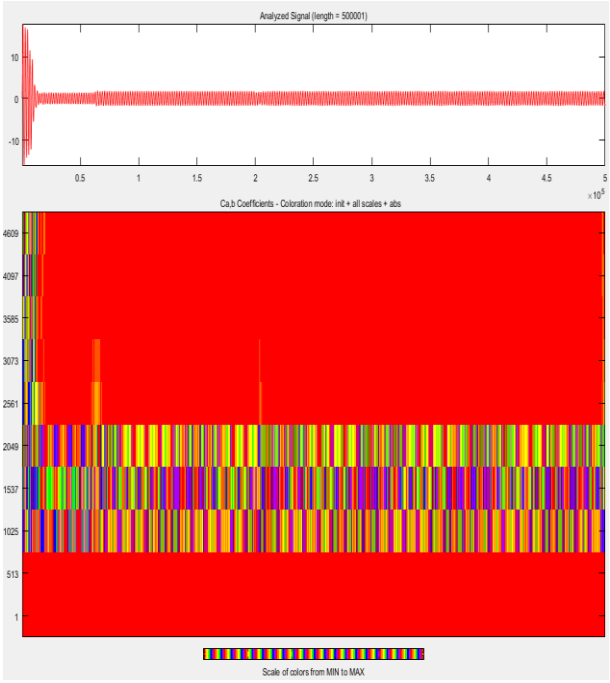

Figure III.10: (b) CWT case of (Dmey)

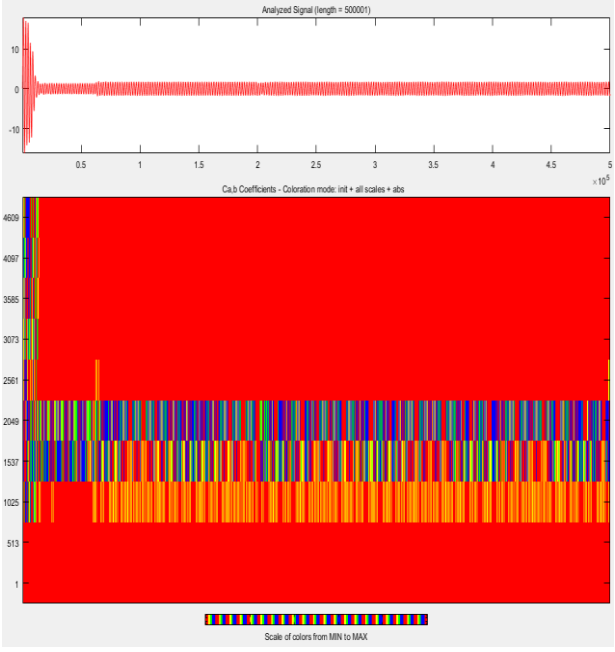

Figure III.10: (c) CWT case of (morl)

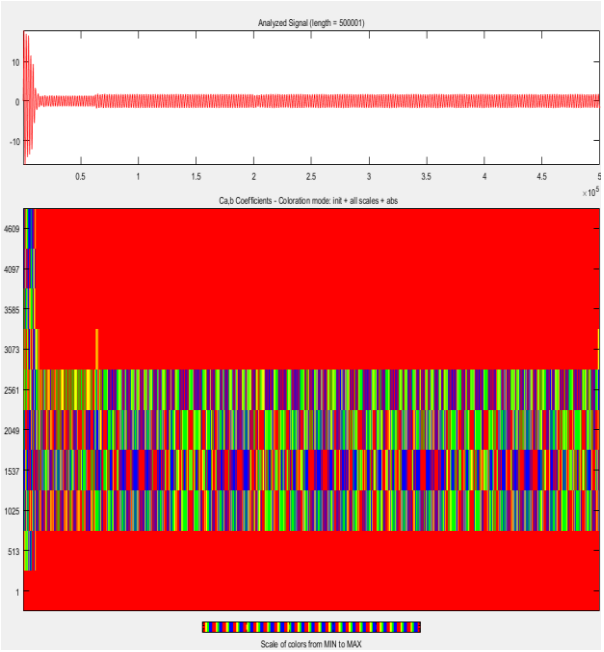

Figure III.10: (d) CWT case of (rbio)

III.2.4.1.3. Case of two broken bars:

The induction motor was second put to the test under duress with two rotor bar destroyed.

Figures (III-11 a, b, c ,and d), show result continuous wavelet transform (CWT) for a motor faults (tow broken bars).

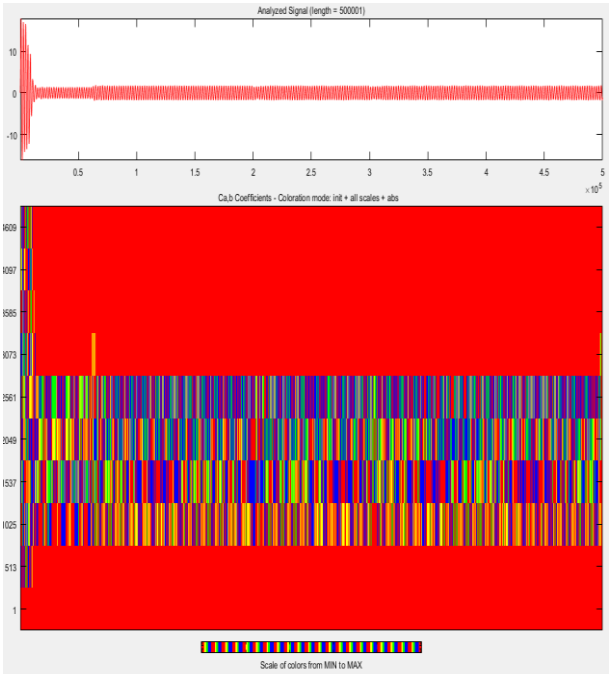

Figure III.11: (a) CWT case of (DB)

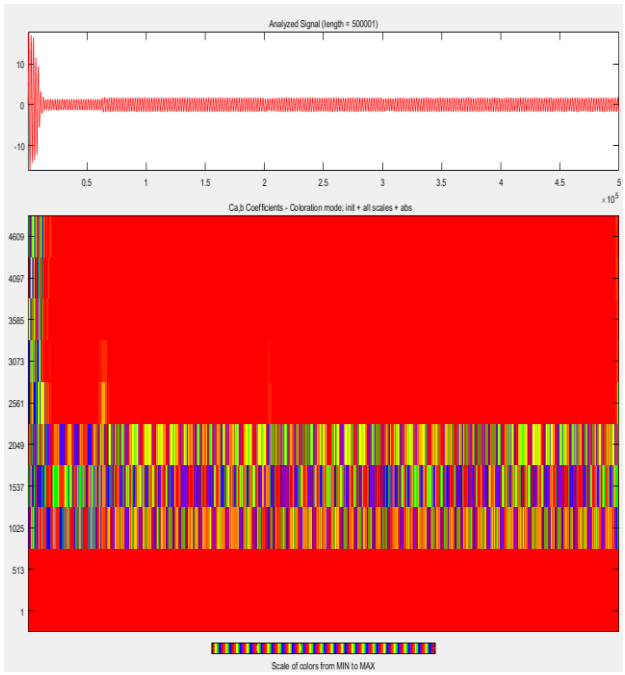

Figure III.11: (b) CWT case of (Dmey)

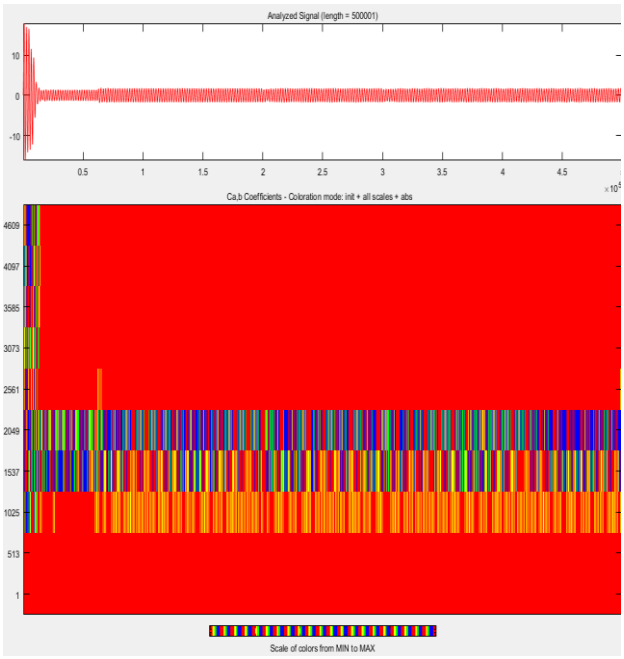

Figure III.11: (c) CWT case of (morl

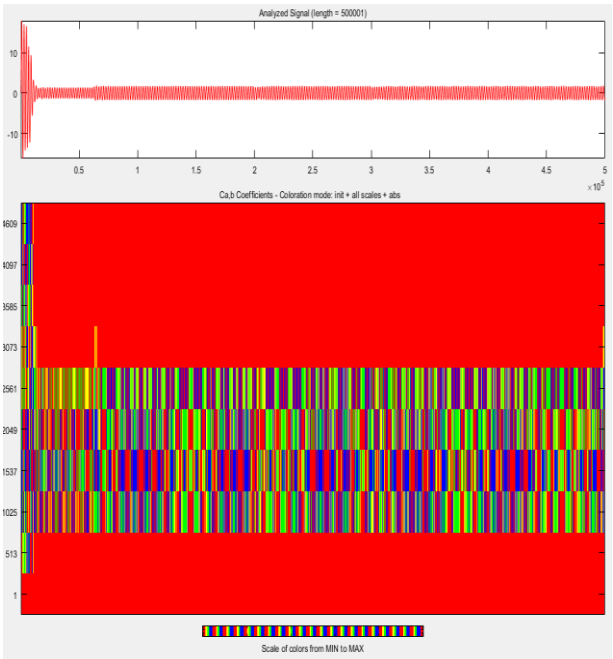

Figure III.11: (d) CWT case of (rbio)

III.2.4.1.4. Case of three broken bars:

The induction motor was third put to the test under duress with three rotor bar destroyed.

Figures (III-12 a, b, c ,and d), show result continuous wavelet transform (CWT) for a motor faults (three broken bars).

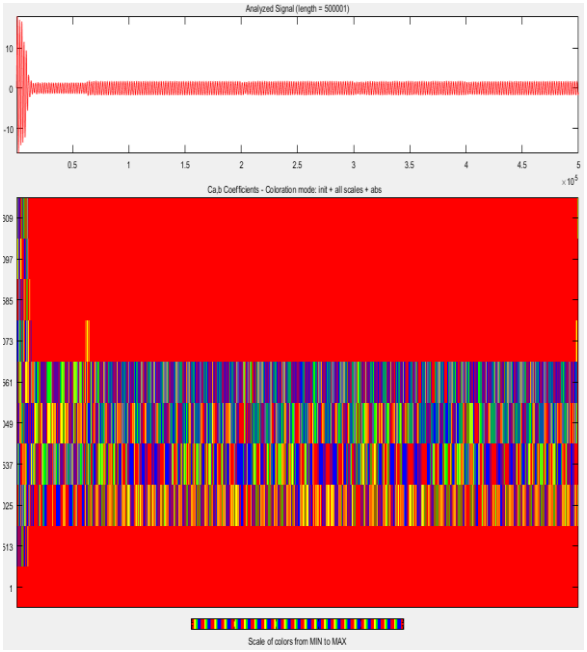

Figure III.12: (a) CWT case of (DB)

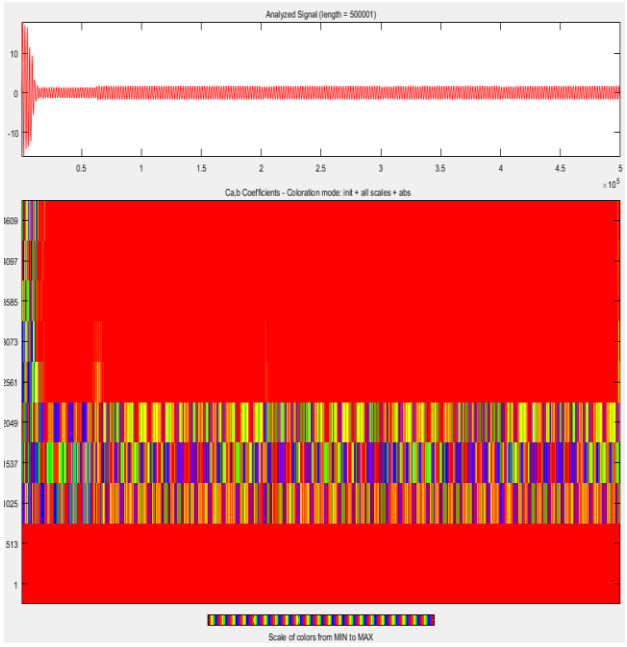

Figure III.12: (b) CWT case of (Dmey)

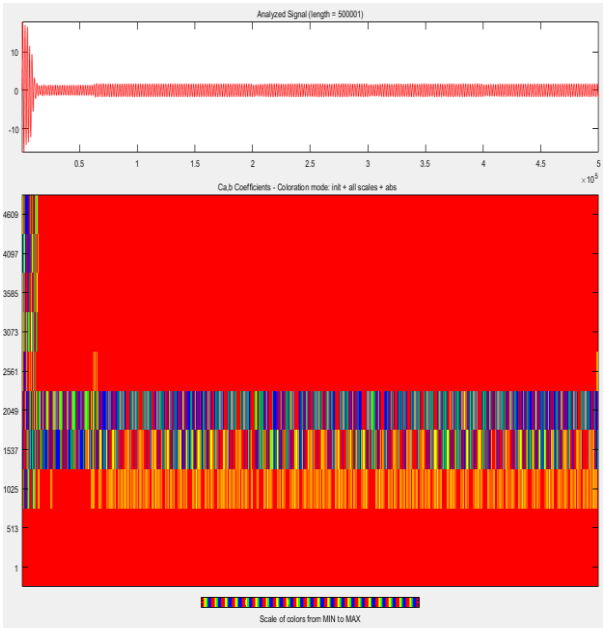

Figure III.12: (c) CWT case of (morl

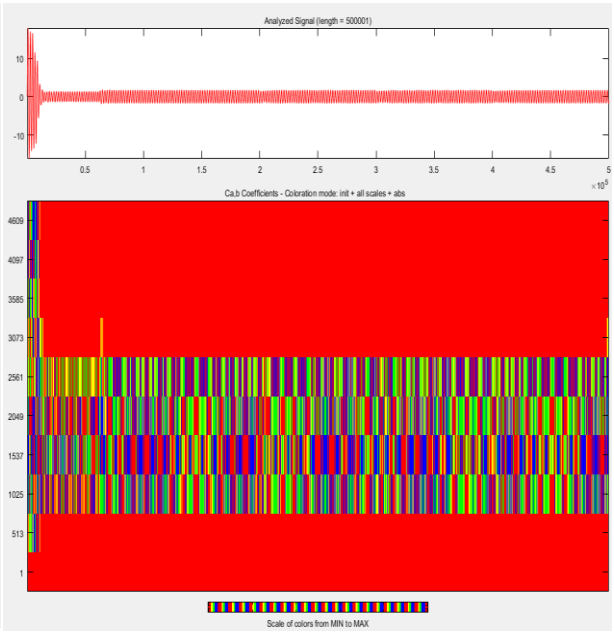

Figure III.12: (d) CWT case of (rbio)

The figures demonstrate the use of continuous wavelet transform (CWT) for stator current for the measurements presented in Figures (III. 9 to III.12).

for the db(04) family and the other families in both a healthy and problematic state of the machine.

Measured using wavelet analysis, the similarity between the signal's fundamental functions (wavelets) and the signal itself is expressed as having the same frequency content. The (CWT) calculated coefficients show how close the signal is to the wave at the current scale.

The current does not alter while the machine is in a healthy state, as opposed to when it is in a damaged one. As the wave coefficients of the kinetic error are stronger than the wave coefficients in the machine's healthy state, we see that the current changes in terms of different degrees of colors and their arrangement in shapes.

These variations show that the wavelet shift may distinguish between the signal components of the healthy and unhealthy motors during the start-up phase. Low frequencies are corresponding to high scales. The higher frequencies match the lower scales.

Figure III. 9 shows the level signals resulting from the wave decay of the stator current to start in a good health condition of the machine, and on the other hand in a defective machine (3 broken bars) Figure III.12 shows the level signals resulting from the wave decay of the stator current .

III.2.4.2. The Discrete Wavelet Transforms simulation results

In order to extract the required features associated to the failure of broken bars at the rotor in varying degrees of severity (one broken bar to three broken bars), the stator current of the phase Isa in regime stationary was analyzed by a technical DWT wavelet.

The original signal is decomposed at the eleventh level with a sample frequency of 5 kilohertz.

At the eleventh level of breakdown, the original signal s is broken down. The signal is divided into two signals: a detailed signal and an approximation signal. Every transmission has a unique frequency range.

While the approximate signal provides low frequency information, the detailed signal contains information at higher frequencies. Here, low frequency information has been extracted using 11 level decomposition. High degrees of decomposition are advised.

In the process of simulation and examination of the results, we relied on four types of the Wavelet family:

a- Biorthogonal wavelets (bior). b- Fejer-Korovkin wavelets (fk).

c- Haar wavelet (haar). d- Symlets wavelets (sym).

III.2.4.2.1. Case of a healthy machine

Figures (III-13 a, b, c, and d), show result Discrete Wavelet Transforms Description (DWT) for a healthy motor.

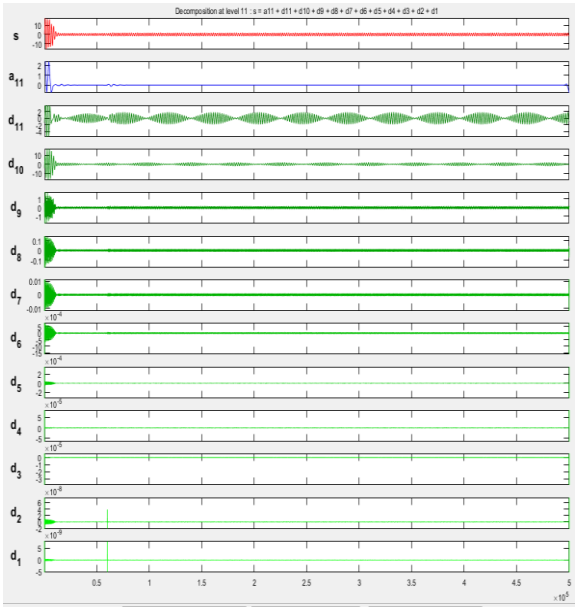

Figure III.13: (a) DWT case of (bior)

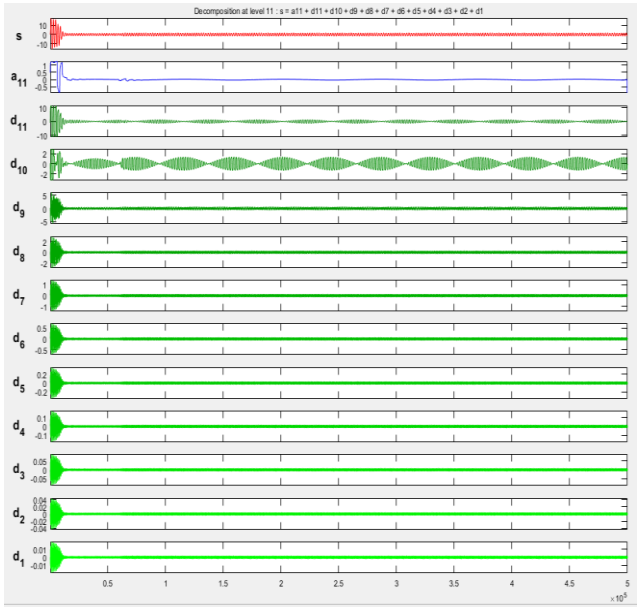

Figure III.13: (b) DWT case of (fk)

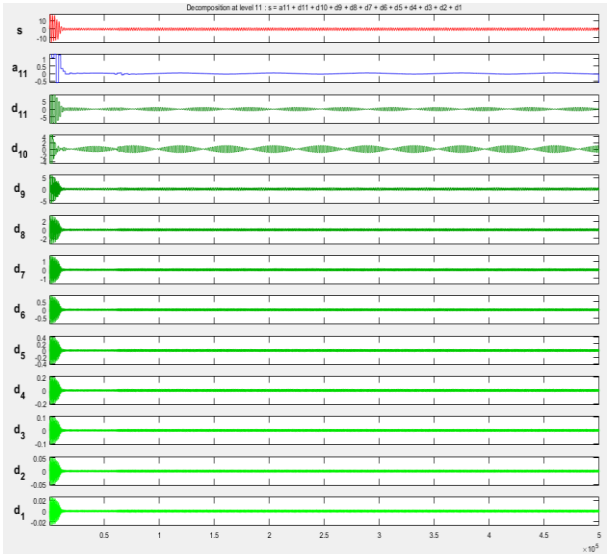

Figure III-.13: (c) DWT case of (haar)

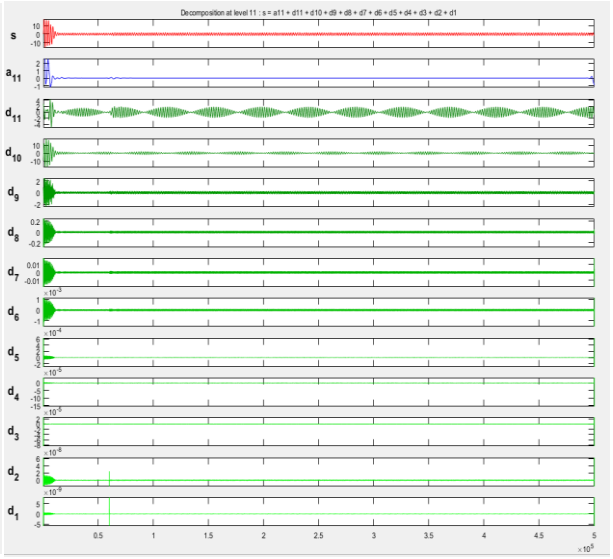

Figure III.13: (d) DWT case of (sym)

III.2.4.2.2. Case of one broken bar:

The induction motor was first put to the test under duress with one rotor bar destroyed.

Figures (III-14 a, b, c and d), show results Discrete Wavelet Transforms Description (DWT) for a motor faults (one broken bar).

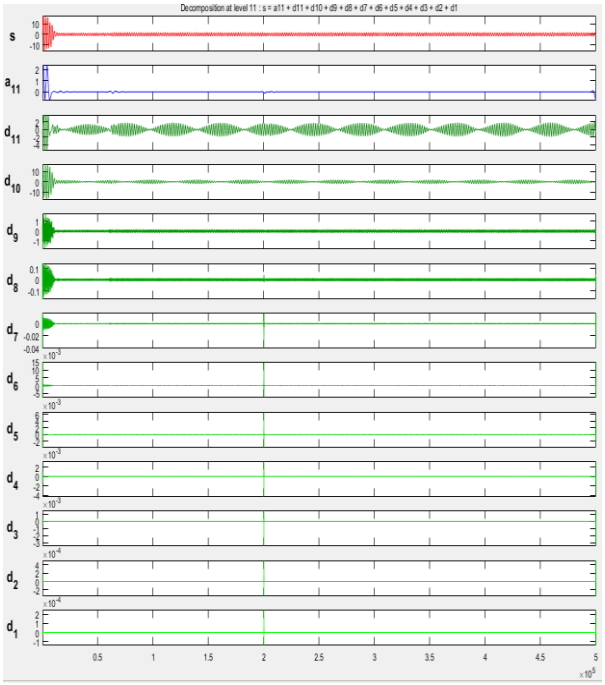

Figure III.14: (a) DWT case of (bior)

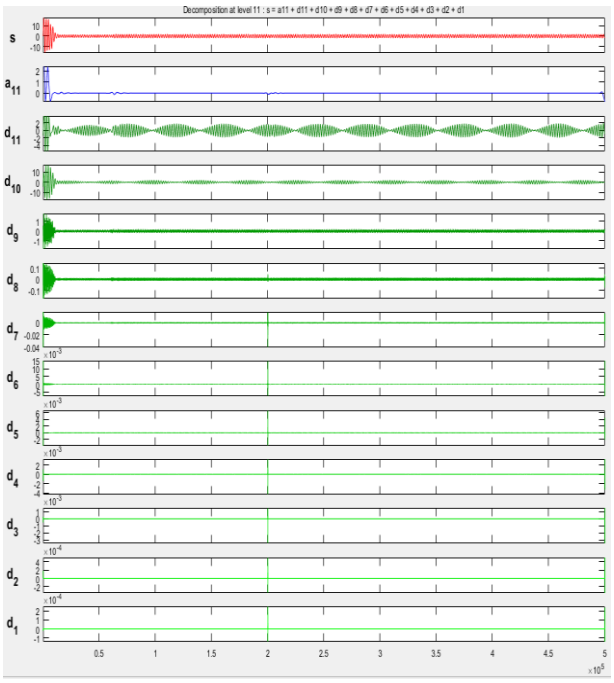

Figure III.14: (b) DWT case of (fk)

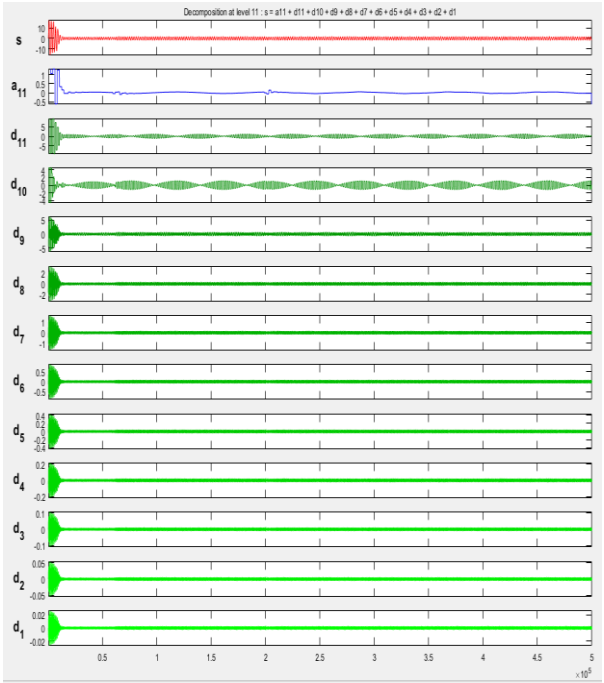

Figure III.14: (c) DWT case of (haar)

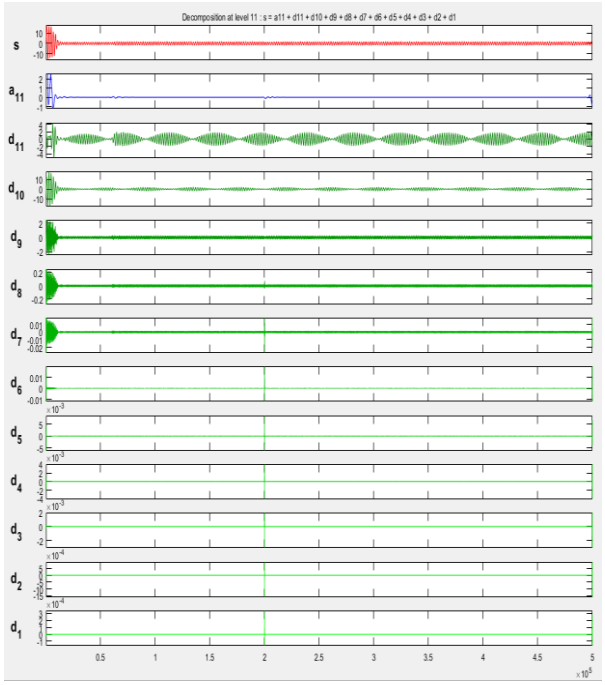

Figure III.14: (d) DWT case of (sym)

III.2.4.2.3. Case of two broken bars:

The induction motor was second put to the test under duress with two rotor bars destroyed.

Figures (III-15 a, b ,c , and d),, show results Discrete Wavelet Transforms Description (DWT) for a motor faults (two broken bars).

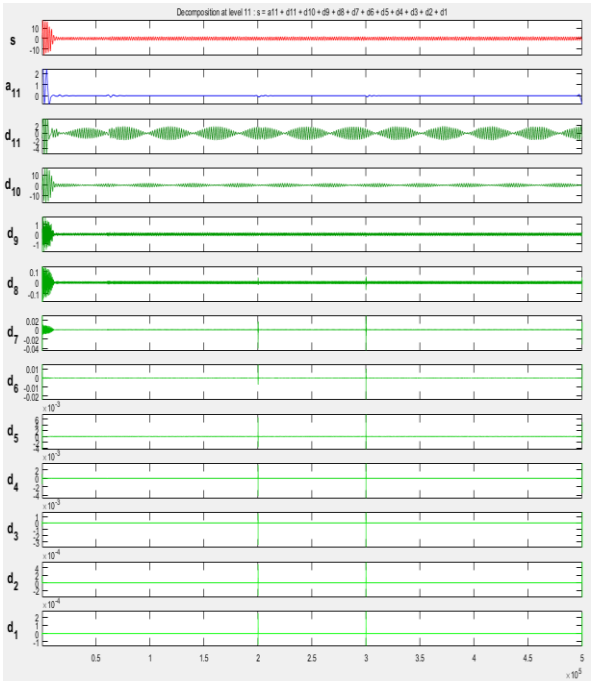

Figure III.15: (a) DWT case of (bior)

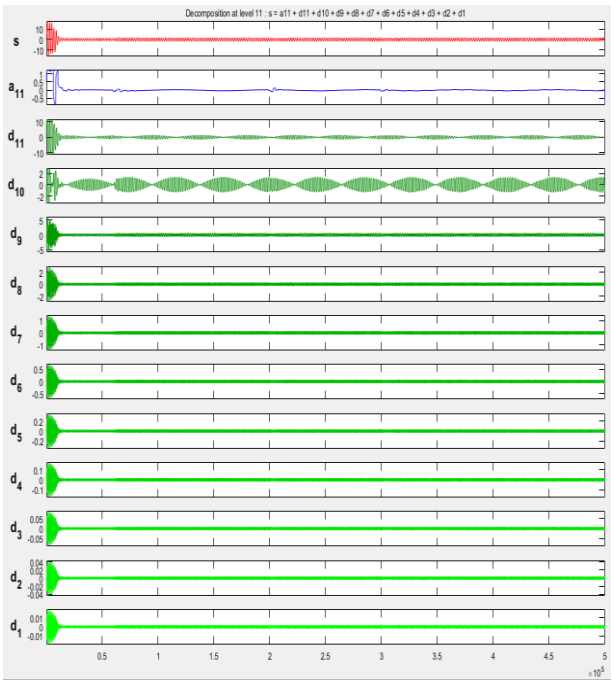

Figure III.15: (b) DWT case of (fk)

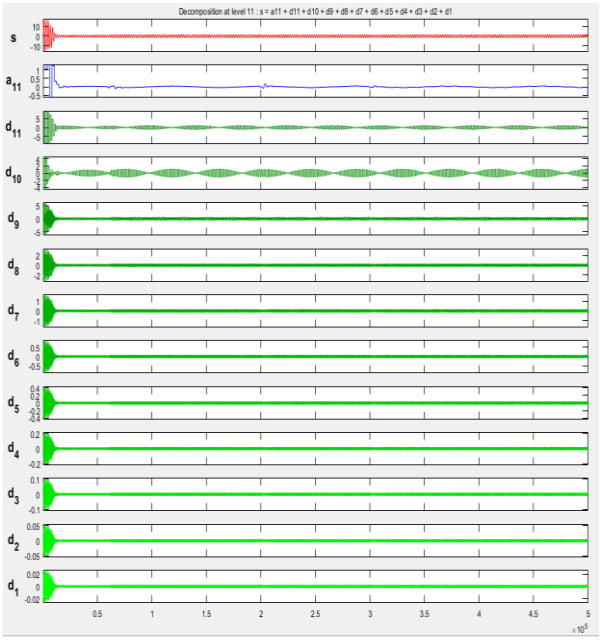

Figure III.15: (c) DWT case of (haar)

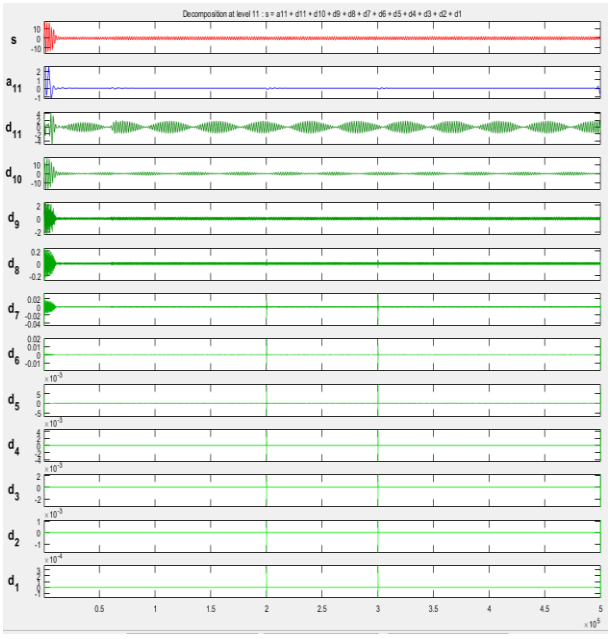

Figure III.15: (d) DWT case of (sym)

III.2.4.2.4. Case of three broken bars:

The induction motor was third put to the test under duress with three rotor bars destroyed.

Figures (III-16 a, b ,c , and d), show results Discrete Wavelet Transforms Description (DWT) for a motor faults (three broken bars).

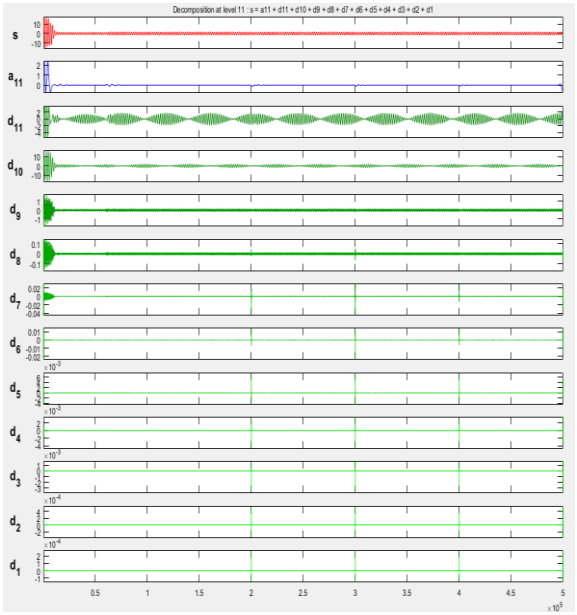

Figure III.16: (a) DWT case of (bior)

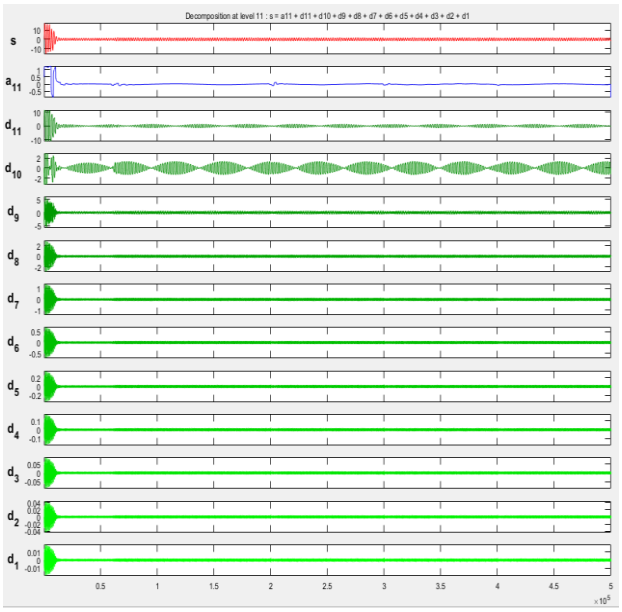

Figure III.16: (b) DWT case of (fk)

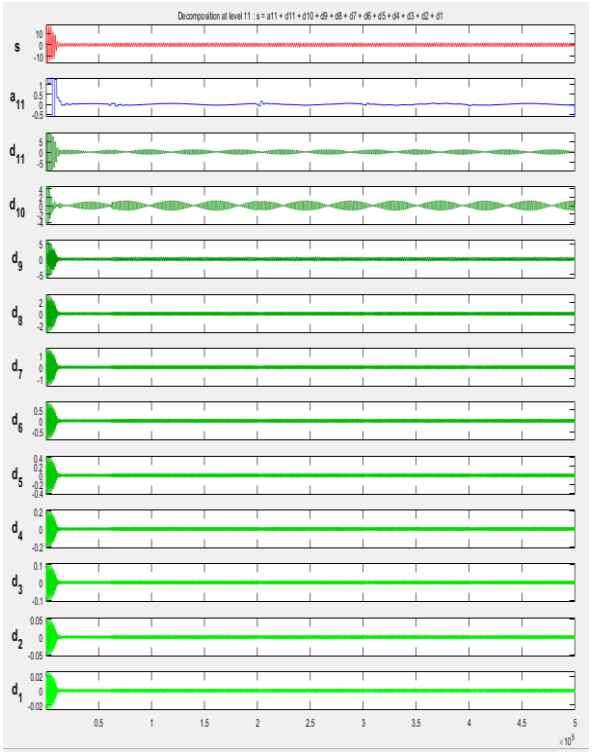

Figure III.16: (c) DWT case of (haar)

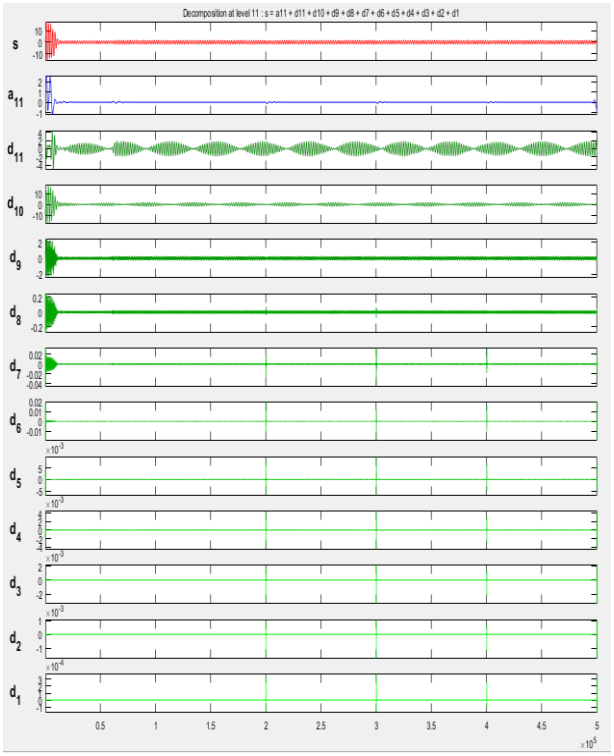

Figure III.16: (d) DWT case of (sym)

The various induction machine circumstances (healthy, loaded with a defect and one broken bar to three broken bars) demonstrate the development of the signals.

This increase in the signals (d11, d10, and a11) is due to the various types of faults that are affecting the corresponding frequency bands, which show the detail signals of d8, d9, and the approximation a9 obtained by multi-level decomposition of the stator current (Isa).

In the instance of 3 damaged bars, Figures (III-16 a, b, c and d) shows a noticeable increase in oscillations. The bands [25-50Hz] correspond to the signals that are most adversely impacted, and this explains why there is a sideband around the fundamental frequency in the stator current spectrum .

In order to accurately detect the rotor bar problems, the approximation signal for the eleventh level has a frequency range of 2.44 to 1.22, which is very low frequency.

In both instances, the signal is different and may be distinguished by the disruptions that manifest at high levels, it is generally seen.

It is noticed that the tenth and eleventh levels are superior to the ninth level, which does not significantly alter, in terms of clarity and meaningful information.

Conclusion: When a fault manifests, the discrepancies in the DWT coefficients are greater than they are under a Healthy Motor situation.

This effect is interpreted by the change in the relative energy associated with each level of decomposition in the band signals in the defective case relative to the healthy case, allowing us to distinguish the healthy machine from the defective ones.

The numerous sorts of defects are having an impact on the respective frequency bands, which is why the signals are increasing.

III.3. results of the the multi-winding model reduced size (with inverter)

We can study the evolution of temporal elements such as stator currents, torque and speed when the rotor cage shows no failure; No-load starting at nominal voltage with a balanced three-phase sinusoidal power supply provided by a three-phase inverter. The simulation is carried out over a period of 5 sec with at the instant t = 0.6 sec the machine is subjected to a resistive torque Cr = 3.5 N.m he simulation of the model allowed us to obtain the different characteristics of stator current, speed and electromagnetic torque; they are shown in Figures respectively (III.18.a, b, c, and d)

Then one, two, and three rotor bar is broken for fault analysis and broken rotor bar detection the simulation results they are shown in Figures respectively (III.19.a, b, c, and d) to (III.21.a, b, c, and d).

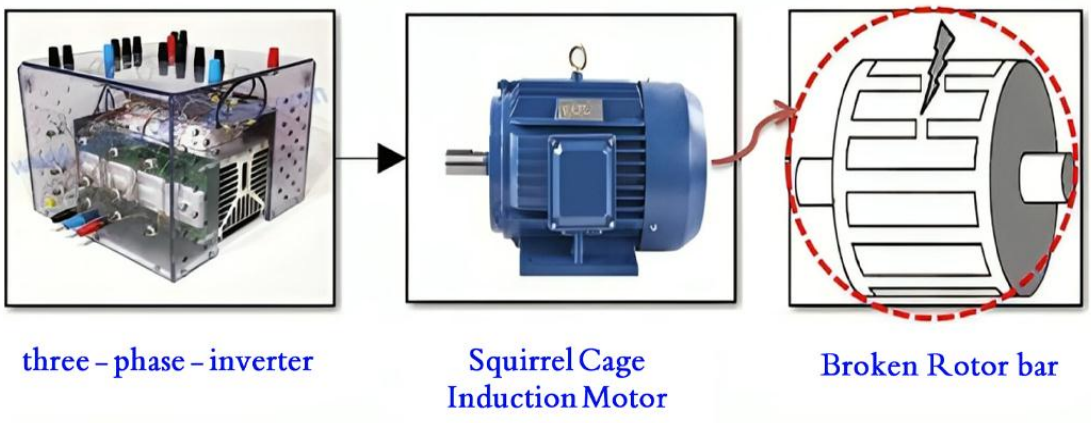

Figure III.17: Model Simulink of the induction motor with fault

III.3.1. Case of a healthy machine :

In this part, a scaled-down simulation of the multi-winding model with inverter is provided by a squirrel cage induction motor.

The accuracy of the model was evaluated throughout a simulation duration of five seconds. A torque of 3.5 Nm was applied to the machine at time t = 0.6 seconds.

When the rotor cage exhibits no signs of failure, it is possible to study the evolution of temporal parameters including stator currents, torque, and speed as well as the current in the

machine's rotor bars. The research's conclusions were shown using the number ten bar. Figures (III.18.a, b, c, and d) show the evolution of the findings.

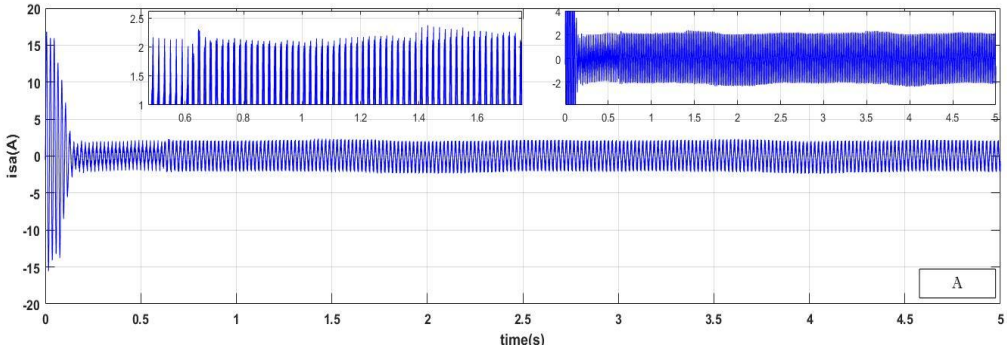

Figure III.18: (a) Evolution of phase a stator current (isa) at no load, on load (healthy).

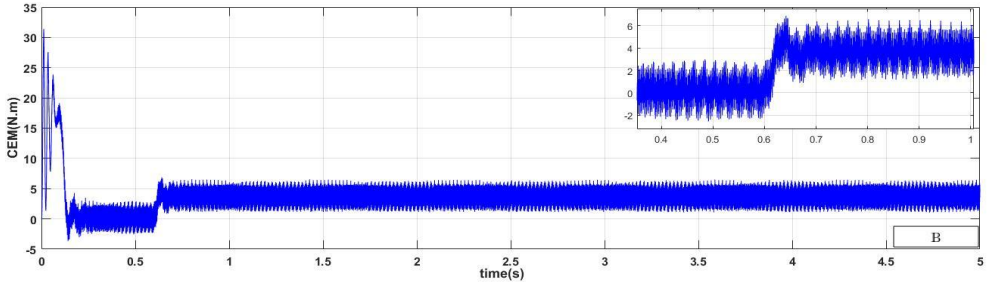

Figure III.18: (b) Evolution of the electromagnetic torque on starting, under load (healthy).

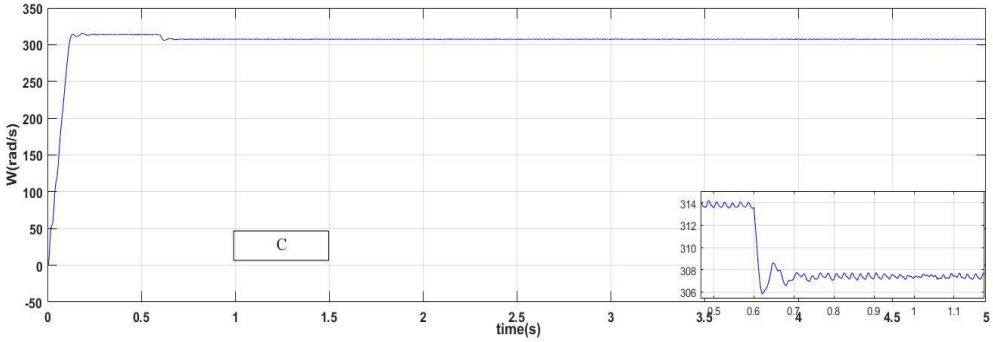

Figure III.18: (c) Rotational speed at start, under load (healthy).

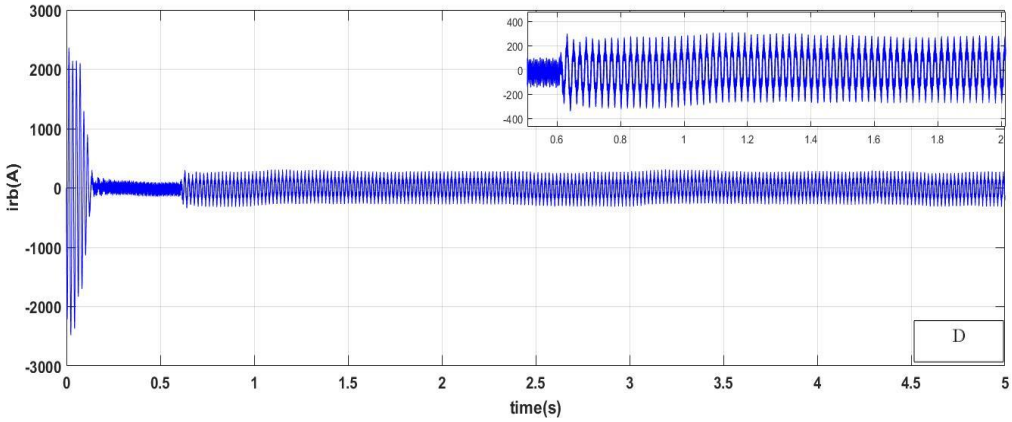

Figure III.18: (d) Evolution of phase a rotor current (irb) bar number ten ,at no load, on load (healthy)

III.3.2. Result of simulation with machine faults:

III.3.2.1. Case of one broken bar:

First, a damaged rotor bar was used to test the induction motor under pressure. In the study, a frequency domain illustration is provided for each stator current.

The machine absorbs a phase as a result of the bar breaking, as shown in Figures (III.19 a, b, c, and d).

The simulation, which lasts for five seconds, applies a resistive torque of 3.5 N.m to the machine at the point t = 0.6 sec.

By increasing the resistance by 11 times, we replicate the first bar's failure at time t=(2)s.

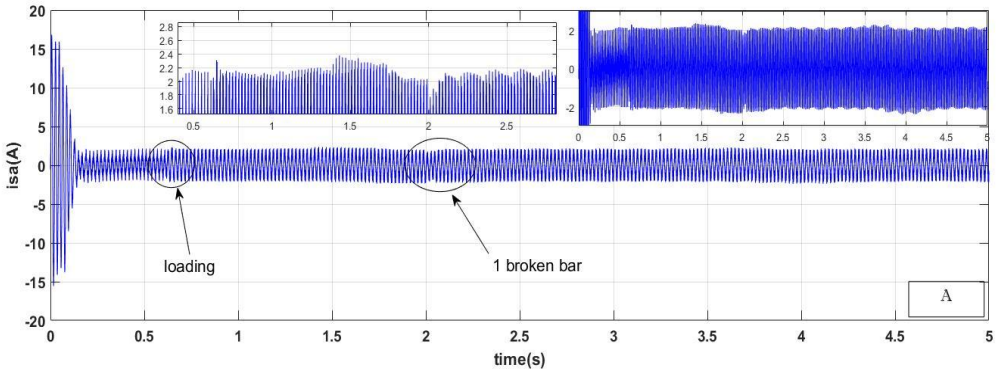

Figure III.19: (a) Evolution of phase a stator current (isa) for one broken bar

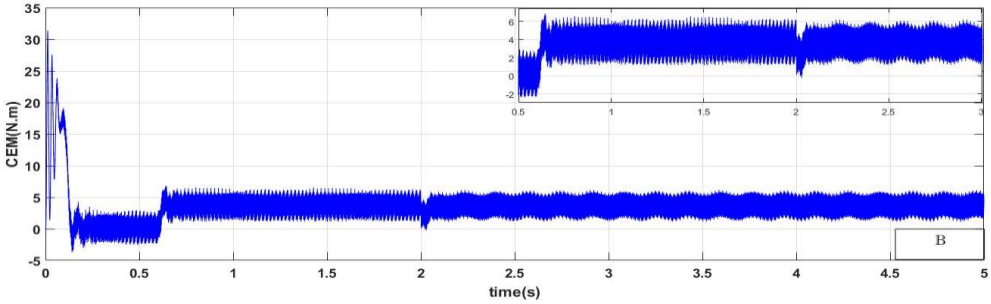

Figure III.19: (b) Evolution of the electromagnetic torque with one broken bar

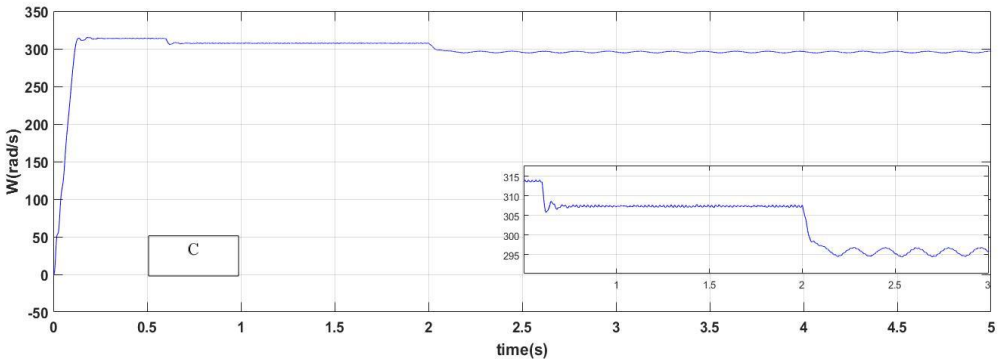

Figure III.19: (c) Rotation speed with 1 broken bar.

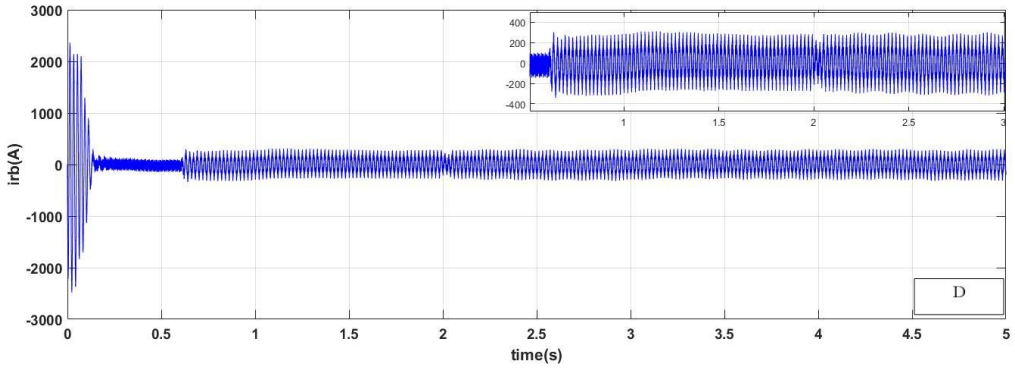

Figure III.19: (d) Evolution of phase a rotor current (irb) bar number ten , with one broken bars

III.3.2.2. Case of two broken bars:

Second, an induction motor stress test was performed using two broken rotor bars. The global quantities (the currents, the electromagnetic torque, and the speed) are shown in the research using the frequency domain.

Figures (III.20 a, b, c, and d) illustrate how a phase that the machine absorbs is impacted by the breaking of two nearby bars (bars number one and number two).

At the time t = 0.6 sec. of the simulation, which lasts for five seconds, the machine is given a resistive torque of 3.5 N.m. We replicate the failure of the first bar at time t= (2) s and the failure of the second bar at time t= (3) s by raising the resistance by 11 times.

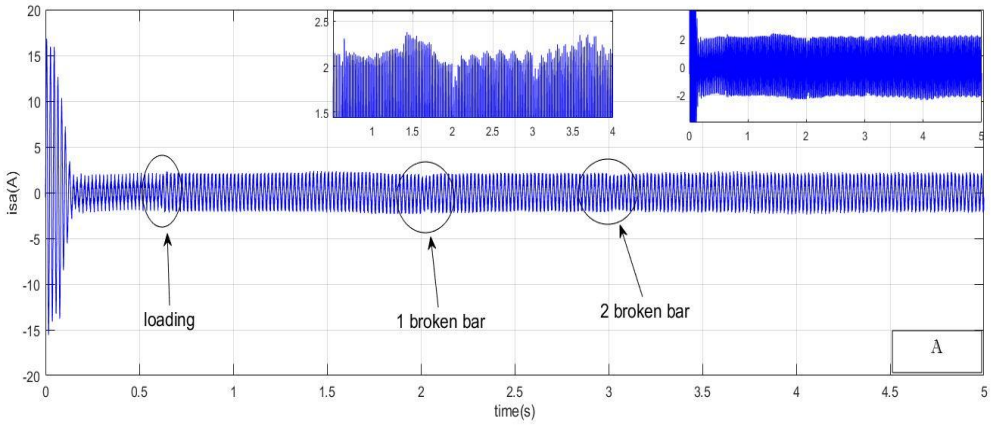

Figure III.20: (a) Evolution of phase a stator current (isa) for two broken bars

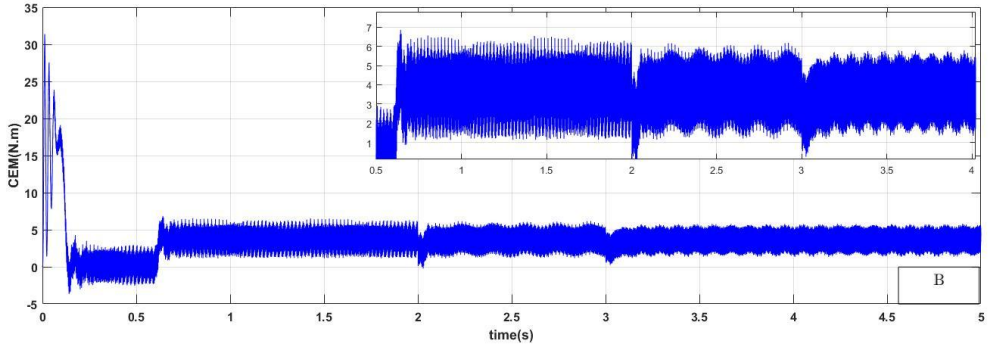

Figure III.20: (b) Evolution of the electromagnetic torque with two broken bars

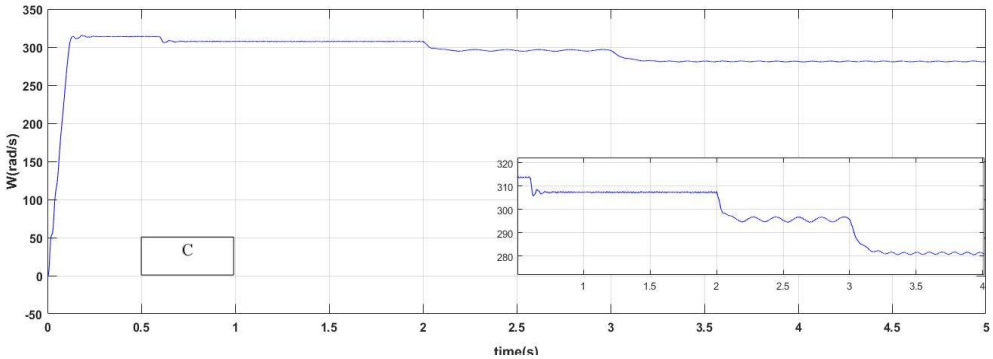

Figure III.20: (c) Rotation speed with two broken bars.

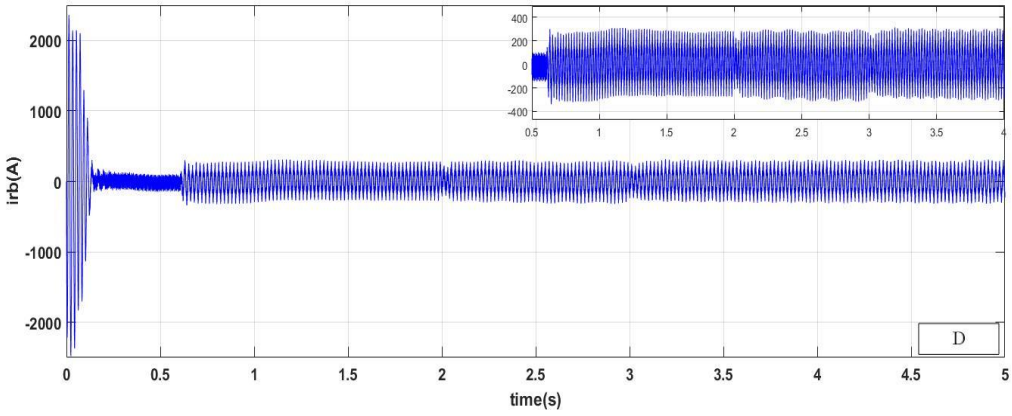

Figure III-20: (d) Evolution of phase a rotor current (irb) bar number ten , with two broken .bars.

III.3.2.3. Case of three broken bars:

Third, the effects of three bar breaking on a phase that the machine absorbs are shown in Figures (III.21 a, b, c, and d).

At the time t = 0.6 sec. of the simulation, which lasts for five seconds, the machine is given a resistive torque of 3.5 N.m. It is possible to successfully duplicate the failures of the first bar at time t=(2) s, the second bar at time t=(3) s, and finally the third bar at time t=(4) s.

Three consecutively broken rotor bars were used in a stress test on the induction motor.

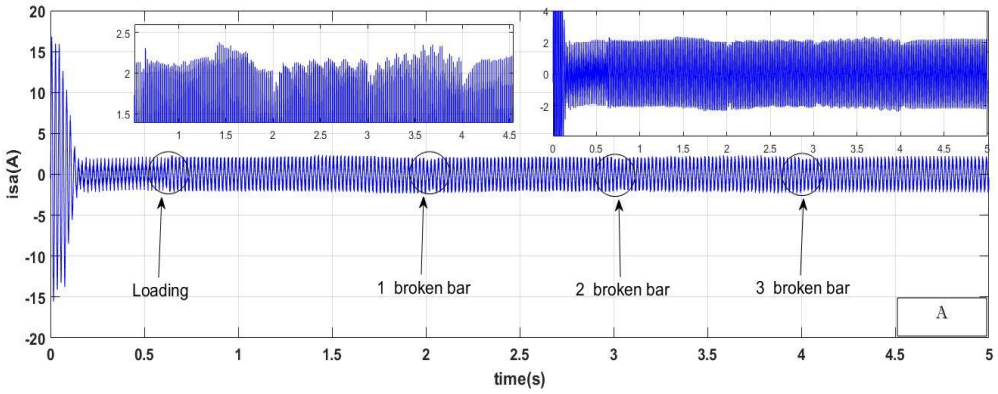

Figure III.21: (a) Evolution of phase a stator current (isa) for three broken bars

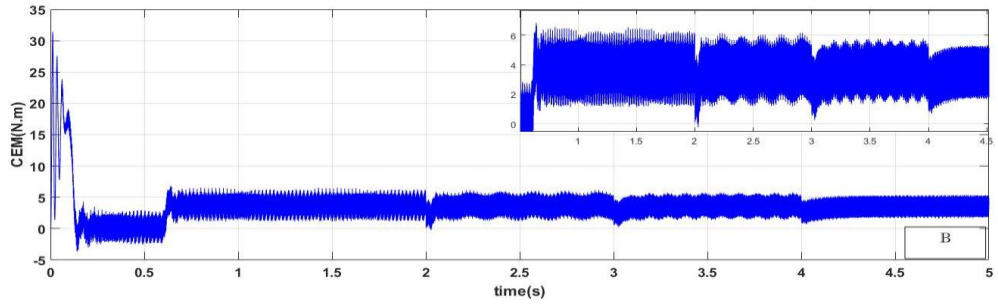

Figure III.21: (b) Evolution of the electromagnetic torque with three broken bars

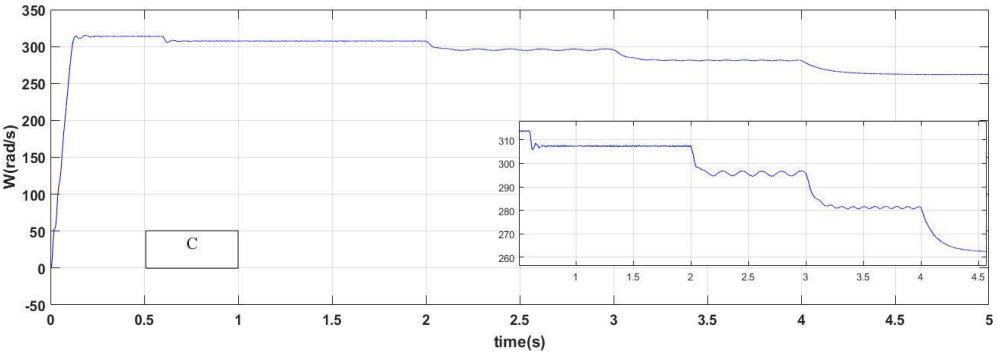

Figure III.21: (c) Rotation speed with three broken bars

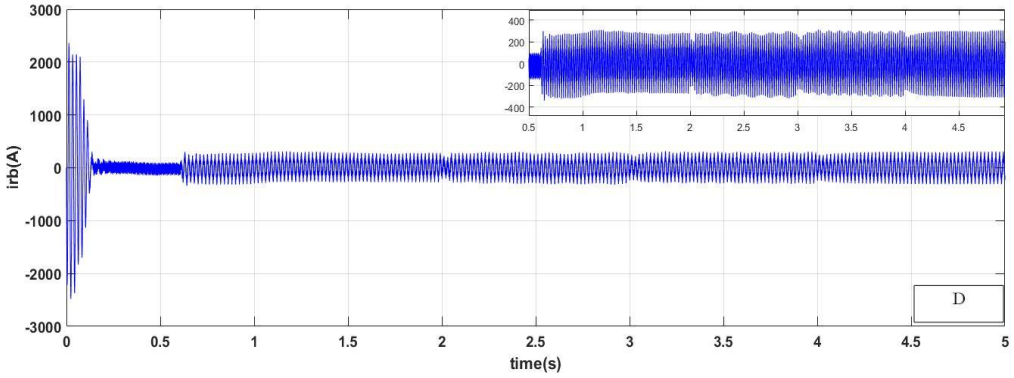

Figure III.21: (d) Evolution of phase a rotor current (irb) bar number ten , with three broken bars.

Figures (III.18.a, b, c, and d) shows that the stator currents, electromagnetic torque, and rotational speed all exhibit constant evolution that is both excellent and stable, causing the speed of the curve to rise until it reaches its peak before settling.

In our research, we found that when three neighboring bars are broken, the speed of rotation progressively slows while the ripples also get larger because the continuous current in the cover is proportional to the number of broken bars. This is shown in Figures (III.19 a, b, c, and d) to Figures (III.21 a, b, c, and d) . The electromagnetic torque grows in exact proportion to the ripples.

We were able to determine the various properties of the stator current, speed, and electromagnetic torque using the model's simulation.

The illustrations demonstrate that when a rotor failure results in broken bars, similar undulations develop on each of the three-stator currents, and the size of these undulations is proportional to the number of broken bars. Keep in mind that as there are more broken bars, the oscillations' amplitude grows.

Similar to this, the electromagnetic torque and speed also exhibit ripples due to the rotor defect. The torque ripples cause the engine to vibrate more and hasten the engine's degeneration.

III.3.3 Fast Fourier Transform (FFT)

We notice here from Figures (III.22 a, b, and c) that the spectral stator current in the healthy state does not register any side line around the base line at 50 Hz.

when the machine is loaded, the speed reaches the nominal value and then decreases slightly so that the torque tends to the value of the load torque. It also shows us additional side lines around the base line fs = 50Hz at frequencies (1±2ks)fs.

When analyzing the speed ripple effect, other frequency components of stator current due to rotor asymmetry were observed around the fundamental at the following frequencies.: fb=(1+2ks)fs

As in in Figures (III.23 a, b, c, and d) to Figures (III.25 a, b, c, and d), displays the harmonic amplitude's increase. as proof that a number of essential criteria are met The emergence of two lateral components with frequencies (1 + 2s)f and (1 - 2s)f to the left and right of the

fundamental f is caused by the existence of a broken bar fault, and the degree of gravity of the fault line amplitudes is (1+2ks)f, suggesting the presence of a two-bar breaking fault.

III.3.3.1 Case of a healthy machine:

Figures (III-22 a, b, and c), show The result of stator current spectral analysis for a healthy motor.

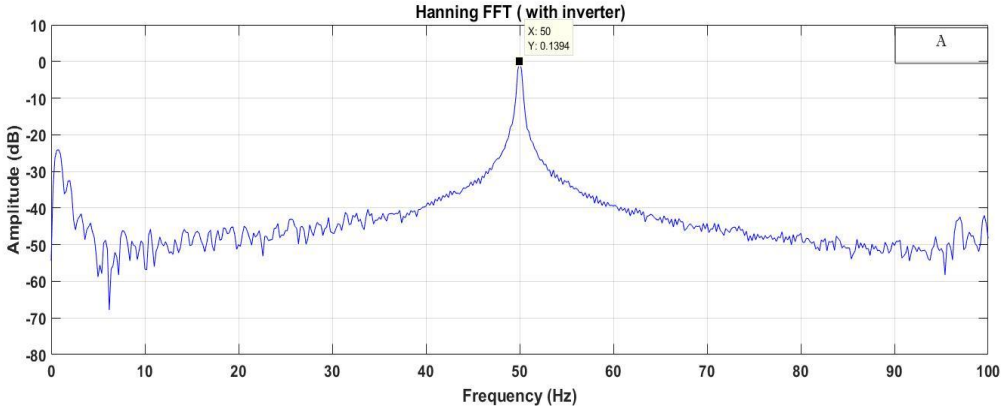

Figure III.22: (a) Spectrum of phase current by hamming spectral analysis .At start-up, under load

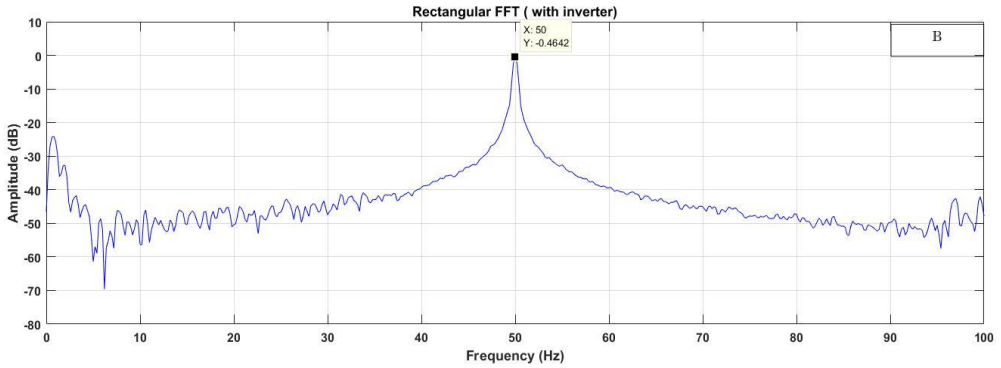

Figure III.22: (b) Spectrum of phase current by hanning spectral analysis .At start-up, under load

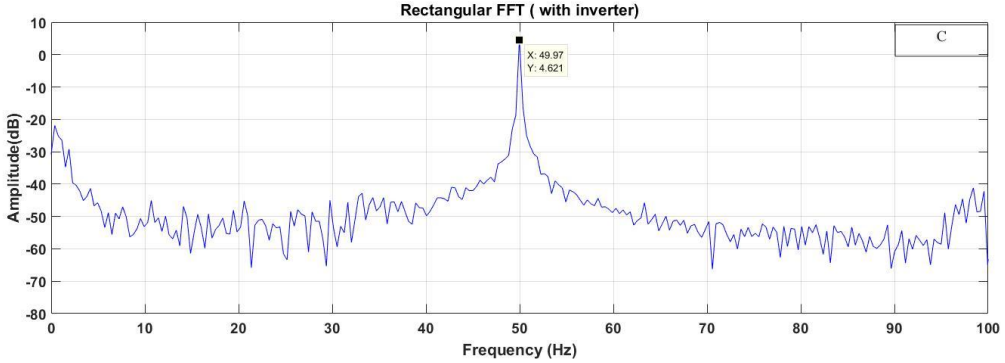

Figure III.22: (c) Spectrum of phase current by Rectangular spectral analysis .At start-up, under load.

III.3.3.2 Case of one broken bar:

The induction motor was first put to the test under duress with one rotor bar destroyed.

Figures (III-23 a, b, and c), show the result of stator current spectral analysis for a motor faults (one broken bar).

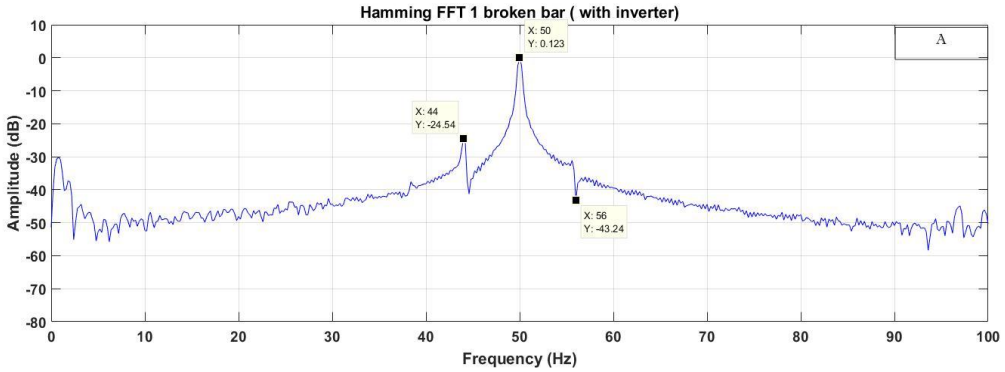

Figure III.23: (a) Spectrum of phase current by hamming spectral analysis . during bar failure(one broken bar)

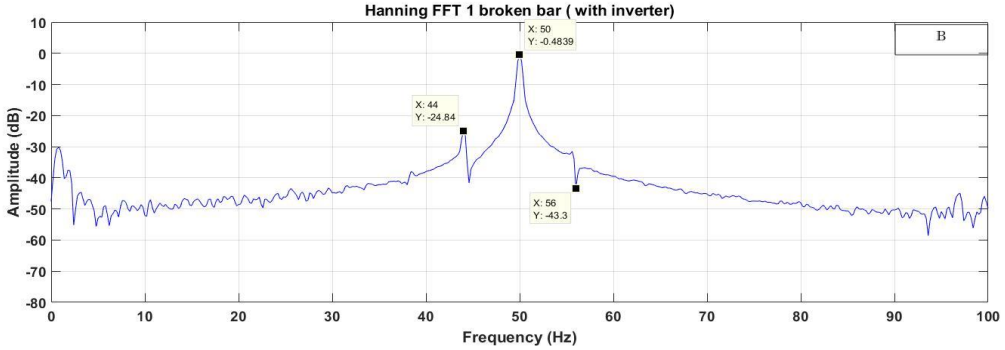

Figure III-.23: (b) Spectrum of phase current by hanning spectral analysis . during bar failure(one broken bar)

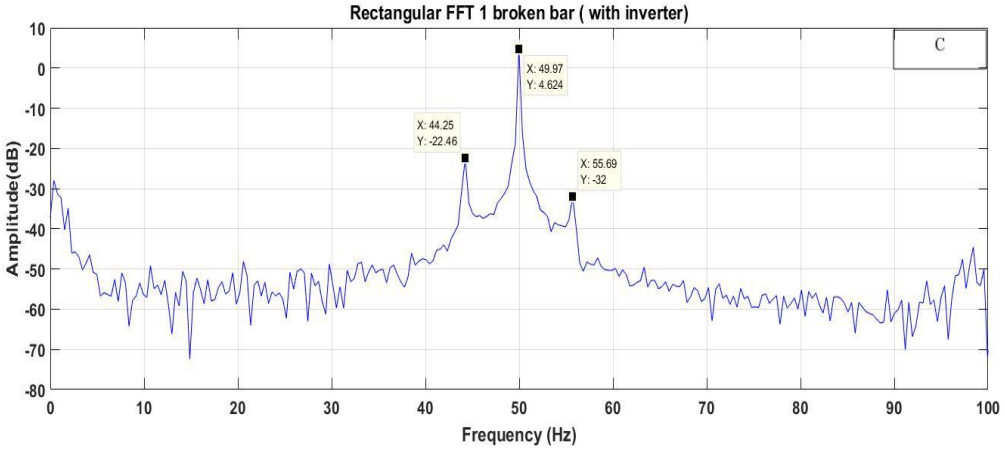

Figure III.23: (c) Spectrum of phase current by Rectangular spectral analysis . during bar failure(one broken bar)

III.3.3.3 Case of two broken bars:

The neighboring rotor bars (bars number one and Number two) were damaged during the second time the induction motor was put under stress.

The results of a stator current spectrum analysis for a motor defect (two broken bars) are shown in Figures (III-24a, b, and c).

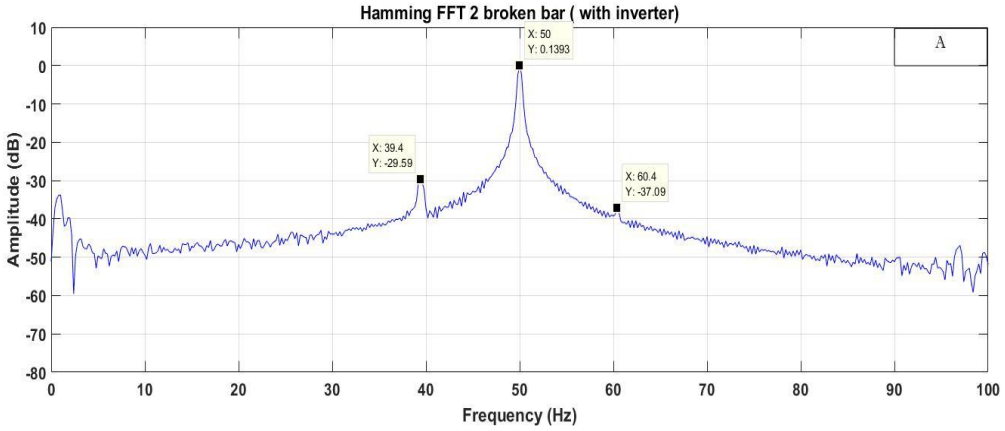

Figure III.24: (a) Spectrum of phase current by hamming spectral analysis . during bar failure(two broken bars)

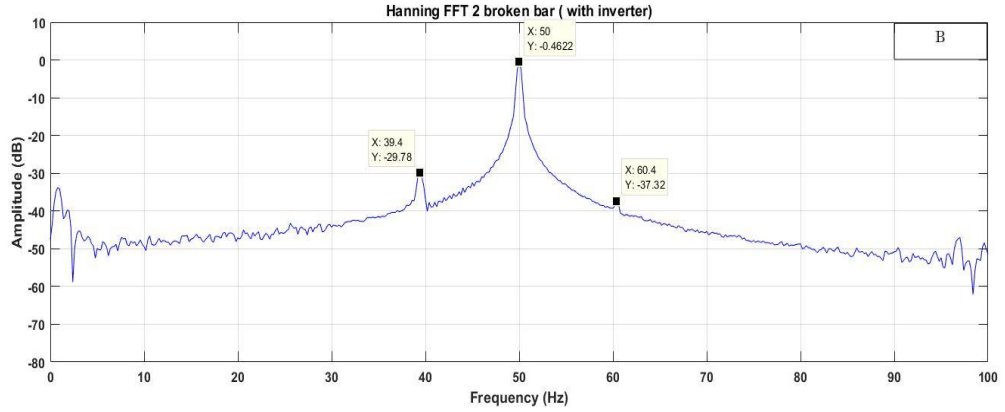

Figure III.24: (b) Spectrum of phase current by hanning spectral analysis . during bar failure(two

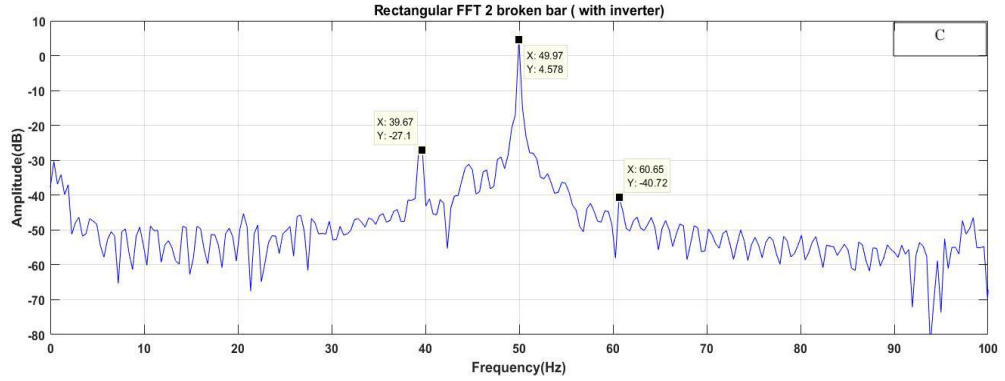

Figure III.7: (c) Spectrum of phase current by Rectangular spectral analysis . during bar failure(two broken bars)

III.3.3.4 Case of three broken bars:

The results of a stator current spectrum analysis for a motor defect (three broken bars) are shown in Figures (III-25 a, b, and c).

The neighboring rotor bars (bar number one, bar number two and bar number three) were damaged during the third time the induction motor was put under stress.

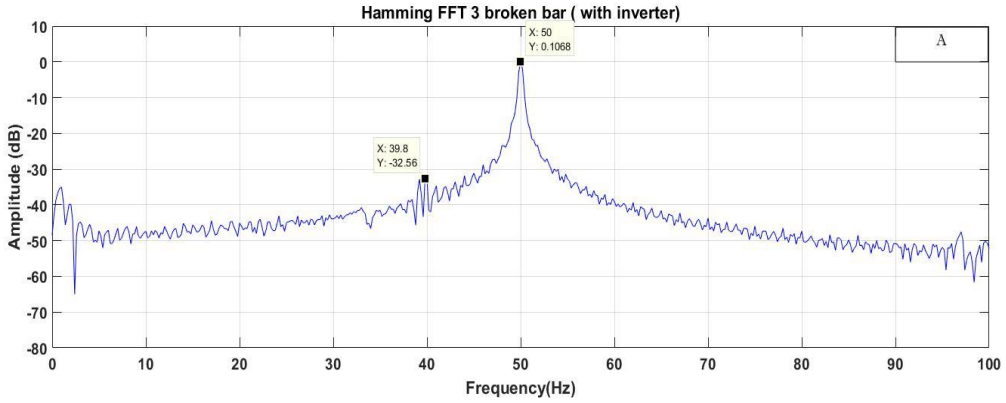

Figure III.25: (a) Spectrum of phase current by hamming spectral analysis . during bar failure(three broken bars)

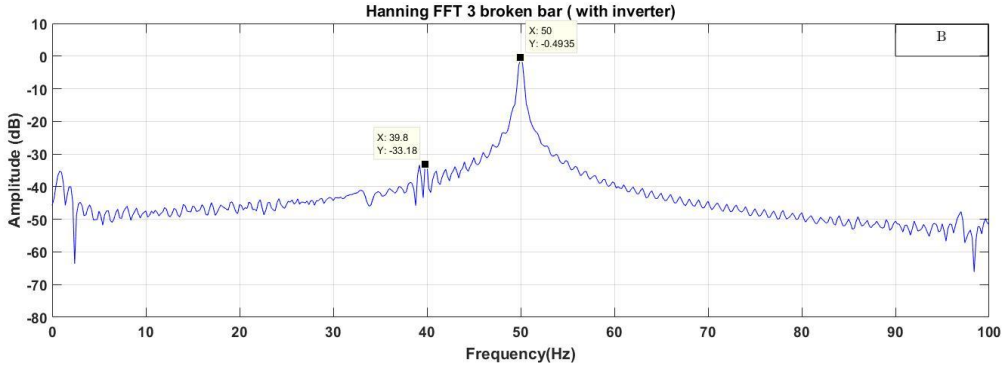

Figure III.25: **(a)** Spectrum of phase current by hanning spectral analysis . during bar failure(three broken bars)

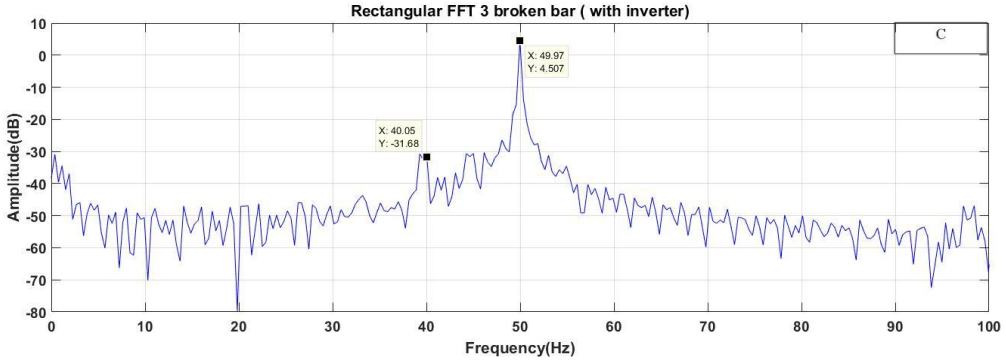

Figure III.25: (a) Spectrum of phase current by Rectangular spectral analysis . during bar failure(three broken bars)

Studied cases	Estimation results Frequency(Hz)/Amplitude(db)		
	Spectrum of phase current	***(1-2s)f (Hz)/(db)***	***(1+2s)f (Hz)/(db)***
healthy machine	**Rectangular window**	**0**	**0**
	Hanning window	**0**	**0**
	Hamming window	**0**	**0**
1 broken bar	**Rectangular window**	**(44.25/-22.46)**	**(55.69/-32)**
	Hanning window	**(44/-24.84)**	**(56/-43.3)**
	Hamming window	**(44/-24.54)**	**(56/-43.24)**
2 broken bar	**Rectangular window**	**(39.67/-27.1)**	**(60.65/-40.72)**
	Hanning window	**(39.4/-29.78)**	**(60.4/-37.32)**
	Hamming window	**(39.4/-29.59)**	**(60.4/-37)**
3 broken bar	**Rectangular window**	**(40/-31.68)**	**0**
	Hanning window	**(39.8/-33.18)**	**0**
	Hamming window	**(39.8/-32.56)**	**0**

TABLE III.2: SPECTRUM OF PHASE CURRENT

We notice that the spectrum of the stator current contains in addition to the fundamental harmonic at the supply frequency fs=50Hz additional harmonics. These are those created by the inverter which are the harmonics of time, these harmonics appear in all the spectra of the stator currents, either with healthy operation or with fault in simulation .

III.3.4 Wavelet Transform Rotor Fault Diagnosis

III.3.4.1 The continuous wavelet transform's simulation results

In this section, we propose to investigate the stator current of the asynchronous motor's signature using the continuous wavelet transform (CWT). use an inverter. The data below show the evolution of the coefficients of the current (CWT) of a stator phase under the conditions of a healthy motor, a broken bar, then two broken bars, then three broken bars at t=2 s, and with the application of a load torque of 3.5 Nm starting at t=0.6 s.

In the process of simulation and examination of the results, we relied on four types of the Wavelet family:

a- Daubechies wavelet (DB). b- Discrete approximation of the Meyer wavelet (Dmey).

c- Morlet wavelet (Morl). d- Reverse biorthogonal wavelets (rbio).

III.3.4.1.1. Case of a healthy machine

Figures (III-26 a, b, c, and d), show result continuous wavelet transform (CWT) for a healthy motor.

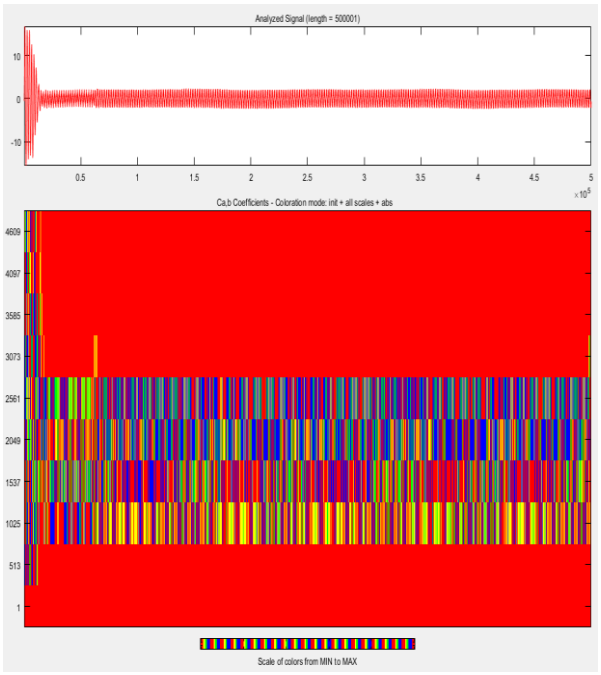

Figure III.26: (a) CWT case of (DB)

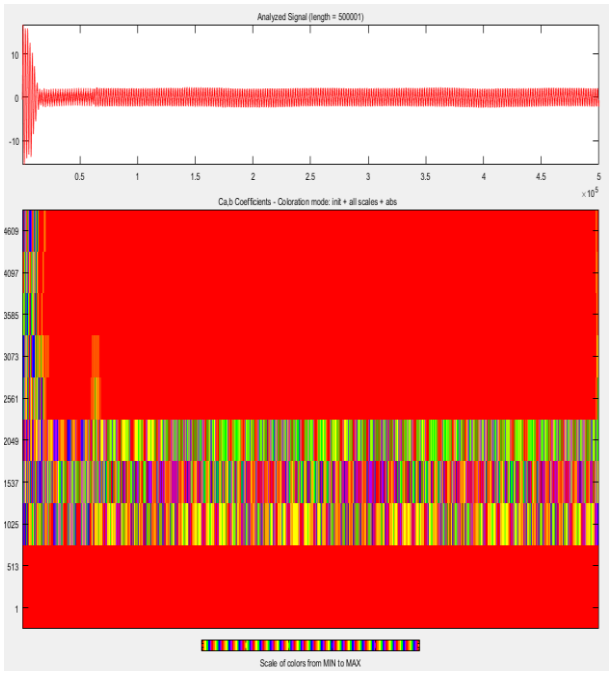

Figure III.26: (b) CWT case of (Dmey)

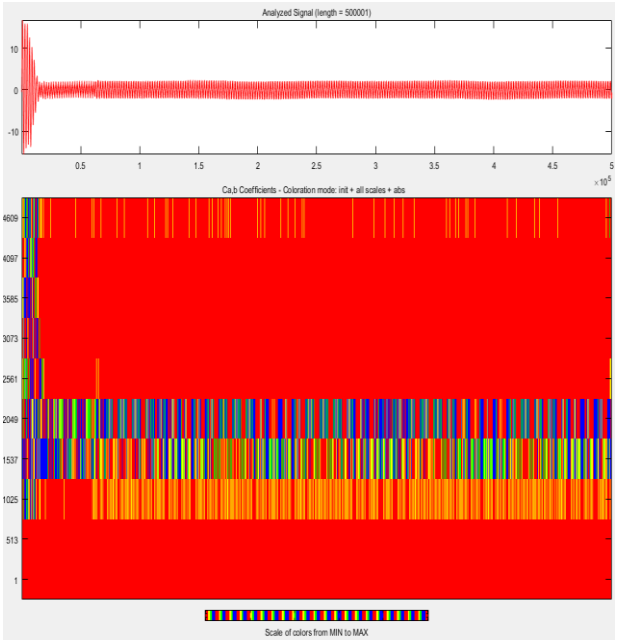

Figure III.26: (c) CWT case of (morl)

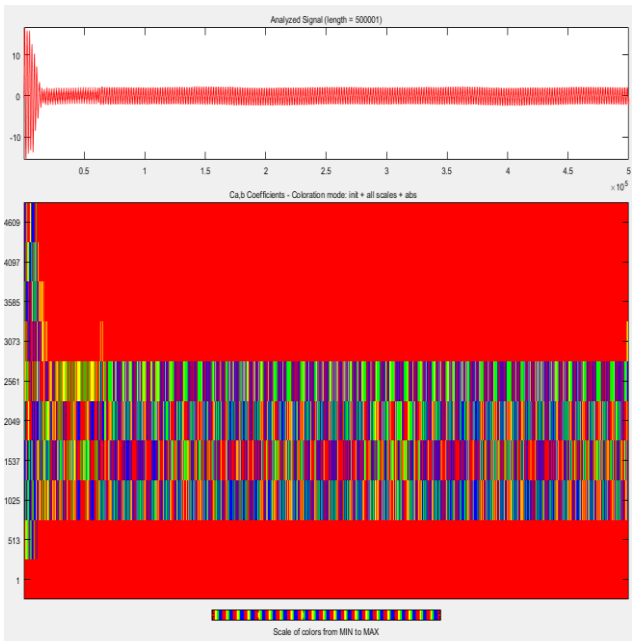

Figure III.26: (d) CWT case of (rbio)

III.3.4.1.2. Case of one broken bar:

The induction motor was first put to the test under duress with one rotor bar destroyed.

Figures (III-27 a, b, c ,and d), show result continuous wavelet transform (CWT) for a motor faults (one broken bar).

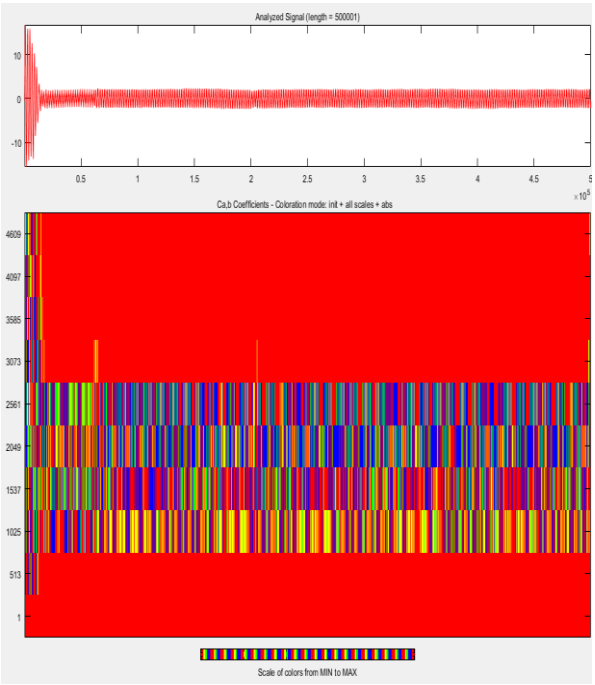

Figure III.27: (a) CWT case of (DB)

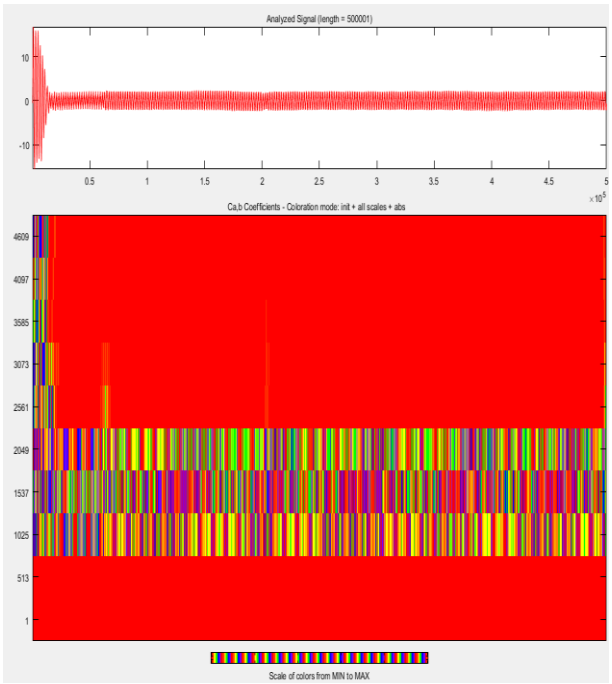

Figure III.27: (b) CWT case of (Dmey)

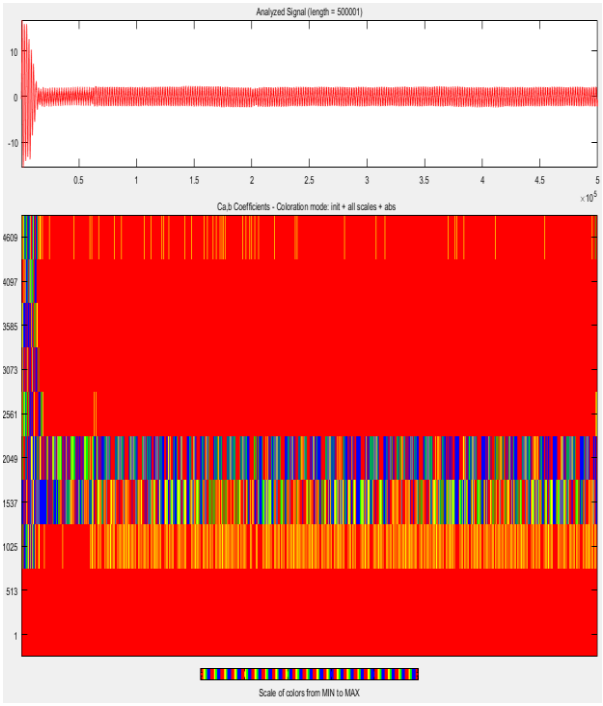

Figure III.27: (c) CWT case of (morl)

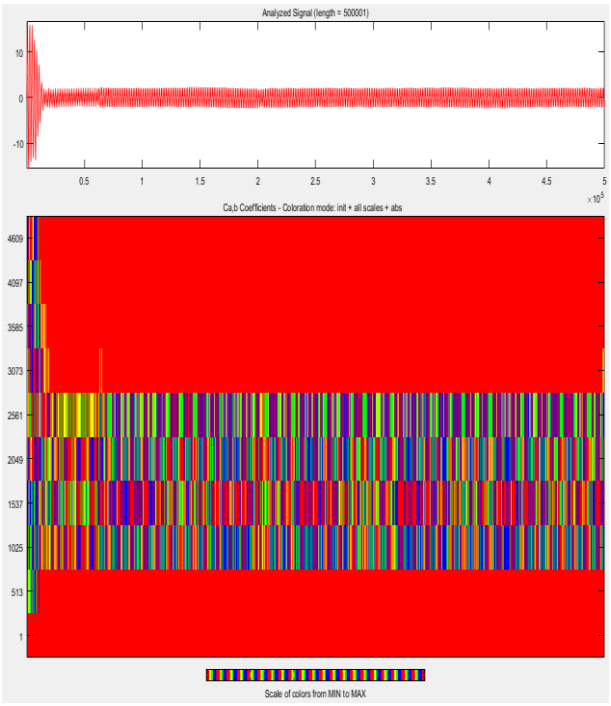

Figure III.27: (d) CWT case of (rbio)

III.3.4.1.3. Case of two broken bars:

The induction motor was second put to the test under duress with two rotor bar destroyed.

Figures (III-28 a, b, c ,and d), show result continuous wavelet transform (CWT) for a motor faults (tow broken bars).

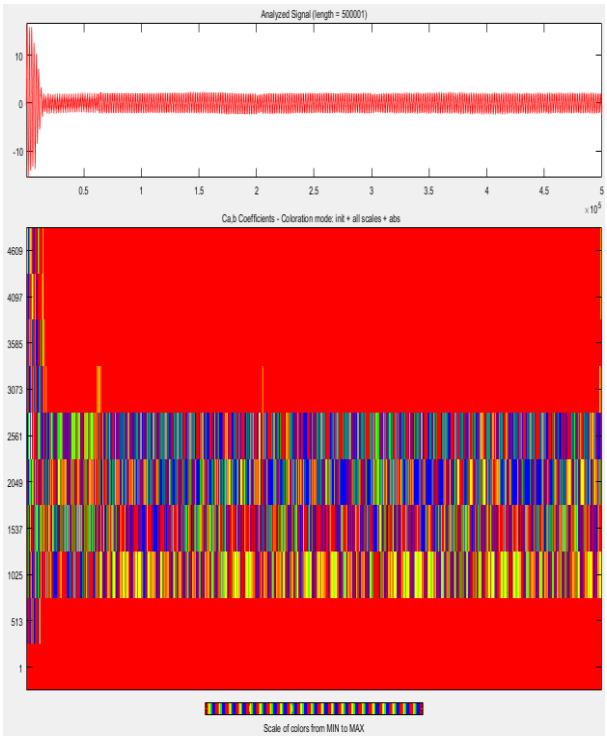

Figure III.28: (a) CWT case of (DB)

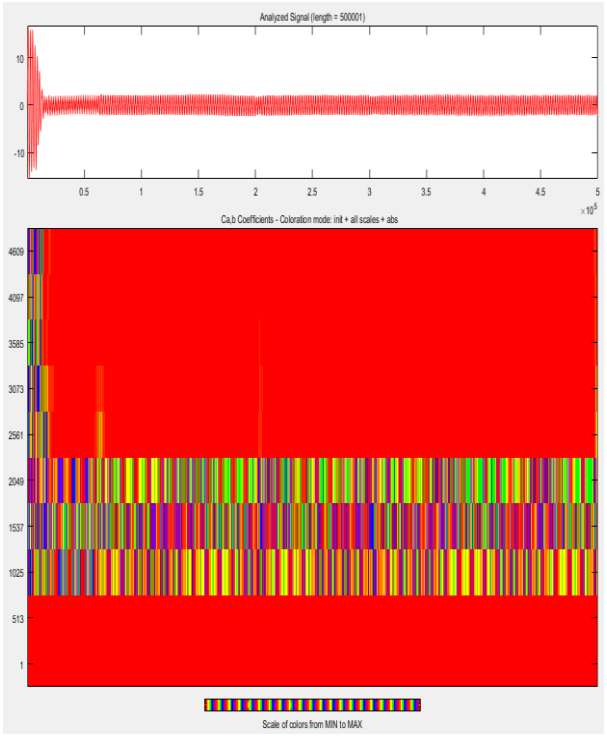

Figure III.28: (b) CWT case of (Dmey)

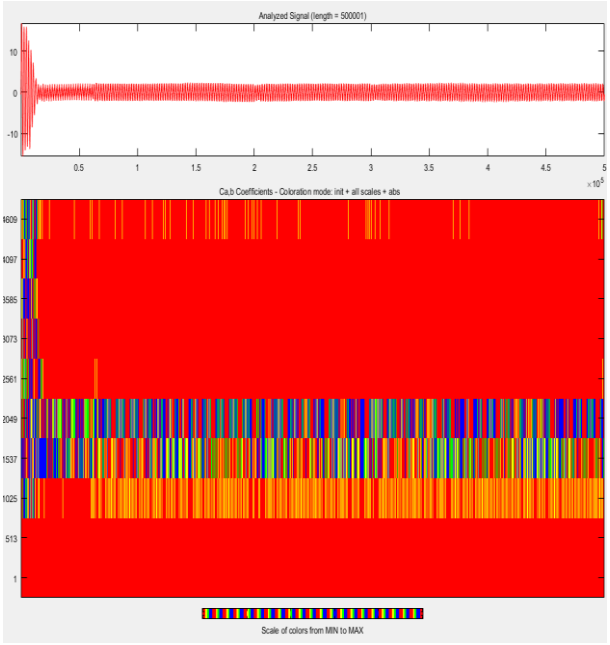

Figure III.28: (c) CWT case of (morl)

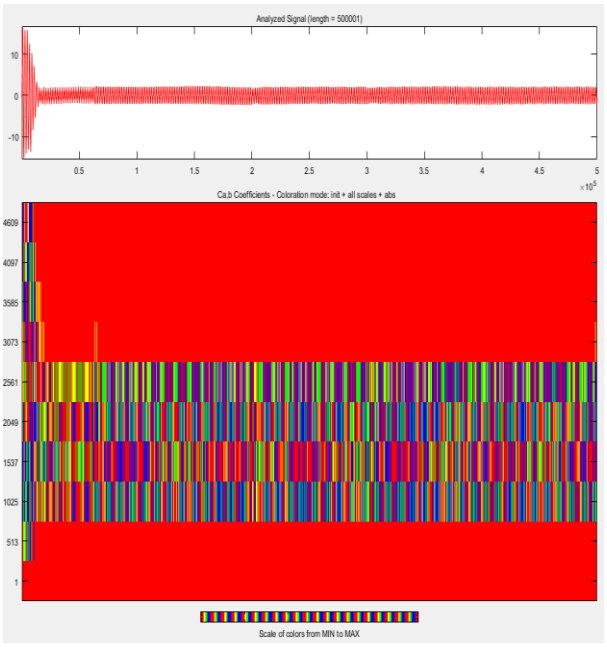

Figure III.28: (d) CWT case of (rbio)

III.3.4.1.4. Case of three broken bars:

The induction motor was third put to the test under duress with three rotor bar destroyed.

Figures (III-29 a, b, c , and d), show result continuous wavelet transform (CWT) for a motor faults (three broken bars).

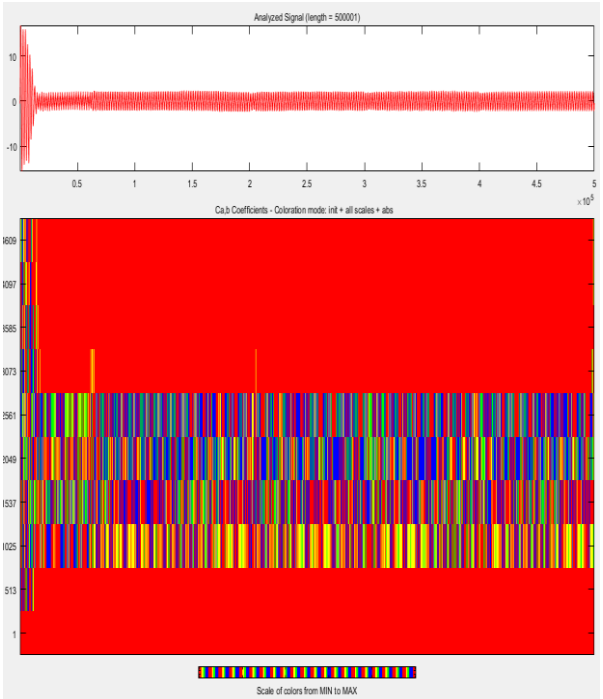

Figure III.29: (a) CWT case of (DB)

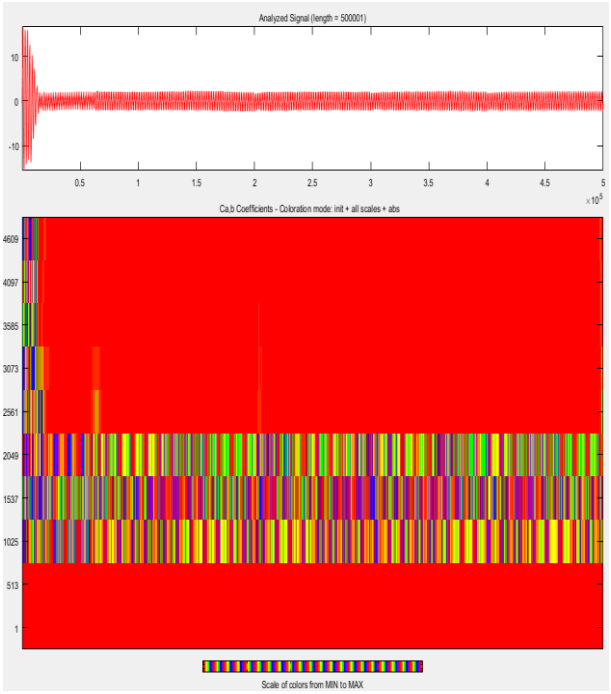

Figure III.29: (b) CWT case of (Dmey)

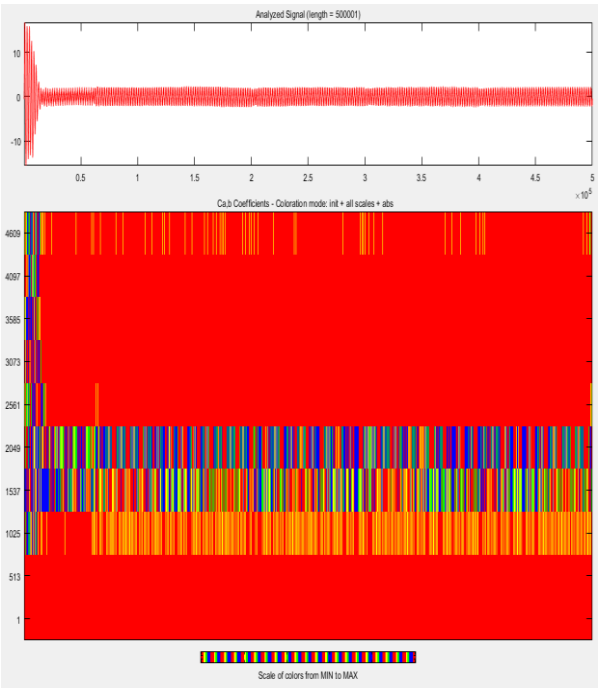

Figure III.29: (c) CWT case of (morl)

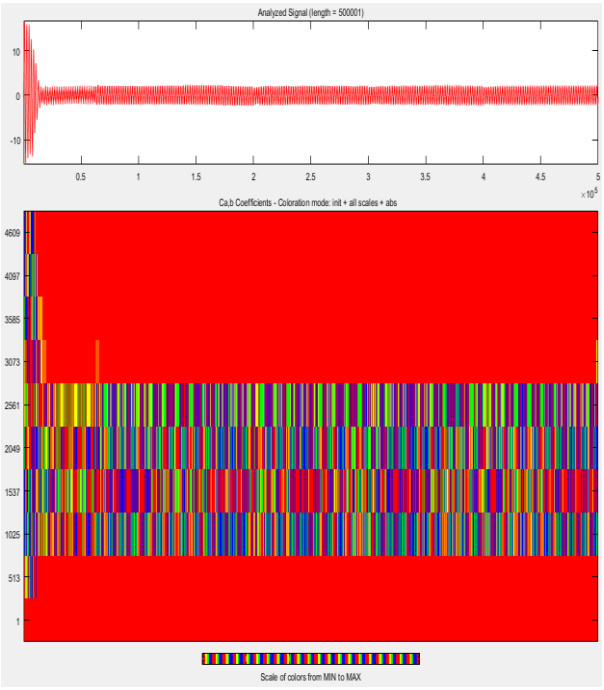

Figure III.29: (d) CWT case of (rbio)

The figures (III-26 a, b, c, and d) to (III-29 a, b, c ,and d) show how continuous wavelet transform (CWT) is used for stator current measurements for the db(04) family and the other families in both a healthy and problematic state of the machine.

The resemblance between the signal's core operations (wavelets) and the signal itself as measured by wavelet analysis is represented as having the same frequency content. The estimated coefficients from (CWT) demonstrate how near the wave the signal is at the present scale.

When the machine is in a healthy state, as opposed to when it is damaged, the current does not change. We see that the current changes in terms of various degrees of colors (the level signals produced by the wave decay of the stator current) and their arrangement in shapes because the wave coefficients of the kinetic error are stronger than the wave coefficients in the machine's healthy condition.

These differences demonstrate that, during the start-up period, the wavelet shift may discriminate between the signal components of healthy and diseased motors. High scales correspond to low frequencies. The lower scales correspond to the higher frequencies.

Figures (III-26 a, b, c, and d) compares the level signals produced by the wave decay of the stator current to start in a healthy machine.

and(3 broken bars) a machine that is malfunctioning The level signals brought about by the wave decay of the stator current are shown in Figures (III-27 a, b, c, and d) to (III-29 a, b, c ,and d).

While a damaged rotor bar and failing motor show a new pattern. It is proposed that a motor that is operating properly can be distinguished from one that isn't by using this extra pattern. These variances are suggested to act as the identifying feature for broken rotor bar defect identification.

III.3.4.2. Analysis using Discrete Wavelet Transforms (DWT)

The level signals produced by the stator current wave decline to start in both a healthy machine and a malfunctioning machine, the figures (III-30 a, b, c, and d) to (III-33 a, b, c ,and d) are shown. explains in detail the variables caused by the broken rotor bars fault and how harmonics arise in transient and steady-state situations.

There is no oscillation in the system when the wavelet signal intensity is strong. The stator current magnitude in the defective condition displays high-level coefficients and variations in coefficients as compared to a healthy state.

Rotor bar failure increases the coefficient and alters the influence of frequency bands.

The original signal is decomposed at the eleventh level with a sample frequency of 5 kilohertz.

In the process of simulation and examination of the results, we relied on four types of the Wavelet family:

a- Biorthogonal wavelets (bior).

b- Fejer-Korovkin wavelets (fk).

c- Haar wavelet (haar).

d- Symlets wavelets (sym).

III.3.4.2.1. Case of a healthy machine

Figures (III-30 a, b, c, and d), show result Discrete Wavelet Transforms Description (DWT) for a healthy motor.

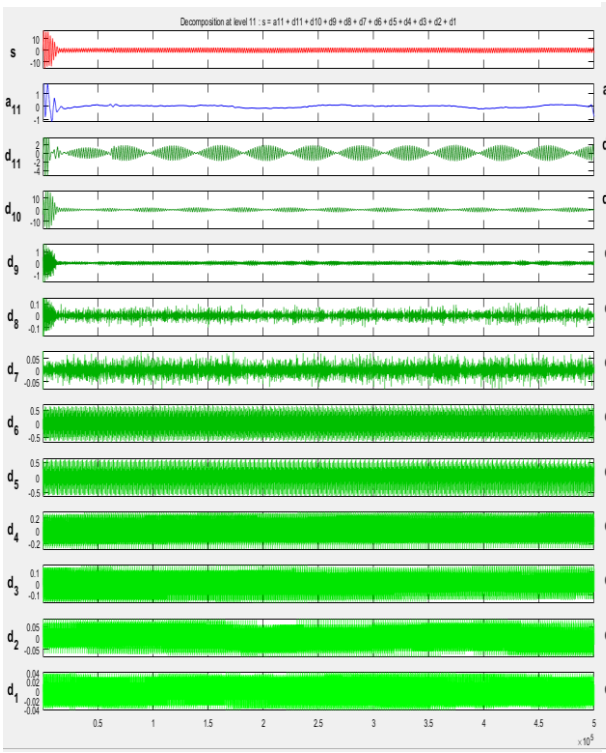

Figure III.30: (a) DWT case of (bior)

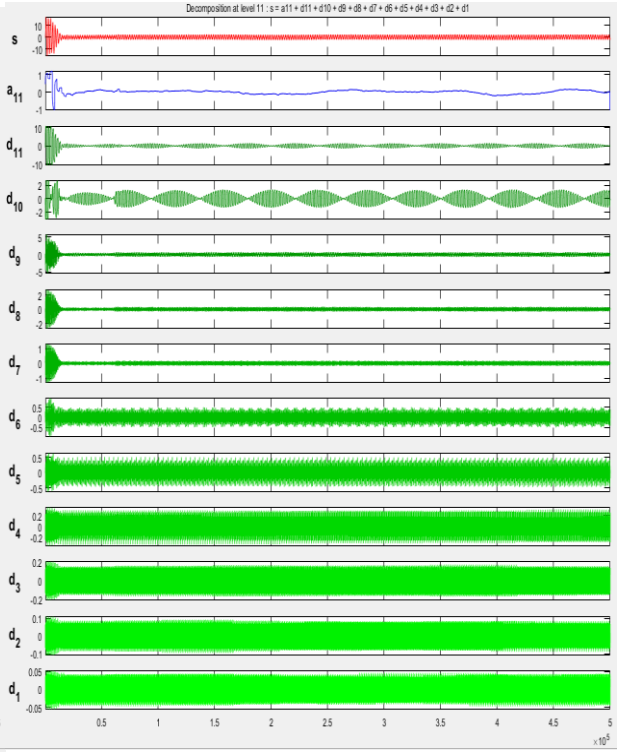

Figure III.30: (b) DWT case of (fk)

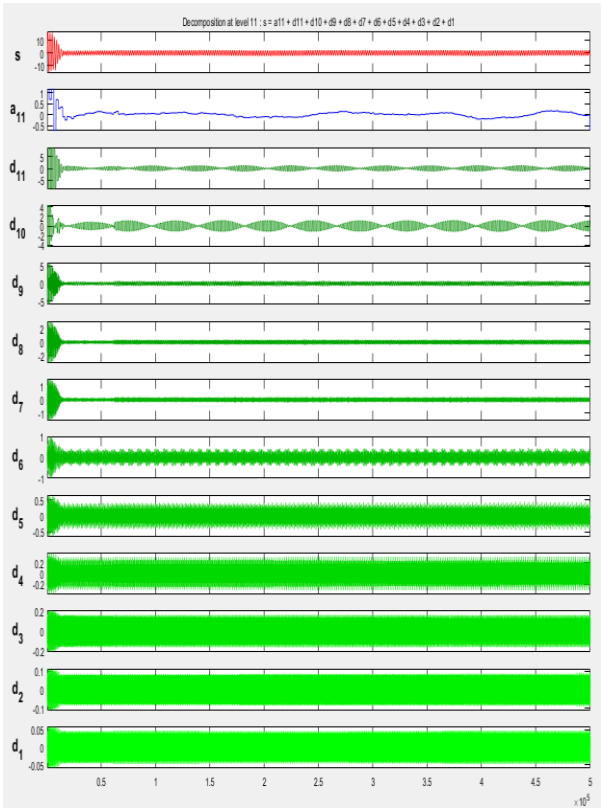

Figure III.30: (c) DWT case of (haar)

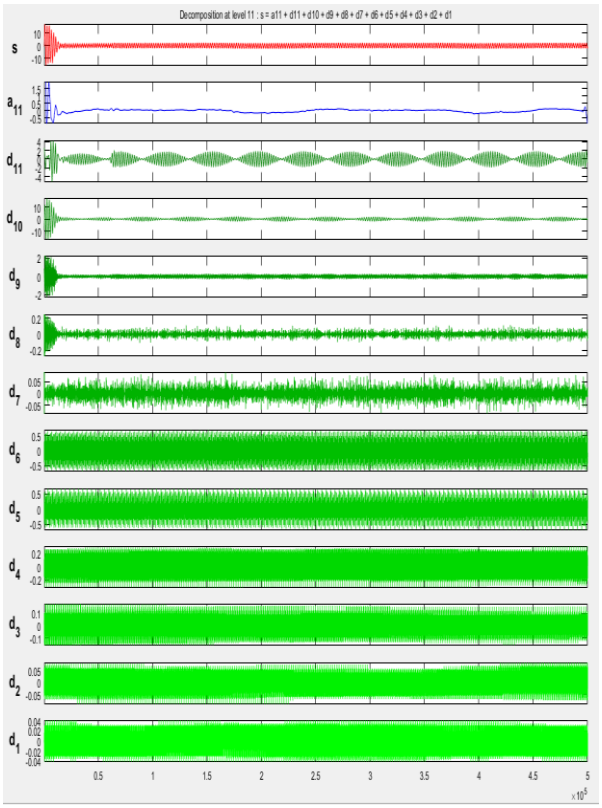

Figure III.30; (d) DWT case of (sym)

III.3.4.2.2. Case of one broken bar:

The induction motor was first put to the test under duress with one rotor bar destroyed.

Figures (III-31 a, b, c and d), show results Discrete Wavelet Transforms Description (DWT) for a motor faults (one broken bar).

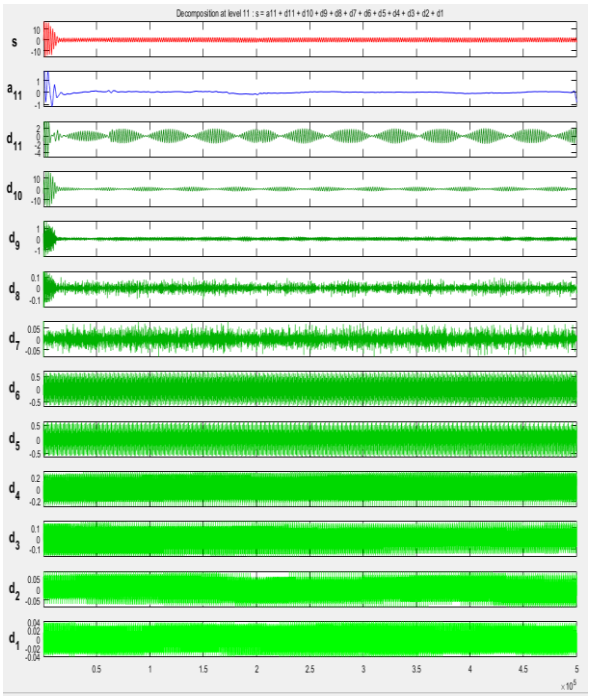

Figure III.31: (a) DWT case of (bior)

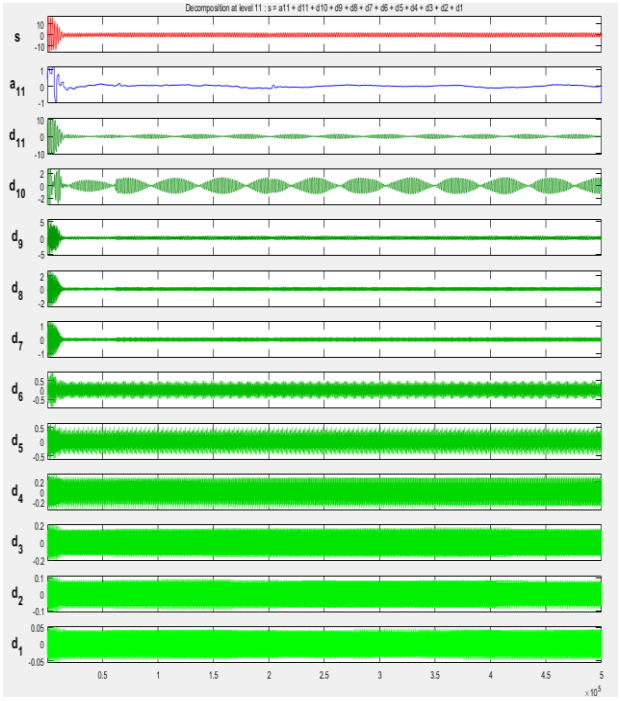

Figure III.31: (b) DWT case of (fk)

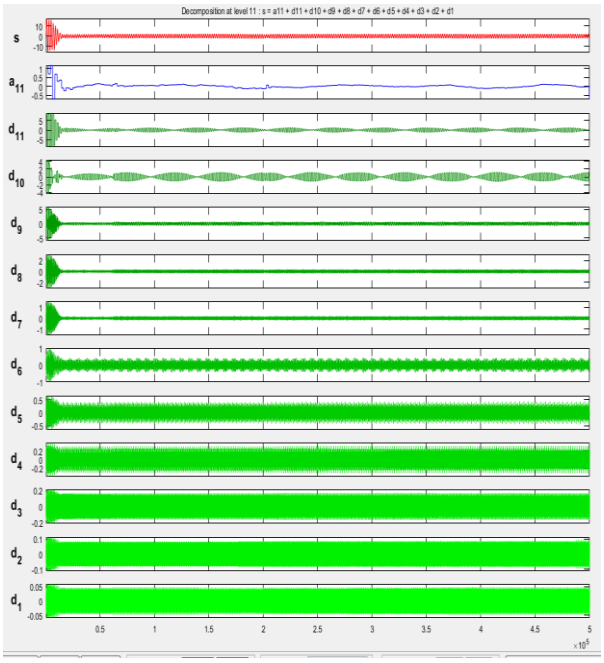

Figure III.31: (c) DWT case of (haar)

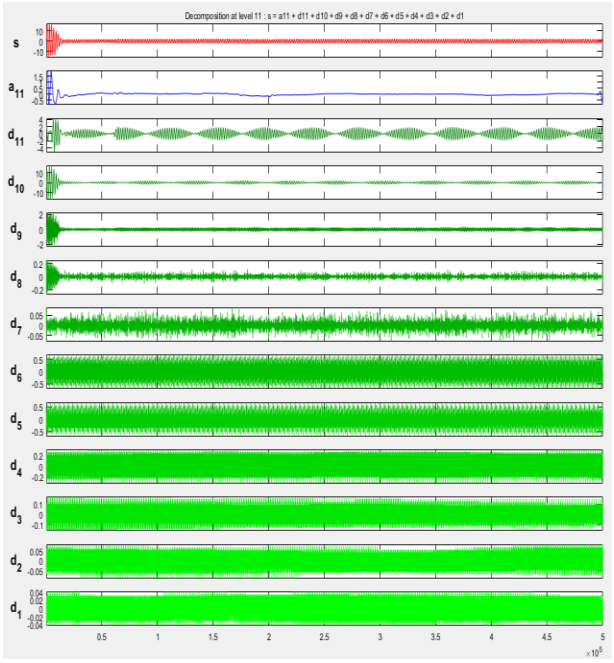

Figure III.31: (d) DWT case of (sym)

III.3.4.2.3. Case of two broken bars:

The induction motor was second put to the test under duress with two rotor bars destroyed.

Figures (III-32 a, b ,c , and d),, show results Discrete Wavelet Transforms Description (DWT) for a motor faults (two broken bars).

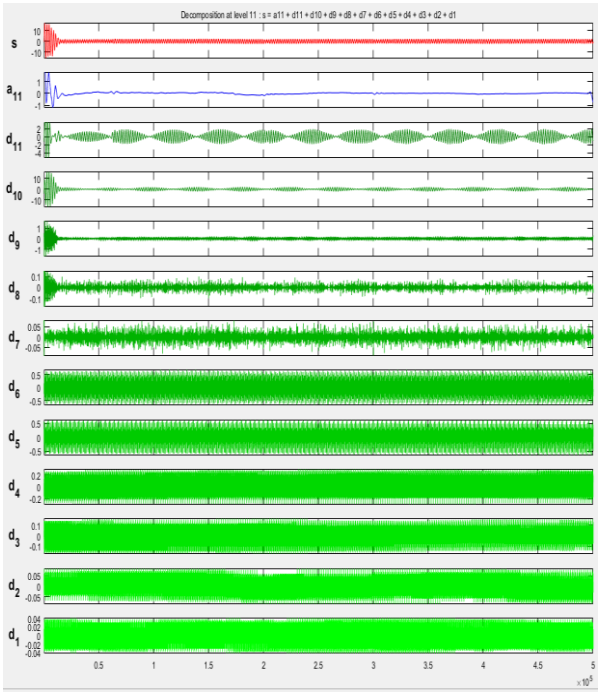

Figure III.32: (a) DWT case of (bior)

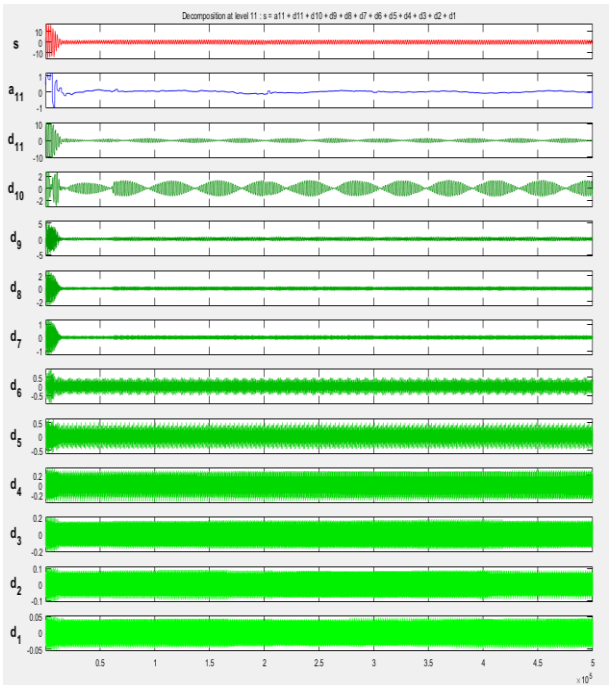

Figure III.32: (b) DWT case of (fk)

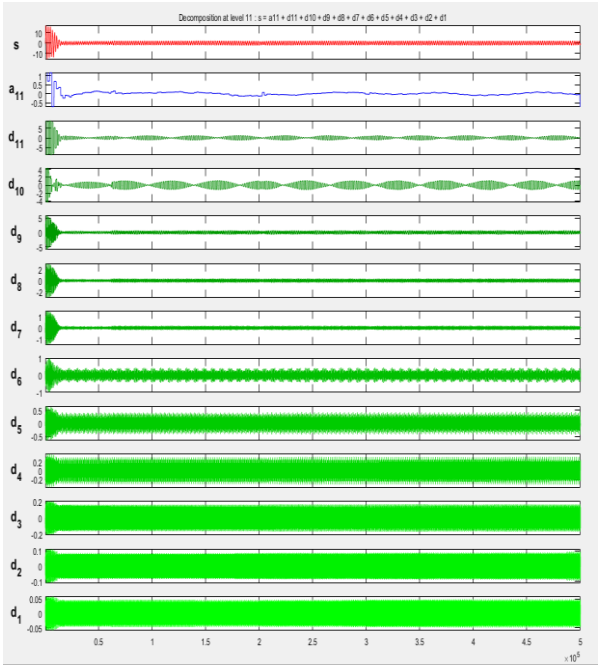

Figure III.32: (c) DWT case of (haar)

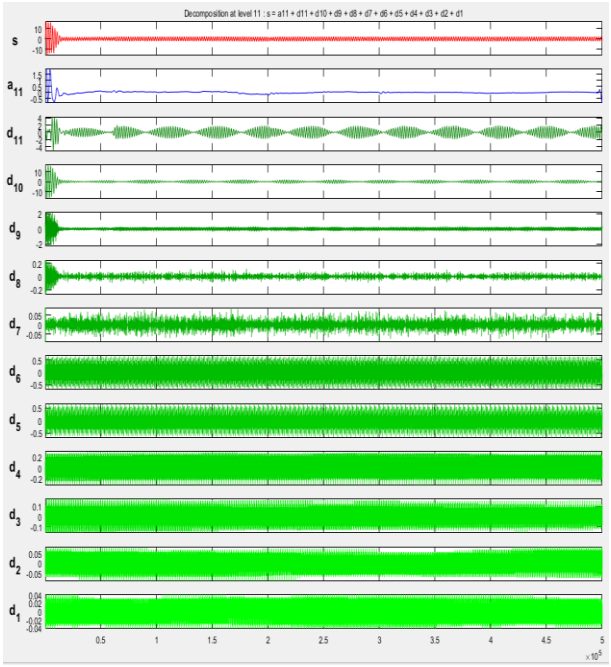

Figure III.32: (d) DWT case of (sym)

III.3.4.2.4. Case of three broken bars:

The induction motor was third put to the test under duress with three rotor bars destroyed.

Figures (III-33 a, b ,c , and d), show results Discrete Wavelet Transforms Description (DWT) for a motor faults (three broken bars).

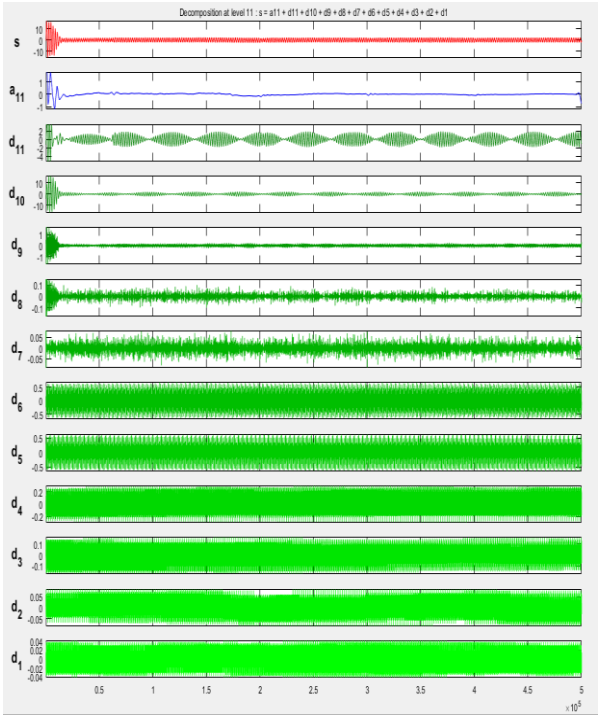

Figure III-33: (a) DWT case of (bior)

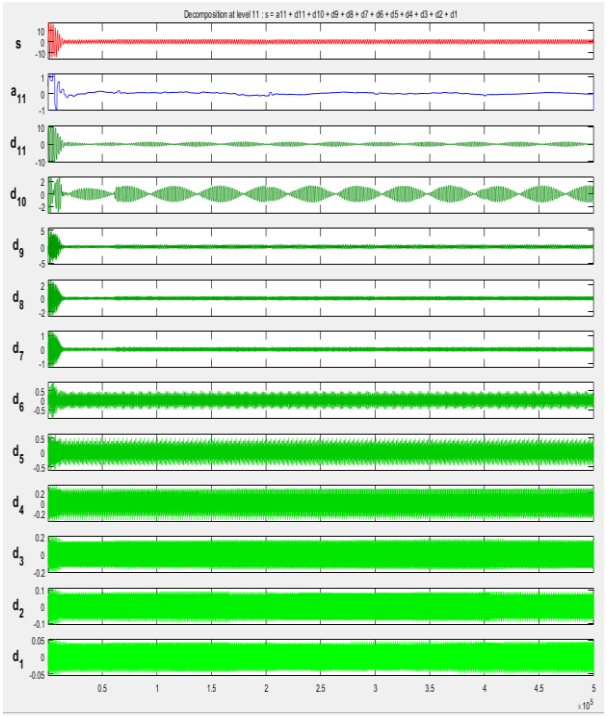

Figure III-33: (b) DWT case of (fk)

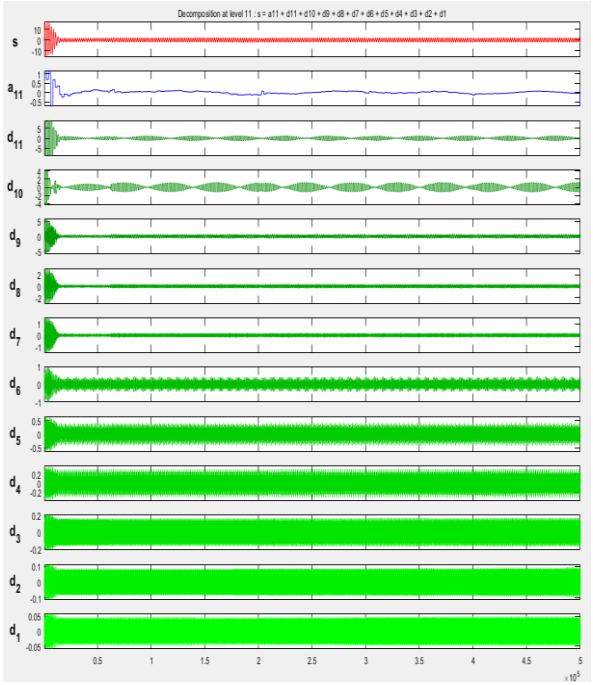

Figure III.33: (c) DWT case of (haar)

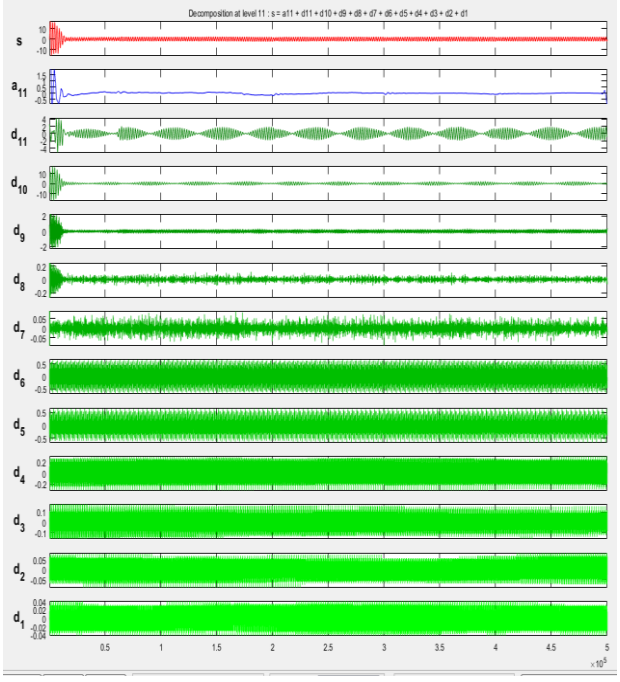

Figure III.33: (d) DWT case of (sym)

While the approximation signal is better at explaining low-frequency information, the detailed signal is better at explaining high-frequency data.

In order to accurately detect the rotor bar problems, the approximation signal for the eleventh level has a frequency range of 2.44 to 1.22, which is very low frequency.

In both instances, the signal is different and may be distinguished by the disruptions that manifest at high levels, it is generally seen.

It is noticed that the tenth and eleventh levels are superior to the ninth level, which does not significantly alter, in terms of clarity and meaningful information.

When comparing the detail and approximation signals produced for the various types of machine operation, it is important to observe that the coefficients D10, D11, and A11 have larger amplitudes than when the machine is in good condition. Signals D10, D11, and A11 have increased amplitudes as a result of the various fault types' effects on the relevant frequency bands.

However, the additional harmonic lines in the spectrum are caused by the inverter's inverter's pulse width modulation (PWM), which uses frequencies that are time harmonics.

It can be inferred from the motor signals and graphs obtained from the samples, together with the 11 levels of decomposition, that when the reading first began, the motor current had higher amplitude because of the higher torque, after which it stabilizes. This signal information for high and low frequencies is particularly helpful in giving specifics. By assessing the energy stored in each, approximation and detail signals, especially in the corresponding plane of the frequency band, are validated with respect to mistake severity and increase.

The signal is divided into various frequency components using wavelet packets so that any irregularities can be examined. By examining the frequency spectrum of the motor current, the wavelet packet analysis is able to identify broken rotor bar problems. Additionally, it may tell you where the defect is and how serious it is. Wavelet packet analysis can also be used to find other induction motor issues. This makes it a useful tool for identifying and resolving induction motor problems.

III.4 Conclusion

The major goal of our research in this chapter is to discover and diagnose asynchronous machine defects using a multi-winding model to simulate bar breakage and assess the machine's behavior in both healthy and defective states. The performance and efficacy of the machine will certainly deteriorate when the breaking bars are increased. The use of signal processing has the advantage of allowing information to be extracted in order to identify and find problems. Also, to ensure that the machine does not stop running as a result of the machine.

The identification of the broken bar fault using spectral analysis of the stator current (MCSA-FFT) provides a plethora of information about the fault's existence, as well as the frequencies and frequency bands that characterize the fault.

Spectral analysis or the Fast Fourier Transform (FFT), from which we observed: Appearance of additional lines in the stator current spectrum, It is by using the Fast Fourier and in the other side the stator current of the phase Isa in regime stationary was analyzed by a technical WT wavelet.

The technique is used to address the problem of using the traditional Techniques like Fourier Transforms signal processing algorithm by analyzing the stator current envelope. The suggested method is based on the use of discrete wavelet transform and continuous wavelet transform.

A waveform can be monitored at any frequency of interest using the suggested discrete wavelet transform and continuous wavelet transform. To identify the rotor broken bar fault, stator current frequency spectrum is analyzed and then examined. Based on a suitable index, the algorithm separates the healthy motor from the defective one, with 1, 2 and 3 broken bars. In comparison to the healthy conditions, the recommended index significantly raises under the broken bars conditions. It can identify the problematic conditions with clarity. The possibility of detecting potential faults has been demonstrated (broken bars), using discrete wavelet transform and continuous wavelet transform. The diagnostic method is adaptable to temporary situations brought on by alterations in load and speed.

Chapter Four :

Validation and Analysis of the Findings Using the Finite Elements

IV.1 Introduction

We have in the past simulated the asynchronous machine in a short period of time using simulation tools like the Park transformation. We can now use these transformations to calculate all the currents of rotor bars and short-circuit rings in the case of the squirrel cage asynchronous machine due to the advancement of computer technology, particularly processors, [21].

In fact, we use either the theory of the electromagnetic field (Maxwell's equations), the theory of electrical circuits (Kirchhoff's laws), or the mixed method combining the theory of the electromagnetic field and the theory of electric circuits to study these induction machines and create a model that takes into account the structure of the rotor, [20].

The finite element technique is one of the approaches based on the theory of the electromagnetic field. Our tool for creating a model that accounts for the topology, size, and composition of the asynchronous machine will be the Maxwell's equations.

The fundamental electromagnetism equations, or Maxwell's equations, convert physical rules into differential forms. These equations are resolved using a variety of techniques, including analytical, numerical, and semi-analytic approaches, [10].

In reality, the numerical approach—more specifically, the finite element method, which is based on the discretization of the research domain—will be of interest to us in this study.

The simulation of a healthy asynchronous machine with breakage defects from the bars to the rotor using the finite element method (FEM) in the magneto dynamic domain will be shown in this chapter. In our model, the conductor connected to the bar in the electrical circuit is removed, and the equivalent surface in the geometry is filled with a non-magnetic substance, simulating the rupture of a bar.

The correctness of the results discussed in the previous chapter using the MATLAB software is further assured by this chapter's results, which we shall explain in both healthy and faulty circumstances using the Flux 2D® tool.

IV.2 Finite element method

The fundamental goal of the finite element approach is to solve complex problems by substituting simpler ones. We will only be able to find an approximation of the answer rather than the actual solution since the original problem gets substituted with a simpler problem during the search for the solution.

Finding the electromagnetic field's structures in a certain area of space is the first step in solving an electro magnetics puzzle. Depending on the geometry of the objects, a limited number of these field configurations can be solved analytically or precisely from the required boundary conditions, [56]. These field configurations must concurrently full fill the Maxwell equations or the wave equations.

Maxwell's equations, along with the constitutive relations of the medium under consideration, are the equations that regulate the electromagnetic field in electromagnetic systems, [22]. Currently, magnetic problem-solving finite element software is widely available on the market. They primarily fit into three groups:

• Static two-dimensional software (such as Maxwell, Opera2D, Flux2D, etc.)

Or the magnetic equation is resolved on its own;

• To account for movement, magnetic and electric equations are concurrently calculated, or dynamic two-dimensional software (Flux2D, etc.);

• Edge effects can be taken into consideration or complicated structures can be calculated using three-dimensional software (Flux3D, TOSCA, ELECTRA, etc.).

Consider the program Flux2D, which enables the drawing of the magnetic circuit diagram on a cutting plane that is perpendicular to the machine's axis of rotation.

Finite element analysis involves these four processes:

- Creation of a 2-D model and definition of geometrical parameters;
- Define physical characteristics like geographic areas, types of materials, etc;
- Building a model of an electric circuit;
- Integration of the research area with problem-solving.

In this part, a squirrel cage induction motor is simulated under both healthy and rotor broken bar situations using time-step FEM. The broken bar current is 0 if the rotor bar is totally destroyed. This raises the rotor current for the other bars. Additionally, the flux distribution surrounding the fractured bar becomes asymmetrical, with an increase in flux density on one side and a reduction on the other. Depending on the magnitude of the breaking, the broken bar may also have non-zero current [80, 82]. In this study, the broken bar current is given a non-zero value, and the broken bar is modelled by a large resistance.

IV.2.1 Principle of the finite element technique

The partitioning of the subject matter into simple areas of limited dimensions is the essential tenet of the finite element approach. The potential vector in a cutting element can be estimated on each domain known as a finite element by approximation functions (also

known as form functions), the expression of which differs from type to type. The continuity of the potential at the intersections of the components must be guaranteed by these approximation functions. Polynomial approximations make up the bulk of methods used to approximate an element's potential [22][86].

For a triangle element:

$$A_e(x, y) = a + bx + cy \tag{IV-1}$$

The following are the quadrilateral elements:

$$A_e(x, y) = a + bx + cy + dxy \tag{IV-2}$$

It is necessary to find the constants a, b, c, and d. Generally speaking, the potential Ae is non-zero in the element and zero everywhere. The following equation gives an approximation of the potential in a point in the resolution domain (Ω):

$$A\ (x, y) = \sum_{e=1}^{ne} A_e(x, y) \tag{IV-3}$$

E : Element number.

ne : The total number of domain elements (Ω).

The values of the potentials of an element's three vertices in figure (IV.1) precisely specify the potential at all of an element's points as well as the current density.

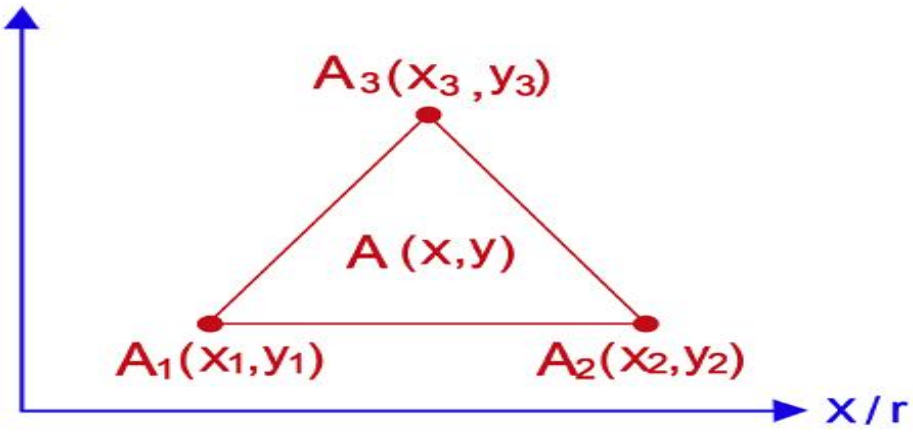

Figure IV.1: Interpolation function of an element

IV.2.2 Equations with partial differentials

There are two different methods of resolution: analytical and numerical. Even though the analytical resolution appears to be straightforward and produces correct answers, it has the significant drawback of neglecting nonlinearity and geometric deformation. We employ numerical approaches for this and to overcome this disadvantage.

Our research reveals that the finite element technique (MEF) has the edge over the other approaches due to its superior ability to adapt to complicated geometries.

The idea behind finite element analysis, which entails breaking down the structure of the machine under study into several components with limited dimensions and then solving Maxwell's equations for each of these elements. Each element's boundary conditions are fixed by those of its neighbours. It is therefore able to do flux, torque, and inductance calculations and determine the magnetic state of the entire structure thanks to the combination of all these calculation components.

The partial differential equation's integral formulation is discretized by the finite element method, which results in a set of algebraic equations that roughly solve the situation under study. The research area is divided into a limited number of polygonal components to create the mesh,

All of the polygons' vertices —also known as the mesh nodes— are used to calculate the vector potential's value. The solution at any point in the domain will be established in accordance with the values at the element's vertices by using the proper interpolation functions.

The techniques most frequently used to convert a system of partial differential equations into an integral formulation are the weighted residuals approach and the variational method.

Despite the significance of its range of application, this approach loses accuracy in two specific circumstances, namely: a) when the field of research becomes infinite; and b) when a singularity exists at the level of the field of study or at specific spots that have infinite derivatives.

-The most frequent kind of items we come across depend on whether the research area is one, two, or three dimensional.

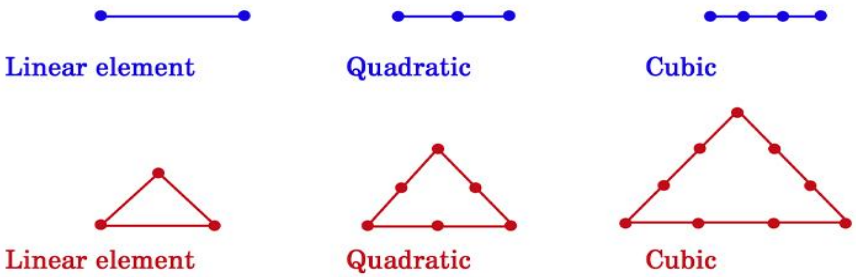

Figure IV.2. Classical elements in one and two dimensions, [61].

First-order triangular components are favoured in the vast majority of two-dimensional applications. We continue to modify the mesh in order to increase the precision of the solution, [87].

The following are the key phases in the creation of a finite element model:

- Construction of the nodal approximation by sub domain;
- Discretization of the continuous medium in sub domain;
- Calculates elementary matrices that correspond to the problem's integral form;
- Assembles elementary matrices; takes boundary conditions into consideration;
- Solves the system of equations.

IV.2.3 Formulations

Consider a certain domain (Ω) in which a field A, scalar or vector, is the solution of the following partial differential equation, [23]:

$$D(A) = F \tag{IV-4}$$

Where D is a differential operator and F is a known function, called the source term.

To fully specify the field A, it is necessary to take into account the boundary conditions Γ of the domain (Ω).

$$L(A) = G\frac{\partial A}{\partial t} + HA \tag{IV-5}$$

In this equation G and H are known functions on the boundaries Γ. It is therefore the same for the function L. We can distinguish two important special cases:

1- If the function G is zero, we will have a Dirichlet condition imposing the value of the field A on the border Γ:

$$L(A) = HA \tag{IV-6}$$

2- If the function H is null, we will have a Neumann condition imposing the value of the derivative of the field A compared to the normal external to the border Γ:

$$L(A) = G\frac{\partial A}{\partial t} \tag{IV-7}$$

A numerical solution approach may be used to find the solution to equation (IV-4) while accounting for the boundary conditions (IV-5). The finite element method's numerical resolution entails dividing the domain Ω into simple sub-domains Ωe, each of which has a field A that is often represented by a polynomial function. As a consequence, the differential equations will be converted into a set of algebraic equations, the solution of which will reveal the distribution of the field A in the domain Ω.

The Maxwell equations linked to the constitutive relations of the medium under consideration are the equations that control the electromagnetic field in electrical equipment.

A. Relationships between electromagnetic couplings

Maxwell-Ampere's equations state that electric currents or variations in an electric field can both produce magnetic fields.

$$r\vec{o}t\vec{H} = J + \frac{\partial \vec{D}}{\partial t} \tag{IV-8}$$

The Maxwell-Faraday equation also shows a magnetic field can be produced by an electric field. Many different types of electrical generators utilise this induced field. An electric field is produced in a neigh boring wire by a revolving permanent magnet that generates a moving magnetic field.

$$r\vec{o}t\vec{E} = \frac{-\partial \vec{D}}{\partial t} \tag{IV-9}$$

B. The relationships of flux conservation

Electric charges produce an electric field in accordance with the Maxwell-Gauss equation. Positive charges are directed toward negative charges in the electric field. This rule describes the electric flow via any closed Gaussian surface more specifically [11][85].

$$div\vec{D} = \rho \quad \text{(IV-10)}$$

$$div\vec{B} = 0 \quad \text{(IV-11)}$$

C. The relationship governing the properties of magnetic materials

$$\vec{D} = \varepsilon\vec{E} \quad \text{(IV-12)}$$

$$\vec{B} = \mu\vec{H} \quad \text{(IV-13)}$$

D. Ohm's law relationship

$$\vec{J} = \sigma\vec{E} \quad \text{(IV-14)}$$

Or :

$\vec{H}$: Magnetic field (A/m);

$\vec{E}$: Electric field (V/m);

$\vec{B}$: Magnetic induction (T);

$\vec{B}_r$: Remanent induction of the magnets (T);

$\vec{J}$: Total current density (A/m^2);

μ : Magnetic permeability (H/m);

σ : Electrical conductivity ($\Omega^{-1}m^{-1}$);

e : The total number of domain elements (Ω).

IV.2.4 The applied model

Three modes of resolution can be employed, depending on the anticipated outcomes and the amount of simulation time available:

IV.2.4.1 Utilizing magneto statics

Due to the fact that this mode needs knowledge of the values of the currents in the various bars of the rotor, it can only be used to replicate a specific moment of the machine operating virtually without a load (and without induced currents). It will mostly be used to calculate the motor's magnetizing inductance, [57].

The sources in this mode are not time-dependent. The phrase:

$$\frac{\partial B}{\partial t} = 0$$

Therefore, the model equations become:

$$r\vec{o}t\vec{H} = \vec{J} \quad \text{(IV-15)}$$

$$div\vec{B} = 0 \quad \text{(IV-16)}$$

$$\vec{B} = \mu\vec{H} + \vec{B}_r \quad \text{(4-17)}$$

It is feasible to create a function in potential vector A in the following way thanks to the condition (IV-12):

$$\vec{B} = r\vec{o}t\vec{A} \quad \text{(IV-18)}$$

Fixing the divergence's value is likewise important for complete definition of A.

The Coulomb gauge condition is then added $div\vec{A} = 0$. This instantly verifies the solution's originality.

We derive the electromagnetic equation in magneto statics by substituting (4-18) and (IV-17) in (IV-15), which is described by the following set of equations:

$$r\vec{o}t(\nu.r\vec{o}t\vec{A}) = \vec{J} + r\vec{o}t(\nu.\vec{B}_r) \quad \text{(IV-19)}$$

Or :

$\nu = \frac{1}{\mu}$: is the magnetic reflectivity

IV.2.4.2 The magneto dynamic mode

Devices with sources of current or voltage that fluctuate over time can use this concept. $\frac{\partial B}{\partial t}$ is not a zero value. Additionally, it simulates steady state and makes use of sinusoidal current density. This enables the accurate measurement of the effective current. Studying a machine analogous diagram is possible in this manner [89]. The following system needs to be resolved:

$$r\vec{o}t(\nu.r\vec{o}t\vec{A}) = j\omega\sigma\vec{A} = \vec{J} \quad \text{(IV-20)}$$

$\omega = 2\pi f$: Electric pulse (rad. s^{-1});

J : imaginary unit ($i^2 = -1$).

IV.2.2.3 Transient magnetic mode

Is the most thorough, it accurately reproduces the engine's rotation. Since the supply is temporary in this situation, discretizing the previous system of characteristic equations step by step in time is necessary. The system to solve is as follows:

$$r\vec{o}t(\nu.r\vec{o}t\vec{A}) + \sigma\frac{\partial\vec{A}}{\partial t} - r\vec{o}t\vec{B}_r + \sigma g\vec{r}adV = 0 \quad \text{(IV-21)}$$

IV.2.5 Overview of the flux2d program

It is a finite element modelling program that allows for evolutionary regimes and accounts for magnetic and thermal phenomena, [36]. Thus, it is software that is well suited to meet our demands. With the aid of the program, engineers may compute and see quantities relevant to two-dimensional or rotationally symmetrical devices made of materials with linear or non-linear, isotropic or non-isotropic properties. The benefit of this comprehensive program is that it enables the linkage with circuit equations and the insertion of a specific surface region termed "tread" for the study of rotating machines with various rotor locations without requiring changes to the geometry and mesh. Specialized modules are needed to solve a problem,The sequence of these 2D Flux modules is shown as :

1- Construction

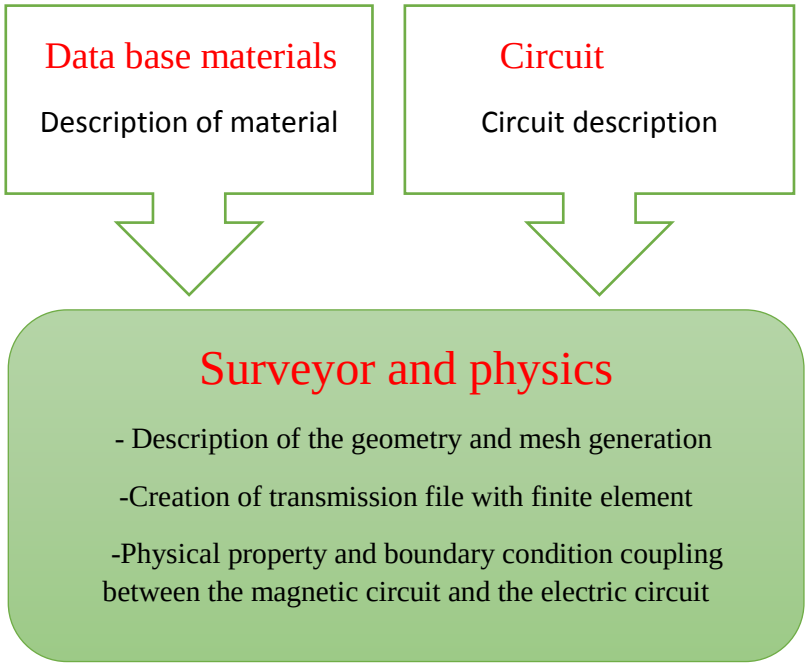

Figure IV.3: The sequence of Flux 2D programs

2- Resolution (Solving Operation Direct)

3- Exploitation (Analysis)

VI.3 Application to the Asynchronous Machine Simulation

Although the slope of the notches and the final consequences would necessitate a 3D display for a detailed investigation, we shall utilize the flux program in its 2D version [30] [32].

Simple factors underlie this decision:

- In comparison to 2D, 3D simulation takes longer.

- The major objective of our investigation is not to determine the impact of the notch inclination.

- Analytically calculated models are used to project the final consequences.

- Resistances and inductances, our model's construction also took into account the following hypotheses:

- Hysteresis and iron losses are disregarded.

- Only sinusoidal power is provided.
- Inter-bar currents are not taken into account.

- The Dirichlet condition (A=0) is applied to the exterior nodes of the stator and those internal to the rotor, forcing the flux lines to be tangential to these two surfaces since the air around the machine and the shaft is not represented.

Parameter	Value	Units
Nominal power	1.1	kW
Nominal voltage	220	V
Rated speed	2850	tr/min
Number of poles	2	----
Frequency	50	Hz
Active length	78.53	mm
Number of phases	3	-----
Connection Type	Y	-----
Number of notches	24	----
Inner stator diameter	100	mm
Stator outer diameter	192.4	mm
Rotor outer diameter	99.3	mm
Rotor internal diameter	87.94	mm
Air gap thickness	0.35	mm
Bars number	16	---

Table IV.1: Characteristic of the studied machine

IV. 3.1. Conductive materials

The resistivity of the copper for a specific temperature of the windings, the expansion, and the number of turns per slot will be allocated to this region for the stator conductors, which will be considered to be spread uniformly throughout the slots.

We shall utilize aluminium's resistance at a certain temperature at the rotor level.

IV. 3.2. The materials are magnetic

In determining the magnetic properties of metallic materials, consideration will be given to the non-linearity of the characters B (H) (Tableau IV.2).

H (A/m)	**0**	**300**	**500**	**1000**	**1500**
B (T)	0	0.66	1.09	1.45	1.56
H (A/m)	2000	3000	4000	5000	6000
B (T)	1.61	1.69	1.73	1.76	1.79
H (A/m)	7000	8000	10000	20000	30000
B (T)	1.83	1.85	1.89	2.04	2.11
H (A/m)	40000	50000	60000	70000	-
B (T)	2.14	2.16	2.18	2.192	-

Table IV.2: B (H) of the magnetic material STEEL_NLIN [60].

IV.3.3. Connecting with equations for circuits

The end effects (inductance, resistance of the coil head, and short-circuit ring) must be taken into consideration in order to accurately describe the motor. The electrical circuit is displayed in Figure IV.4.

The sources of supply voltage (V _U, V_V, and V_W), (B_U, B_V, B_W), the stator winding (L_U, L_V, and L_W), the leakage inductances.

R1, R2, and R3 are voltage drop resistors in the networks (R_U, R_V, and R_W) that represent the resistances of the voltmeters used to monitor the stator voltage, according to [88] .With:

Ql: Is a closed circuit that contains rotor bars (Figure IV.5) (Bar k), resistors (Rik), and leakage inductances (Laik), which correspond to the inter-bar regions of short-circuit rings (arcs between two adjacent bars). It is used to model the squirrel cage of the machine.

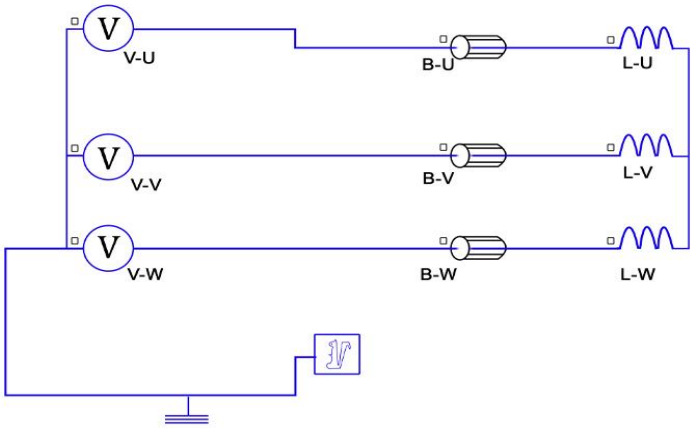

Figure IV.4: Circuits representing end effects related to geometry

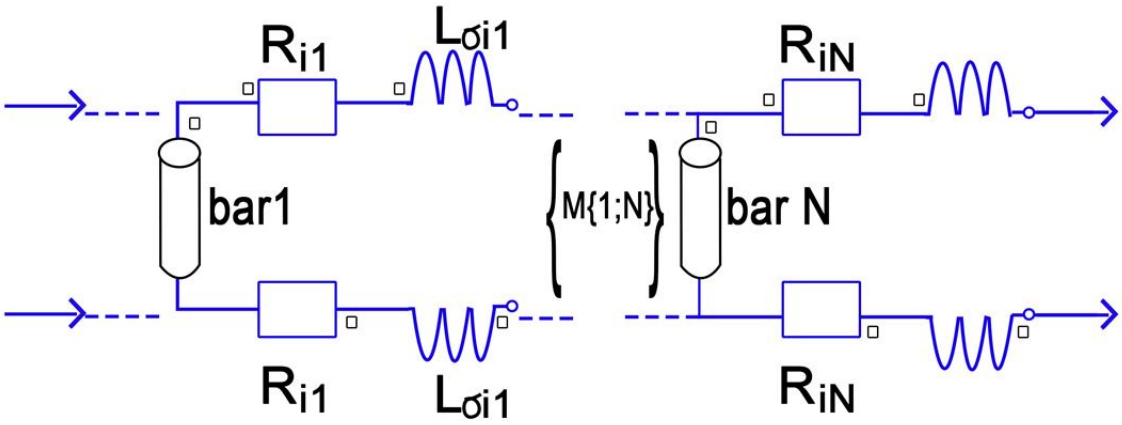

Figure IV.5: Equivalent circuit of the rotor cage

This connection is made because the simulations planned attempt to replicate the engine's fluctuations while running under load. It is necessary to simulate the short-circuits of the cage since the currents created in the rotor can no longer be disregarded, as was the case when there is no load. Additionally, this approach allows for the direct delivery of voltage to the motor rather than current, which would otherwise be required in the absence of this connection.

IV.4 Result of simulation by dynamic magneto in transitional regime (healthy machine)

The relative position of the rotor stator, often known as "the initial position of the rotor," is what determines the outcomes of magneto dynamic simulations. By determining the relative rotor-stator location at which the electromagnetic torque equals the average value,

we have reached our conclusion. The "initial position" of the rotor serves as input information for Flux2D®'s SOLVER_2D processor.

The transitory operating regime is seen as being highly significant. In fact, by validating the design and optimization findings in this mode, it is able to provide a notion of the dynamics and the machine's rejection of disturbances.

In this part, a squirrel cage induction motor is simulated using time-step FEM under both healthy and rotor broken bar situations.

The model from the previous chapter is simulated in this chapter using Flux2D®.

At time t = 0.6 seconds, the machine was subjected to a torque of 3.5 Nm, which corresponds to the investigated machine's nominal torque, in order to observe the model's good performance.

When the rotor cage does not exhibit any signs of failure, we can study the evolution of temporal elements like stator currents, torque, and speed. We have shown on Figures (IV-6 to IV-11) the evolution of both local and global quantities, such as magnetic field lines and magnetic induction.

The induction motor was sent to the test under load first with a sound rotor, then with two damaged rotor bars. The frequency domain is used to illustrate each stator current in the research.

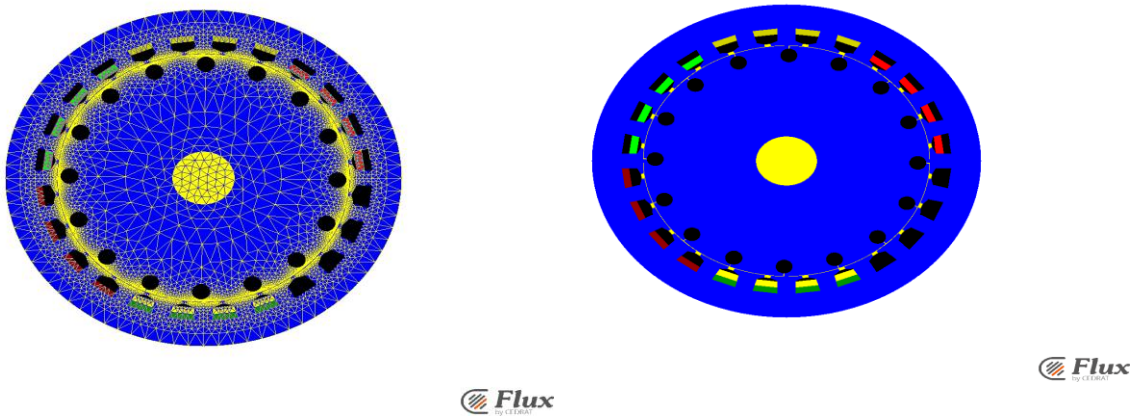

Figure IV.6: Regions of the electromagnetic field calculation domain and mesh distribution (healthy machine)

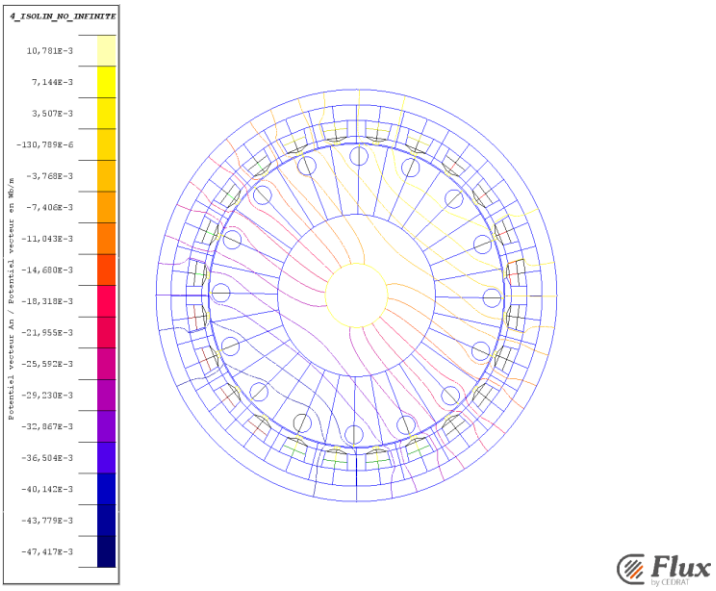

Figure IV.7: Distribution of equiflux lines for nominal operation(healthy machine)

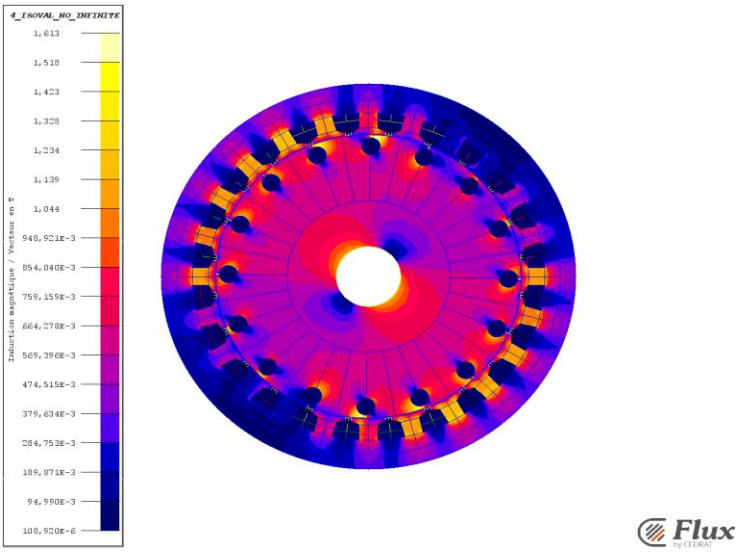

Figure IV.8: Magnetic induction for nominal operation(healthy machine)

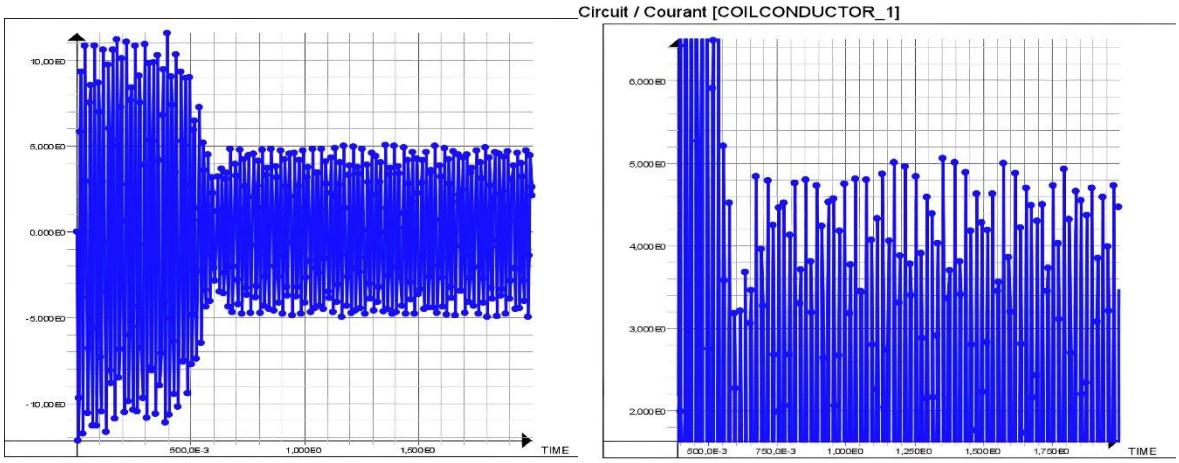

Figure IV.9: Evolution of phase a stator current (isa), on load (healthy)

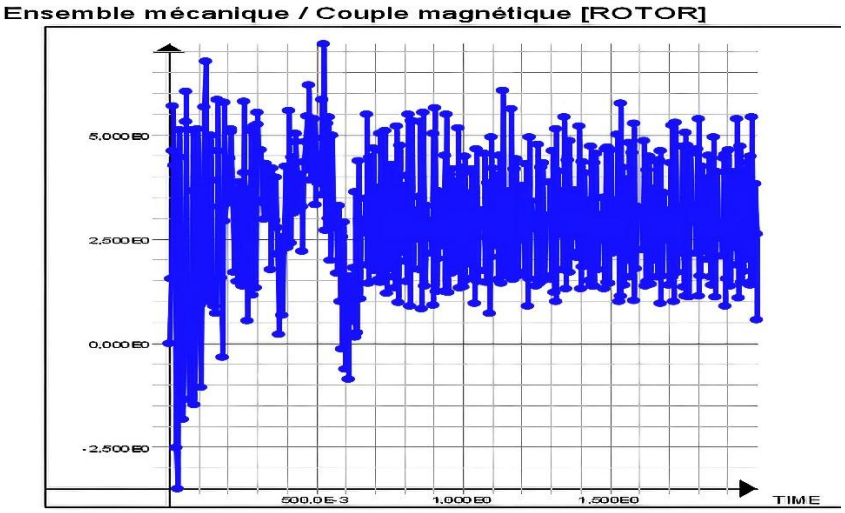

Figure IV.10: Evolution of the electromagnetic torque on starting, under load (healthy)

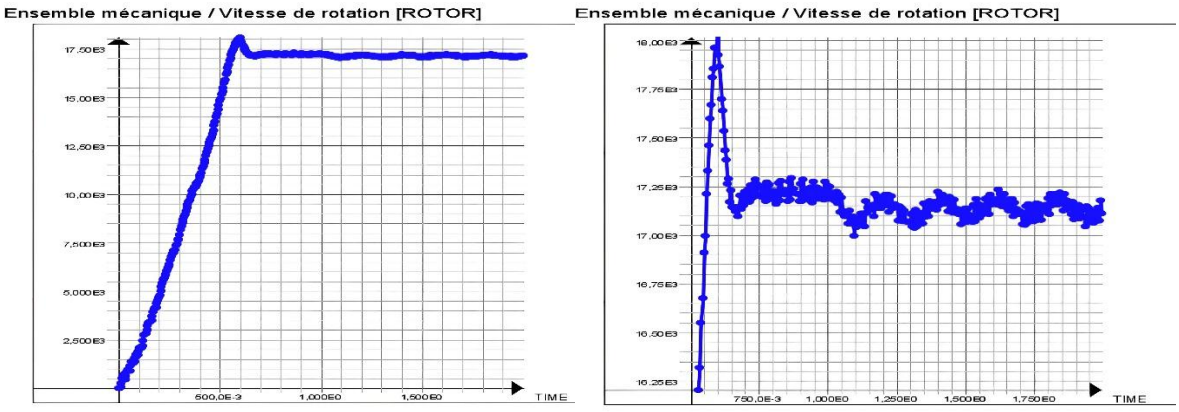

Figure IV.11: Rotational speed at start, under load (healthy).

We have shown the evolution of the local quantities (the lines of the magnetic field, the magnetic induction) and the global quantities (the currents, the electromagnetic torque, and the speed) on the Figures (IV.6 to IV.11).

The Figures (IV.6 through IV.8) have two poles that are quite obvious to see. In relation to the poles' axis, the distribution of the lines is approximately symmetrical. The flux lines between the stator and rotor are slightly shifted in the rotor's direction of rotation. The induction distribution is similarly almost symmetrical, and we can see that the start-up current in the bars is higher than the start-up current under normal operation.

The currents in the bars result in a symmetrical distribution of the flux lines around each pole for a healthy motor.

We were able to determine the various speed, electromagnetic torque, and stator current parameters through the simulation of the asynchronous motor model with a rotor. It should be noted that when the machine is loaded, the speed reaches its nominal value and then slightly lowers. The torque will then tend to equal the load torque value.

The rotor is initially in a shutdown condition, which causes current amplitudes to reach their maximum levels. After then, a permanent regime is formed, which causes the currents to decline with sinusoidal oscillations around zero. We apply a nominal resistive torque of 3.5Nm at time t = (0.6 s). Figure (IV.9) depicts the stator phase current's form.

The impact of the rising currents is brought on by the rising magnetic response of the rotor, which is brought on by the rising amplitude of the rotor currents.

The electromagnetic torque is seen in Figure (IV.10) as it evolves, with the transient phase lasting, manifesting, and capable of reaching a maximum value. The torque then rapidly decreases to virtually zero, matching the fluid friction torque. We apply a 3.5 Nm torque at (0.6 s), and the electromagnetic torque naturally responds in the opposite manner to counter the resistive torque.

The progression of the rotor's rotational speed is seen in Figure (IV.11). As soon as the engine starts, the speed rises, bringing it to a stable condition. A resistive torque of 3.5 Nm is then provided at time (0.6 s), which tends to slow the motor shaft and cause the speed drop.

IV.5 Result of simulation by dynamic magneto in transitional regime (machine with default)

The most prevalent rotor defects are bar breakage. Their simulations allow us to recognize the symptoms of these defects and forecast the deteriorations the machine will experience. We used the finite element technique (FEM) to simulate an engine in various situations where rotor bar breakage faults were present in order to demonstrate the failure of the bars to break.

IV.5.1 Case of one broken bar

First, the induction motor was put through a stress test with one damaged rotor bar. The frequency domain is used to illustrate each stator current in the research.

Figures (IV.12 to IV.17) show how bar breaking affects a phase that the machine absorbs.

The simulation lasts for five seconds, with the machine being exposed to a resistive torque of 3.5 N.m. at the point t = 0.6s. By increasing the resistance by 11 times, we reproduce the first bar's failure at time t=2s.

We have shown the evolution of the local quantities (the lines of the magnetic field, the magnetic induction) and the global quantities (the currents, the electromagnetic torque, and the speed). The simulation of the model allowed us to obtain the various characteristics of the stator current, speed, and electromagnetic torque.

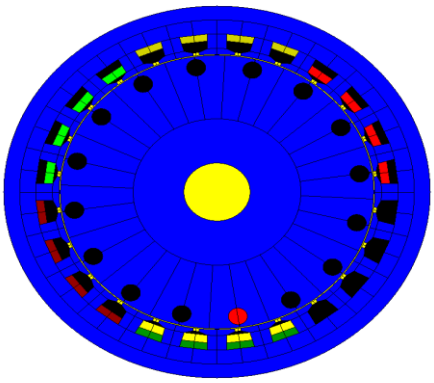

Figure IV.12: Regions of the electromagnetic field calculation domain. (one broken bar)

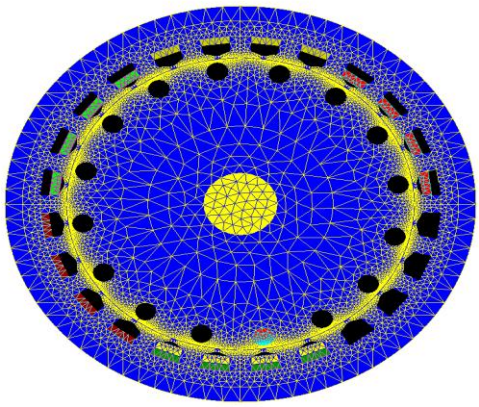

Figure IV.13: Distribution of the mesh (one broken bar)

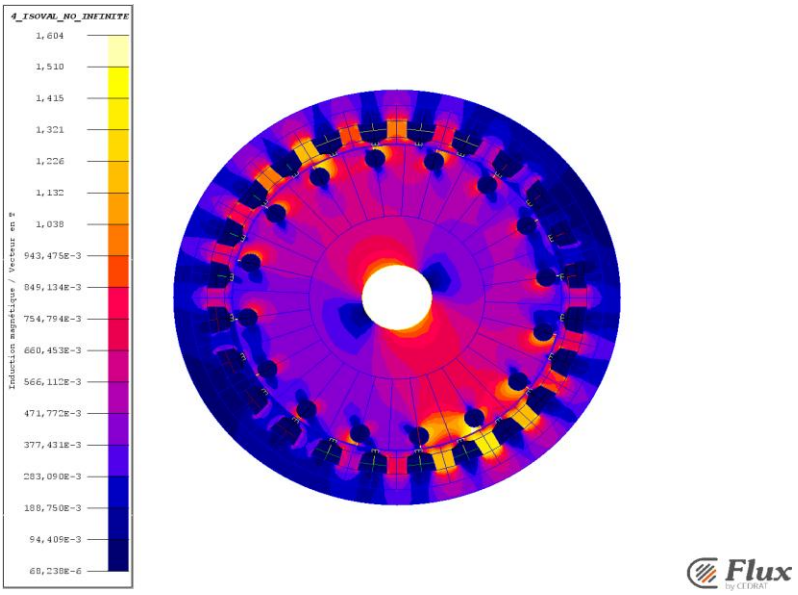

Figure IV.14: Magnetic induction for operation for one broken bar

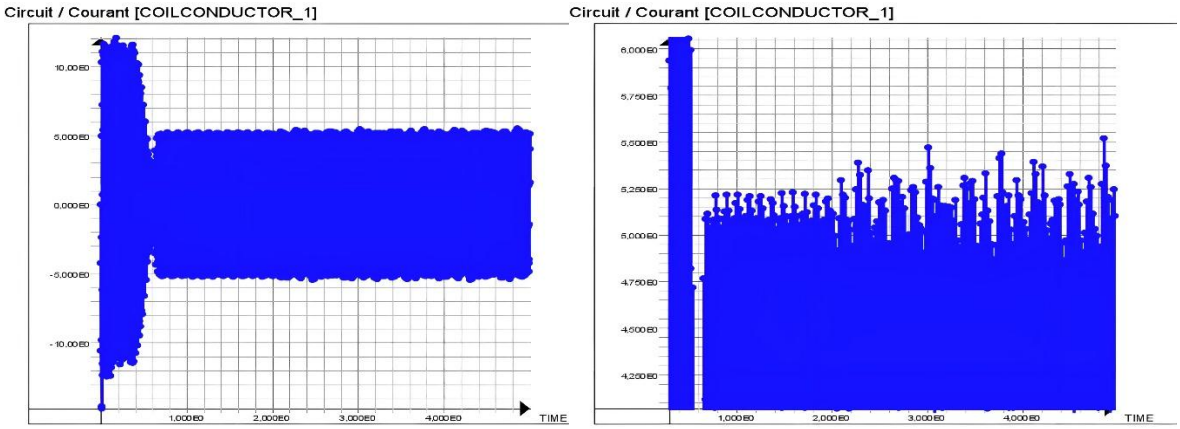

Figure IV.15: Evolution of phase a stator current (isa) for one broken bar

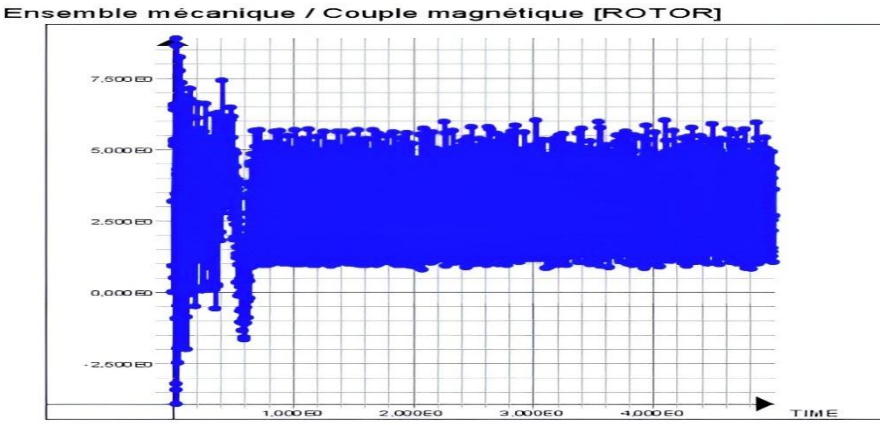

Figure IV.16: Evolution of the electromagnetic torque on starting, under load for one broken bar

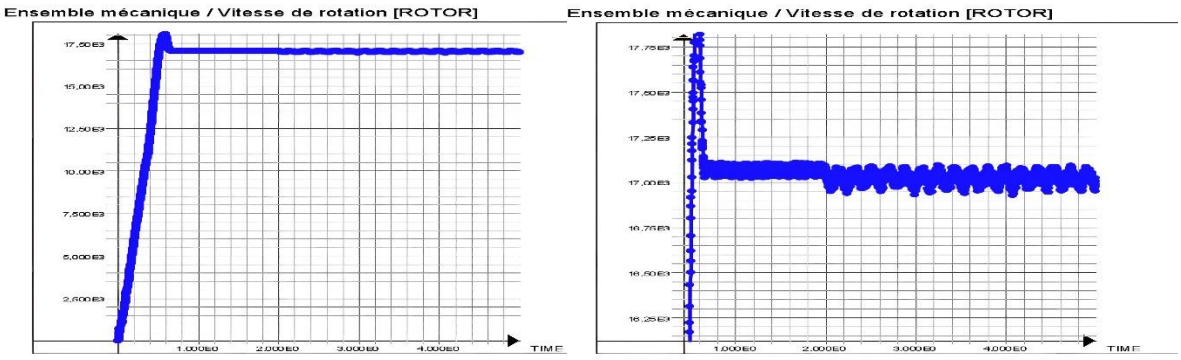

Figure IV.17: Rotational speed at start, under load for one broken bar.

IV.5.2 Case of two broken bars

Second, an induction motor stress test was conducted with two rotor bars that were damaged. We have demonstrated the evolution of the local quantities (the lines of the magnetic field, the magnetic induction) and the global quantities (the currents, the electromagnetic torque, and the speed) in the research using the frequency domain.

Figures (IV.18 to IV.23) depict how a phase that the machine absorbs is impacted by two bar breaking.

A resistive torque of 3.5 N.m is applied to the machine at the point t = 0.6 sec during the simulation, which lasts for five seconds. We replicate the first bar's failure at time t= 2s and the second bar's failure at time t= 3s by raising the resistance by 11 times.

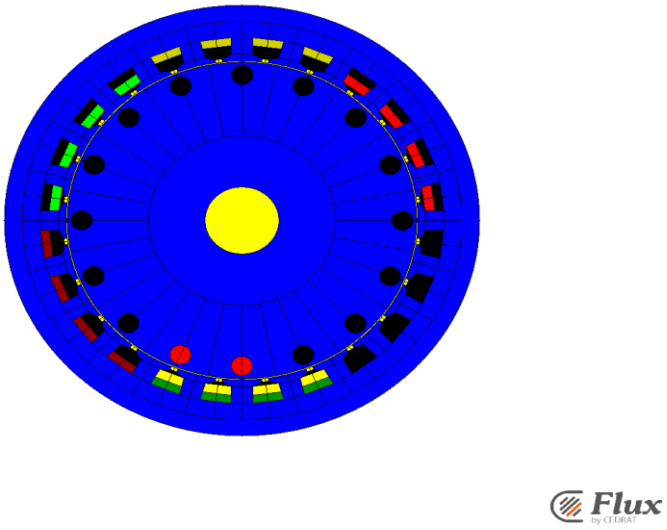

Figure IV.18: Regions of the electromagnetic field calculation domain. (two broken bars)

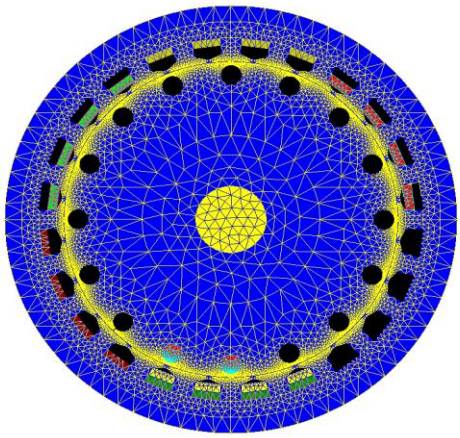

Figure IV.19: Distribution of the mesh (two broken bar)

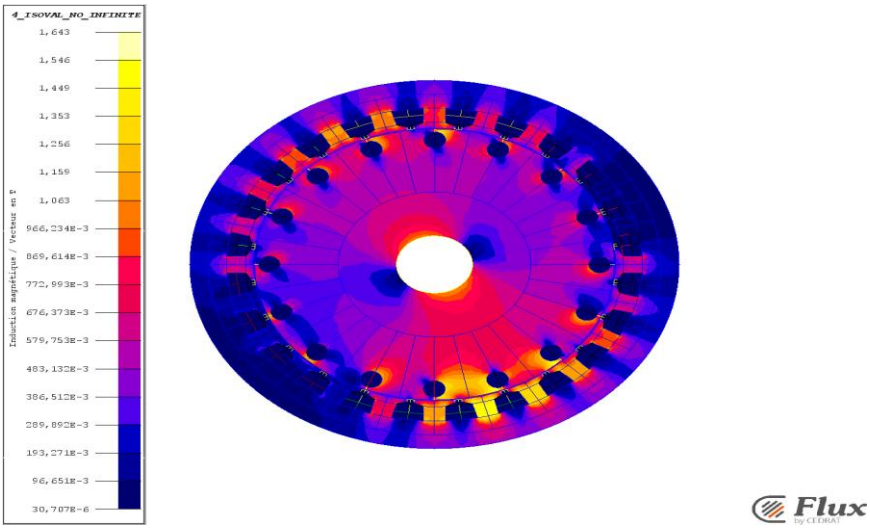

Figure IV.20: Magnetic induction for operation for two broken bars

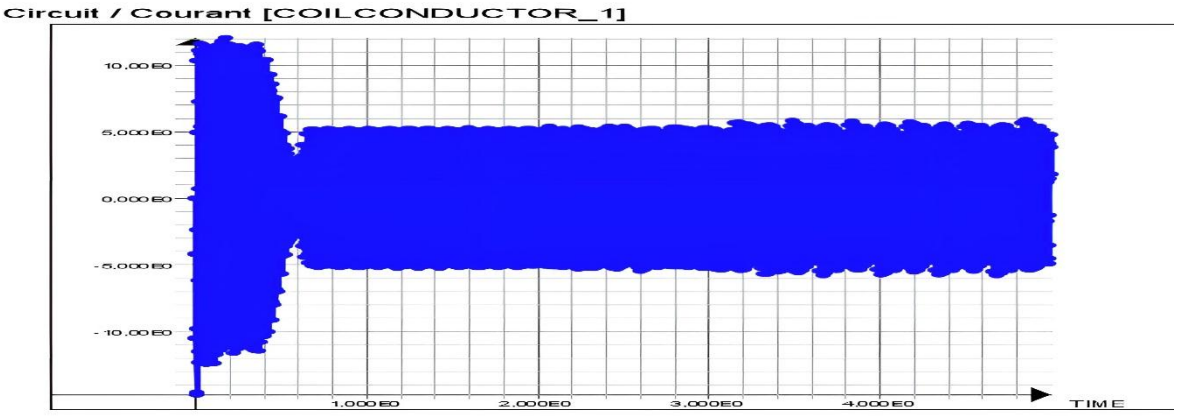

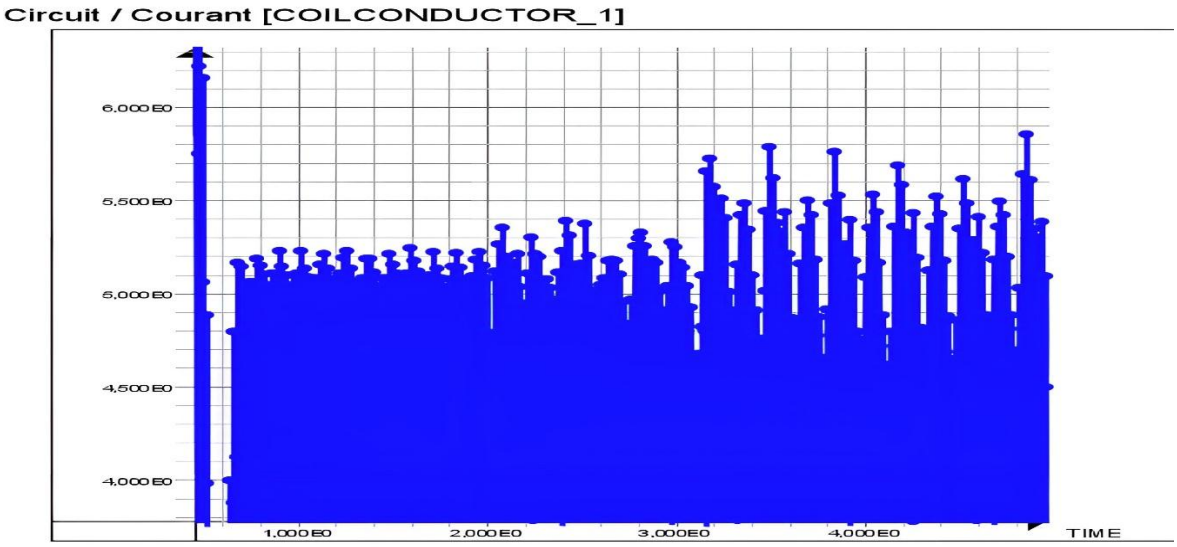

Figure IV.21: Evolution of phase a stator current (isa) for two broken bars

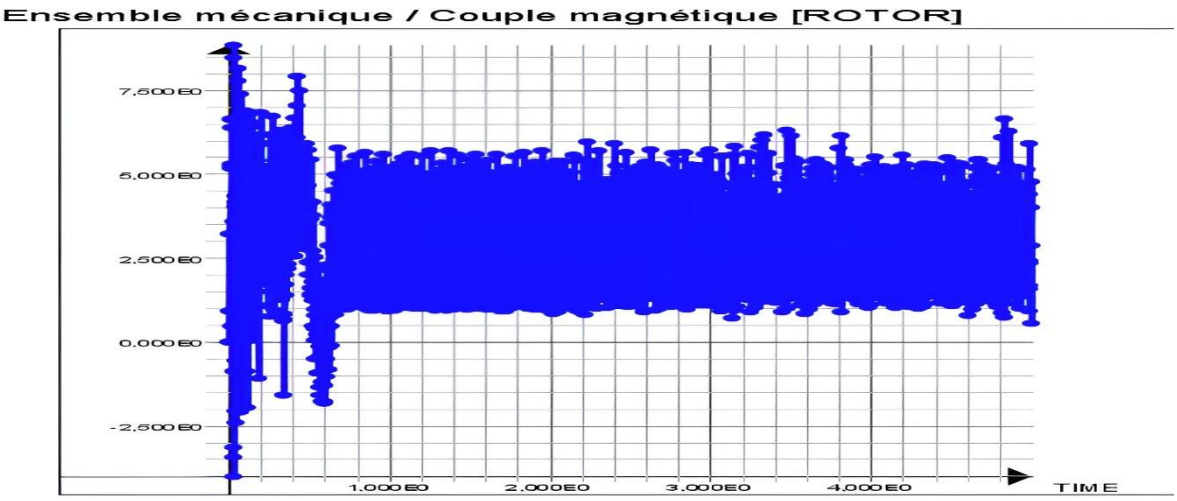

Figure IV.22: Evolution of the electromagnetic torque on starting, under load for two broken bars.

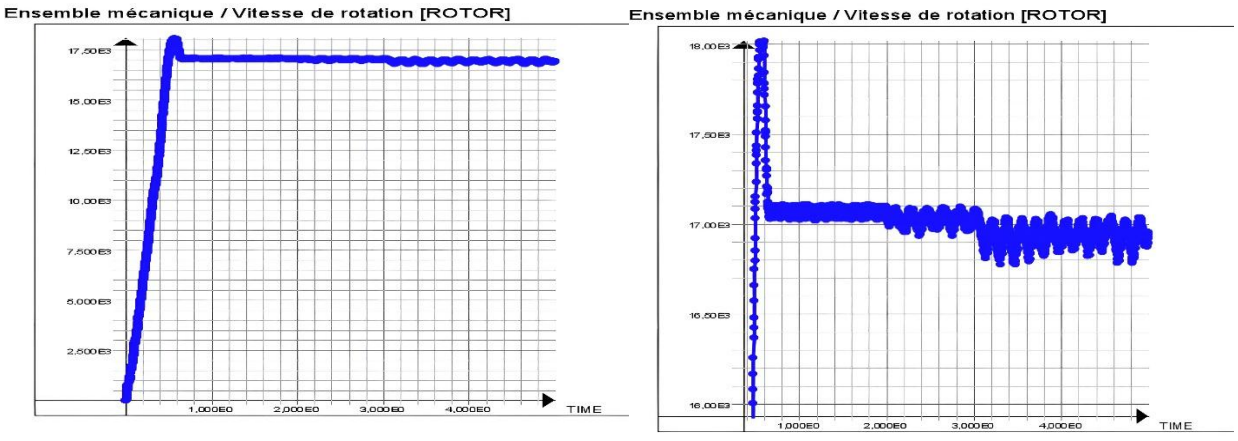

Figure IV.23: Rotational speed at start, under load for two broken bars.

IV.5.3 Case of three broken bars

Third, the effects of three bar breaking on a phase that the machine absorbs are shown in Figures (IV.24 to IV.29). A resistive torque of 3.5 N.m is applied to the machine at the point t = 0.6 s during the simulation, which lasts for five seconds. By raising the resistance by a further 11 times, we are able to replicate the failures of the first bar at time t=2s, the second bar at time t=3s, and finally the third bar at time t=4s.

Three broken rotor bars were used in a stress test on the induction motor. We have demonstrated the evolution of the local quantities (the lines of the magnetic field, the magnetic induction) and the global quantities (the currents, the electromagnetic torque, and the speed) in the research using the frequency domain.

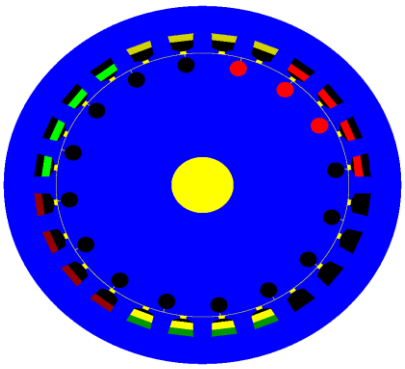

Figure IV.24: Regions of the electromagnetic field calculation domain. (Three broken bars)

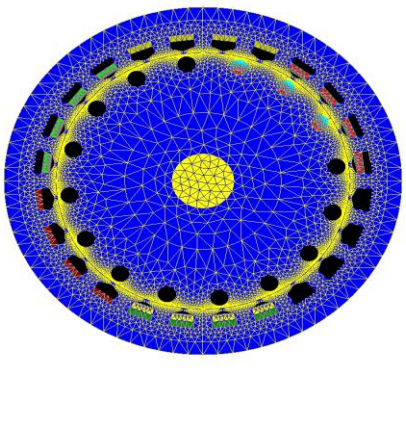

Figure IV.25: Distribution of the mesh (three broken bar)

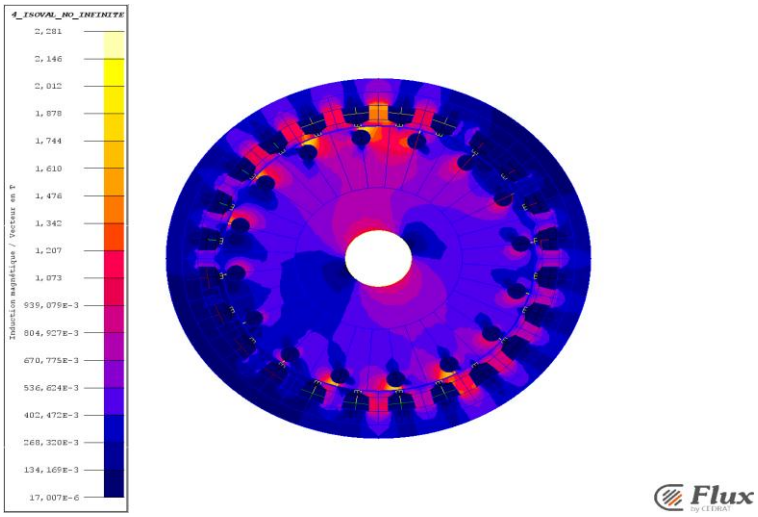

Figure IV.26: Magnetic induction for operation for three broken bars

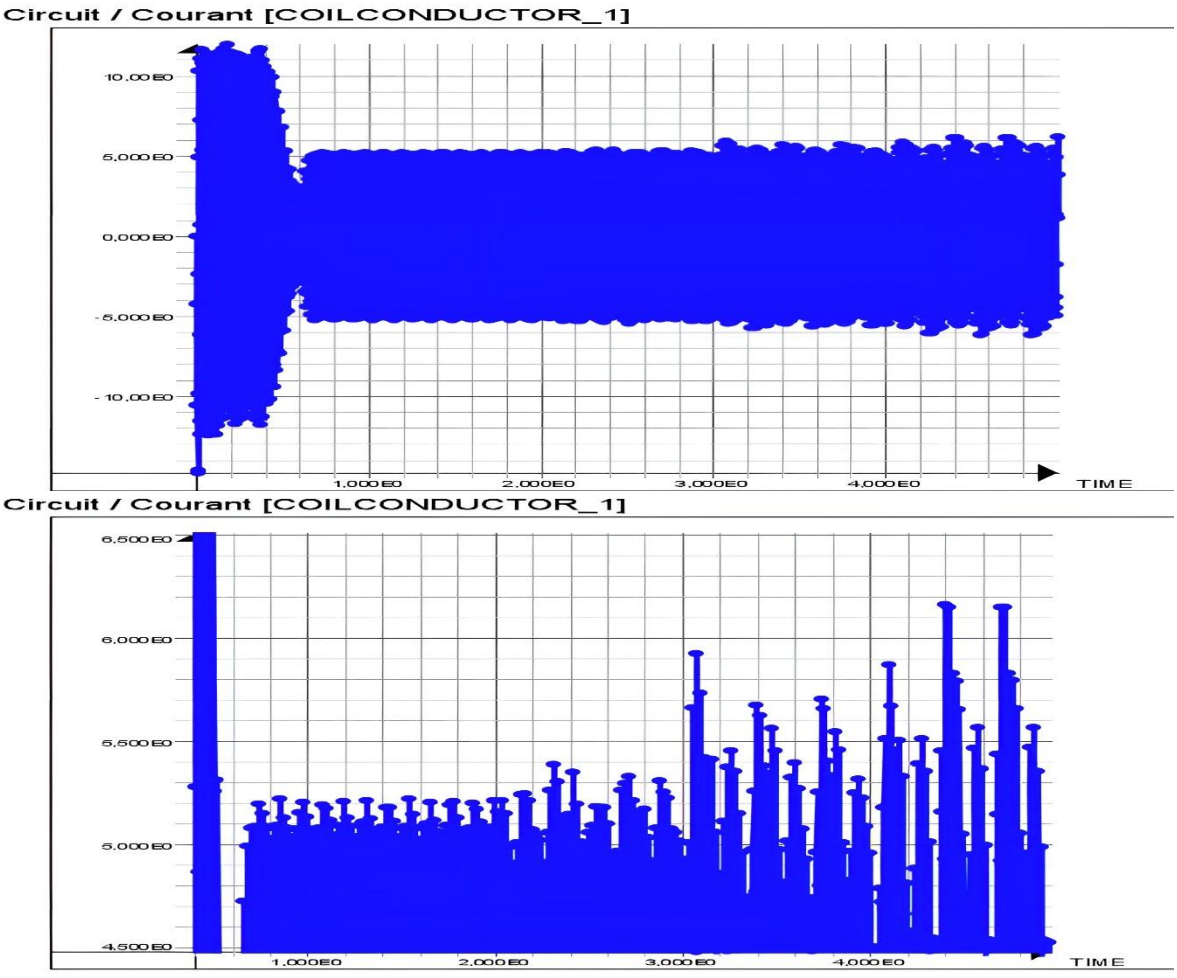

Figure IV.27: Evolution of phase a stator current (isa) for two broken bars

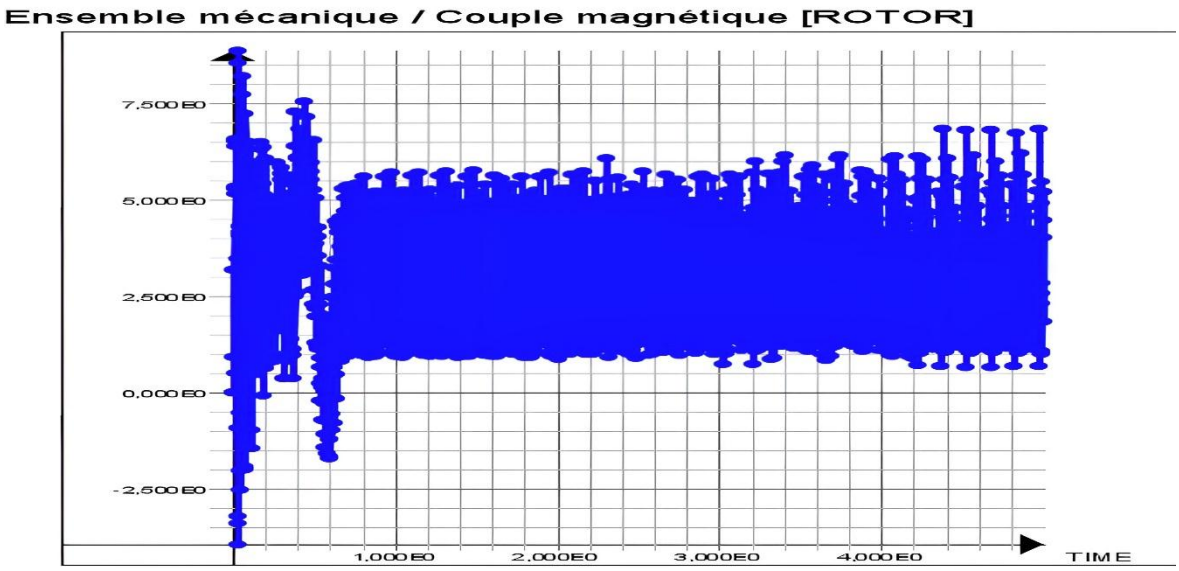

Figure IV.28: Evolution of the electromagnetic torque on starting, under load for three broken bars.

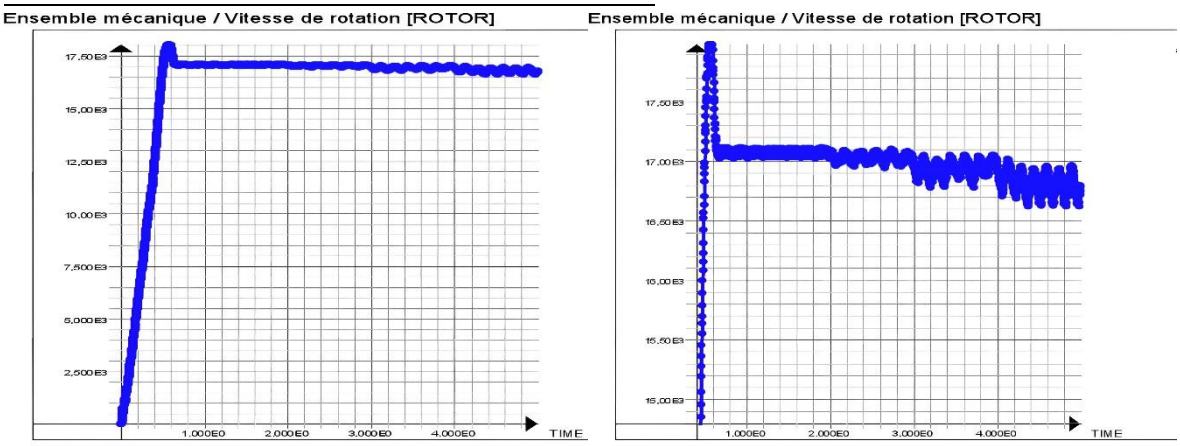

Figure IV.29: Rotational speed at start, under load for three broken bars

We have investigated the machine in three circumstances by breaking the bars, as shown by the prior findings:

- In the first experiment, we fractured the first rod in the squirrel cage rotor, as seen in Figures IV-12 and IV-13. The rod was broken at time t = 2s, and its effects were visible up to t = 5s.
- As illustrated in Figures IV-18 and IV-19, we broke two neighboring bars (bars number one and number two) in the squirrel cage rotor in the second scenario. The first bar was broken at time t = 2s, and we observed its impact until t = 3s. The second rod broke at time t=3s, and its effects were visible until t=5s.

- As shown in Figures IV-24 and IV-25, in the third scenario, we broke three adjacent bars (bars numbers one, two, and three) in the squirrel cage rotor since the first bar was broken at time t = 2s and we observed its impact until t = 3s. The third rod was broken at time t = 4s after the second rod was broken at time t = 3s, and its effects were visible until t = 4 s. We observed its impact up to t=5s.

We will discuss these modifications in our examined model from four perspectives in order to understand these consequences in the three cases:

1. **Magnetic induction and for machine operation**

The magnetic induction operation machine is shown in figures (IV-14), (IV-20), and (IV-26) in three successive examples. The accentuation of the imbalance when the faults arise is also visible in the induction distributions.

We note that the induction is rather high around the fault. The stators complete induction imbalance between the machine's poles accounts for the distortions in the supply currents and electromagnetic torque.

This fault rises higher and becomes more obvious as the number of broken bars rises, which explains why it was easier to see the problem in the third example than it was in the second and in the first instance, breaking one bar had the least detrimental effects.

2. **Changes in phase a current in a stator**

The rupture of the bars causes an undulation in the currents' amplitude. The number of broken bars directly relates to the oscillation's magnitude. The charts below demonstrate this dependency.

In the Figures (IV-15), (IV-21), and (IV-27) the broken bars reflect the current in the bar next to the broken bars in each of the three examples.

The distribution of the currents in the machine's bars is shown in the figures above; when the machine's bars break, the current between the rotor's bars becomes unbalanced and its amplitude increases. Along with the number of broken bars, its amplitude grows. Be aware that this value is also related to the oscillations' amplitude.

Because the neighboring bars carry more current, this causes them to heat up and age more quickly, which accounts for the cumulative effect on the breakage of the bars.

3. The torque impact of bar fracture

We can see that the mechanical characteristic in a transitory condition, along with the number of broken bars, swiftly provides information on the status of the engine in Figures (IV-16), (IV-22), and (IV-28). The machine and the traction chain's component degradation are sped up by the oscillations' high amplitude.

We see that the torque is increasingly impacted as the number of broken bars increases. In actuality, the disintegration of the bars lowers the average value and raises oscillations.

Through analysis of these defects in the third situations, which demonstrated to us in each instance that the rise in damage grows exponentially with the number of broken bars, these oscillations increase with the number of broken bars in the squirrel cage rotor.

4. Rotational speed

As the number of broken bars slowing the motor shaft rises, we can see from the findings in Figures (IV-17), (IV-23), and (IV-29) that the speed is degrading and dropping.

The inverse link between machine speed and the quantity of broken bars was validated in the first, second, and third examples in our investigation of the evolution of machine speed. These lead to oscillations in rotational speed, which produce mechanical vibrations and, as a result, irregular machine operation.

IV.6 Conclusion

In this chapter, a squirrel cage induction motor is simulated under both healthy and rotor broken bar situations using time-step FEM. The if the rotor bar is totally destroyed. This raises the rotor current for the other bars. Additionally, the asymmetric flux distribution and increased flux density surrounding the fractured bar cause an increase in electromagnetic torque oscillations and a decrease in rotational speed.

Let's come to the conclusion that the machine will have more issues the more broken bars there are.

In this study, the broken bar current is given a non-zero value, and the broken bar is modeled by a large resistance. The FEM machine fault model is used to study the behavior of the machine under various fault conditions, such as fault (broken bar). We have shown

the evolution of the local quantities (the lines of the magnetic field, the magnetic induction), as well as the global quantities (the currents, the electromagnetic torque, and the speed).

The analysis provided by the finite element approach then demonstrates that it is a useful and affordable way to analyze the impact of rotor defects on the behavior of asynchronous machines, and has enabled us to comprehend and quantify the local effects of rotor faults.

These outcomes provided compelling evidence for the efficiency of the approach employed in our investigation in identifying flaws (broken bars) in the squirrel cage rotor and anticipating future issues with the device.

A validation of the accuracy of our work from the third chapter, where we utilized the MATLAB software, is also expressed in this chapter utilizing the Flux2D® SOLVER tool.

General Conclusion

Since asynchronous machines are becoming more prevalent in industrial settings, certain users are required to take precautions against the emergence of a problem, which most frequently results in a premature machine shutdown. Therefore, the work discussed here focuses on the identification of rotor failures, particularly bar fractures that may happen inside an asynchronous machine's squirrel cage.

Our work's primary goal is to employ a multi-winding model to mimic the break of bars and identify the machine's behaviours in both a healthy and faulty condition in order to discover and diagnose defects in asynchronous machines. Increasing the breaking bars inevitably causes the machine's efficiency and performance to decline. The benefit of using signal processing is that information may be extracted to find and identify faults.

Results

In the first chapter, we reviewed the machine's component parts and described the numerous defects that may arise on them. The examination of signals showing an electrical and/or mechanical flaw in the frequency domain is then made possible by a number of instruments derived from signal processing techniques.

Finally, we outlined the benefits and drawbacks of the diagnostic techniques currently used to determine whether a defect exists in an asynchronous system to confirm the existence of an electrical and/or mechanical breakdown, as well.

It immediately became essential to have a simulation tool that was adequately representational of the various conditions (healthy and broken system), given how challenging it is to experimentally recreate fault situations. Therefore, in the second section of this thesis, we present a model that enables the simulation of an asynchronous squirrel-cage machine in the (Park) frame by using a multi-winding model to simulate the break of bars and assess how the machine behaves under normal and abnormal electrical conditions (at the motor or voltage inverter level case).

Through this method, it was feasible to examine how an asynchronous machine's dynamic behaviours were affected by a rotor error.

In the third chapter, simulation software on Matlab was created. Results on the signals acquired as a function of time, including the stator current, mechanical speed, electromagnetic torque, and bar currents.

For the spectrum study of the stator current for broken rotor bar faults, we also employed the transformations Fast Fourier (FFT) and Wavelet.

There is a wealth of information concerning the broken bar fault's existence, as well as the frequencies and frequency bands that define the fault, when it is identified using spectral analysis of the stator current (MCSA-FFT).

We observed the following via spectral analysis or the Fast Fourier Transform (FFT): Appearance of new lines in the stator current spectrum, We have emphasized more representative criteria, such as the presence of frequency lines ((1± 2ks) fs) on both sides, utilizing the Fast Fourier Transform (FFT). Another fundamental error that leads to bars breaking.

It has been discovered that rotor flaws lead to oscillations in stator current, speed, and torque. As the fault severity grows, so does the amplitude of these oscillations.

When the machine was powered by an inverter with PWM control, new harmonics began to arise in the signal spectrum. The most significant of these harmonics, as we have already said, are those that are centeredaround the carrier frequency. Others close to the fundamental, however, have modest amplitudes. Additionally, it was discovered that the fault harmonics may be easily separated from the inverter's other harmonics.

These diagnostic methods have the benefit of alerting us to defects even while the equipment is being powered by an inverter.

The outcomes demonstrate that the FFT can detect a bar break defect by looking for lines that are opposite the fundamental.

In this study, the diagnostic method is based on the analysis of the stator current during the start-up electromagnetic torque and uses both discrete wavelet transform and continuous wavelet transform.

This technique can demonstrate the time-frequency properties of fault signals clearly. The performance of these two strategies was shown by their ability to construct a local

representation of non-stationary current signals for both a working machine and one with a defect by raising the peaks of the time domain waveform analysis function.

Using wavelet transform and wavelet packets to decompose the signal is a useful method for multi-resolution analysis.

The orthogonality of the wavelet function ensures the independence of the decomposed signals. The separated frequency bands include no duplicate data.

Mechanical condition monitoring and problem diagnostics may be successfully carried out using data from a number of separate frequency bands.

Additionally, to ensure that the machine would run continuously while using the wavelet continuous transformation approach. The produced simulation results demonstrate this technique's use in broken bar detection. Additionally, wavelet quality may be employed to enhance fault identification and increase the efficacy of detection and diagnostics. This technique, which makes use of specific technologies for motor status monitoring and fault analysis, identifies issues early, helping to prevent damage and total failure. The shorter period of time ensures that defects will be found and that the equipment will be maintained without suffering any damage. This work shows a new approach in detection of broken rotor bars in squirrel cage induction motors with inverter or without inverter

Fourthly, We have created a model based on finite elements utilizing Flux 2D® software to depict numerous flaws that may arise during normal operation, the FEM confirmed the simulation results to Chapter 3's results credibility and confirm the potency of the suggested index for rotor broken bar fault detection in the fourth chapter. When compared to healthy settings, the suggested index significantly increases at broken bars situations, and it may identify defective conditions with clarity.

We considered the possibility of rotor bar failure defect in order to meet the goal of our study. As a consequence, we discovered that the electromagnetic torque degraded and that the bars next to the fractured bars are under the highest stress. This study helped us to understand how the failed system behaved and to identify the distinctive fault signatures, enabling us to create appropriate diagnostic procedures and serving as a starting point for problem identification.

Furthermore, in this chapter, FEM is used to analyze the magnetic field and establish the characteristics of the machine under various failure scenarios. Additionally, two situations

(health machines and destructive machines) show that machine broken bars have an impact.

Outlook

REFERENCES

[1] BAZINE Sadok, “Conception et implémentation d’un méta-modèle de machines asynchrones en défaut” , thèse de doctorat, Université de Poitiers, Année 2009.

[2] M. BOUHARKAT, “Etude de l'évolution des courants rotoriques d'une machine asynchrone à cage en régime dynamique”, Thèse de doctorat, Université de Batna, Faculté des sciences de l'Ingénieur, Année Février 2006.

[3] Abid M., Laribi S., Larbi M., Allaoui T, “Diagnosis and localization of fault for a neutral point clamped inverter in wind energyconversion system using artificial neural network technique”, Electrical Engineering &Electromechanics, 2022, no. 5, pp. 55-59. doi:https://doi.org/10.20998/2074-272X.2022.5.09.

[4] Talhaoui. H, Ameid. T, Aissa. O, Kessal. A, “Wavelet packet and fuzzy logic theory for automatic fault detection in induction motor”, Soft Computing, 2022, 26:11935–11949. doi:https://doi.org/10.1007/s00500-022-07028-5.

[5] Ghirmay.A, Ghebremeskel.H, Ghebrehiwet.R, “Comparative Analysis of Signal Processing Techniques for Fault Detection in Three Phase Induction Motor”, Journal of Electronics and Informatics, 2021, Vol.03/ No.01.doi: https://doi.org/10.36548/jei.2021.1.006

[6] DEHINA .W, BOUMEHRAZ. M, KRATZ .F, “Diagnosis and Detection of Rotor Bars Faults in Induction Motor Using HT and DWT Techniques”, 18th International Multi-Conference on Systems. 2021.Biskra, Algeria, doi: https://doi.org/10.1109/SSD52085.2021.9429381

[7] N. Bessous, S.Sbaa, and A.Toumi, (2018), “A detailed study of the spectral content in the stator current of asynchronous machines under broken rotor bar faults using MCSA technique, ” .

[8] J. Cusidó, and L.Romeral, “Fault Detection in Induction Machines Using Power Spectral Density in Wavelet Decomposition”, IEEE TRANSACTIONS ON INDUSTRIAL ELECTRONICS, VOL. 55, NO. 2, FEBRUARY 2008 .

[9] Khadim .M- S ,Kuldeep .S, “Rotor broken bar fault detection in Induction Motor Using Transformative Techniques"Institute of Engineering & Technology”, Lucknow, INDIA, Journal of Electrical Engineering www.jee.ro.

[10] Martin Brandt, Miroslav Gutten, “ Analysis of Winding Fault in Electric Machines by Frequency Method ” ,Measurement and Applied Electrical Engineering, ©2018 IEEE.

[11] SZABÓ .Loránd , DOBAI .Jenő Barna, BIRÓ .Károly Ágoston, “ ROTOR FAULTS DETECTION IN SQUIRREL-CAGE INDUCTION MOTORS BY CURRENT SIGNATURE ANALYSIS ” ,2004 IEEE-TTTC - International Conference on Automation, Quality and Testing, Robotics (2004).

[12] Bousseksou. Radouane, “Analytical modeling of asynchronous machines application to diagnosis”, thesis of Magister, Mentouri University of Constantine 2007.

[13] A. H. Bonnett, "Cause and analysis of Anti-Friction Bering Failures in A.C Induction Motors", IEEE Transactions on Industry Application, pp 14 - 23, Sept/Oct 1993.

[14] A.Bouzida, "Diagnosis of faults of the asynchronous cage machine by the wavelet technique", Memory of Magister National Polytechnic School of Algiers. Algeria 2008.

[15] Saliou .Diouf, "Contribution to the industrial diagnosis of rolling bearing faults and Imbalance by Neuronal techniques Application to the asynchronous machine", doctoral thesis, University of Paris XII Val De MARNE-CRETEIL, 2007.

[16] Géaton .Didier, "Modeling and diagnosis of the asynchronous machine in presence of failures", doctoral thesis, Henri Poincaré University, Nancy1, 2004.

[17] Oumaamar Mohamed El Kamel, "Fault monitoring and diagnosis rotors of the induction machine with different types of power supply", doctoral thesis Mentouri University of Constantine 2010.

[18] Ali Ibrahim, " Contribution At diagnostic machinery electromechanics: Exploitation of electrical signals and instantaneous speed ", Thesis doctorate University of Saint Etienne 2009.

[19] Rodrigo S. Miranda ,Clarissa Cruz,Noé Cheung and Adilto P. A. Cunha " Fatigue Failure Analysis of a Speed Reduction Shaft ", Department of Mechanical Engineering, State University of Maranhão-UEMA, São Luís 65055-310, MA, Brazil 24 May 2021, https://doi.org/10.3390/met11060856.

[20] Hossein. Hooshmandi, Mohammad .Ebrahimi, Ali. Davoudi " Analytical Derivation of Induction Motors Inductances under Eccentricity Conditions ", Progress In Electromagnetics Research B, Vol. 60, 95–110, January 2014; DOI:10.2528/PIERB14051704.

[21] Bui Viet Phuong, "Diagnosis of electrical machines by field analysis magnetic leakage application to the identification of rotor faults of an alternator void", Doctoral thesis, National Polytechnic Institute, University of Grenoble 2007.

[22] M. Melfi, A.M. Jason Sung, S. Bell, G.L. Skibinski, "*Effect of surge voltage risetime on the insulation of low-voltage machine fed by PWM converters*" ,IEEE Transactions on Industry Applications, vol. 34, pp.766-775, July/August 1998.

[23] A. H. Bonnett and G. C, "Soukup. analysis of rotor Failures in A.C Induction Motors", *IEEE Transactions on Industry Application*, VOL. 24(6):1124-1130, nov/dec 1988.

[24] Babak Vaseghi , "Contribution to the study of electrical machines in the presence of fault between turns Modeling – Reduction of the fault current", Doctoral thesis the National Polytechnic Institute of Lorraine, University of Nancy, 2009.

[25] Hamid A, Toliyat, Mohammed S, Arefeen, and Alenxender G, Parlos "A method for dynamic Simulation of Air-Gap Eccentricity in Induction Machines", IEEE Transaction on Industry Applications,32(4);910-917, July–August1996.

[26] Mohamed. Khaleel, Mehmet. ŞİMŞİR, Zıyodulla. Yusupov, Nassar .Yasser, Hala. Elkhozondar, Abdussalam. Ali Ahmed, "The Role of Fault Detection and Diagnosis in Induction Motors",

Department of Electrical-Electronics Engineering, Faculty of Engineering, Karabuk University, Karabuk, Turkey, February 4, 2023.

[27] Kim, K., and Parlos, A.G., (2002), "Model-Based Fault Diagnosis of Induction Motors Using Non-Stationary Signal Segmentation " ,Mechanical Systems and Signal Processing, vol. 16, no. 2-3, pp. 223-253.

[28] A. Menacer, "Contribution to the identification of parameters and states of an induction machine for diagnosis and development of robust control: robustness against faults", Doctoral thesis, University of Batna .December 2007.

[29] Abed. A "Contribution to the study and diagnosis of the asynchronous machine", doctoral thesis, Henri Poincaré Nancy University, 2002.

[30] Saadi SAKHARA, "DIAGNOSTIC DES DEFAUTS D'UN ENTRAINEMENT ELECTRIQUE PAR LA TECHNIQUE ONDELETTE", THESE diplôme de DOCTORAT, DEPARTEMENT D'ELECTROMECANIQUE, Université Badji Mokhtar- Annaba, 2017.

[31] T. BOUMEGORA , "Recherche des signatures électromagnétiques des défauts dans une machine asynchrone et synthèse d'observateurs en vue du diagnostic", Thèse de doctorat ; Ecole centrale de Lyon, Année 2001

[32] MERABET. S, D. HOUSSINE, "Diagnostic de d'défauts de la machine asynchrone `a cage d'écureuil par la méthode de reconnaissance des formes", Thèse d'ingénieur ; Ecole Nationale Polytechnique d'Alger, Année Juin 2007.

[33] BELAIDE Ammar, "diagnostic de la machine asynchrone par la méthode d'identification paramétrique", Université de M'sila, diplôme d'ingénieur d'état, Année 2012.

[34] S. Bashir, "Contribution to the diagnosis of the asynchronous machine by parametric estimation", Doctoral thesis, University of Poitiers, 2002. 26

[35] T. J. Sobczyk, A. Izworski, "Recognition of rotor eccentricity of induction motor based on the fourier spectra of phase currents" ,Proc. ICEM'98, pp. 408–413, Vol 1, September 2–4 1998 Istanbul Turkey.

[36] M. E. H. Benbouzid and G. B. Kliman, "What stator current processing based technique to use for induction motor rotor faults diagnosis," *IEEE Trans. Energy Convers.*, vol. 18, no. 2, pp. 238–244, Jun. 2003.

[37] Khadim Moin Siddiqui, V.K.Giri, "Broken Rotor Bar Fault Detection in Induction Motors using Transient Current Analysis" ,International Journal of Electronics and Communication Technology, Volume 2, Issue 4, Oct-Dec 2011.

[38] G. B. Kliman *et al.*, "Non-invasive detection of broken rotor bars in operating induction motors", *IEEE Trans. Energy Convers.*, vol. EC-3, no. 4, pp. 873–879, Dec. 1988.

[39] F. Filipetti *et al.*, "AI techniques in induction machines diagnosis including the speed rifle effect", in *Proc. IEEE Industry Applications Society Annu. Meet. Conf.*, San Diego, CA, Oct. 6–10, 1996, pp. 655–662.

[40] Neelam Mahala, Ratna Dahiya, "Rotor Faults Detection in Induction Motor by Wavelet Analysis", International Journal of Engineering Science and Technology Vol.1(3), 2009, 90-99.

[41] H.Douglas, P.Pillay, A.Ziarani, "Detection of Broken Rotor Bar in Induction Motors using Wavelet Analysis", Proc. Of IEEE International Electric Machines and Drives Conference (IEMDC'03), vol. 02, pp. 923-928, 2003.

[42] Harlisca Ciprian, SZABÓ Loránd, "Wavelet Analysis and Park's Vector Based Condition Monitoring of Induction Machines", Journal of Computer Science and Control Systems, Volume 4, Number 2, October 2011.

[43] N. Hariharavarshan, Jeyaram Durga Manian, and R. Me lvinaMinny, "Online Monitoring and Analysis of Induction Motor Using Cu rrent Signature Analysis Implementing Wavelet Analysis and FFT Analysis", *International Journal of Electrical Engineering & Technology*, 7(6), 2016, pp. 36–54.

[44] Yaghobi, H., Ansari K., Rajabi, H. (2011). "Analysis of magnetic flux linkage distribution in salient pole synchronous generator with different kinds of inter turn winding faults", Iranian Journal of Electrical & Electronic Engineering, 7(4): 260-272.

[45] Nemec, M., Ambrožič, V., Fišer, R., Nedeljković, D., Drobnič, K. (2019). "Induction motor broken rotor bar detection based on rotor flux angle monitoring", Energies, 12(5): 794-811. https://doi.org/10.3390/en12050794

[46] Rababaah, A.R., Arumala, J., Dabipi, I.K., Fotouhi, K., Hura, G., Dudi, A. (2016). " Mechanical system fault detection using intelligent digital signal processing", Journal of Machinery Manufacturing and Automation, 5(1): 27-39.

[47] Bellini A, Filipetti F, Tassoni C, Capolino GA, "Advances in diagnostic techniques for induction machines", IEEE Trans Ind Electron 2008;55:4109–26.

[48] Filippeti F, Franceschinni G, Tassoni C, Vas P, "AI techniques in induction machines diagnosis including the speed ripple effect", IEEE Trans Ind Appl 1998;34:98–108.

[49] Garcia-Perez, A., Romero-Troncoso, R.J., Cabal-Yepez, E., Osornio-Rios, R.A., 2011. " The application of high-resolution spectral analysis foridentifying multiple combined faults in induction motors", IEEE Trans. Ind. Electron. 58 (May (5)), 2002–2010

[50] Hedayati Kia, S., Henao, H., Capolino, Gérard-André, 2009. "Diagnosis of broken-bar fault in induction machines using discrete wavelet transformwithout slip estimation", IEEE Trans. Ind. Appl. 45 (July/August (4)), 1395–1404.

[51] Jung, J.-H., Lee, J.-J., Kwon, B.-H., 2006. "Online diagnosis of induction motors using MCSA", IEEE Trans. Ind. Electron. 53 (December (6)),1842–1852.

[52] Ujjan, S. M., Kalwar, I. H., Chowdhry, B. S., Memon, T. D., & Soother, D. K. (2020). "Adhesion level identification in wheel-rail contact using deep neural networks", 3C Tecnología. Glosas de innovación aplicadas a la pyme. Edición Especial, Abril 2020, 217-231.

[53] DEHINA .W, BOUMEHRAZ. M, KRATZ .F. "*Diagnosis and Detection of Rotor Bars Faults in Induction Motor Using HT and DWT Techniques*", 18th International Multi-Conference on Systems. 2021.Biskra, Algeria

[54] Kia, S.H., Henao, H., Capolino, G.-A., 2007. "A high-resolution frequency estimation method for three-phase induction machine fault detection",IEEE Trans. Ind. Electron. 54 (August (4)), 2305–2314

[55] K. Gyftakis, J. Antonino-Daviu, R. Garcia-Hernandez, M. McCulloch, D. Howey, A. Cardoso, "Comparative Experimental Investigation of the Broken Bar Fault Detectability in Induction Motors", IEEE Transactions on Industry Applications, 10 (2015) 1-1.

[56] W. W. Tan and H. Huo, "A generic neurofuzzy model-based approach for detecting faults in induction motors" ,*IEEE Trans. Ind. Electron.*, vol. 52, no. 5, pp. 1420–1427, Oct. 2005.

[57] B. Ayhan, M.-Y. Chow, and M.-H. Song, "Multiple discriminant analysisand neural-network-based monolith and partition fault-detection schemesfor broken rotor bar in induction motors," *IEEE Trans. Ind. Electron.*, vol. 53, no. 4, pp. 1298–1308, Jun. 2006.

[58] Daubechies. I, "The wavelet transform, time-frequency localization and signal analysis", IEEE transactions on information theory. 1990; 36.5: 961–1005.

[59] Peng .ZK, Chu. FL, "Application of the wavelet transform in machine condition monitoring and fault diagnostics: a review with bibliography", Mechanical Systems and Signal Processing. 2004; 18.2: 199–221.

[60] Kia SH, Henao H, Capolino G-A, (2009). " Diagnosis of broken-bar fault in induction machines using discrete wavelet transform without slip estimation", IEEE Trans Ind Appl 45:1395–1404. https://doi.org/10.1109/TIA.2009.2018975.

[61] Bouzida A, Touhami O, Ibtiouen R et al (2011). " Fault diagnosis in industrial induction machines through discrete wavelet transform", IEEE Trans Ind Electron 58:4385–4395. https://doi.org/10.1109/IE.2010.2095391.

[62] Zhenxing, L., Xianggen, Y., Zhang, Z., Chen, D. and Chen, W. (2004), "Online rotor mixed fault diagnosis way based on spectrum analysis of instantaneous power in squirrel cage induction motors", IEEE Transactions on Energy Conversion, Vol. 19 No. 3.

[63] Bhola Jha and K. Ram Mohan Rao, " Doubly Fed Induction Generator Analysis through Wavelet Technique", Journal of Engineering Science and Technology Review 2 (1) (2009) 63-67.

[64] G. A. Jiménez, A.O. Munoz, M. A. Duarte-Mermoud, "Fault detection in induction motors using Hilbert and Wavelet transforms", Springer- Verlag 2006.

[65] Purushotham, V.; Narayanana, S.; Prasad, S.A.N; "Multi-fault diagnosis of rolling bearing elements using wavelet analysis and hidden Markov model based fault recognition", NDTE Int. **2005**, 38, 654–664.

[66] Douglas, H., Pillay, P. and Ziarani, A.K. (2004), "A new algorithm for transient motor current signature analysis using wavelets", IEEE Transactions on Industry Applications, Vol. 40 No. 5, pp. 1361-1368

[67] Osipov, D. S., Lyutarevich, A. G., Gapirov, R. A., Gorunov, V. N., & Bubenchikov, A. A. (2016). "Applications of wavelet transform for analysis of electrical transients in power systems: the review", Przeglad Elektrotechniczny, 4, 162-165.

[68] Mehrjou M R, Mariun N, Karami M, Misron N, Toosi S, Zare MR, "Evaluation of waveletfunctions for broken rotor bar detection of induction machine using coefficient-related features", International Journal of Applied Electronics in Physics & Robotics. 2013; 1.1: 18–23.

[69] Ekici S, Yildirim S, Poyraz M, "Energy and entropy-based feature extraction for locating fault on transmission lines by using neural network and wavelet packet decomposition", Expert System Application. 2008; 34.4: 2937–2944.

[70] Ameid T, Talhaoui H, Azzoug Y, Chebaani M, Laidoudi A (2021). "Rotor fault detection using hybrid signal processing approach for sensorless backstepping control driven induction motor at lowspeed operation", Int Trans Elect Energy Syst 31:1–26. https:// doi.org/10.1002/2050-7038.13150

[71] Cherif H, Menacer A, Bessam B, Kechida R ,(2015). "Stator inter turns fault detection using discrete wavelet transform. In: International symposium on diagnostics for electrical machines", power electronics and drives (SDEMPED). IEEE, Guarda, Portugal.
doi:https://doi.org/10.1109/DEMPED.2015.7303681

[72] S. R. Kapoor, N. Khandelwal, P. Pareek, "Bearing fault analysis by signal energy calculation based signal processing technique in Squirrel Cage Induction Motor", International Conference on Signal Propagation and Computer Technology, pp. 33–38 (2014).

[73] J.A. Antonino-Daviu, M. Riera-Guasp, J. Roger-Folch, M.P. Molina, "Validation of a new method for the diagnosis of rotor bar failures via wavelet transform in industrial induction machines", IEEE Transactions on Industry Applications 42 (4) (2006) 990–996.

[74] Z. Ye, A. Sadeghian, B. Wu, "Mechanical fault diagnostics for induction motor with variable speed drives using Adaptative Neurofuzzy Inference System", Electric Power Systems Research 76 (9–10) (2006) 742–752.

[75] Z. Ye, B. Wu, A. Sadeghian, "Current signature analysis of induction motor mechanical faults by wavelet packet decomposition", IEEE Transactions on Industrial Electronics 50 (6) (2003) 1217–1228.

[76] S. Nandi, H.A. Toliyat, "Condition monitoring and fault diagnosis of electrical motors—A review, IEEE Transactions on Energy Conversion 20 (4) (2005) 719–729.

[77] T. Tarasiuk, "Hybrid wavelet-Fourier spectrum analysis ", IEEE Transactions on Power Delivery 19 (3) (2004) 957–964.

[78] Bourkoua A / Ouhab et Hamrat Amar, "développement du système automatique de diagnostic des défaillance des machines asynchrones par l'application de la technique des réseaux de neurones " , thèse d'ingéniorat ; spécialité d'électromécanique,Université de boumerdes.1999.

[79] A. Abed, L. Baghli, H. Razik, A. Rezzoug, "Modelling Induction Motors for Diagnostic Purposes", EPE'99, 7-9 September 1999, 233.pdf, Lausanne, Suisse, pp. 1-9.

[80] N.Benouzza , "Approche des Vecteurs de Park Appliquée à la Détection des Défauts dans les Moteurs Asynchrones à Cage d'Ecureuil ", Thèse de Doctorat, Université des Sciences et de la Technologie d'Oran, 06 Décembre 2006.

[81] S.Bouslimani , " Commande Vectorielle de la Machine Asynchrone avec Régulateurs Classique et Flou en Présence de Défauts", Université Larbi Ben M'hidi Oum El Bouaghi, 14 Décembre 2011

[82] A. Abed, "Contribution à l'Etude et au Diagnostic de la Machine Asynchrone", Thèse de Doctorat, Université Henri Poincaré, Nancy-1, mars 2002.

[83] Pu. Shi, zheng chen, Y. Vagapov, Z. Zouaoui , "A new diagnosis of broken rotor bar fault extent in three phase squirrel cage induction motor", Mechanical System and Signal Processing, Vol 42, pp 388-403, 2014.

[84] Arvind Singh, bevon Grant, R. DeFour, C Charma, Bahadoorsingh, "a review of induction motor fault modeling", Eectric power Systems Research, Vol 133, pp 191- 197, 2016.

[85] BOUCHIBI Abbes et Boualem ZERROUKI, " commande par logique floue d'une machine asynchrone ", thèse d'ingéniorat ; spécialité d'Electronique option contrôle 2003.

[86] S.Laribi , "Synthèse des Méthodes de Diagnostic Appliquées à la Détection des Défauts dans les Machines Asynchrones", Mémoire de Magister, USTO Oran, 03 Juillet 2005

[87] M. G. Say , " The Performance and Design of Alternating Current Machines ", Sir Isaac Pitman &Sons Ltd., London, 1983.

[88] D.Toumi, N.Benouzza, B.Kraloua, A.bendiabdellah et A.Benyettou , " Emploi de l'Analyse Spectrale du Courant de Ligne pour la Détection des Défauts d'Excentricités dans les Moteurs Asynchrones à Cage d'Ecureuil", Procession of SNGE'2001 3 ème Séminaire National en Génie Electrique Université Mohamed Khider de Biskra, 29-30 octobre 2001.

[89] H.Austin, George, "Analysis of Rotor Failures in Squirrel Cage Induction Motors", IEEE Trans-actions on Industrial Electronics 1987.

[90] N.Benouzza, A.Benyettou, .Bendiabdellah, B.Kraloua et D.Toumi, " Rotor Cage Faults Diagnosis in 3-Phase Induction Motors, by Park's Vector Approach".4th, Jordanian International Electrical Electronicsnn Engineering Conference, 2001.

[91] S. Nandi, RajMohan Bharadwaj, H.A. Toliyat, and A.G. Parlos, "Performance Analysis of a Three Phase Induction Motor under Incipient Mixed Eccentricity Condition ", IEEE PEDES'98 Conference proceedings, Perth, Australia, Nov.30-Dec.3, 1998.

[92] I. Chouidira, D. Khodja, S. Chakroune, (2019), " Continuous Wavelet Technique for Detection of Broken Bar Faults in Induction Machine " , Traitement du Signal ,vol.36,No.2. pp.171-176.

[93] Abu Ibaid. O. Z. I, Belhamdi. S, Abid. M ,CHAKROUNE.S, " Diagnosis of rotor faults of asynchronous machine by spectral analysis of stator currents", 5 th INT ERNATIONAL AEGEAN

Symposium on Innovation Technologies & Engineering. February 25-2 6, 2 022. Izmir, Turkey.https://www.aegeanconference.com/symposium-book.

[94] Djalal Eddine Khodja, " Elaboration d'un système intelligent de surveillance et de diagnostic automatique en temps réel des défaillances des moteurs à induction", Thèse de Doctorat, Boumerdès, 2007.

[95] Chouidira. I, Khodja. D. E, Chakroune. S, "Fuzzy Logic Based Broken Bar Fault Diagnosis and Behavior Study of Induction Machine", Journal Européen des Systèmes Automatisés, Vol. 53, No. 2, April, 2020, pp. 233-242.https://doi.org/10.18280/jesa.530210.

[96] M. G. Say, " The Performance and Design of Alternating Current Machines ", Sir Isaac Pitman &Sons Ltd., London, 1983.

[97] F.Ameur, "Contribution à l'Amélioration de la Commande Directe du Couple de la Machine Asynchrone :Utilisation de la MLI Vectorielle", Mémoire d'ingénieur, centre universitaire Dr M.Tahar, Saïda, Algérie. 2006

[98] M.Arezki, " MODÉLISATION FRÉQUENTIELLE DE LA MACHINE ASYNCHRONE EN VUE DE L'ANALYSE DES PERTURBATIONS CONDUITES BASSES FRÉQUENCES ", Thèse de Doctorat, Université de Batna, 06 Décembre 2008.

[99] Y. Soufi , T. Bahi, M. F. Harkat, R. Rouaibia, "Diagnosis and Fault Detection in Induction Motor drive Fed by PWM Voltage Source Inverter", Journal of Electrical Systems, Vol.6, N. 2, pp. 186-194, 2010.

[100] Tarek Ben Slimen, "A new technique for simultaneous Detection of one for Two Open-Switch Faults in Three phase Voltage – inverter – Fed PM Brushless DC Motor drive " , Journal of Electrical Engineering (JEEEC), VOL.59,NO.2,2008,97-100.

[101] M. Trabelsi , "simulation multiple IGBTs Open circuit Faults Diagnosis in Voltage Source Inverter Fed Induction Motor Using Modified Slope Method", International Conference on Electrical Machines _ ICEM 2010, Rome.

[102] F.Labrique and G.Séguier, "Les Convertisseurs de l'Electronique de Puissance", Edition Tech & Doc/Lavoisier 1995.

[103] Mehdi BELHAJ, "Contribution à l'Identification des Paramètres et des Etats d'une Machine à Induction pour Diagnostic et Développement de Commande Robuste : Robustesse vis à vis de Défauts ", Thèse de Doctorat, Université de Nantes, Le 18 Juin 2007.

[104] Y. Soufi , T. Bahi, M. F. Harkat, R. Rouaibia, " Diagnosis and Fault Detection in Induction Motor drive Fed by PWM Voltage Source Inverter", Journal of Electrical Systems, Vol.6, N. 2, pp. 186-194, 2010.

[105] M. Trabelsi , "simulation multiple IGBTs Open circuit Faults Diagnosis in Voltage Source Inverter Fed Induction Motor Using Modified Slope Method", International Conference on Electrical Machines _ ICEM 2010, Rome.

[106] Tarek Ben Slimen, "A new technique for simultaneous Detection of one for Two Open-Switch Faults in Three phase Voltage – inverter – Fed PM Brushless DC Motor drive " , Journal of Electrical Engineering (JEEEC), VOL.59,NO.2,2008,97-100.

[107] Sakhara .Saadi, " Diagnostic dans un entraînement électrique : Composé d'un onduleur et un moteur à cage" Mémoire de magister, Université de Badji Mokhtar Annaba 2006.

[108] BELHAMDI .Saad, "Fault Diagnosis of Asynchronous Machine Controlled by Different Control Techniques" , Thesis a Doctorate of Science degree,Option Electrical Engineering, Mohamed Khider University - Biskra,2014.

[109] G.P. Mehta, B. Singh, M. s. Manna, "Performance Analysis of rotating induction machines for Air-Gap eccentricity & Rotor bar faults using finite element method", International Journal of Research in Computer and communication technology", vol. 2, 2013, No. 5, pp: 267-272.

[110] Nicola Bianchi, "Electrical Machine Analysis Using Finite Elements", by Taylor & Francis Group, LLC, 2005, France.

[111] Jawad Faiz, B.M. Ebrahimi, "Locating rotor broken bars in induction motors using finite element method", Energy conversion and Management, vol. 50, 2009, pp: 125-131.

[112] Williamson, S., Lim, L.H. and Smith, A.C. (1990), "Transient analysis of cage-induction motors using finite-elements", IEEE Transactions on Magnetics, Vol. 26 No. 2, pp. 941-944.

[113] Ebrahami, B.M., Faiz, J., Lotfi-fard, S. and Pillay, P. (2012), "Novel indices for broken rotor bars fault detection in induction motors using wavelet transform", Journal of Mechanical System Signal Processing, Vol. 30, pp. 131-145.

[114] M. Feliachi, " Contribution au Calcul du Champ Electromagnétique par la Méthode des Eléments Finis en Vue d'une Modélisation Dynamique de Machines Electriques ", thèse de doctorat, Conservatoire National des Arts et Métiers,France 1981.

[115] MERABET .S et D. HOUSSINE ; "Diagnostic de d'défauts de la machine asynchrone `a cage d'écureuil par la méthode de reconnaissance des formes" , Thèse d'ingénieur ; Ecole Nationale Polytechnique d'Alger ; Année Juin 2007.

[116] B. M. Ebrahimi, J. Faiz, M. Javan-Roshtkhari, A. Z. Nehad, " Static Eccentricity fault Diagnosis in Permanent Magnet Synchronous motor using time stepping finite element method ", IEEE Transactions on Magnetics, vol. 44, No. 11, 2008, pp: 4297-4300.

[117] N. Bianchi, S. Bolognani, G. Comelato, "Finite Element Analysis Of Three-Phase Induction Motors: Comparison Of Two Different Approaches", Ieee Trans. On Energy Conversion, Vol. 14, No. 4, December 1999, Pp. 1523–1528.

[118] Sprooten, Jean-Claude Maun, "Influence of saturation level on the effect of broken bars in induction motors using fundamental electromagnetic laws and finite element simulations", IEEE Transactions on Energy Conversion, 2009, vol. 24, No. 3.

[119] A. Zorig, " Identification des Machines Asynchrones en Vue de leur Diagnostic ", mémoire de magister, Université de Setif 2010.

[120] W. Zaabi, Y. Bensalem and H. Trabelsi, " Fault Analysis of Induction Machine using Finite Element Method(FEM) v, 15th international conference on Sciences and Techniques of Automatic control & computer engineering - STA'2014, Hammamet, Tunisia, December 21-23, 2014.

[121] B. Silwal, "Computation of eddy currents in a solid rotor induction machine with 2-D and 3-D FEM ", MSc Thesis, Aalto University. Helsinki, 2012.

[122] ZEGHBA. Oussama, " Conception Optimisée d'une Machine Asynchrone à Cage Utilisant les Algorithmes Génétiques Modifiés ", Thèse Présentée pour l'obtention du diplôme de Doctorat Troisième Cycle Filière : Electromécanique Option : Electromécanique, UNIVERSITE MOHAMED BOUDIAF - M'SILA, 2021.

[123] T. TUDORACHE et L. MELCESCU, " FEM optimal design of energy efficient induction machines", Advances in Electrical and Computer Engineering, Volume 9, Année 2009

[124] M. BOUHARKAT, " Etude de l'évolution des courants rotoriques d'une machine asynchrone à cage en régime dynamique", Thèse de doctorat, Université de Batna, Faculté des sciences de l'Ingénieur, Année Février 2006.

[125] Devanneaux. V, " Modélisation des machines asynchrones triphasées à cage d'écureuil en vue de la surveillance et du diagnostic", Thèse de doctorat, Institut National Polytechnique de Toulouse, Année 2002.

[126] A. Ceban, R. Pusca, R. Romary, "Study of rotor faults in induction motors using external magnetic field analysis", IEEE Transactions on Industrial Electronics, vol. 59, No. 5, 2012, pp: 2082-2093.

[127] D. Marcsa, "Parallel finite element methods to solve coupled electrodynamic problems", PhD dissertation, Széchenyi István University, 2017.

Appendices A

❖ **ASYNCHRONOUS MACHINE SIZING PROGRAM RESULTS SHEET**

1. SPECIFICATION DATA

Useful Power (W)	Pu... 1100.00
Single Phase Voltage (V)	V1... 220.00
Number of Machine Phases m1	m1... 3.00
Supply frequency (Hz)	fs .. 50.00
Number of Pole Pairs	p... 1.00
Rotating Field Speed (rps)	ns... 50.00
Yield Esteem	Eta... 0.85
Estimated Power Factor	Cosfie... 0.90
Estimated Dispersion Coefficient	Kdisp... 0.70
Power Absorbed by the Machine (W)	Pabs... 1294
Machine Phase Current (A)	I1... 2.179
Apparent Internal Power (VA)	If .. 1006.5
Const. Shape Non Sinusoidal Induction	Kfind .. 4.000
Induction Form Factor in Air gap	Kf .. 1.085
Pole Coverage Coefficient	Kfnp .. 0.700
Geometry Factor Estimate Machine	Landae1 .. 0.500
Estimated Linear Current Density (A/m)	A1 .. 15000
Induction magnet. Estimated Air gap (T)	Bd .. 0.550
Estimated virtual length (m)	lie .. 0.079
Pitch Polar estimate (m)	Taue .. 0.157
Coef.Usage estimated minimum	Cest1 .. 0.427
Air gap Estimate (m)	Deltae .. 0.00035
Estimated Apparent Tangential Force (N/m²)	Sigmae .. 2597.0
Number Slot/Pole and /Phase	q1 .. 4
Fact. Distribution Fundamental wave	Kd1 .. 0.958
Shortening coefficient	Kp1 .. 0.940

2. PART ONE

2.1. PRELIMINARY CALCULATIONS

Coefficient of Winding	Kw1 .. 0.900
Number Slots of the machine	Z1 .. 24

2.2. GEOMETRIC DIMENSIONS

Determination of Diameter (m)	D1 .. 0.10000
Calculation Pole Pitch (m)	Tauc1 .. 0.15708

Virtual length (m)	lic .. 0.07854
Calculation of the Geometry Factor	Landac1 .. 0.500
Calculation of the Utilization Coefficient	Ccal1 .. 0.427

3. PART TWO STATOR SIZING

3.1. Number of Turns Per Phase

Pole Pitch Area(m²)	Spp1 .. 0.01234
Number of Turns Per Phase	Nsph11 .. 166.0
Number of Turns Chosen Per Phase	NsphCh11 .. 166
Total number of stator conductors	z1 .. 996
Number Conductors/stator slot	Nz1 .. 42
Recalculated Induction in Air gap(T)	Bdr .. 0.550
Air gap Delta--Asynchronous machines(m)	Deltac1 .. 0.00035
Useful flux in air gap (Wb)	FluxU .. 0.00475
Dispersion Coefficient	SigH1 .. 0.42857
Total Flux (Wb)	FluxT .. 0.00679
Linear density (A/m)	A1c .. 7423

3.2. Stator Winding Sizing

Stator Current Density (A/mm²)	Jcond1 .. 4000000
Conductor insulation thickness (mm)	Episcd .. 0.00004
Thickness Sheath Protection Coil Iron(m)	EpG .. 0.00050
Gap between insulation sheath conductors (m)	Gap .. 0.00050
Calles thickness (m)	EpCal .. 0.00050
Notch width (m)	LEnc .. 0.00816
Notch depth (m)	PEnc .. 0.00633
Throat thickness Notch (m)	EpgorZd1 .. 0.00200
Resistivity Stator Winding(Ohm.m)	Rho1 .. 3e-08
Copper Volume Density (kG/m3)	GamaCu1 .. 8890
Iron Volume Density (kG/m3)	GamaFe1 .. 7600
Estimated Induction in Cylinder Head(T)	BCul1 .. 1.300
Filling coefficient (Expansion)	Kr .. 0.900

3.3. Dimensioning of the stator slots

Stator Winding Section (mm²)	Scond1 .. 5.45e-07
Conductor Diameter (mm)	Dcond1 .. 0.00083276
Selected Normalized Diameter (mm)	Dnorcd1 .. 0.00087276
Chosen Normalized Width (mm)	Lnorcd1 .. 0.00073801
Selected Normalized Height (mm)	Hnorcd1 .. 0.00073801
Normalized section (m²)	Snorcd1m .. 5.45e-07
Insulated conductor width (mm)	Lcdis .. 0.001

Insulated conductor height (mm)	Hcdis .. 0.001
Section Insulated conductor (m²)	Scdism .. 6.05e-07
Stator tooth pitch (m)	Pdz1 .. 0.013
Calculated Notch Depth (m)	PEncc .. 0.006
Notch Fill Factor	FREncm .. 0.700

3.4. Stator Resistance per Phase

Coil Head Coefficient	KTB .. 2.000
Average Coil Head Width (m)	lf .. 0.294
Long. Avg. (half-turn) Conduct. (m)	LavgCond .. 0.373
Total length Stator Winding (m)	LTCond1 .. 371.466
Stator Winding Phase Resistance (Ohm)	Rph1m .. 6.820

3.5. Total Leakage Reactance Per Stator Phase

Permeance Zone Dent.Stator Perm	Z1..2.69e-08
Permeance Flux diff.Stator Perm	D1 .. 1.23e-07
Permeance Head Coil Stator Perm	B1 .. 8.95e-08
React. Total Leak/Stator Phase (Ohm)	Xf1 .. 4.140

4. PART THREE ROTOR SIZING

Number of Conductors Per Rotor Phase	Nsph2 .. 0.5
Number of Rotor Slots	Z2 .. 16
Number of Notches per Phase	Kq .. 1
Shortening coefficient	Ks .. 1
Ventilation-Friction Loss Coef (pcent)	KPVF .. 0.0
Coef Loss Superf.-Pulsat.Teeth (pcent)	KPSup .. 0.0
Estimated Slip (pcent)	Slip .. 0.050
Ring Current Density (A/mm²)	JAn .. 5000000
Resistivity Al. Winding Rotor(Ohm.m)	RhoAl2 .. 3.6e-08
Bar Current Density (A/mm²)	JBar .. 5000000
Aluminum Volume Density (kG/m3)	GamaAl2 .. 2700
Rotor Iron Volume Density (kG/m3)	GamaFe2 .. 7600
Induction Rotor Cylinder Head (T)	BCul2 .. 1.008

4.1. Sizing of the Rotor Cage

Rotor Tooth Pitch (m)	TauZ2 .. 0.017
Empty EMF of each Rotor Bar (V)	E2Bar .. 0.515
Wind losses. and Friction (W)	PVF .. 5,500
Additional losses (W)	PSup .. 5,500
Rotoric Bar Current (A)	IBar .. 141.831
Current in Rotor Ring (A)	IAn .. 363.500
Cage Ring Thickness (mm)	EpAn .. 0.009
Cage Ring Depth (mm)	ProfAn .. 0.009

Ring average length (mm)	LAn .. 0.295

4.2. Equivalent Resistance Calculation by Rotor Phase

Resistance Anneau a 75°C (Ohm)	RAn .. 6.99e-06
Epaisseur Barre Cage (mm)	EpBar .. 0.005
Profondeur Barre Cage (mm)	ProfBar .. 0.005
Longeur Barre Cage (mm)	LBar .. 0.097
Resistance de la Barre a 75°C (Ohm)	RBar .. 0.000123
Resist.Equival./Phase Rotor 75°C(Ohm)	Rph2 .. 0.000159

4.3. Rotor Total Leakage Reactance Calculation

Permeance Rotoric Dental Zone Perm	Z2 .. 1.3e-06
Permeance Rotoric Differential Flux Perm	D2 .. 2.1e-07
Permeance Rotor Coil Head Perm	B2 .. 1e-07
Total Rotor Reactance (Ohm)	Xf2 .. 0.000505

5. PART FOUR TOTAL ENGINE WEIGHT CALCULATION

5.1. Total Stator Weight Calculation

Cylinder Head Stator Thickness (m)	EpCul1 .. 0.037
Outer Diameter Cylinder Head Stator (m)	DExCul1 .. 0.192
Stator Yoke Iron Weight (kG)	PFeCul1 .. 9.690
Weight Iron Tooth area of Stator(kG)	PFeZd1 .. 0.902
Notch pitch (m)	TauEnc .. 0.013
Shortening Factor 11Enc/12Enc	FRac .. 0.778
Stator Copper Weight (kG)	PCu1m .. 1.799
Total Stator Weight (kG)	PT1 .. 12.391

5.2. Total Rotor Weight Calculation

Weight of Bars (kG)	PBar .. 0.118
Weight of Radial Rings (kG)	PAn .. 0.115
Weight of Iron Rotoric Tooth Area(kG)	PFeZd2 .. 0.675
Rotor Yoke Thickness (m)	EpCul2 .. 0.033
Weight of Rotor Cylinder Head (kG)	PCul2 .. 3.051
Shaft diameter (m)	Shaft .. 0.021
Weight of iron shaft (kG)	PfeAr .. 2.951
Total Weight of Radial Cage Rotor (kG)	PT2 .. 6.910

5.3. TOTAL ENGINE WEIGHT

TOTAL ENGINE WEIGHT (kG)	GTM .. 22,791
MOTOR MASS POWER (kW/kG)	PMASM .. 0.048

6. TOTAL INERTIA OF THE ASYNCHRONOUS MACHINE MOTOR (QUALITY AND PERFORMANCE FACTOR)

6.1. Total Resistance Returned to the Stator

Vacuum permeability	Mu0 .. 1.3e-06
Reduction coefficient of the machine	Kred.. 16743.3
resist. Rotor Brought to Stator(Ohm)	Rr21 .. 2.65409
resist. Total Returned to Stator(Ohm)	RTot .. 9.55546

6.2. Total Reactance Brought Back to the Stator

Reactance Rotor Brought to Stator (Ohm)	Xf21 .. 8.76473
Total Reactance Returned to the Stator (Ohm)	XfTot .. 13.17297

6.3. MAGNETO-MOTORING FORCES IN THE MACHINE

FMM in the Air Gap Zone (At)	FmmDelta .. 333.6
Induction B at 1/3 head stator tooth (T)	BdZ13 .. 1.571
FMM Stator Tooth Zone (At)	FmmZ1 .. 78.6
Recalculated induction Cylinder head Stator (T)	BCulr1 .. 1.300
FMM in the Stator Yoke Zone (At)	FmmCul1 .. 195.4
Induction B 2/3 tooth head Rotor (T)	BdZ23 .. 0.897
FMM in the Rotoric Tooth Zone (At)	FmmZ2 .. 2.8
Recalculated induction Cylinder head Rotor (T)	BCulr2 .. 1.008
FMM in the Rotor Yoke Zone (At)	FmmCul2 .. 26.3
Total FMM/Pole Pair (At)	FmmTot .. 636.7
Calculated Saturation Coefficient	KSAT .. 1.300
Total Saturation Coefficient	KSATot .. 1.300
Stator Magnetizing Current Im (A)	Im .. 1.578
Stator Short Circuit Current (A)	I1cc .. 14.395
Short-Circuit Current Phase Angle	fiCC .. 54.043
Starting Torque Tstart (Nm)	Tstart .. 4.1
Nominal Torque Tn (Nm)	Tn .. 3.7

7. PART SIX PERFORMANCE CALCULATION

7.1. TOTAL IRON LOSSES

Losses In Stator Iron (W)	PFerStat .. 56.4
Losses In Rotor Iron (W)	PFerRot .. 3.6
TOTAL LOSSES IN IRON (W)	PFerTot .. 60.0

7.2. TOTAL LOSSES PER FLOW PULSATION

Stator Pulse/Flux Iron Losses (W)	Ppuls1 .. 0
Rotor Pulse/Flux Iron Losses (W)	Ppuls2 .. 11,000

TOTAL LOSSES PER FLOW PULSE (W)	PpulsTot .. 11,000

7.3. TOTAL COPPER LOSSES IN THE MACHINE

Winding Copper Losses of Stator (W)	PCopper1 .. 97.1
Rotor Cage Copper Losses (W)	PCopper2 .. 51.0
TOTAL LOSSES-COPPER IN MACHINE (W)	PCopperTot.. 148.1

7.4. TOTAL FRICTION/VENTILATION LOSSES

Losses Friction/Ventil.(W)	PFrotVent.. 5.5

7.5. SUM OF LOSSES IN MACHINE

Sum of Losses in the Machine (W)	SumPer .. 224.616

7.6. MACHINE PERFORMANCE

Machine yield in (pcent)	YieldM .. 0.830

8. PART SEVEN PARAMETERS FOR DEVELOPING THE CIRCLE DIAGRAM

No-load active current (A)	Iact0 .. 0.094
No-load current (A)	I0 .. 1.581
No-load Phase Angle (Degree)	fi0 .. 86.592
Nominal Slip 1 (pcent)	SlipN .. 4.377
Nominal Power Factor	Cosfi .. 0.921
Nominal Phase Angle (Degree)	fi1 .. 22.896
Maximum Power Factor	CosfiMax .. 0.802
Coeff. of Overload at Startup	COverch .. 6.4

9. PART EIGHT PROPORTION VERIFICATION CALCULATION

Product Yield Power Factor	PETAFP .. 0.765
No-load Current/Rated Current Ratio	RT1 .. 0.72573
Total Section Stator Conductors (m^2)	STotCond1.. 0.00054259
Total Section Stator Conductors (m^2)	STotCond2.. 0.00045386

10. PART NINE DETERMINATION OF PARAMETERS EQUIVALENT DIAGRAM

Stator Leakage Inductance (H)	lsf1 .. 0.01318
Induct.Rotor Leak Returned to Stator(H)	lfr21 .. 0.02692
No-load reactive power (VAR)	Q0 .. 1041.7
Stator Self-Phase Inductance (H)	Ls1 .. 0.44369

Mutual Inductance Stator - Rotor (H)	M .. 0.43051
Induct.Clean Rot.Returned to Stator (H)	Lr21 .. 0.45743

Appendices B

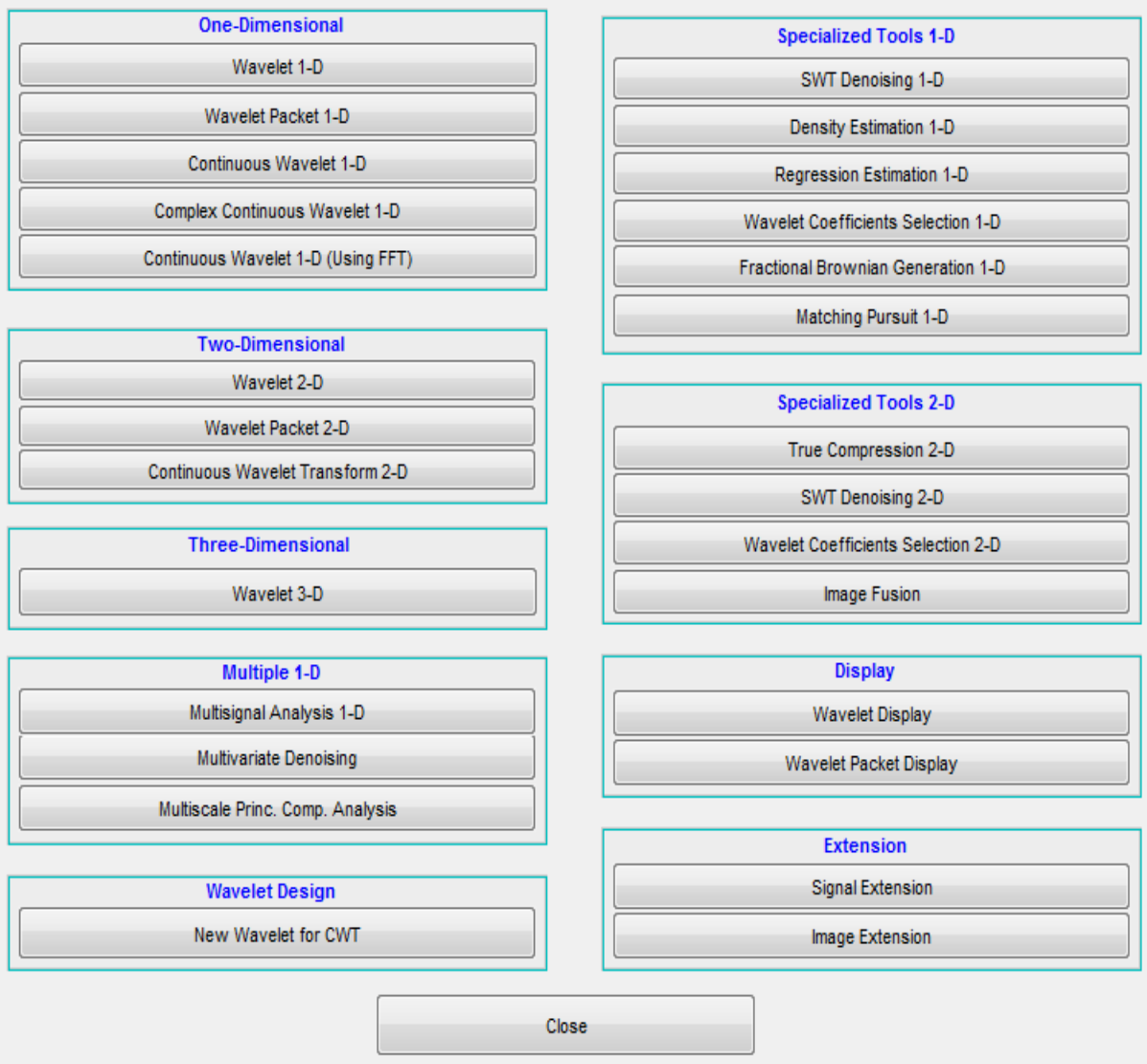

Figure : Matlab Toolbox Wave menu editor windows .[108]

[108] BELHAMDI Saad "Fault Diagnosis of Asynchronous Machine Controlled by Different Control Techniques" , Thesis a Doctorate of Science degree,Option Electrical Engineering, Mohamed Khider University - Biskra,2014.

Abstract

Machine monitoring, for the diagnosis and forecasting of breakdowns, has given rise to a lot of work in recent years, and has caused its considerable influence on the operational continuity of many industrial processes, squirrel cage induction motors are widely employed. These motors can be used in harsh situations, such as non-ventilated spaces, due to their high strength and longevity.

In this thesis, we have first presented rotor faults in asynchronous machines, mentioning the diagnostic methods currently used, as well as their advantages and disadvantages. Secondly, a model of squirrel cage with multiple turns in a closed loop was presented to simulate the breaking bars. We used an analytical technique to illustrate the development of the model using the Park criterion. We also use the inverter with two voltage levels in MAS.

In the third chapter, we present the simulation results of the machine scale model in both intact and defective condition (with and without inverter), by performing a spectral analysis of the stator current signature of an asynchronous cage motor under different fault conditions of the rotor (broken rod), in the first using the method Fast Fourier transform FFT the second using WT wavelet analysis techniques in both directions continuous transform and discrete transform to determine the breakage problems of the rods in the induction motor predicting a deterioration in her condition. Confirming the validity of the simulation results in the previous chapter, in Chapter 4, we presented a simulation model using finite element approach in Flux 2D® software in order to evaluate how the machine behaves in the absence and presence broken bars. So that, this work and the results we have reached are a scientific reference to be used in diagnosing faults of asynchronous machines with a squirrel cage.

Key words—Squirrel cage induction motors, BRB, WT, FFT, continuous wavelet transform, discrete wavelet transform, FEM.

خلاصة

لقد أدت مراقبة الآلات لتشخيص الأعطال والتنبؤ بها إلى ظهور الكثير من العمل في السنوات الأخيرة، وكان لها تأثير كبير على الاستمرارية التشغيلية للعديد من العمليات الصناعية، ويتم استخدام المحركات الحثية ذات القفص السنجابي على نطاق واسع. يمكن استخدام هذه المحركات في المواقف القاسية، مثل الأماكن غير جيدة التهوية، نظرًا لقوتها العالية وطول عمرها الافتراضي.

في هذه الأطروحة، قمنا أولاً بعرض أخطاء الدوار في الآلات غير المتزامنة، مع ذكر طرق التشخيص المستخدمة حالياً، بالإضافة إلى مزاياها وعيوبها. ثانياً، تم تقديم نموذج لآلة غير متزامنة بقفص سنجابي متعدد اللفات في حلقة مغلقة لمحاكاة كسر القضبان. استخدمنا تقنية تحليلية لتوضيح تطور النموذج باستخدام معيار بارك. قمنا أيضًا باستخدام العاكس بمستويين من الجهد في.MAS

في الفصل الثالث، نقدم نتائج المحاكاة لنموذج مقياس الآلة في كل من الحالة السليمة والمعيبة (مع وبدون عاكس)، من خلال إجراء تحليل طيفي لتيار الجزء الثابت لمحرك قفص غير متزامن تحت ظروف خطأ مختلفة للدوار. (القضيب المكسور)، في الأول باستخدام طريقة تحويل فورييه السريع FFTوالثاني باستخدام تقنيات تحليل الموجات WT في كلا الاتجاهين التحويل المستمر والتحويل المنفصل لتحديد مشاكل كسر القضبان في المحرك التحريضي متوقعا تدهور حالتها.

قدمنا في الفصل الرابع نموذج محاكاة باستخدام منهج العناصر المحدودة في برنامج Flux 2D® من أجل تقييم كيفية تصرف الآلة في ظل غياب ووجود العيوب (الأعمدة المكسورة) والتأكد من صحة نتائج المحاكاة في الفصل السابق، بحيث يكون هذا العمل والنتائج التي توصلنا إليها مرجعاً علمياً يستخدم في تشخيص أعطال الآلات الكهربائية غير المتزامنة ذات القفص السنجابي.

الكلمات المفتاحية ـ المحركات الحثية ذات القفص السنجابي، القضيب المكسور ، ، تحويل المويجات المستمر، تحويل المويجات المنفصلة.

Résumé

La surveillance des machines, pour le diagnostic et la prévision des pannes, a donné lieu à de nombreux travaux ces dernières années, et a eu une influence considérable sur la continuité opérationnelle de nombreux processus industriels. Les moteurs asynchrones à cage d'écureuil étant largement utilisés, ces moteurs peuvent être utilisés dans des situations difficiles, telles que des espaces non ventilés, en raison de leur résistance et de leur longévité élevées.

Dans cette thèse, nous avons d'abord présenté les défauts rotoriques des machines asynchrones, en mentionnant les méthodes de diagnostic actuellement utilisées, ainsi que leurs avantages et inconvénients. Dans un deuxième temps, un modèle de machine asynchrone à cage d'écureuil à multi-enroulements en boucle fermée a été présenté pour simuler la rupture de barres. Nous avons utilisé une technique analytique pour illustrer le développement du modèle en utilisant le critère de Park. Nous avons également utilisons l'onduleur avec deux niveaux de tension dans MAS.

Dans le troisième chapitre, nous présentons les résultats de simulation du modèle réduit de machine à la fois intact et défectueux (avec et sans inverseur), en effectuant une analyse spectrale de la signature du courant statorique d'un moteur asynchrone à cage dans différentes conditions de défaut du rotor. Dans la première en utilisant la méthode de transformée de Fourier rapide FFT, la seconde en utilisant les techniques d'analyse par ondelettes WT dans les deux sens, transformée continue et transformée discrète, pour déterminer les problèmes de cassure des barres prédisant une détérioration de son état.

En fin, dans le dernier chapitre nous avons présenté un modèle de simulation utilisant l'approche éléments finis dans le logiciel Flux 2D® afin d'évaluer le comportement de la machine en absence et en présence de défauts. Confirmant la validité des résultats de simulation du chapitre précédent, de sorte que ce travail et les résultats auxquels nous sommes parvenus constituent une référence scientifique à utiliser dans le diagnostic des défauts des machines asynchrones à cage d'écureuil.

Mots clés : Moteurs à induction, BRB, WT, transformation en ondelettes continue FFT, transformation en ondelettes discrète, MEF.